Functional interfaces for the immobilization of membrane proteins : concept, characterization and interactions

Hajra Basit

UNIVERSITÉ DE GRENOBLE

THÈSE

Pour obtenir le grade de

DOCTEUR DE L'UNIVERSITÉ DE GRENOBLE

Spécialité : Chimie Biologie

Arrêté ministériel : 7 août 2006

Présentée par

Hajra BASIT

Thèse dirigée par **Pascal DUMY** et
par **Pierre LABBÉ**

préparée au sein du **Laboratoire Ingénierie et Interactions Biomoléculaires (I2BM)**
dans **l'École Doctorale de Chimie et Science du Vivant**

INTERFACES FONCTIONNELLES POUR L'IMMOBILISATION DES PROTÉINES MEMBRANAIRES : CONCEPT, CARACTÉRISATION ET APPLICATIONS

Thèse soutenu publiquement le **04 Mai 2011**,
devant le jury composé de :

Dr. Claire-Marie PRADIER
Directrice de Recherche CNRS, UPMC, Paris (Rapporteur)
Dr. Ralf RICHTER
Professeur CIC biomaGUNE, San Sebastián, Espagne (Rapporteur)
Dr. Jean-Luc POPOT
Directeur de Recherche CNRS, IBPC, Paris (Président du jury)
Dr. Angéline VAN DER HEYDEN
Maître de Conférences DCM, Grenoble (Co-encadrante, Membre)
Prof. Pierre LABBÉ
Professeur DCM, Grenoble (Co-directeur, Membre)
Prof. Pascal DUMY
Professeur DCM, Grenoble (Directeur, Membre)

Acknowledgements

It is good to have an end to the journey toward; but it is the journey that matters, in the end...

Ursula Le Guin

A journey of about three years perhaps doesn't sound very long, but well, it surely is when it is on a foreign land, around 7000 kilometers away from home. Nonetheless, these years spent as a PhD student at the Département de Chimie Moléculaire, Grenoble were indeed very special and memorable, and herein, I wish to acknowledge all those who helped me either professionally or personal during this course.

At the outset, I wish to thank Prof. Pascal Dumy, director of Département de Chimie Moléculaire, Grenoble for accepting me as a PhD student in his team, and under his supervision. I also wish to acknowledge him for providing the necessary financial support.

I would like to express my sincere gratitude to my jury members Dr. Claire-Marie Pradier, Directrice de Recherche, Université Pierre et Marie Curie, Paris and Dr. Ralf Richter, Principal Investigator, CIC biomaGUNE, Spain for meticulously reading my dissertation, and for accepting to be a part of my thesis-defense jury.

I am greatly indebted to Dr. Jean-Luc Popot, Directeur de Recherche, Institut de Biologie Physico-Chimique, Paris for having accepted to preside over my thesis-defense jury. His scientific advices and suggestions on various aspects of this work were extremely valuable.

I am grateful to Prof. Pierre Labbé, my thesis co-supervisor, for all the valuable discussions and suggestions, especially during the "formative" years of my thesis work. I wish to thank him for giving me the freedom to venture upon newer ideas and techniques, and for the confidence he bestowed upon me and my work. I wish to particularly thank him for giving me an opportunity to learn AFM, from the expert hands of Prof. Bernard Nysten in Louvain.

I sincerely thank Dr. Angéline Van der Heyden, for all her help and support, especially during the "latter" part of my work. I thank her for embarking into the field of membrane proteins along with me, and for strongly suggesting a "tenure extension"; I can now affirm that a significant amount of very crucial results were produced in those 3 months. Lastly, I thank her for establishing those "troubleshooting" collaborations and contacts with people across Grenoble in moments of severe distress!

I truly wish to thank Dr. Chantal Gondran, for all her time, efforts and enthusiasm in guiding me and helping me understand Electrochemical Impedance Spectroscopy. I deeply cherish all those moments spent with her, when she would make a subject as complex as Impedance, appear very simple and lucid. I am really glad that I had an opportunity to work with her. Merci beaucoup Chantal!

I wish to thank Prof. Bernard Nysten (UCL Louvain, Belgium), for teaching me AFM, especially the "liquid-medium" and the "MAC-mode" technique for imaging soft samples.

I also wish to thank Dr. Cécile Breyton (IBS, Grenoble), for her generosity in lending us her proteins and for the scientific discussions. I also thank Prof. Françoise M. Winnik (Univ. of Montreal, Canada) for providing us the biotinylated amphipol.

I would like to thank Dr. Christophe Travelet (CERMAV Grenoble), for helping me perform DLS experiments. I also wish to thank Dr. Patricia Renesto, and Prof. Winfried Weissenhorn (EMBL Grenoble), for their help in the sucrose gradient density measurements.

I acknowledge all the permanent staff members of DCM for their cordiality, kindness, and for providing a very pleasant working ambience at the department. I would specially like to thank Dr. Didier Boturyn, for allowing me to access the synthesis facilities and for the very useful suggestions on the various protecting groups. I would also like to thank Dr. Liliane Guerente, Mr. Ludovic Guillard and Mr. Hugues Bonnet, for all their scientific help. Thanks to Prof. Jean-Claude Moutet, for the various discussions, for all his kind words and his appreciation of my spoken "French".

Thanks must also go to Dr. Jean-François Constant, for always being available and ready to share his knowledge of molecular biology. I truly enjoyed all the long discussion with him, both scientific and non-scientific. I would also like to thank Dr. Alain Deronzier and all the permanent members of CIRE, for being so kind and warm during the time we shared our "working spaces". My thanks to Sébastien Morin as well, for his immense help in the infotech related problems.

My sincere thanks to Mme. Régine Rozand and Mme. Véronique Gineste, for all the administrative help they provided.

I wish to convey my thanks to the non-permanent members of DCM, for the various light moments spent together on either tea/coffee breaks or the famous "crêpes" parties. I would like to begin with Ludivine (my QCM-D expert), Aurélien (the smiling guy) and Jessica (the kind girl). I thank Raoudha, for her pleasant company and the laughter riots at the foyer, Cedric (for all the discussions on AFM, publications, iPhone, etc., etc...), Gareth (for the electrochemical cell), Abdel-Kader and Kamal (for those evening eat-outs and for those rib-tickling jokes), Marcello (for the 'tac-tac' and definitely for all his help with the distilled THF), Sébastien, Isabelle Anil, Dhruv and Meenakshi. I am sure to have forgotten many people in this list, to whom I apologize profusely!

I owe special thanks to Audrey Conti and Mohammed Habib (EMBL, Grenoble), for helping me tremendously during each of my frequent visits to EMBL. Merci Audrey et Choukran Habib!

A special word of gratitude to Sumana (Sumo), for helping me train my hands on the NMR machine, and for the good moments we shared during the "syntheses" days. Special thanks to Fabien as well, for being such a nice and helping friend and colleague, and for being magnanimous in lending me "his" potentiostat for impedance measurements!

My acknowledgements cannot be complete without expressing my gratitude to Prof. Santanu Bhattacharya (IISc Bangalore). It was in his lab that I was first introduced to the wondrous world of scientific research (during my master's internship project). I also thank him for giving me an opportunity to work in his group, which not only helped me strengthen my skills in chemistry, but also helped me learn several aspects of research and science in general, which were very useful during the course of my PhD.

I would like to thank Prof. Sampath (IISc Bangalore), for his generous help with the atomically flat gold surfaces, and for initiating me into Electrochemical Impedance Spectroscopy, a technique that later turned out very useful to my research.

My three year long stay in Grenoble was made really pleasant by all my friends of the "Foyer de l'etudiante", who also helped me speak French, as fluently as I do today. I cannot thank my friends Mouna and Rached enough, for their joyful company and their enormous help in organizing my thesis-defense party. I also thank Afzal Khan, for his warm, friendly and family-like company during these years.

Last but certainly not the least; I thank my family for their unconditional love and support, and their unwavering faith on my abilities. Special thanks to my mom for being this beautiful person that she is! A lovable thank-you to my little nephew, for convincing me very endearingly, to come back home with a bag full of chocolates for him! I also thank Saikat, for being this pillar of strength and support, through thick and thin. I thank him for the formidable patience with which he lent an ear to my discussions and problems, despite being so far away.

INDEX

List of Abbreviations

AFM	Atomic Force Microscopy
Alloc	allyl oxycabonyl
Apols	Amphipols
B-PCApol	Biotin tagged Phosphoryl choline based amphipol
cmc	critical micellar concentration
ConA	Concanvalin A
C_{dl}	Electrical double layer capacitance
C_m	Membrane capacitance
CPE	Constant Phase Element
DCC	*N-N'*-Dicyclohexyl carbodiimide
DIPEA	*N-N'*-Diisopropylethylamine
DMEM	Dulbecco's Modified Eagles Medium
DMF	*N-N'*-Dimethylformamide
DLS	Dynamic Light Scattering
E.coli	Escherichia Coli
ECM	Extracellular Matrix
EDC	*N*-(3-Dimethylaminopropyl)-*N'*-ethylcarbodiimide hydrochloride
EIS	Electrochemical Impedance Spectroscopy
ESI	Electron Spray Ionisation
FhuA	Ferric hydroxamate uptake receptor
Fmoc	9-Fluorenylmethoxycarbonyl
HD	High Density
HEK(293)	Human embryonic kidney cell line
LDAO	Lauryldimethylamine oxide
LD	Low Density
MeOH	Methanol
NHS	N-Hydroxysuccinimide
NMR	Nuclear Magnetic Resonance
OG	Octyl-β-glucoyranoside
OTs	Tosylate
PEG	Polyethylene glycol
POPC	1-Palmitoyl-2-oleoyl-*sn*-glycero-3-phosphocholine
Pmc	(*4-(2-hydroxyethyl)-1-piperazineethanesulfonic acid*)
PyBOP	2,2,5,7,8-pentamethylchromane-8-sulfonyl (Benzotriazol-1-yloxy)tris(pyrrolidino)phosphonium hexafluorophosphate
QCM-D	Quartz crystal Microbalance with Dissipation

RAFT	Regioselectively Addressable Functional Template
R_h	Hydrodynamic Radius
R_m	Membrane Resistance
RP-HPLC	Reverse Phase High Performance Liquid Chromatography
r.t.	Room temperature
RU	Resonance/Response Units
SAM	Self-Assembled Monolayer
SDS	Sodium dodecyl sulfate
SLB	Supported Lipid Bilayer
SPPS	Solid Phase Peptide Synthesis
SPR	Surface Plasmon Resonance
SUV	Small Unilamellar Vesicles
TFA	TrifluoroAcetic Acid
tBLM	Tethered Bilayer Lipid Membrane
TIS	Triisopropyl Silane
TLC	Thin Layer Chromatography
Tris	Tris[hydroxymethyl]aminomethane hydrochloride
TSG	Template Stripped Gold
UV	Ultraviolet

Synopsis

SYNOPSIS (English)

Organization, compartmentalization and communication constitute the ways in which nature is structured and through which it functions. The finest example of this fact is the cytoplasmic cell membrane. The cell membrane, although being a complex self-assembly of phospholipids, sphingolipids, membrane proteins and other structural components is an organization *'par excellence'*. The cell membrane maintains a selective barrier between the extracellular matrix and the cytoplasm by permitting the transport of specific molecules/ions only when they are required by the cell. However, it also acts as a medium through which communication is maintained between the interior and the exterior of a cell. The last mentioned function of the cell membrane is actually mediated through the agency of the membrane proteins embedded within the membrane.

These membrane proteins which are integral to the cell membrane are known to perform myriads of functions which are vital to life. They are for example transporters which carry nutrition into the cell in the form of glucose *etc.*; they are receptors, which perform a very crucial role of recognition at the cell surface interface. These important functions of the membrane proteins thus make them an important feature in both pharmaceutical and drug research. However, taking into account the increasing interests that the membrane proteins draw in since several years, their *in vitro* studies call for the design of rational models which can protect/stabilize their special structural features.

These proteins being amphiphilic in nature are quite difficult to work with in pure aqueous medium. They thus require specialized systems which provide them conditions similar to that of the cell membrane. These specialized systems, called the cell membrane mimic models are being vastly developed in the interest of studying membrane proteins.

To this context several model systems have been described in the literature, each of them tend to address different structural features of the cell membrane and each one provides an advantage or disadvantage over the other.

In our present work, our goal is to design such model membranes at the interface of surfaces. These systems often called solid Supported Lipid Bilayers (SLBs) or Tethered Bilayer Lipid Membranes (tBLMs) are two systems studied quite intensively in the literature. The former being introduced much before the latter, has been exploited not only in the incorporation of membrane proteins but has also been used as a support for studying biomolecular interactions. The tBLMs are developed lately as an improvement

to the SLB models. These systems essentially target to achieve successful incorporation of the membrane proteins by reduced frictional interference from the surface as in the case of SLBs.

Another system, which is not really a membrane mimic, but rather provides amphiphilic nature to the membrane proteins, is currently being used quite extensively. Such systems, involve the use of amphiphilic polymers called Amphipols (Apols). These Amphipols are shown to render excellent stability to membrane proteins and they offer a general ease and convenience to the studies of membrane proteins.

Aim of the present study and Organization of the Thesis

A major aim of the present work is the design, characterization and applications of functional interfaces, which facilitate the study of membrane proteins and biomolecuar interaction events. To this goal, three specific model systems were studied in the present context namely the Supported Lipid Bilayers (SLBs), the Tethered Bilayer Lipid membrane (tBLM) and Phosphorylcholine based Amphipols.

The present thesis is thus organized in the following five chapters:

1. Bibliography

This section gives a brief overview of the general structure of a cytoplasmic cell membrane; it highlights its structural characteristics which are convivial to the stability of the embedded membrane proteins. It also highlights the general structural features of membrane proteins, in particular the structure and the functions of FhuA (an *E.coli* outer membrane protein) and the $\alpha_v\beta_3$ integrin (an angiogenic factor in human cells), as these two proteins are widely studied in this thesis. This chapter also details the various cell membrane mimic models present in the literature. It also briefs about the various techniques such as Quartz Crystal Microbalance with Dissipation (QCM-D), Atomic Force Microscopy (AFM), Electrochemical Impedance Spectroscopy (EIS), Surface Plasmon Resonance (SPR) and Dynamic Light Scattering (DLS) used in the present thesis to characterize the various functional interfaces.

2. Supported Lipid Bilayers as platforms for studying biomolecular interactions

This chapter highlights the general features of Supported Lipid Bilayers and their viability as a platform for studying biomolecular interactions. However, this chapter is dedicated to the study of two principal systems and is hence sub-divided into two parts.

2.1 cRGD Induced Cell Adhesion of HEK-β3 Cells on Supported Lipid Bilayers

This subsection describes the adhesion of HEK- β_3 cells (over expressing the $\alpha_v\beta_3$ integrin) on a Supported Lipid Bilayer doped with lipidic-*c*RGD ligands. The objective of this chapter is to offer a systematic study of cell adhesion delineating the concentration of the lipidic cRGD ligands in the SLB on the morphology of the adhered cells. To this effect two lipidic ligands were selected, a ligand offering multivalent (4) *c*RGD groups and a ligand bearing a single *c*RGD group.

The objective was to understand the effects of the ligand spacing on inducing cell adhesion and a change in the morphology of the adhered cells. The use of complementary techniques like Quartz Crystal Microbalance with Dissipation (QCM-D) and Optical microscopy have been employed here to both quantify and visualize the cell adhesion on various SLBs.

2.2 Incorporation of FhuA in SLBs to monitor its Interaction with pb5 by QCM-D

This chapter aims to incorporate FhuA (an *E. coli* outer membrane protein) in liposomes. The influence of the presence of FhuA in the proteoliposomes is intended to be characterized and discussed using techniques like Dynamic Light Scattering (DLS). Moreover, the influence of increasing concentrations of FhuA on the fusion behavior of these proteoliposomes on a SiO_2 substrate is looked upon by (QCM-D). The other

objective of this study is to characterize the interactions of SLB-embedded FhuA with pb5 (a bacteriophage T5 protein) which specifically recognizes FhuA.

3. Design and characterization of tBLMs based on mixed SAMs: Influence of the SAM composition on bilayer formation

This chapter is targeted towards the design and characterization of tethered lipid bilayer membranes (tBLMs) based on mixed SAMs. The objective of this study is divided into two aspects. The first one being the formation and characterization of mixed SAMs made up of two thiols. To this end, the two tailor made thiols, are designed in such a way that one of these thiols bearing lipidic chains is highly hydrophobic and non polar while the other one bearing ethylene glycol groups is polar. We intend to highlight on the preferential adsorption of the hydrophobic thiol over the hydrophilic one and characterize the heterogeneity in the self-assembled monolayers observed by mixing the two thiols.

The second aspect of this objective was to study the influence of the composition of the SAM on the fusion behavior of the liposomes. This study is done in view of the contemporary interest in designing tBLMs with minimum possible quantities of the anchoring hydrophobic thiol to observe better fluidity in the structure. Thus this chapter aims to delineate with the help of techniques like QCM-D, AFM and EIS, a relationship between the composition of the SAM and the properties of the formed tBLMs.

4. Amphipols – Molecular toolkits for manipulating membrane proteins

This section is inclined towards studying the use of Amphipols (a class of amphipathic polymers) on the stability and surface immobilization of proteins (both FhuA and $\alpha_v\beta_3$ integrin). It thus describes the use of biotinylated phosphorylcholine based amphipols (B-PCApols) in maintaining the two above mentioned proteins soluble in their natural state. The goal here is thus to define the optimum working conditions *i.e.* the ratio of Apol: protein for each of the two above mentioned proteins. Not only was their surface immobilization on SPR chips looked at carefully, but also their interactions with pb5 and

vitronectin, their respective natural partners were examined. The approach is to probe into the measurements of affinity constants for the interactions of both FhuA with pb5 and $\alpha_v\beta_3$ integrin with vitronectin. Techniques like dot-blot, Nanodrop UV-visible spectroscopy and SPR are exploited for the present study.

5. SPR Study of Lectin Recognition by Small Multivalent Carbohydrates Ligands

The final section of this thesis is rather more like an annexe, because it does not deal with membrane proteins. It is rather dedicated to the study of biomolecular recognition events between proteins and small multivalent molecules.

In the past decade, multivalent interactions have appeared to be an essential element in the mediation of biological processes. Living organisms have developed different characteristics (coupling of receptors of the same function at the cell surface, showing multiple ligand sites on a single receptor) to allow an efficient and sensitive signal transmission. Fundamental understanding of multivalency has since become of high interest. However, multivalent binding interactions are necessary complex due to the multiple binding modes available, each of them having a potency to enhance the functional affinity of the multivalent ligand. To generate ligands with particular biological properties, however, a single binding mode could be required. Besides the importance of an optimal ligand design, knowledge on the individual mechanism involved in the recognition event is thus crucial. In the present chapter, the interaction between Concanavalin A (ConA) and mannosyl residues grafted on a cyclodecapeptide scaffold was studied as a model for the interaction of multimeric lectin with multivalent low molecular weigh glycoclusters. We proposed a direct SPR binding assay to explore the fundamental mechanisms involved in the global recognition event. The proximity/statistical effect induced by the close proximity of epitopes on the scaffold have been well evidenced and evaluated.

SYNOPSIS (Français)

L'organisation, la compartimentation et la communication constituent les moyens par lesquels la nature est structurée et à travers lesquels elle fonctionne. Le plus bel exemple de cette structuration est la membrane cellulaire cytoplasmique. La membrane cellulaire bien qu'étant un auto-assemblage complexe de phospholipides, de sphingolipides, de protéines membranaires et autres composants structurels, est une organisation «par excellence». La membrane cellulaire maintient une barrière sélective entre la matrice extracellulaire et le cytoplasme en autorisant le transport de molécules / ions spécifiques seulement lorsque ceux-ci sont requis par la cellule. En parallèle, la membrane représente un espace à travers lequel la communication entre les milieux intracellulaire et extracellulaire s'effectue. Cette dernière fonction est en fait régie par la présence de protéines membranaires ancrées dans la membrane.

Ces protéines membranaires qui font partie intégrante de la membrane cellulaire sont connues pour effectuer une multitude de fonctions essentielles à la vie. Elles agissent par exemple comme transporteurs qui apportent la nutrition dans la cellule sous forme de glucose ou autre; elles agissent également comme récepteurs, jouant un rôle crucial dans la reconnaissance à surface de la cellule. C'est grâce aux fonctions importantes qu'elles remplissent que les protéines membranaires sont devenues des sujets d'étude primordiaux pour la recherche pharmaceutique et thérapeutique. Toutefois, de part l'intérêt croissant que suscite ces protéines, leurs études *in vitro* requièrent la conception de modèles rationnels capable de protéger / stabiliser leurs particularités structurales.

Compte tenu de leur nature amphiphile, il est assez difficile de travailler avec ces protéines en milieu aqueux pur. En effet, elles nécessitent des systèmes spécifiques qui leur fournissent des conditions similaires à celles de leur environnement naturel, la membrane cellulaire. Différents systèmes mimant la membrane cellulaire ont ainsi été développés afin de permettent leur étude.

Dans ce contexte, plusieurs modèles de systèmes ont été décrits dans la littérature. Chacun d' entre eux ayant tendance à viser des caractéristiques structurales spécifiques de la membrane cellulaire, chacun présente donc un avantage ou un désavantage par rapport aux autres.

Dans le travail ici présenté, notre objectif est de concevoir des membranes modèles sur des surfaces solides. Les bicouches lipidiques supportées sur support solides (SLBs pour

solid supported lipid bilayers) ou suspendues (tBLMs pour tethered Lipid Membranes) sont deux systèmes étudiés de manière intensive dans la littérature. Les SLBs, introduites bien avant les tBLMs, ont été exploitées non seulement pour l'incorporation de protéines membranaires, mais aussi comme support pour étudier les interactions biomoléculaires. Les tBLMs, récemment développées, apparaissent quand à elles comme une amélioration aux modèles SLBs. Ce dernier système vise essentiellement améliorer l'intégration de la protéine au sein de la membrane en réduisant les interférences de friction entre la protéine et la surface comme cela peut être le cas avec les SLBs.

Un autre système, impliquant l'utilisation de polymères amphiphiles appelés amphipols (Apols) commence à être largement utilisé pour stabiliser les protéines membranes. Ce système, qui n'est pas vraiment un modèle de membrane, fournit un environnement amphiphile à la protéine. Les amphipols se sont donc avérés être d'excellents agents stabilisateurs pour les protéines membranaires, généralisant et facilitant ainsi l'utilisation de ces protéines.

Objectif de ces travaux et organisation du manuscrit

Un des objectifs majeurs de ce travail est le concept, la caractérisation et les applications d'interfaces fonctionnelles, pour faciliter l'étude des protéines membranaires et leur processus de reconnaissance biomoléculaire. Pour atteindre cet objectif, trois systèmes modèles spécifiques ont été étudiés, à savoir les bicouches lipidiques supportées (SLBs), les bicouches lipides suspendues (tBLM) et des amphipols fonctionnalisés par la phosphorylcholine.

La présente thèse est donc organisée en cinq chapitres dont figure ci-dessous un bref résumé :

1. Bibliographie

Cette section donne un bref aperçu de la structure générale de la membrane cytoplasmique d'une cellule, et met en évidence ses caractéristiques structurelles, propices à la stabilité des protéines membranaires. Les caractéristiques générales de la structure des protéines membranaires y sont décrites, ainsi que la structure et les fonctions des deux protéines étudiées lors de cette thèse : FhuA (protéine de la membrane externe de la bactérie *E. coli*) et de l'intégrine αvß3 (un facteur angiogénique des cellules humaines). Ce chapitre détaille également les différents modèles de membranes cellulaires présents dans la littérature. Les différentes techniques utilisées lors de cette thèse pour caractériser les diverses interfaces fonctionnelles sont décrites, à savoir, la microbalance à cristal de quartz avec mesure de la dissipation (QCM-D pour Quartz Crystal Microbalance with Dissipation), la microscopie à force atomique (AFM pour Atomic Force Microscopy), la spectroscopie d'impédance électrochimique (EIS pour electrochemical impedance spectroscopy), la résonance plasmonique de surface (SPR pour Surface Plasmon Resonance) et la diffusion dynamique de la lumière (DLS pour Dynamic Light Scattering)

2. Bicouches lipidiques supportées comme plateforme pour l'étude d'interactions biomoléculaires

Ce chapitre met en évidence les caractéristiques générales des bicouches lipidiques supportées et leur viabilité en tant que plateforme pour étudier les interactions biomoléculaires. Toutefois, ce chapitre est dédié à l'étude de deux systèmes principaux et est donc sous-divisé en deux parties.

2.1. Adhésion cellulaire induite par les groupements cRGD – Adhésion des cellules HEK-β3 sur des SLB

Ce paragraphe décrit l'adhésion des cellules HEK-β3 (sur exprimant l'intégrine αvß3) sur des bicouches lipidiques supportées dopées avec des ligands lipidiques cRGD. L'objectif de ce chapitre est de proposer une étude systématique de l'adhésion cellulaire en reliant la concentration des ligands lipidiques cRGD dans les SLBs à la morphologie des cellules adhérées. A cet effet, deux ligands lipidiques ont été sélectionnés, l'un offrant une présentation multivalente des groupes cRGD et l'autre ne portant qu'un seul groupe cRGD. L'objectif est de comprendre les effets de l'espacement entre les ligands sur le déclenchement de l'adhésion des cellules et sur les changements de morphologie des cellules adhérées. L'utilisation de techniques complémentaires comme la microbalance à quartz avec mesure de la dissipation (QCM-D) et la microscopie optique a été mise à profit pour les quantifier et visualiser l'adhésion cellulaire sur les différentes SLBs.

2.2. Incorporation de FhuA dans les SLBs pour étudier ses interactions avec pb5 par QCM-D

Ce chapitre vise à intégrer FhuA, une protéine de la membrane externe d'*E. coli,* dans des liposomes. L'influence de la présence de FhuA dans les protéoliposomes est caractérisée puis discutée en utilisant des techniques comme la diffusion dynamique de la lumière (DLS). En parallèle, l'influence de concentrations croissantes de FhuA sur le processus de fusion de ces protéoliposomes sur un substrat de SiO_2 est étudiée par QCM-D. Enfin, la caractérisation des interactions de FhuA ancrée dans la SLB avec un de ses ligands spécifiques, pb5 (une protéine du bactériophage T5) est présentée.

3. Conception et caractérisation de tBLMs basées sur des SAMs mixtes : influence de la composition de la SAM sur la formation de la bicouche

Ce chapitre est dédié à la conception et à la caractérisation de membrane de bicouches lipidiques suspendues (tBLMs pour tethered Bilayer Lipid Membranes) basées sur des monocouches auto-assemblées (SAMs pour Self-Assembled Monolayers) mixtes. Cette étude est divisée en deux parties. La première concerne la formation et la caractérisation des SAMs mixtes constituées de deux thiols. À cette fin, deux thiols sur mesure, ont été conçus de sorte que l'un de ces thiols, porteur des chaînes lipidiques, est hautement hydrophobe et non polaire tandis que l'autre thiol, porteur de groupements éthylène glycol, est polaire. Nous avons mis en évidence l'adsorption préférentielle du thiol hydrophobe sur le thiol hydrophile et caractériser l'hétérogénéité dans les SAMs obtenues à partir de mélanges des deux thiols. La deuxième partie de cette étude est dédiée à la caractérisation de l'influence de la composition des SAMs sur le comportement de fusion des liposomes. Cette étude est réalisée en relation avec l'intérêt actuel qu'est la conception de tBLMs avec des quantités minimales de thiol hydrophobe d'ancrage afin d'obtenir une meilleure fluidité de la structure. Ainsi, ce chapitre vise à définir, à l'aide de techniques comme la QCM-D, l'AFM et l'EIS, une relation entre la composition de la SAM et les propriétés des tBLMs formées.

4. Amphipols – outils moléculaires pour la manipulation de protéines membranaires

Cette section se concentre sur l'utilisation d'amphipols, une classe de polymères amphiphiles, pour assurer la stabilité et l'immobilisation de deux protéines, FhuA et l'intégrine $\alpha v\beta 3$. L'utilisation d'amphipols biotinylés à base de phosphorylcholine (B-PCApols) dans le maintien de ces deux protéines solubles dans leur état naturel y est décrite. Le but ici est donc de définir les conditions optimales de travail, à savoir le ratio molaire Apol: protéine, pour chacune des deux protéines mentionnées ci-dessus. Dans un premier temps, leur immobilisation à la surface de puces SPR a été examinée attentivement, puis leurs interactions avec leurs partenaires naturels respectifs, pb5 et la vitronectine, ont été étudiées. L'approche utilisée a été de mesurer les constantes

d'affinité pour les interactions des deux protéines membranaire FhuA avec pb5 et de l'intégrine αvß3 avec la vitronectine. Pour cette étude, des techniques comme le dot-blot, la spectroscopie UV-visible sur nanogouttes et la SPR ont été exploitées.

5. Etude par SPR de la reconnaissance de lectines avec de petits ligands carbohydrate multivalents.

La section finale de cette thèse est à considérer comme une annexe, car elle ne traite pas de protéines membranaires. Elle est, en effet, dédiée à l'étude de la reconnaissance biomoléculaire entre des protéines et des petites molécules multivalentes.

Au cours de cette dernière décennie, les interactions multivalentes sont apparues comme un élément essentiel de la médiation des processus biologiques. Les organismes vivants ont développé différentes caractéristiques (couplage à la surface cellulaire de récepteurs ayant la même fonction, exposition de plusieurs sites de reconnaissance sur un seul récepteur) afin de permettre une transmission efficace et sensible du signal. La compréhension fondamentale de la multivalence est dès lors devenue du plus haut intérêt. Toutefois, les interactions multivalentes sont nécessairement complexes en raison des multiples modes individuels de liaison disponibles, chacun d'entre eux ayant un pouvoir de renforcer l'affinité fonctionnelle du ligand multivalent. Cependant, pour générer des ligands ayant des propriétés biologiques spécifiques, un seul mode de liaison pourrait être requis. Outre l'importance d'une conception optimale du ligand, la connaissance des mécanismes individuels impliqués dans la reconnaissance est donc cruciale. Dans ce chapitre, l'interaction entre la concanavaline *A* (ConA) et des résidus mannosyl greffés sur un châssis cyclodecapeptidique a été étudiée comme un modèle d'interaction de lectines multimériques avec des ligands sucre multivalents de faible poids moléculaire. Nous proposons un test de liaison direct par SPR pour l'étude des mécanismes fondamentaux impliqués dans le processus de reconnaissance globale. L'effet de proximité /statistique induit par la proximité des épitopes sur le châssis moléculaire a ainsi été mis en évidence et évalué.

1. Bibliography

1. Bibliography

1.1. Cytoplasmic cell membranes: The living frontiers of nature

Nature's ways of defining frontiers are commendably different from that of man, and this fact is extremely well illustrated by the cytoplasmic cell membrane. This supramolecular structure *i.e.* the cytoplasmic cell membrane, which is ubiquitous in all living organisms, serves primarily as a barrier between the extracellular matrix and the cytoplasm (a function extremely important for the cellular process). Nonetheless, it is bestowed upon with a wide variety of mediators (called the membrane proteins). These mediators/membrane proteins by means of transport, signal transduction etc. ensures the harmonious functioning of biological processes on both sides of the frontier (cell membrane).

The structure of the cell membrane was proposed about 40 years ago by S.J.Singer and G.L.Nicolson, where by means of a collection of data of the 10 precedent years, they described the cell membrane to be a like a fluid-mosaic.[1]

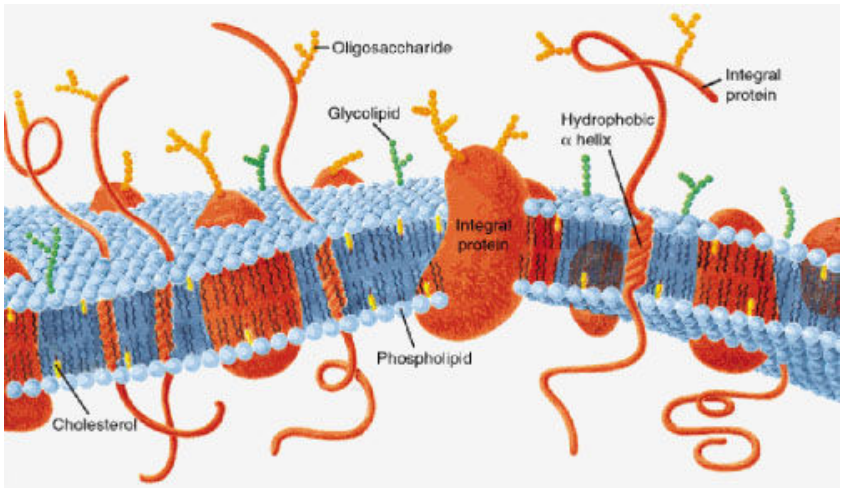

Figure 1.1 An adaptation of the representation of the fluid mosaic model of the cell membrane proposed by Singer and Nicolson. The phospholipids are colored blue, the cholesterol groups are colored light yellow and the membrane proteins are colored orange.

This model demonstrated that the cell membrane consists of a bilayer of phospholipids, which are organized in such a way that the hydrophilic heads of the lipids are at the two extremities of the membrane (facing the aqueous interior and the exterior of the cell) and the hydrophobic lipid chains form the inner part of the membrane (shielded away from

water). The stability of this arrangement of lipids in the bilayer was shown to be arising from like-like interactions (*i.e.* van der Waals forces and hydrophobic forces in the lipidic regions and electrostatic forces in the polar domain).

However, another important feature that this model highlighted was the fact that the cell membrane has membrane proteins embedded within them, thus making it a mosaic like structure. These membrane proteins could either span the membrane from one side to the other (transmembrane proteins) or they could sit on one surface of the membrane (peripheral proteins). This model also suggested that in the cell membrane, not just the membrane proteins, but also the phospholipids possessed an innate fluidity in 2 dimensions. Thus an ensemble of the two above mentioned features of the membrane led to its name "Fluid-mosaic". However, the cell membrane besides being fluid is still highly ordered in the membrane plane. Later on, advanced studies on the cell membranes demonstrated that lipids move laterally at a fast rate with a lateral diffusion coefficient on the order of 1 $\mu m^2/s$, but they cross the membrane by flip-flop only once every few hours.[2]

1.2. Membrane Proteins

1.2.1. General Structural Features of Membrane Proteins and their Functions

The above mentioned fluid-mosaic model by S.J.Singer and G.L.Nicolson, not only threw light on the structure of the cell membrane, but also highlighted a very important feature about the structure of the membrane proteins. In that, the model demonstrated that membrane proteins are bifunctional in nature. In which, they posses two clear structural domains *i.e.* a hydrophobic domain which is embedded within the cell membrane and a hydrophilic domain which is present outside the cell membrane. It is well understood by now, that about 20-30% of the eukaryotic genome codes for membrane proteins.[3] Further, membrane proteins carry out many pivotal roles in a cell. For example, they control the uptake of nutrients and ions, they sense the external environment, they generate energy during respiration, they modulate cell-cell

interactions and most importantly they are receptors to specific proteins of the extracellular matrix.[4] They are classified based on their functions as well as their structures. Figure 1.2 gives a schematic picture about the various functions of membrane proteins, indicating also schematically the different conformations adapted by these proteins for each of their function.

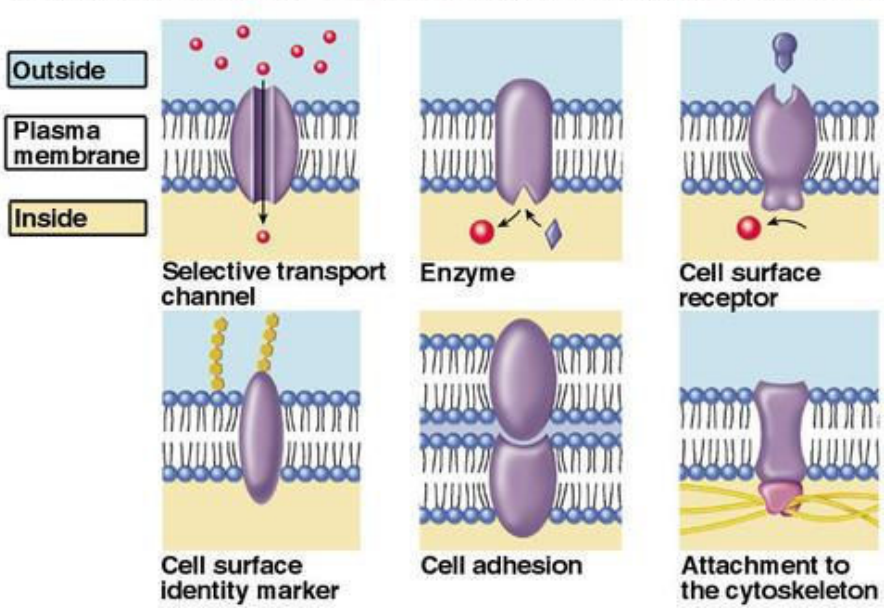

Figure 1.2 A schematic representation describing the different functions of the transmembrane proteins.

Hence, it is understood beyond doubt that these proteins form a very important part of the cell membrane and are involved in several important cellular functions. However, their direct investigation upon isolation from the cell membrane has always observed to be quite delicate. This is because of the amphiphilic nature of these proteins, which limits their solubility and stability in aqueous media. The part of their structure, which is embedded in the bilayer (composed of lipidic chains), is highly hydrophobic. Thus, a solution of membrane proteins in an aqueous buffer does not stay monomeric because of the hydrophobic effect, which tends to minimize the number of water molecules in contact with hydrophobic region.[5] This results in aggregation of the membrane protein and more often than not in its precipitation. This situation is found to improve greatly, by addition of surfactants to the membrane proteins. Surfactants are amphiphilic molecules, which when present above a particular concentration, self-assemble in aqueous medium to form micelles. The surfactant micelles organize themselves around the hydrophobic regions of the membrane proteins. They organize themselves in such a way that

hydrophobic interactions between the micelle structure and that of the protein are maximized, while the polar head groups of the surfactant are in contact with the aqueous medium. This renders a global solubility to the protein and thus improves its stability. However, the micelles surrounding the protein are in dynamic equilibrium with the monomers and this has shown to negatively affect the stability of the membrane proteins.[6]

Moreover, the reconstitution of these detergent stabilized proteins into artificial bilayers or liposomes requires the careful removal of the surfactant.

1.2.2. Introduction to Membrane Proteins Explored In the Present Study

Among the various classes of membrane proteins described above, we were principally interested in the study of the following two types of proteins as follows.

1. A Ferric hydroxamate uptake receptor (FhuA) in *E.coli* cells, which is a porin that carries out the transport of Ferrichrome in *E.coli* cells by the help of another membrane protein (see section 1.2.2.a).
2. The human $\alpha_v\beta_3$ integrin, a protein that has been of interest to our group since several years due to its various biological functions as described in section 1.2.2.b.

The present section details the structural features and functions of each of these proteins and their respective roles in their host organisms.

1.2.2.a FhuA; an Outer Membrane Protein in *E.coli* Cells

FhuA is an outer membrane protein present in gram negative bacteria called *Escherichia coli* (*E. coli*). *E. coli* are commonly present in the intestines of human beings and animals worldwide. They were first discovered and isolated by a German pediatrician and bacteriologist Theodor Escherich in 1885 and were eventually named after him. Their cells are typically rod-shaped and are about 2 μm long and 0.5 μm in diameter, with a cell volume of 0.6 - 0.7 μm^3. [7] They are a special class of bacteria called facultative

anaerobes *i.e.* they can survive in an environment with or without air and, depending on the environment, may or may not produce thin hair-like structures (flagella or pili) that allow the bacteria to move and to attach to human cells. Most of the *E. coli* are normal inhabitants of the small intestine and colon and can benefit their hosts[8,9]. However, they can cause diseases if they spread outside the intestines *e.g.* in the urinary tract where they cause bladder or kidney infections. Unlike the gram positive bacteria, *E. coli* have two membrane layers separated by a periplasmic space as seen in Figure 1.3.

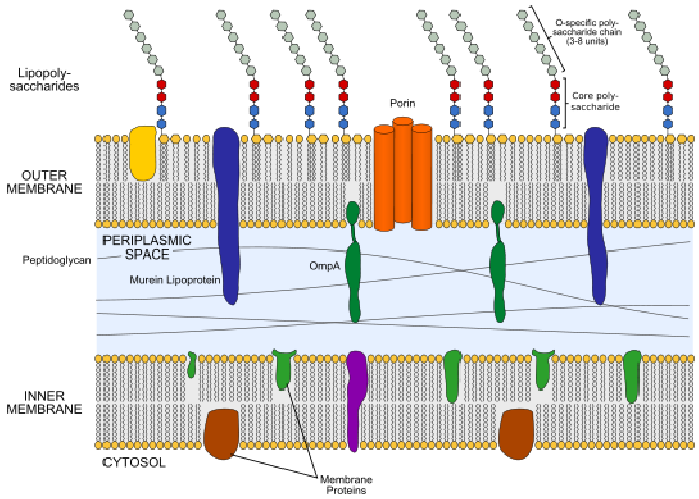

Figure 1.3 Diagram representation of the cell membrane of gram-negative bacteria

As clearly seen in Figure 1.3 a gram-negative bacterial cell membrane is largely composed of three distinct, characteristic layers.

1. An inner membrane or plasma membrane. This consists of phospholipids as well as various membrane proteins (called inner membrane proteins). The inner membrane defines the edge of the cytoplasm of cells.
2. A periplasmic space, *i.e.* a volume found between the inner (plasma) membrane and the outer membrane. It is known that the periplasmic space is filled with a loose network of peptidoglycans and is more a gel than a fluid-filled space. The periplasmic space of gram-negative bacteria contains many proteins that participate in nutrient acquisition such as for example hydrolytic enzymes attacking nucleic acids and phosphorylated molecules as well as binding proteins involved in transport of materials into the cell.

3. An outer membrane, that consists of phospholipids, various membrane proteins (called outer membrane proteins), lipoproteins, and lipopolysaccharides (LPS). The outer membrane of the gram negative bacteria confers several functions. Most importantly, it serves as a protective barrier *i.e.* a selective transport across the cell membrane is facilitated through the outer membrane proteins (porins) which can transport small molecules like glucose, but it prevents the transport of toxic substances like bile salts and penicillin G. Thus, as opposed to gram-positive cells, gram-negative cells are resistant to lysozyme and penicillin attack. Although, transport across the outer membrane is primarily mediated by passive diffusion through non-specific or substrate specific porins.[10] However, the transport of substances like iron is severely limited because they exist as highly insoluble ferric hydroxide complexes. Thus in order to acquire iron, microorganisms secretes compounds called siderophores. These compounds chelate the ferric ion thereby rendering it soluble. Because siderophore-iron complexes are found at exceedingly low concentrations in the external media, their rate of passive diffusion across the outer membrane is insufficient for supporting the requirements of cellular growth. Therefore, a class of high-affinity siderophore receptors exists within the outer membrane, which mediates the transport of Fe^{3+}-ferrichrome complex. FhuA in the outer membrane of *Escherichia coli* is the receptor for ferrichrome-iron. In addition to binding ferrichrome-iron,[11] FhuA also functions as the primary receptor for the structurally related antibiotic albomycin and for several bacteriophages (T1, T5, UC-1, and f80).

The crystal structure of FhuA in its unliganded/free state solved by Locher *et al.* is shown in Figure 1.4. It consists of a barrel of 22 β strands which has a bean-shaped cross section of 35 × 24 Å.[12]

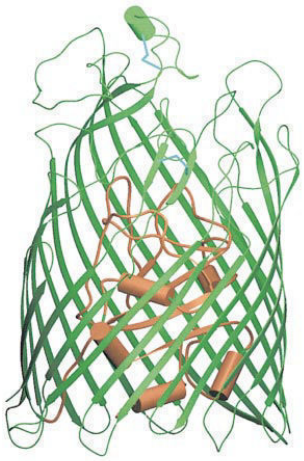

Figure 1.4 Overall crystal structure of free FhuA as solved by Locher et al.[12] The β barrel (green strands) are formed by 22 anti parallel strands. A plug is found to snug inside the barrel. The top part of the protein faces the cell surface while the bottom is in the periplasm of the bacterial cell.

A plug formed by the N-terminal of the protein clogs the barrel (brown structure in Figure 1.4). This plug comprises of five α helices and six β strands. Its surface interacts extensively with the barrel lining, as witnessed by the presence of nine salt bridges and more than 60 hydrogen bonds. The plug has been demonstrated to change conformation upon interaction with specific gating ligands such as ferrichrome, and is thus shown to play a role in its transport. However, the exact transport mechanism of ferrichrome is yet unknown

Bacteriophages are viruses that infect bacteria in a very specific manner. They are usually called in their shortened term as phage. Typically, bacteriophages consist of an outer protein capsid enclosing genetic material. The genetic material can be *ss*RNA, *ds*RNA, *ss*DNA, or *ds*DNA ('*ss*-' or '*ds*-'denotes single-strand or double-strand respectively) along with either circular or linear arrangement. The most commonly present phages are the *ds*DNA tailed phage Figure 1.5. The infection of gram-negative bacteria by a bacteriophage takes place by the recognition of the phage through irreversible binding to a receptor which is an outer membrane protein. This binding is followed by a conformational change that allows the ejection of the *ds*DNA from the viral capsid and its transfer into the bacterial cell membrane. Entry of this viral DNA into the cytoplasm of the bacteria leads to its expression into the bacterial cell, thus causing a mass production of the virus and the lysis of the bacterial cell.

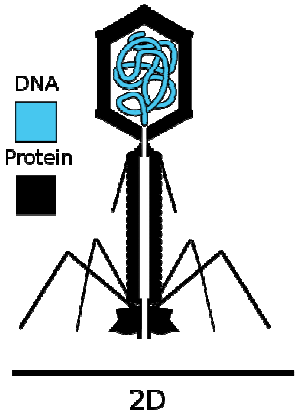

Figure 1.5 Cartoon representation of a typical DNA tailed phage.

In the case of bacteriophage T5, its binding to the *E. Coli* cells is mediated by specific interactions between the outer membrane protein FhuA (of the *E.coli*) and the receptor-binding protein pb5 of the phage T5.[13] pb5 is located at the distal end of the phage tail. Isolated pb5 is known to interact with *E.coli* cells, indicating that its activity is retained upon isolation. (See section 2.2)

1.2.2.b $\alpha_v\beta_3$ Integrin; a Transmembrane Protein

Integrins are transmembrane proteins that traverse the cytoplasmic membranes of the cells in such a way that they have an extracellular domain at the surface of the cell. This extracellular domain acts as a receptor and forms the link between the cytoskeleton inside the cells and the extracellular matrix outside the cells.

All Integrins are obligate heterodimers, containing two distinct chains, called the α (alpha) and β (beta) subunits. In mammals, eighteen α and eight β subunits have been characterized (see Figure 1.6)[14]

Each of the 24 integrins shown in Figure 1.6 are known to have a specific non-redundant function mediated by the binding of the integrin to its extracellular matrix (ECM) protein as shown. As it can be seen in Figure 1.6, the $\alpha_v\beta_3$ Integrin is a receptor of the peptidic sequence RGD.

Hence, the $\alpha_v\beta_3$ integrin binds specifically to the ECM proteins such as vitronectin, which bears the sequence RGD. It also is known to mediate the adhesion of cells in a

promiscuous manner, to a large number of other extracellular matrix proteins, including fibronectin, fibrinogen etc. through the key recognition motif Arg-Gly-Asp (RGD), which was first demonstrated by Pierschbacher and Ruoslahti.[15]

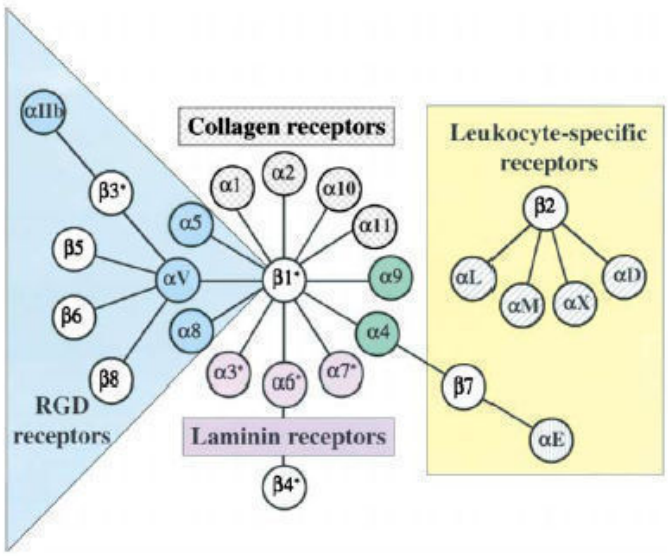

Figure 1.6 The integrin receptor family. Integrins are heterodimers; each subunit crosses the membrane. Figure adapted from a review on integrins by O'Hynes.[14]

Concerning the structure of the Human $\alpha_v\beta_3$ integrin (237 kDa), only the structure of its extracellular domain has been solved by crystallography.[16] However, a cartoon representation of its structure was proposed much earlier by Horton *et al.* (shown in Figure 1.7).[17] Its structure is known to be characterized by an α_v chain of 145 kDa, containing seven- 60 amino acid long tandem repeats; the C-terminal of this strand which is in the extracellular region binds divalent cations via an E-F hand-like structure. Whereas, the β subunit of 92 kDa is known to have a high cysteine content concentrated mainly in four repeat domains.[17]

Although the exact mechanism of binding of the $\alpha_v\beta_3$ integrin to its ECM proteins is still unknown, it has been demonstrated recently that Integrins depend on divalent cations to bind their extracellular ligands.[18] This fact was confirmed lately by the crystal structure of extracellular domain of the $\alpha_v\beta_3$ integrin in complex with the RGD ligand.[18] In these studies they observed that the $\alpha_v\beta_3$ integrin-RGD complex consisted of Mn^{2+} ions at the binding site of the protein. Thereby highlighting that Mn^{2+} ions are involved in the binding of the RGD based ligands (ECM proteins, to the $\alpha_v\beta_3$ integrin.

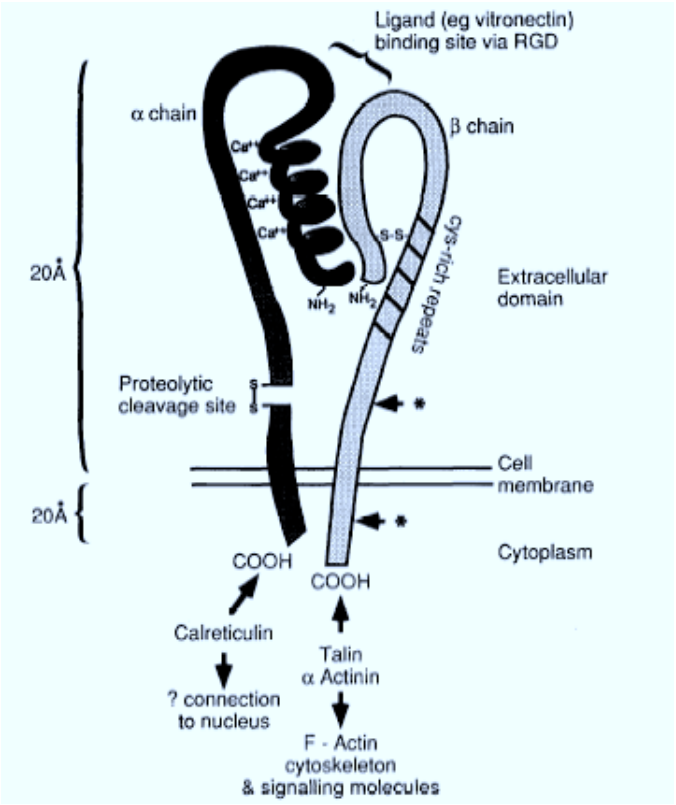

Figure 1.7 A stylized view of the αvβ3 "vitronectin receptor". Structure adapted from Horton *et al.* [17]

There are three main clinical areas where the upregulation of $\alpha_v\beta_3$ integrin has been found in disease and they are being developed as targets for drug development. These are: in angiogenesis in tumours; in melanoma when it progresses from the horizontal to vertically invasive and metastatic stages; and in coronary arteries following angioplasty leading to vascular restenosis.[19,20] Thus, the general approach in the treatment of these diseases has thus been towards modifying the integrin adhesion receptor behavior by the use of blocking monoclonal antibodies or agents developed to mimic the amino acid motifs (RGD) in ligands.[21,22] This approach deals with blocking the active site of the $\alpha_v\beta_3$ integrin by these artificial ligands, thus blocking the natural interactions with the ECM proteins (in particular to vitronectin), leading to a hysteresis of the effects of upregulation of $\alpha_v\beta_3$ integrin.

Thus, for the past few years, several molecular motifs bearing the RGD ligand have been developed towards this interest.[23,24] Thereby, making this protein a major candidate in pharmaceutical and drug research.

1.3. Design of functional interfaces that mimic the cell membrane

For direct investigation on these membrane proteins and the membrane related process, the need of the hour is to design functional interfaces, which most faithfully resemble the cell membrane. Towards this end, the last few years has seen immense developments towards designing membrane model mimics. Hitherto, the most accepted models reported in the literature are few, namely vesicles, black lipid membranes, supported lipid bilayers and tethered lipid bilayers (Figure 1.8).

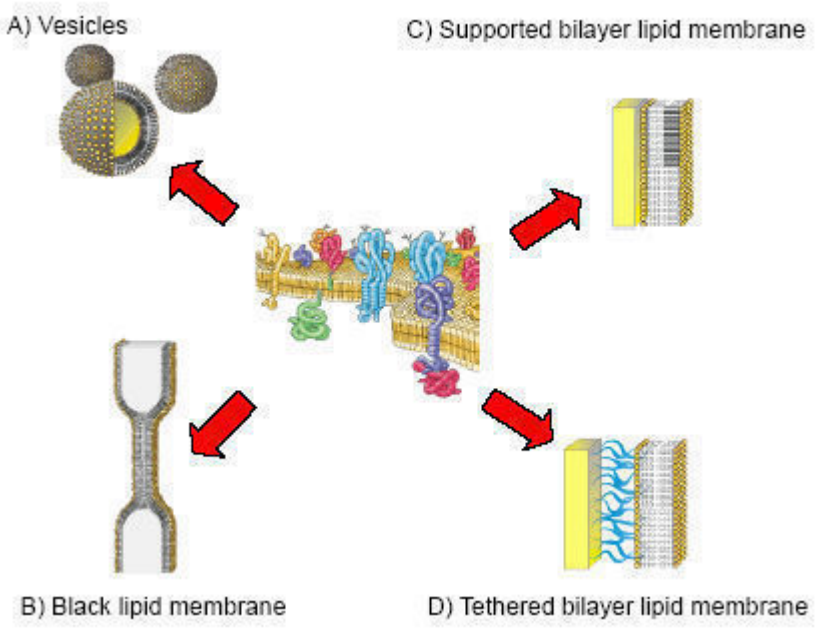

Figure 1.8 Schematic representations of the most common membrane model systems (A) Vesicles (B) Black lipid membranes (C) Supported Lipid Bilayers and (D) Tethered bilayer lipid membrane

The present section deals with a quick recall and discussion on the various membrane model systems listed above, their methods of preparation, their advantages and their drawbacks over each other.

1.3.1. Vesicles

Vesicles as shown in Figure 1.8 represent an alternative to free standing Bilayer Lipid Membranes (BLMs). They also have a bilayer structure and can be thought of a spherical bag of bilayer, filled with water inside it. A wide range of vesicle sizes can be prepared by various methods with hydrodynamic radii (R_h) from ~ 20 nm to 100 μm. Their rough classification is as follows: small unilamellar vesicles (SUVs) R_h< 100 nm, large unilamellar vesicles (LUVs) R_h = 100 nm – 1 μm, giant unilamellar vesicles R_h = (GUV) > 0.5 μm. SUVs are mainly used for protein research in suspension where many aggregates are present.[25] They are also used as precursors for preparing supported lipid bilayers (discussed later). Furthermore they have proved to be an excellent system for the *in vitro* expression of membrane proteins.[26]

Vesicles in general are more stable than BLMs with lifetimes from days to weeks without alteration. However, a major drawback they offer is that the vesicle interior is not accessible as an ion/analyte reservoir which makes them unsuitable for electrochemical methods. Furthermore, the use of vesicles as bilayer models is essentially restricted to studies in solution/ vesicular dispersions.

1.3.2. Black Lipid Membranes

The free standing lipid bilayer as it is sketched in Scheme 2 B spans the aperture of a Teflon film. This creates an interaction free membrane model and is accessible from both sides. The name *black lipid membrane* (BLM) is derived from the fact that the lipid film appears black when it is spanning the aperture. The black "color" is the result of destructive interference between the reflected light at the two respective hydrophilic/hydrophobic interfaces. The first preparation of BLMs was reported in 1962 where an organic lipid solution was "painted" across such an aperture. [27] After the successful bilayer formation some solvent still remains inside the hydrophobic core so that in can interfere with sensitive membrane proteins. A solvent free method was first developed by Montal *et al.*.[28] By lowering the aperture through a monomolecular Langmuir film at the air water interface a lipid monolayer is spanned over the hole from both sides resulting in a bilayer. BLM proved to be especially useful for electrochemical measurements investigating membrane pores and of proton pumps.[29,30] A general

disadvantage of BLMs is the low mechanical stability. BLM setups have to be installed in a vibration free environment but still last only several hours.[31]

1.3.3. Supported Lipid Bilayers

In a quest to produce a model system that quite closely resembles the biological cell membranes, planar lipid bilayers supported on a solid substrate (Supported Lipid Bilayer) were developed nearly a quarter century ago.[32-35] These Supported Lipid Bilayers (SLBs) which are essentially composed of phospholipids were found to be quite robust and stable. They have an advantage over vesicles or black lipid bilayers, in that, the solid support can also serve as a means for employing surface specific analytical techniques. These solid Supported Lipid Bilayers are separated from the substrate by a thin layer of 10-20 Å of hydration see Figure 1.9 [34,36]

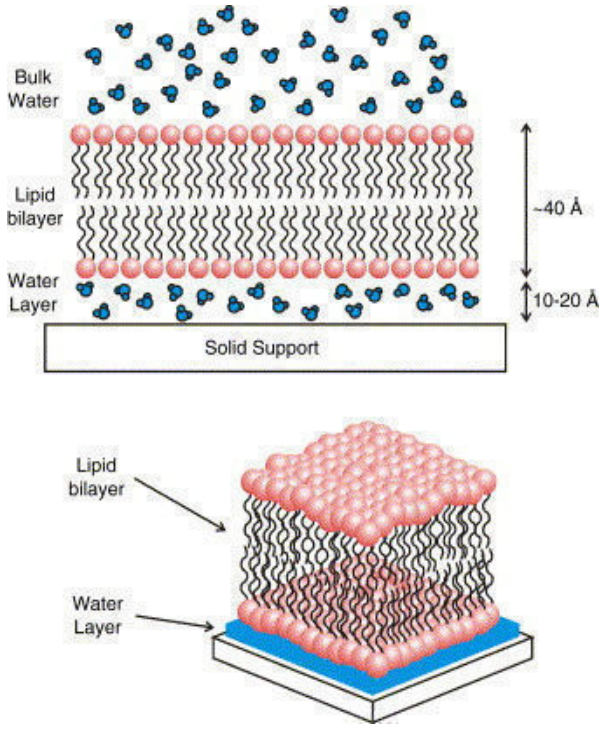

Figure 1.9 Cartoon representation of a solid supported lipid bilayer. The phospholipid membrane is separated from the substrate by a 10-20 Å layer of water.

Supported phospholipids membranes are known to be held in place above a solid support by a combination of molecular forces such as hydration (between the substrate and the phospholipid head groups), electrostatic (between the phospholipid head groups), van der

Waals (lipid part of the phospholipids) and steric forces.[37] Besides the binding forces that keep the bilayer confined to the support, the bilayers still possess a remarkable fluidity. The phospholipids are found to be freely moving with a lateral diffusion coefficient of approximately 1- 4 $\mu m^2/s$.[38] It is this feature of these supported lipid bilayers which make them attractive models for mimicking cell membranes. Another reason for the increasing attention that SLBs have received from both chemists and biologists is their ease of preparation.

There are three general methods adopted for the formation of Supported Lipid Bilayers.

1. Langmuir Blodgett/Langmuir-Schäfer (LB/LS) technique

This technique is historically the first one used to prepare supported bilayers.[34,35,39] In this method a lipid monolayer is spread from a desired lipid solution (in organic solvent) onto a pure water surface in a Langmuir trough. After evaporation of the solvent, the monolayer is compressed slowly to reach a surface pressure of 32 mN/m (the equivalent pressure of a bilayer) and equilibrated. A hydrophilic substrate (glass, SiO_2 etc.) is then immediately submerged into the trough and then slowly withdrawn using an automated mechanism, while maintaining a constant surface pressure (Figure 1.10). This step transfers a single monolayer of lipids known as the Langmuir-Blodgett (LB) layer onto the substrate. The lipid bilayer is then completed by the addition of a second monolayer known as the Langmuir-Schäfer (LS) layer. A monolayer of phospholipids is spread and compressed on the trough in the same way as described earlier. A LB-coated substrate is attached to an automated suction tip and its face is lowered slowly to contact the LS monolayer at the air/water interface for a few seconds (Figure 1.10). To complete the process, this slide is then pushed through the interface into water to hydrate/fill in water molecules between the surface and the phosphlipid head groups. Although this method is useful for the formation of asymmetric bilayers, it is not the best adapted for incorporation of transmembrane/membrane proteins because prior to transfer of the second monolayer, the proteins within the monolayer are exposed to air, which can lead to their denaturation.

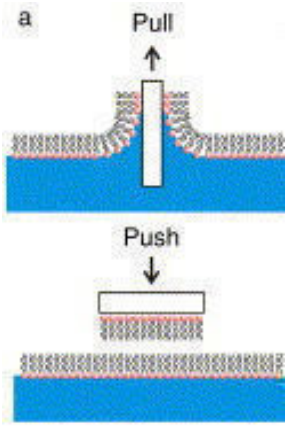

Figure 1.10 Langmuir-Blodgett/ Langmuir-Schäfer technique for formation of a SLB. A lipid monolayer is spread at the air/water interface of a Langmuir trough and transferred to a solid substrate keeping the surface pressure constant. A second monolayer (SLB) is transferred onto the first one by horizontal apposition of this monolayer on another monolayer of phospholipids on an air/water interface.

2. Vesicle Fusion (VF) technique

This technique first demonstrated by McConnell *et al.*, is one of the simplest ways of forming a supported lipid bilayer.[33] Here, vesicles are brought into contact with a hydrophilic surface (SiO_2, mica) for a short period of time (10- 60 minutes in most cases) where the adsorption and spreading of vesicles to bilayer occurs. The vesicle fusion pathway to form a bilayer on SiO_2 was first demonstrated using QCM-D by Keller and Kasemo to be a two step pathway.[40] This featured the initial adsorption of intact vesicles (indicated by a decrease in frequency and increase in dissipation) followed by their spreading and fusion to form a bilayer (indicated by a subsequent increase in frequency and decrease in dissipation to reach a stable value $\Delta F_n/n \sim 25$ Hz and $\Delta D_n \sim 0.2 \times 10^{-6}$ respectively) as seen in Figure 1.11. Henceforth, a lot of investigation has been devoted to the mechanism and kinetics of vesicles spreading, the impact of the vesicle size on bilayer formation, the influence of bivalent cations on fusion kinetics in order to provide a comprehensive understanding of the driving forces on the SLB formation.[41-43] This method of SLB formation by vesicle fusion has since then emerged to be one of the most commonly employed ones. Although, besides the fact that it is the easiest way of generation a SLB, this technique offers less control over the orientation of the incorporated membrane protein. In that, the membrane protein besides orienting itself at the bilayer/water interface can also orient itself at the substrate/bilayer interface.[44]

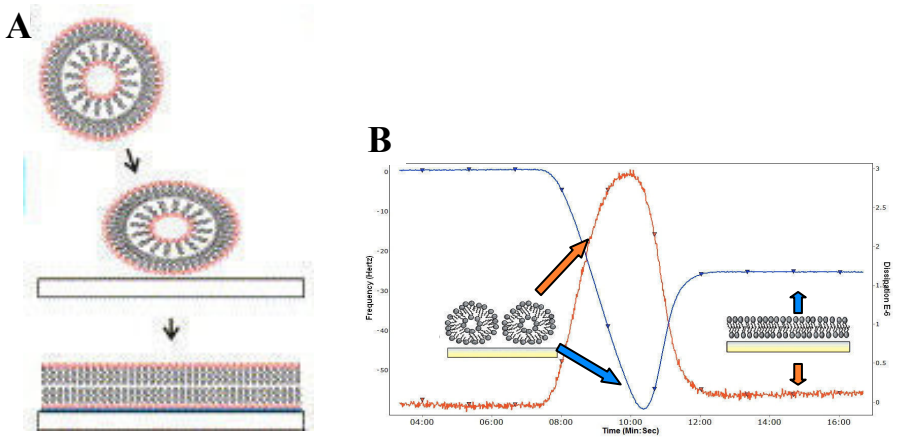

Figure 1.11 (A) Cartoon representation of direct vesicle fusion on a hydrophilic surface to give a Supported Lipid Bilayer (SLB) **(B)** Typical QCM-D profile of the vesicle fusion process on a SiO_2 surface to give a SLB. In blue is the normalized frequency and in red is the Dissipation, the initial decrease in frequency and increase in dissipation are suggestive of the adsorption of intact vesicles which later fuse to form a bilayer as indicated by an increase in frequency and decrease in dissipation to stable values.

3. Langmuir-Blodgett followed by Vesicle Fusion (LB/VF)

This method is a combination of both the above mentioned methods. Herein, a LB monolayer of phospholipids is prepared on hydrophilic substrates as described above.[44] This monolayer-coated slide is then incubated with vesicles or proteoliposomes for typically 60-120 minutes followed by washing off the excessive vesicles. Since the second monolayer is completely vesicle derived and because membrane proteins are introduced as proteoliposomes only in the second step, they tend to be oriented almost unidirectionally in the SLB.

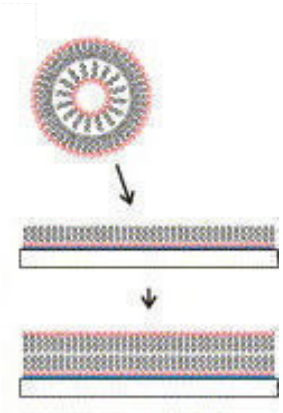

Figure 1.12 A combination of Langmuir-Blodgett and vesicle fusion to form a SLB. A monolayer is initially formed by pulling a hydrophilic surface through a lipid monolayer on an air/water interface followed by interaction with vesicles.

Owing to their ease of fabrication, and their close resemblance to the natural cell membrane besides other factors like their stability, SLBs have evolved into reliable model-membrane systems, which allowed for various applications. In particular, they SLBs constitute models of choice for measuring ligand-receptor interactions between membrane proteins and their receptors, as well as interesting platforms for cell adhesion studies. Nonetheless, they present certain drawbacks which are discussed in the following section.

1.3.4. Tethered Lipid Bilayer Membranes

The above mentioned Supported lipid Bilayers although quite versatile, present a disadvantage in terms of their application in incorporation of transmembrane proteins. This advantage arises from the fact that they are too close to their solid support (see Figure 1.9). This close proximity to the support could be a major hindrance for the fluidity and the stability of transmembrane protein and in particular, when they exhibit large intracellular domains.

This feature puts forward a major question on the rationality of the SLBs. Thus, research is now oriented towards designing model systems where the bilayer is decoupled from the surface by a spacer or a tether. These bilayer systems are thus called Tethered Bilayer Lipid Membrane (tBLMs) see Figure 1.13.

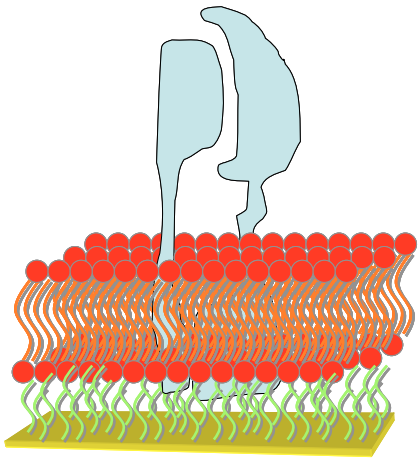

Figure 1.13 Schematic diagram representing a protein inserted in a tBLM. The hydrophilic spacer groups (colored green) ensure a good decoupling of the protein and the bilayer from the substrate.

These systems, besides separating the bilayers from the solid support, also confer a higher stability to the assembly. The tethering layer is on one end covalently attached to the surface and in the other end anchored into the bilayer (through hydrophobic interactions). The covalent attachment of one end of the tether to the surface renders good stability to the thus formed tBLM. Various functional groups have been used as tethers for the tBLM. The two most popularly used and studied tethering groups in the construction of tBLMs comprise of polymer cushions and self-assembled monolayers (SAMs). The present sections will thus take a quick glance over the most highlighted studies done over these systems.

Polymer tethered bilayer membranes These systems use polymers as the tethers/tethering groups to separate the bilayer from the surface. These soft, water-swollen polymer systems not only create a substantially larger separation between the substrate and the bilayers, but also help in stabilizing the hydrophilic extracellular domain of the incorporated proteins. In this context, several such systems have been defined, which employ the use of various polymeric functions. However, one of the most interesting systems studied involved the use of lipid conjugated-PEG polymers (Figure 1.14) by M.L. Wagner and L.K. Tamm.[45]

In their studies, they reported the formation of tBLMs on the polymer cushions made with the molecule described in Figure 1.14 where the phospholipids possessed a high lateral diffusion (~1.2×10^{-8} cm^2/s)

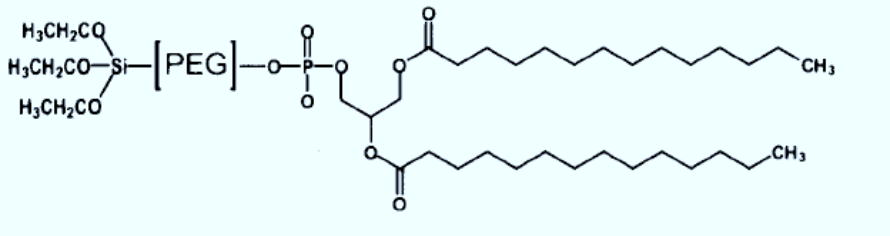

Figure 1.14 Structure of the Lipid-conjugated polymer used by Wagner and Tamm[45] for tethering lipid bilayers.

Moreover, they also demonstrated that almost 25-30% of cytochrome b_5 (a transmembrane protein) incorporated in these polymer tethered bilayers had a lateral diffusion of (~1.2×10^{-8} cm^2/s) which is quite high. These results clearly elucidated that the decoupling of the bilayer from the surface is an important aspect in the mobility of

the membrane proteins. Several other systems based on polymer cushion tBLMs have since then evolved.[46-48]

Self-Assembled Monolayers as tethers for lipid bilayers This architecture is to date, the most exploited one in the literature. Herein, the tethering groups are comprised of Self-Assembled Monolayers (SAMs). The SAMs used to tether or anchor bilayers are usually made up of thiols bearing bifunctional groups *i.e.* a hydrophilic group which acts as a spacer between the surface and the membrane and a hydrophobic group which acts as the tethering group for the bilayers. Among these anchoring thiols, several molecular entities defining the tethering hydrophobic region have been used and discussed in the literature[49,50] However, it has been demonstrated by several groups that SAMs made up of pure anchoring lipid thiol is inefficient in accommodating small peptides and obviously bigger proteins.[51,52] This has thus shifted the focus towards designing tBLMs where the anchoring thiol is diluted with a small hydrophilic thiol, often called the backfilling thiol. This process however seems limiting as the dilution may not always lead to the successful formation of a tBLM. Our present work described in Chapter 3 discusses the effects of dilution of the anchoring thiol on the tBLM formation process.

1.3.5. Amphipols

Amphipols (Apols) are short-chain amphipathic polymers designed to keep membrane proteins soluble in aqueous solutions. Although, in the present thesis they are incongruently classified under the subclass of model systems that mimic cell membranes, they are rather surfactant substitutes which make the studies of membrane proteins in detergent-free aqueous solution much less cumbersome. Although several amphipols are known in the literature[53], a huge contribution towards the development of these systems comes from the group of J-L. Popot.[54] The most well studied amphipols in the context of its structure, characterization, trapping and stabilization of the membrane protein and several other features is the Apol called "A8-35" developed in the group of J-L.Popot.[55]
Its structure as shown in Figure 1.15 is composed of a relatively short polyacrylate chain labeled x, in which some of the carboxylates are linked to octylamine groups labeled y and some with isopropylamine labeled z. The free acid groups offer the charge to the

entire structure, which makes the polymer highly water soluble, whereas the octylamide moieties provide the hydrophobic nature to the structure, thus rendering it globally amphipathic.

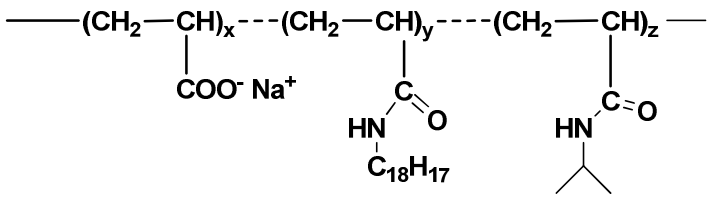

Figure 1.15 Chemical structure of the Amphipol "A8-35" developed in the group of J.-L. Popot.[55]

Although, this amphipol has seen unbeatable success in terms of its applications towards solubilization and long-term stability of membrane proteins as well as activation of denatured membrane proteins[56] and many more. It has also shown a small disadvantage, arising form its structure. Since the polar group of this Apol consists of a carboxylic acid group, the stability of this structure is greatly dependent on the medium in which it is used. The presence of high concentrations of salts like NaCl, Ca^{2+} and low pH are factors which are detrimental to its stability.

Replacement of this group to a zwitterionic phosphorylcholine group has been demonstrated as a good alternative structure (Amphipol) by the group of F.Winnik.[57] As will be discussed in subsection 2.2, the use of phosphorylcholine groups is advantageous in aspects of studying biomolecular interaction studies, as they offer an excellent inertness towards biomolecules thereby avoiding non-specific interactions.

The structure and applications of such an Amphipol (phosphorylcholine based) is discussed in detail in Chapter 4 of the present thesis.

1.4. Techniques used in studying biomolecular interactions

The present section gives an overview of a list of the few techniques that were extensively used in the present thesis. Their general principles, applications, limitations and scope are described here in brief.

1.4.1. Quartz Crystal Microbalance with Dissipation (QCM-D)

The quartz crystal microbalance (QCM) is a nanogram sensitive technique that utilizes acoustic waves generated by oscillating a piezoelectric crystal quartz plate to measure mass. The sensor is a thin quartz crystal disk sandwiched between two electrodes. The quartz being piezoelectric is deformed when an electrical field is applied between the electrodes (Figure 1.16 Band C). Under an alternative electric field, (Figure 1.16C) the quartz is made to oscillate and its resonance is excited when a sufficient voltage is applied with a frequency close to the resonant frequency (f_0) or to odd overtones n (n = 3, 5, 7, …) of the piezoelectric crystal. Small mass deposited onto the crystal surface induces decreases of the resonance frequency. Since the resonance frequency can be measured precisely, even small amount of an adlayer can be easily quantified.

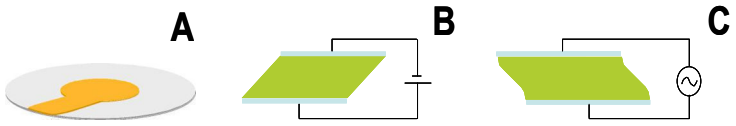

Figure 1.16 Schematic representation of A) a quartz Crystal sensor and of the strain induced in the quartz by application of B) a DC field and C) an AC field

In 1959, Sauerbrey had demonstrated that the mass of an adsorbed film (Δm) is related to the shift in the resonance frequency (Δ*f*) of the oscillating piezoelectric surface by a linear relationship given in Equation 1.1:[58]

$$\Delta m = -C\frac{\Delta f_n}{n} \qquad \textbf{Equation 1.1}$$

Where Δf_n is the variation of frequency recorded on the harmonic number n and C is the mass sensitivity of the QCM device described as follows:

$$C = \frac{\delta_q \rho_q}{f} \qquad \textbf{Equation 1.2}$$

Where, δ_q and ρ_q are the thickness and the density of the quartz respectively, f its oscillating frequency. At a fundamental frequency, f_0, of 5 MHz, C is equal to 17.7 $ng.cm^{-2}.Hz^{-1}$. Thus, an increase in mass will be observed through a decrease in frequency. The mass evaluated is solely based on the quartz crystal properties and is independent of the adlayer nature. However, for the Sauerbrey equation to be valid, three conditions need to be fulfilled (i) the mass of the adlayer should be smaller compared to the mass of the quartz disk (ii) the film should be homogeneously deposited on the quartz surface area and (iii) the film should be rigid and coupled to the mechanical oscillation of the sensor under non slipping conditions.

This acoustic method was initially developed to follow the deposition of thin films on solid support under gaseous or vacuum atmosphere and was further applied to measurements in liquid environment[59] and to adsorption of soft films (protein, polymers,…). The last mentioned applications, however, often deviate from the Sauerbrey assumption since the adsorbed film is usually not rigid and dissipates energy through frictional dissipative losses. In addition, acoustic coupling between the oscillating quartz surface and the liquid environment also induces a damping of oscillations. Interpretation of QCM data thus needs to take into account not only the viscous character of the liquid (that is generally considered as a pure Newtonian liquid) but also the visco-elastic mechanical properties of the adsorbed film. The study of soft adsorbed films in presence of a liquid was thus made possible via the measurement of an additional parameter, the energy dissipation D,[60] defined as follows:

$$D = \frac{1}{\pi f t_D}$$ **Equation 1.3**

With, f, the resonance frequency and $t_{D,}$ the decay time. The dissipation is addressed by measuring the oscillation decay of the sensor after a short excitation close to its resonance frequency. (Figure 1.17) A soft layer adsorbed on the quartz will dissipate more energy than a rigid one and the corresponding decay time will be lowered (Figure 1.17 B).

Figure 1.17. Representation of the frequency decay induced by the adsorption of A) a rigid and B) a soft film on oscillating quartz.

By switching the driving voltage on and off periodically during the adsorption of viscoelastic films, changes of the resonant frequency ($\Delta F_n/n$) and of the dissipation (ΔD_n) are monitored in real time for several harmonics. Quantitative interpretation on the film properties could be then obtained by fitting the experimental data using adequate models that take into account the properties of the liquid environment as well as the viscoelastic properties of the adlayer. From the model developed by Voinova,[61,62] meaningful parameters of the film such as the mass, the viscosity and the shear modulus could be extracted.

It is important to note here that the mass obtained by QCM-D corresponds to the whole acoustically coupled mass including the film "dry matter" and the associated hydration water or solvent.

This acoustic mass differs from values obtained by optical methods such as Ellipsometry or Surface Plasmon Resonance, which sense only the "dry mass" of the film adsorbed.[63-65]

In some cases, as for example monitoring DNA hybridization, the coupled water of the film increases the sensitivity of the technique.[63] This coupled water contribution to the total acoustic mass could however sometimes be unfavorable. A typical example concerns the quantification of affinity measurement between a protein and a recognition surface. In such a situation, the contribution of coupled water depends on the packing density of the protein in the film. Therefore, the mass of the adsorbed protein is not linearly related to the acoustic mass observed and affinity constant can not be unambiguously quantified.[66]

Thanks to the determination of viscoelastic parameters in addition to the adsorbed mass, QCM-D is now a widely used technique for characterization of thin film as well as to follow biomolecular interactions and phase transition. For example, QCM-D has been proven to be an efficient tool to characterize conformational change of polymer chains and polymer multilayers formation, [67-69] to study the adsorption of protein on recognition surface,[64,70] DNA hybridization[63,71] or cell adhesion and spreading.[72,73]

While one of the major applications of QCM-D to biomolecular studies is probably the recognition of protein to specific surface, this technique has been also extensively used to characterize lipid model membranes. Indeed, the dissipation measurement is particularly relevant in these systems where the viscosity and elasticity of the lipid assemblies play a key role. As demonstrated by the initial work of Keller,[40] this technique is well adapted to differentiate model membrane assemblies on surfaces. As represented in Figure 1.18, the adsorption of vesicles on various substrates can result in the formation of mono or bilayer as well as to the formation of an intact vesicles monolayer. Each of this system can be clearly identified by a signature ($\Delta F_n/n$, ΔD_n).

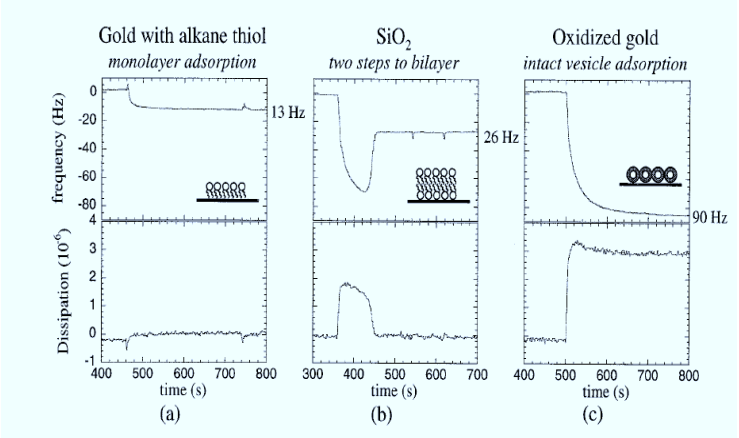

Figure 1.18. QCM-D profile observed for the interaction of small unilamellar vesicles with different kind of surface. The interaction leads a) to a monolayer formation on an alkane thiol self-assembled monolayer b) to a bilayer formation on a SiO_2 and c) to a layer of intact vesicles on oxidized gold. This picture is extracted from reference.[40]

A phospholipid monolayer formed on a hydrophobic layer leads to a $\Delta f_n/n$) value of ca. −13 Hz. No change in dissipation are recorded during the process and the dissipation of the phospholipid monolayer is zero (Figure 1.18A) meaning that this monolayer behaves as a rigid film. For oxidized gold surfaces, adsorption of intact vesicle (Figure 1.18C) lead to large variation in ($\Delta F_n/_n$) and ΔD_n values. This strongly enhanced energy dissipation was attributed to the deformation of the intact adsorbed vesicles which behave as a highly viscoelastic layer. Figure 1.18B represents the QCM-D profile observed during the interaction of vesicles with a SiO_2 surface which leads to the final formation of a lipid bilayer. The ($\Delta F_n/n$) value observed, ca. −26 Hz correspond to the double of the one observed for a monolayer. The phospholipid bilayer dissipation is almost 0. Interestingly, from the QCM-D profiles, it has established that the bilayer formation occurs in two stages. Firstly, the vesicles are adsorbed intact as indicated by a large variation of the signals that resembles the case of oxidized gold. After a certain time, a second stage occurs. The increase of frequency (loss of mass) and corresponding decrease in dissipation (loss in viscoelasticity) is interpreted to the vesicle fusion and spreading with release of the entrapped water. The frequency combined to the dissipation variations measurements lead to crucial information on the final assembly as well as on its formation pathway. Comprehensive studies involving the influence of parameters such as the surface chemistry, the vesicle size, salts, etc onto the supported lipid bilayer formation have been based on QCM-D studies.[74-77]

1.4.2. Electrochemical Impedance Spectroscopy

Almost well known to everyone is the concept of Resistance in electrochemistry. It is the ability of a circuit element to resist the flow of electrical current. Ohm's law (Equation 1.4) defines resistance in terms of the ratio between voltage, E, and current, I.

$$R = \frac{E}{I} \qquad \textbf{Equation 1.4}$$

While this is a well known relationship, its use is limited to only one circuit element- the ideal resistor. An ideal resistor has several simplifying properties:

- It follows Ohm's Law at all current and voltage levels.
- . Its resistance value is independent of frequency,. AC current and voltage signals though a resistor
- The elements are in phase with each other.

However, in real systems, the circuit elements exhibit much more complex behaviors. These elements force us to abandon the simple concept of resistance, and in its place we use impedance, a more general circuit parameter. Like resistance, impedance is a measure of the ability of a circuit to resist the flow of electrical current, but unlike resistance, it is not limited by the simplifying properties listed above.

Electrochemical impedance can be measured by applying an AC potential to an electrochemical cell and then measuring the current response through the cell. However, for studying electrical impedance, the system under study should be linear *i.e.* it should show a linear response in current for a small change in potential. Unfortunately, most electrochemical systems are never linear. Thus electrochemical impedance is normally measured using a small excitation signal. This is done so that the cell's response falls on a linear zone of the curve. In a linear (or pseudo-linear) system, the current response to a sinusoidal potential (around a fixed value E_c with an amplitude ΔE) will be a sinusoid at the same frequency but shifted in phase (see Figure 1.19). Thus, this sinusoidal current response around a value I_c would have an amplitude ΔI which would reflect the slope of the stationary curve. This method thus permits the extraction of information on the elementary steps constituting an electrochemical process.

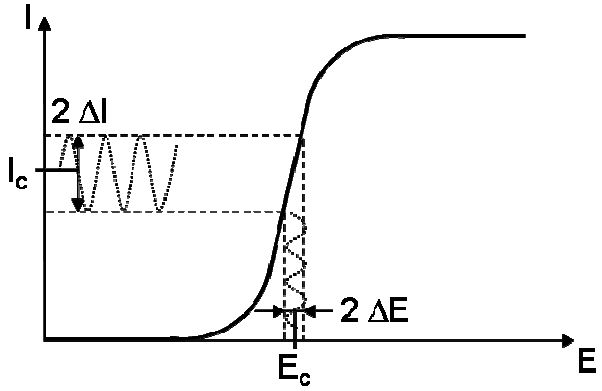

Figure 1.19 Sinusoidal current response upon application of a sinusoidal potential

The electrical impedance Z(ω) is thus defined as the relation between the sinusoidal wave equation E(ω) = E × exp (j(ωt) applied to a system and the resulting current I(ω) = I × exp [j(ωt + φ)] as

$$Z(\omega) = \frac{E}{I} \times exp(-j\varphi) = |Z(\omega)| \times exp(j\varphi) \qquad \textbf{Equation 1.5}$$

Where the Cartesian coordinates can be defined as

$$Z(\omega) = \mathrm{Re}[Z(\omega)] + j\,\mathrm{Im}[Z(\omega)] \qquad \textbf{Equation 1.6}$$

Where, j is an imaginary number, $j = (-1)^{1/2}$, $\omega = 2\pi f$, where f is the frequency, Re [Z] and Im[Z] are the real and imaginary components of Z(ω) respectively.

Various Representations of Impedance Data

Nyquist Plot: Impedance results can be presented using various representations. However, one of the most commonly used presentation for studying systems where charge transfer can occur at the interface is the Nyquist representation Figure 1.20. Looking at equation 1.6, we observe that the expression of impedance Z(ω) is composed of a real and imaginary component. The plot of the Imaginary part of impedance (-Im [Z(ω)]) in function with its real part (Re [Z(ω)]) gives the Nyquist representation (Fig. 1.20). Each point in this diagram thus represents the real and imaginary components of impedance at a given frequency. The low frequency data are on the right side of the plot

whereas the high frequency data are on the left side. On the Nyquist representation the modulus of impedance | Z(ω)| (arrow) can be represented as the length of the vector. The angle between this vector and the X-axis is commonly called as the phase angle φ.

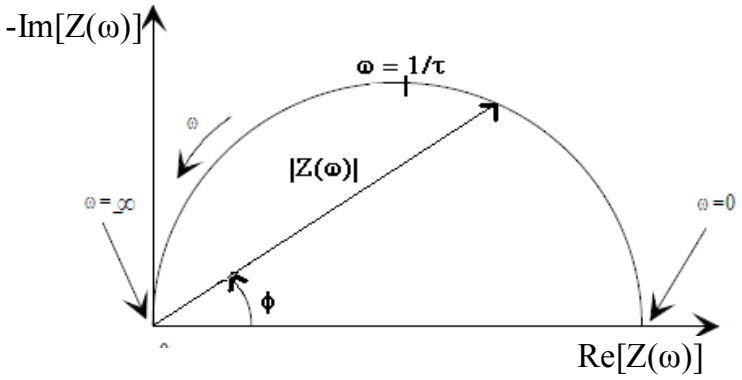

Figure 1.20 Representation of impedance data as a Nyquist plot with Impedance vector

Complex capacitance-plane plot:

Another common representation of impedance data is the complex-capacitance plane plot. The complex-capacitance plane plot as shown in Figure 1.21 is quite similar to the Nyquist plot except that the axes represent the imaginary component of the capacitance as a function of its real component. Each point in this diagram, as for the Nyquist plot, represents the real and imaginary components of the capacitance at a given frequency.

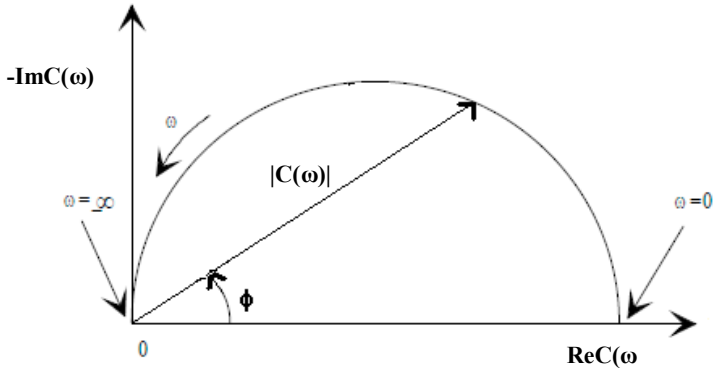

Figure 1.21 Complex-capacitance plane representation of impedance data.

The low frequency data are on the right side of the plot whereas the high frequency data are on the left side. On this representation, the modulus of capacitance | C(ω)| (arrow) can be represented as the length of the vector. The angle between this vector and the X-

axis is commonly called as the phase angle φ. The Cartesian coordinates in this representation can be defined as shown in equation (1.7) and they are the inverse function of Z.

$$C(\omega) = Re\,C + j\,Im\,C = \frac{1}{j\omega Z} \qquad \textbf{Equation 1.7}$$

A complex capacitance-plane plot has shown to be specifically useful in studying dielectric materials, where no redox probe is used in solution. Thus, this representation has been widely employed in studying systems like self-assembled monolayers and tethered/suspended lipid bilayers, both fabricated on conducting substrates like gold.

One such recent example in the literature of complex capacitance-plane representation as a means for analyzing impedance data has been demonstrated by Heinrich *et al.*[78]. They described the use of this method of representation to study the tBLM formation on mixed SAMs obtained from various concentration ratios of two different thiols (Figure 1.22).

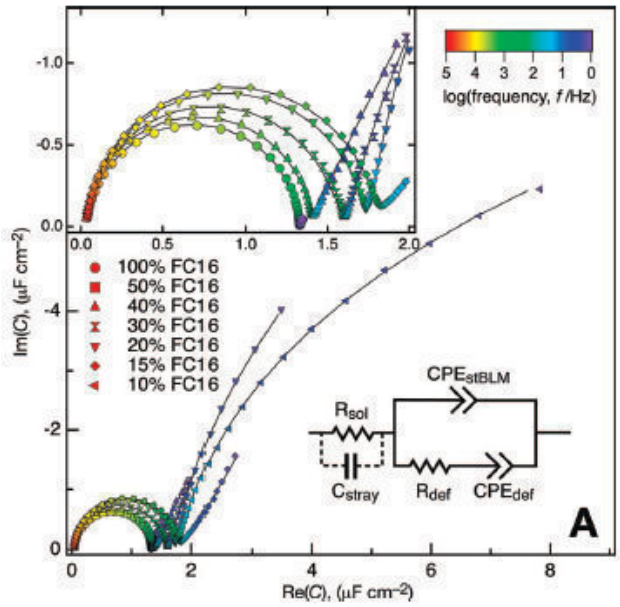

Figure 1.22 Complex-capacitance plane representation of the EIS data obtained by Heinrich et al.[78] for tBLMs formed over mixed SAMs of varying ratios of thiol FC16 and β-mercaptoethanol. The inset represents the zoom on the experimental data with the frequency scale as a color gradient scale. The electrical circuit on the right hand demonstrates the equivalent circuit model used by them to fit the results.

As seen in the figure above, the curves exhibit semicircular shapes at high and moderate frequencies, whereas tails at low frequencies.

It is important to note that all the data obtained by impedance measurements have to be treated by fitting them into an electrical equivalent circuit model (ECM). The fitting into an ECM helps in extracting the electrical and dielectric parameters of the system.
As shown in the figure above, the ECM used by Heinrich *et al.* (bottom right corner of the Figure 1.22) uses elements like resistance and capacitance in a particular sequence to fit the data points. These results of fits are plotted on the data points (the straight lines passing over each data point) in the curve.
To understand how an ECM is chosen for fitting, it is important to know that each frequency region of these plots represents or characterizes one of the several elementary steps that constitute the global electrochemical process. The parameters characterizing each step have to be taken into account in their order of frequency, for defining an electrochemical circuit model to analyze or fit the experimental data.
For example, in the above case, the high frequency regions define a parameter called solution resistance, whereas the moderate frequency region define parameters characteristic of the membrane deposited on the electrode (*i.e.* Resistance and Capacitance of the membrane) and the low frequency points describe the electrical double-layer capacitance. These parameters in their respective orders are explained as follows.

Solution resistance (R_s) is often a significant factor in the impedance of an electrochemical cell. A modern 3 electrode potentiostat compensates for the solution resistance between the counter and the reference electrodes. However, any solution resistance between the reference electrode and the working electrode must be considered while modeling the cell. The resistance of an ionic solution depends on the ionic concentration, type of ions, temperature, and the geometry of the area in which current is carried.

Membrane Resistance and membrane capacitance (R_m and C_m): The electrical resistance is defined as the property of a material to resist the flow of electrons. Although each electrode material has a characteristic resistance, the films deposited on the

electrode material can alter the electrode resistance drastically. This resistance offered by the deposited film is often termed as membrane resistance R_m. Membrane resistance of thiol based SAMs have been discussed quite intensively in the literature.[79] This property has been shown to be directly related to the structure, packing and organization of thiols in the SAM. In general, long chain hydrophobic thiols are shown to be more resistive than short chain thiols.

Further, the formation of tethered bilayer lipid membranes on SAMs is known to increase the membrane resistance. This increase is due to the addition of a compact layer of phospholipids on the SAMs which offer higher resistance to the flow of current.

Membrance capacitance (C_m) on the other hand, is defined as the ability of a material to store charge. A capacitor is formed when two conducting plates are separated by a non-conducting media, called the dielectric. In the case of self-assembled monolayers (SAMs) and tethered bilayer lipid membranes (tBLMs), these layers (mono- or bilayer respectively) act as the dielectric material between the charged electrode and the charged electrolyte solution. The capacitance associated with these layers/membranes can be defined as

$$C = \frac{\varepsilon\varepsilon_o}{d} S \qquad \textbf{Equation 1.8}$$

Where,

ε= the dielectric constant of the material

ε_o= the permittivity of vacuum 8.85×10^{-14} F/cm

S = the area of the surface and

d = the thickness of the film/membrane

Thus, following this equation we observe that the capacitance of a membrane is inversely proportional to its thickness. And hence, in general SAMs of long chain thiols are less capacitive than SAMs of shorter chain thiols. Also, the formation of tBLMs on SAMs is characterized by a decrease in the membrane capacitance as the length of the film increases.

Double-layer capacitance (C_{dl}): An electrical double layer exists on the interface between an electrode and its surrounding electrolyte. This double layer is formed as ions from the solution "stick on" to the electrode surface. The charged electrode is separated from the charged ions. The separation is very small, often of the order of angstroms. Charges separated by an insulator form a capacitor. The value of the double layer capacitance depends on many factors. The most important ones being the property of the electrode material at the interface, the electrolyte used the ionic strength and the electrode geometric area.

It is also essential to note that Heinrich *et al.*[78] in their ECM use Constant phase elements CPE instead of true capacitors. This can be explained by taking into account the generic representation of a complex-capacitance plane plot (Fig. 1.21), herein we notice that the semicircles are perfect arcs centered on the x-axis. However, the curves in figure 1.22 (experimental results by Heinrich *et al.*) display arcs instead of semicircles. In such arcs, as better described using another Nyquist representation (Figure 1.23), the centre of this arc is somewhere below the x-axis (see the cross indicated on the red line in Figure 1.23. These slightly distorted semicircles are known to be arising due to inhomogeneities in some properties. To account for these inhomogenities, a CPE is used instead of a true capacitor. Thus, a CPE is best defined as a non ideal capacitor.

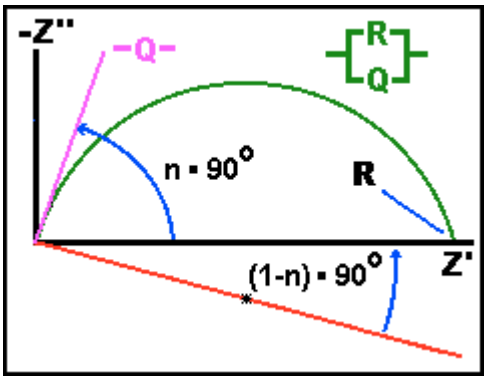

Figure 1.23 Concept of a CPE described on the Nyquist presentation

The impedance of a CPE is defined as $Z_{CPE} = Q^{-1}(j\omega)^{-\alpha}$, where Q is the amplitude of the CPE, ω is the angular frequency and α is the exponent which is a real number that varies between 0 and 1. When $\alpha = 1$, purely capacitive behaviour is observed (i.e. $Q = C$).

1.4.3. Dynamic Light Scattering

Dynamic Light Scattering (DLS), sometimes referred to as Photon Correlation Spectroscopy (PCS) or Quasi-Elastic Light Scattering (QELS) is a technique for measuring the size of particles typically in the sub micron region.

It is based on the principle of semi-classical light scattering theory, where when light impinges on matter; the electric field of the light induces an oscillating polarization of electrons in the molecules. Since particles are in Brownian motion, the interaction with light causes a Doppler Shift when the light hits the moving particle thus changing the wavelength of the light. This change is related to the size of the particle. It is possible to compute the sphere size distribution and give a description of the particle's motion in the medium, measuring the diffusion coefficient of the particle and using the autocorrelation function.

The experimental set up for DLS is schematically described in Figure 1.24.

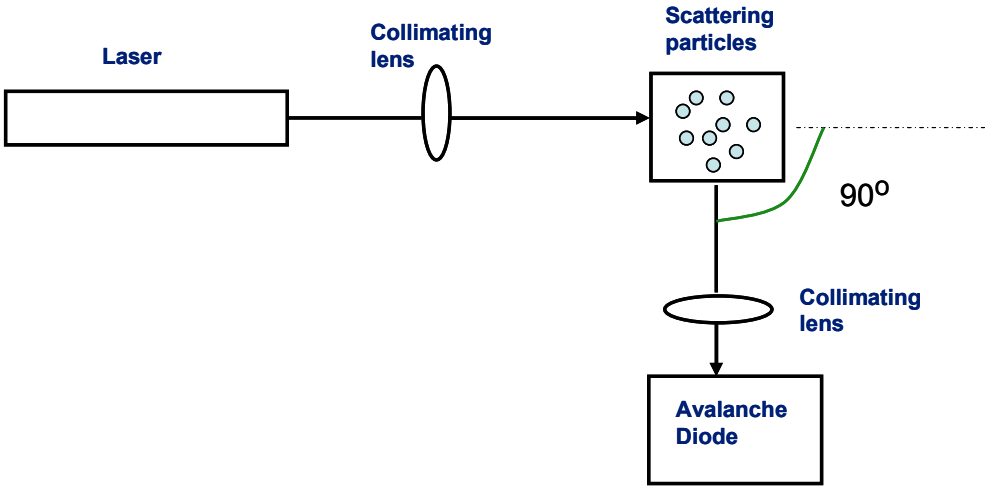

Figure 1.24 Schematic representation explaining the experimental set up of a typical DLS device

The PCS method consists in determining the velocity distribution of particles movement by measuring dynamic fluctuations of intensity of scattered light. The disperse particles or macromolecules suspended in a liquid medium undergo Brownian motion which causes the fluctuations of the local concentration of the particles, resulting in local inhomogeneities of the refractive index. This in turn results in fluctuations of intensity of the scattered light.

The mechanism of DLS can be understood by following scheme in Figure 1.25

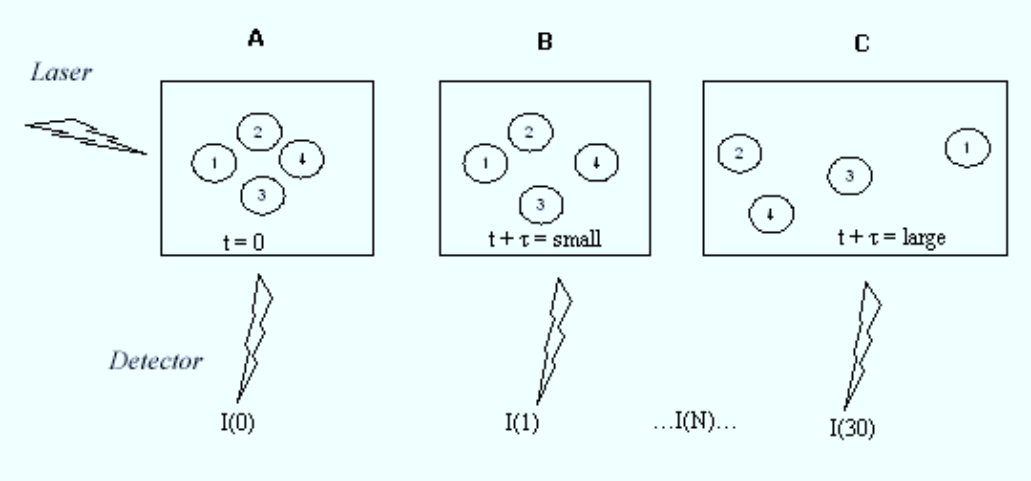

Figure 1.25 A schematic diagram explaining the functioning of DLS

The following parameters are introduced in order to describe and quantify DLS phenomenon:

- Light intensity is I(t) at time t
- At the time t + τ, which is a very small time later than t, the diffusing particles will have new positions and the intensity at the detector will have a value I(t+ τ)
- The detector saves the values for I(t + τ) at numerous times (Actually, the autocorrelator automatically calculates the function instead of the discrete intensities)
- Shown below is an example of a light scattering experiment. -A- shows time zero. -B- is after a short time. -C- is after a longer time period.
- I(t+ τ) correlates with I(t), the closer the measurement is to time zero, the more similar I(t+ τ) is to I(t) since the particles have not had much time to move (Panel B):

$$\lim_{\tau \longrightarrow 0} I(t+\tau) = I(t)$$

Equation 1.9

- As time goes on there is no more similarity between the starting state and the current state (Panel C). The measured intensities do no correlate anymore to the beginning one. This happens faster if the particles are smaller since smaller particles move faster. One needs a method for quantifying how fast the correlation takes to break down between the starting measurement and one a short time later.
- The function used to calculate this correlation is the *time-intensity autocorrelation function G (also mentioned as r)*: this function describes how a given measurement relates to itself in a time dependent manner:

$$r_\tau = \frac{\sum_{i=1}^{N-k}(Y_i - \overline{Y})(Y_{i+k} - \overline{Y})}{\sum_{i=1}^{N}(Y_i - \overline{Y})^2}$$

Equation 1.10

- At time zero, r = 1 i.e. there is a 100% autocorrelation. With progress in time, the autocorrelation diminishes, reaching zero as there is no more similarity between starting and final states.
- The decay of the autocorrelation is described by an exponential decay function $g_2(t)$-1 which relates the autocorrelation to the diffusion coefficient D of the particle and the scattering vector q as

$$g_2(t) - 1 \propto e^{-2Dq^2t}$$

Equation 1.11

$$q = \frac{4\pi\eta}{\lambda} sin\frac{\theta}{2}$$

Equation 1.12

n = refractive index of the solution (1.33 for water)

λ = wavelength of the laser (632.8 nm ALV device for a He-Ne laser)

θ = angle of measurement/scattering angle = 90º

- By fitting the points of autocorrelation to the function G (t), the diffusion coefficient can be measured and related to the equivalent sphere of diameter d using the Stokes - Einstein equation (1.13):

$$D = \frac{k_B}{3\pi\eta d} T \qquad \textbf{Equation 1.13}$$

η = solvent viscosity (water = 8.94×10^{-4} Pa.s)
T = Temperature (K) (room temparature = 298 K)
D = diffusion coefficient (m^2/s)
k_B = Boltzmann constant (1.3807×10^{-23} J/K)
d = sphere diameter (m)

1.4.4. Surface Plasmon Resonance

When a monochromatic, plane polarized light propagating in a dielectric medium approaches the interface with another dielectric medium of lower refractive index, it is either reflected or refracted depending on the angle of incidence, θi. As θi approaches the critical angle (θc), more light is reflected back. At θc and beyond, total internal reflection of the incident light occurs, and thus no light is refracted. If the interface between the two dielectric medium is coated by a thin metallic layer (Au or Ag), instead of being internally reflected, some of the light energy may resonate and couple with the electrons cloud (plasma) which propagates at the metal surface. The energy of the light which is coupled to this surface electron cloud may create an evanescent wave field which travels several hundreds of nanometers into the adjacent dielectric medium of low refractive index. The amplitude of the wave field dissipates exponentially with the distance from the metal surface. Thus, light energy is absorbed by the surface, and less light is reflected. At a certain angle above θc, which corresponds to the surface plasmon resonance angle, θspr, the coupling of light energy to the plasma is at its most efficient, reducing the intensity of reflected light (Ir). A minimum amount of light is reflected at θspr (Figure 1.26).

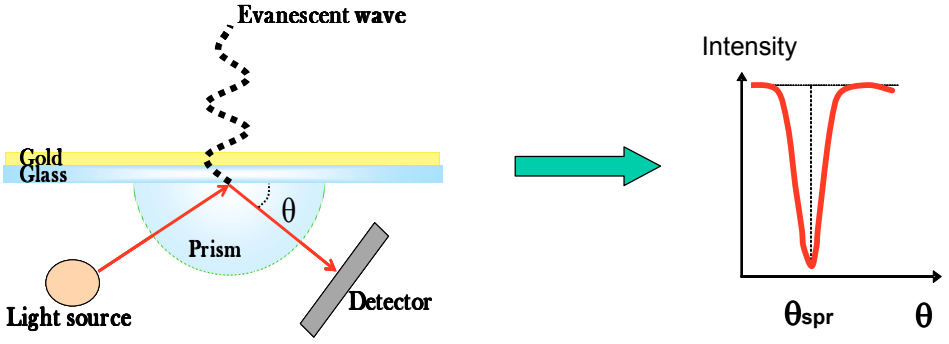

Figure 1.26 Schematic diagram of the principals of SPR.

The evanescent wave field is dependent on the refractive nature of the metal boundary. Therefore, any change occurring near to this interface which alters the refractive index will change the resonant energy of this wave field. As the monochromatic light shining at the surface does not change in θi, a change in the intensity of the reflected light is observed. Thus, any change in these environments may be measured quantitatively with respect to the intensity of reflected light.

Although the effect of surface plasmon resonance was discovered over 100 years ago, applications as biosensors evolved in the 1980s and 1990s. In the context of our studies, SPR measurements were performed with a BIAcore T100 device. This device equipped with a micro fluidic system is especially dedicated to kinetic and affinity determination between an immobilized ligand and an analyte in solution. For this application, one binding partner is immobilized on a gold or gold modified surface so as to form the internal surface of a flow cell. The corresponding analyte is then injected into the flow cell in buffer solution. As the analyte binds to the immobilized ligand, a shift in the refractive index occurs. This in turn shifts θspr leading to a measureable change in reflected light intensity (see Figure 1.27 A-B). As more analyte binds to the surface, the change in θspr increases in magnitude giving rise to the association curve recorded in the sensorgram by the detector. As the amount of analyte associating with the surface equilibrates with the amount of analyte dissociating, equilibrium is reached. During the post-injection phase, only buffer passes through the flow cell and the analyte dissociates from the surface leading to a decrease in the signal and the recording of the dissociation curve (Figure 1.27A). In order to extract affinity of the binding, this

association/dissociation cycle is repeated for several concentrations (Figure 1.27C). At the end of each association/dissociation cycle, a regeneration step is performed to ensure a similar initial surface for the following cycles. Simultaneous injections are performed on a reference flow cell in order to remove bulk and non specific contributions to the signal. The sensorgrams are then subjected to mathematical treatment using analysis software in order to calculate association and dissociation rates and, if possible, equilibrium binding constants.

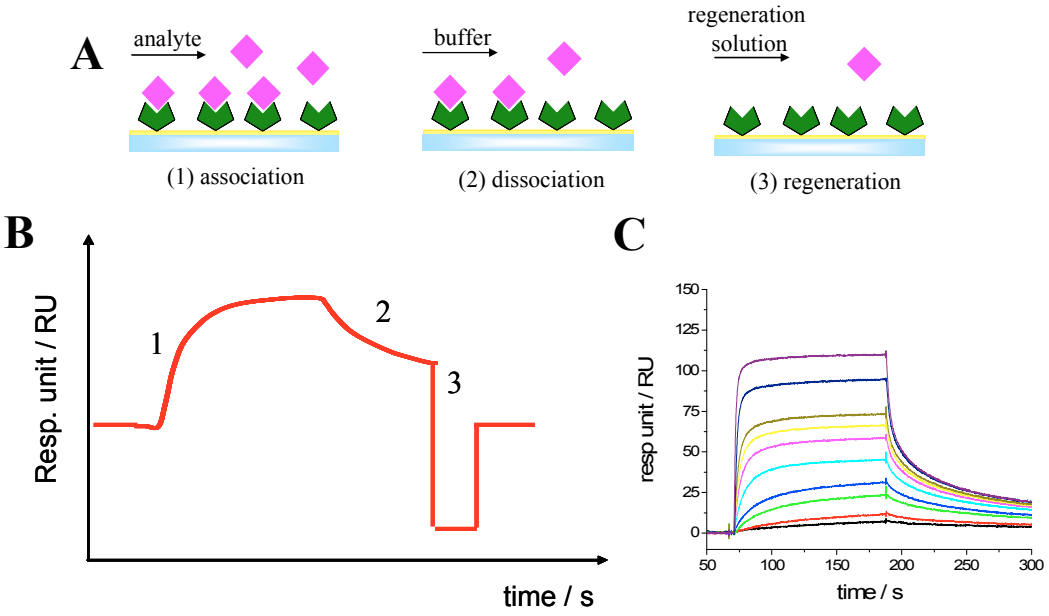

Figure 1.27 A) Scheme and B) associated sensorgram representing the different steps involved in a kinetic analysis of the interaction between an analyte in solution and its corresponding immobilized ligand C) sensorgrams representing association/dissociation cycles for increasing concentration in analyte.

With BIAcore device, the variation of shift angle is expressed as resonance units (RU), whereby 1000 RU corresponds to a $\Delta\theta$spr of 0.1°. The RU value (or $\Delta\theta$spr) could be related to the quantity of adsorbed analyte using a conversion factor depending on both the surface and on the refractive index of the molecules.[63] As an example, 1000 RU is equivalent to 1 ng mm^{-2} of protein attached to a CM5 sensorchip (gold surface functionalized with carboxymethyl dextran of lengths about 100 nm).

Considering a 1:1 interaction, the maximum response signal $R_{anal,max}$ expected for the analyte could be evaluated from the following relationship:

$$R_{anal,\max} = R_{lig} \times \frac{MW_{anal}}{MW_{lig}} \times \left[\left(\frac{dn}{dc} \right)_{lig} \Big/ \left(\frac{dn}{dc} \right)_{anal} \right] \qquad \textbf{Equation 1.14}$$

with R_{lig} the quantity in RU of immobilized ligand, MW_{lig} et MW_{ana} respectively the molar weight of the ligand and of the analyte and $(dn/dc)_{lig}$ and $(dn/dc)_{ana}$ the refractive index increment respectively for the ligand and the analyte.

Assuming similar refractive index increment for the ligand and the analyte, it is could be easily understood from this equation that most of the time, immobilization of the partner presenting the lowest molecular weight is preferred. However, sometimes the immobilization of the larger partner is required where detection of small molecular weight molecules is limited, even with a high level of immobilized ligand. Therefore, inhibition assays are chosen to overcome this difficulty.

1.4.5. Atomic Force Microscopy

AFM is a special method of scanning probe microscopy (SPM) which is able to measure surface topography, mechanical properties and interactions on a surface with nanometric resolution.[80] A nanometer sharp tip attached to a cantilever is scanned over the surface and the deflection of the cantilever due to objects or interactions with the substrate is read out by measuring the position of a laser beam reflected from the backside (Figure 1.28). AFM is a method image surfaces with a resolution which is up to 1000 times higher than in optical microscopy. In addition it does not require labeling and is non-invasive. There are two main fields of application. The first is molecular metrology especially in the field of semiconductor research and testing. Apart from this, AFM has found its way into biological science. The huge advantage of AFM over high resolution techniques like scanning electron microscopy (SEM) is the ability to measure in water at physiological conditions in a non-invasive fashion. It can even be used to monitor biological processes like cell migration *in situ*. All the named features have made AFM a highly flexible method that is used in research labs all over the world.

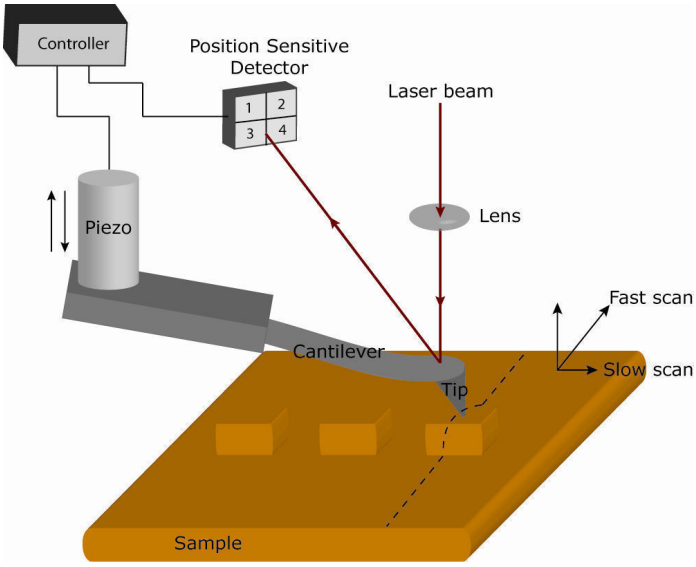

Figure 1.28 Demonstrating the principle of working of AFM

There are three basic measurement modes for AFM. The first one is the so called contact mode where the tip is scanned over the surface at constant force by applying a feedback mechanism (Figure 1.29A).

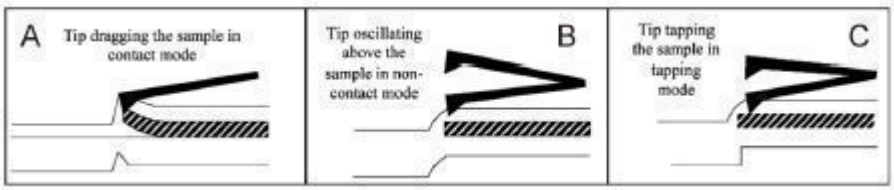

Figure 1.29 Diagram demonstrating the 3 principal modes of working of AFM (A) contact mode, (b) non-contact mode and (C) conventional acoustic/tapping mode.

This mode is comparably insensitive to perturbations through the environment and is mostly used for hard and dry surfaces. The only drawback of this method is that the tip can alter the surface through scratching. Another mode is called non-contact mode AFM (Figure 1.29B). In this mode the tip is oscillating near its resonance frequency. When the tip starts to interact with the surface through van der Waals forces for example, the oscillation is damped. By mapping the damping relative to the lateral-position of the cantilever, surface images are obtained. This method is mainly used for very soft samples like cells because there is no danger of alteration of the sample by the cantilever. It is

possible to get very high resolution images but therefore low oscillation amplitudes and flat surfaces are needed. A major disadvantage of non-contact mode AFM is the susceptibility to perturbations through the environment. An example is the thin water film due to humidity which is almost always present when measuring in air. Due to the very low exerted force on the sample the cantilever will only stick to that liquid film without mapping the actual topography.

A method to get the best out of the two operation modes is the tapping mode – also termed intermittent contact mode (Figure 1.29C). Again the cantilever is actively excited by a piezoelectric element to vibrate at or close to its resonance frequency. Then unlike in non-contact mode it is brought so close to the surface that it starts to tap on the sample which results in a lowered resonance amplitude. By mapping the amplitude versus the lateral position it is possible to extract exact height information of a sample. Because the cantilever is only in contact with the surface for a very short time the likelihood of changing the sample with the tip is reduced. Due to the stronger oscillation compared to non-contact mode it is less susceptible to perturbation through the environment. Furthermore there is secondary information available which is the phase of the oscillation. Depending on the mechanical properties of the surface the cantilever oscillation is shifted in phase relative to the excitation frequency. A soft surface results in a higher phase shift than a hard one so that mechanical contrast can be extracted from the phase image.

Another field of application of AFM apart from imaging is force spectroscopy.[81] This is a direct way to measure the surface interactions as a function of the tip-sample separation. However, in the present thesis the only mode which will be employed for imaging is the top MAC mode of imaging. This mode of imaging is principally the same as the non-contact or the acoustic mode, except that the oscillations in the cantilever are driven by a magnetic field. With MAC Mode, a magnetically coated cantilever called a MAC Lever is driven by an oscillating magnetic field. The magnetic field is applied directly to the MAC Lever from either above (Top-MAC). Thus, there is less system noise, less confusion in determining the true cantilever resonance, and the cantilever can be operated at much smaller amplitudes

1.5. References

(1) Singer, S. J.; Nicolson, G. L. *Science* **1972**, *175*, 720-731.
(2) Saxton, M. J.; Jacobson, K. **2003**.
(3) Krogh, A.; Larsson, B. È.; Von Heijne, G.; Sonnhammer, E. L. L. *J. Mol. Biol.* **2001**, *305*, 567-580.
(4) Daley, D. O. *Curr. Opin. Struct. Biol.* **2008**, *18*, 420-424.
(5) Tanford, C. *The Hydrophobic Effect: Formation of Micelles and Biological Membranes 2d Ed*; J. Wiley., 1980.
(6) Brotherus, J. R.; Jost, P. C.; Griffith, O. H.; Hokin, L. E. *Biochemistry* **1979**, *18*, 5043-5050.
(7) Kubitschek, H. E. *J. Bacteriol.* **1990**, *172*, 94.
(8) Bentley, R.; Meganathan, R. *Microbiol. Mol. Biol. Rev.* **1982**, *46*, 241.
(9) Reid, G.; Howard, J.; Gan, B. S. *Trends Microbiol.* **2001**, *9*, 424-428.
(10) Braun, V.; Hantke, K.; Köster, W.; Sigel, A.; Sigel, H.; Marcel Dekker Inc., New York: 1998.
(11) Coulton, J. W.; Mason, P.; Cameron, D. R.; Carmel, G.; Jean, R.; Rode, H. N. *J. Bacteriol.* **1986**, *165*, 181.
(12) Locher, K. P.; Rees, B.; Koebnik, R.; Mitschler, A.; Moulinier, L.; Rosenbusch, J. P.; Moras, D. *Cell* **1998**, *95*, 771-778.
(13) Bonhivers, M.; Ghazi, A.; Boulanger, P.; Letellier, L. *EMBO J.* **1996**, *15*, 1850.
(14) Hynes, R. O. *Cell* **2002**, *110*, 673-687.
(15) Pierschbacher, M. D.; Ruoslahti, E. *Nature* **1984**, *309*, 30-33.
(16) Xiong, J. P.; Stehle, T.; Diefenbach, B.; Zhang, R.; Dunker, R.; Scott, D. L.; Joachimiak, A.; Goodman, S. L.; Arnaout, M. A. *Science* **2001**, *294*, 339.
(17) Horton, M. A. *The International Journal of Biochemistry & Cell Biology* **1997**, *29*, 721.
(18) Xiong, J. P.; Stehle, T.; Zhang, R.; Joachimiak, A.; Frech, M.; Goodman, S. L.; Arnaout, M. A. *Science* **2002**, *296*, 151.
(19) Wilder, R. L. *Annals of the rheumatic diseases* **2002**, *61*, ii96.
(20) Brooks, P. C.; Clark, R. A.; Cheresh, D. A. *Science* **1994**, *264*, 569.
(21) Haubner, R.; Finsinger, D.; Kessler, H. *Angew. Chem., Int. Ed.* **1997**, *36*, 1374-1389.
(22) Pfaff, M.; Tangemann, K.; Müller, B.; Gurrath, M.; Müller, G.; Kessler, H.; Timpl, R.; Engel, J. *J. Biol. Chem.* **1994**, *269*, 20233.
(23) Massia, S. P.; Hubbell, J. A. *J. Cell Biol.* **1991**, *114*, 1089.
(24) Garanger, E.; Boturyn, D.; Coll, J. L.; Favrot, M. C.; Dumy, P. *Org. Biomol. Chem.* **2006**, *4*, 1958-1965.
(25) Kalmbach, R.; Chizhov, I.; Schumacher, M. C.; Friedrich, T.; Bamberg, E.; Engelhard, M. *J. Mol. Biol.* **2007**, *371*, 639-648.
(26) Nomura, S. M.; Kondoh, S.; Asayama, W.; Asada, A.; Nishikawa, S.; Akiyoshi, K. *J. Biotechnol.* **2008**, *133*, 190-195.
(27) Mueller, P.; Rudin, D. O.; Ti Tien, H.; Wescott, W. C. *Nature* **1962**, *194*, 979-980.
(28) Montal, M.; Mueller, P. *Proc. Natl. Acad. Sci. U. S. A.* **1972**, *69*, 3561.
(29) Schulte, A.; Ruamchan, S.; Khunkaewla, P.; Suginta, W. *J. Membr. Biol.* **2009**, *230*, 101-111.

(30) Schmies, G.; Lüttenberg, B.; Chizhov, I.; Engelhard, M.; Becker, A.; Bamberg, E. *Biophys. J.* **2000**, *78*, 967-976.
(31) Schmitt, E. K.; Vrouenraets, M.; Steinem, C. *Biophys. J.* **2006**, *91*, 2163-2171.
(32) Mueller, P.; Rudin, D. O.; Tien, H. T.; Wescott, W. C. *Nature* **1962**, *194*, 979-&.
(33) McConnell, H. M.; Watts, T. H.; Weis, R. M.; Brian, A. A. *Biochim. Biophys. Acta* **1986**, *864*, 95-106.
(34) Tamm, L. K.; McConnell, H. M. *Biophys. J.* **1985**, *47*, 105-113.
(35) Tamm, L. K. *Klin. Wochenschr.* **1984**, *62*, 502-503.
(36) Johnson, S. J.; Bayerl, T. M.; McDermott, D. C.; Adam, G. W.; Rennie, A. R.; Thomas, R. K.; Sackmann, E. *Biophys. J.* **1991**, *59*, 289-294.
(37) Cremer, P. S.; Boxer, S. G. *J. Phys. Chem. B* **1999**, *103*, 2554-2559.
(38) Stelzle, M.; Miehlich, R.; Sackmann, E. *Biophys. J.* **1992**, *63*, 1346-1354.
(39) Lahiri, J.; Fate, G. D.; Ungashe, S. B.; Groves, J. T. *J. Am. Chem. Soc.* **1996**, *118*, 2347-2358.
(40) Keller, C. A.; Kasemo, B. *Biophys. J.* **1998**, *75*, 1397-1402.
(41) Reviakine, I.; Brisson, A. *Langmuir* **2000**, *16*, 1806-1815.
(42) Richter, R.; Mukhopadhyay, A.; Brisson, A. *Biophys. J.* **2003**, *85*, 3035-3047.
(43) Richter, R. P.; Brisson, A. R. *Biophys. J.* **2005**, *88*, 3422-3433.
(44) Kalb, E.; Frey, S.; Tamm, L. K. *Biochim. Biophys. Acta, Biomembr.* **1992**, *1103*, 307-316.
(45) Wagner, M. L.; Tamm, L. K. *Biophys. J.* **2000**, *79*, 1400-1414.
(46) Naumann, R.; Baumgart, T.; Graber, P.; Jonczyk, A.; Offenhausser, A.; Knoll, W. *Biosens. Bioelectron.* **2002**, *17*, 25-34.
(47) Knoll, W.; Bender, K.; Foerch, R.; Frank, C.; Goetz, H.; Heibel, C.; Jenkins, T.; Jonas, U.; Kibrom, A.; Kuegler, R. *Polymer Membranes/Biomembranes*, 87-111.
(48) Ye, Q.; Konradi, R.; Textor, M.; Reimhult, E. *Langmuir* **2009**, *25*, 13534-13539.
(49) Schiller, S. M.; Naumann, R.; Lovejoy, K.; Kunz, H.; Knoll, W. *Angew. Chem., Int. Ed.* **2003**, *42*, 208-211.
(50) Jeuken, L. J. C.; Daskalakis, N. N.; Han, X.; Sheikh, K.; Erbe, A.; Bushby, R. J.; Evans, S. D. *Sens. Actuators, B* **2007**, *124*, 501-509.
(51) He, L.; Robertson, J. W. F.; Li, J.; Kärcher, I.; Schiller, S. M.; Knoll, W.; Naumann, R. *Langmuir* **2005**, *21*, 11666-11672.
(52) Kendall, J. K. R.; Johnson, B. R. G.; Symonds, P. H.; Imperato, G.; Bushby, R. J.; Gwyer, J. D.; van Berkel, C.; Evans, S. D.; Jeuken, L. J. C. *Chemphyschem*, *11*, 2191-2198.
(53) Rajesh, S.; Knowles, T.; Overduin, M. *New Biotechnol.*
(54) Popot, J. L. *Annu. Rev. Biochem.* **2010**, *79*, 737-775.
(55) Tribet, C.; Audebert, R.; Popot, J. L. *Proc. Natl. Acad. Sci. U. S. A.* **1996**, *93*, 15047.
(56) Dahmane, T.; Damian, M.; Mary, S.; Popot, J. L.; Bane res, J. L. *Biochemistry* **2009**, *48*, 6516-6521.
(57) Diab, C.; Tribet, C.; Gohon, Y.; Popot, J. L.; Winnik, F. M. *Biochim. Biophys. Acta, Biomembr.* **2007**, *1768*, 2737-2747.
(58) Sauerbrey, G. *Z. Phys* **1959**, *155*, 206–222.
(59) Konash, P. L.; Bastiaans, G. J. *Anal. Chem.* **1980**, *52*, 1929-1931.
(60) Rodahl, M.; Hook, F.; Krozer, A.; Brzezinski, P.; Kasemo, B. *Rev. Sci. Instrum.* **1995**, *66*, 3924-3930.
(61) Krozer, A. *Faraday Discuss* **1997**, *107*, 246.
(62) Voinova, M. V.; Rodahl, M.; Jonson, M.; Kasemo, B. *Phys. Scr.* **1999**, *59*, 391.
(63) Larsson, C.; Rodahl, M.; Höök, F. *Anal. Chem.* **2003**, *75*, 5080-5087.

(64) Hook, F.; Voros, J.; Rodahl, M.; Kurrat, R.; Boni, P.; Ramsden, J. J.; Textor, M.; Spencer, N. D.; Tengvall, P.; Gold, J.; Kasemo, B. *Colloids Surf. B* **2002**, *24*, 155-170.
(65) Reimhult, E.; Larsson, C.; Kasemo, B.; Höök, F. *Anal. Chem.* **2004**, *76*, 7211-7220.
(66) Wilczewski, M.; Van der Heyden, A.; Renaudet, O.; Dumy, P.; Coche-Guérente, L.; Labbé, P. *Org. Biomol. Chem.* **2008**, *6*, 1114-1122.
(67) Notley, S. M.; Eriksson, M.; Wågberg, L. *J. Colloid Interface Sci.* **2005**, *292*, 29-37.
(68) Ishida, N.; Biggs, S. *Langmuir* **2007**, *23*, 11083-11088.
(69) Zhang, G.; Wu, C. *Macromol. Rapid Commun.* **2009**, *30*, 328-335.
(70) Höök, F.; Rodahl, M.; Brzezinski, P.; Kasemo, B. *Langmuir* **1998**, *14*, 729-734.
(71) Caruso, F.; Rodda, E.; Furlong, D. N.; Niikura, K.; Okahata, Y. *Anal. Chem.* **1997**, *69*, 2043-2049.
(72) Fredriksson, C.; Kihlman, S.; Rodahl, M.; Kasemo, B. *Langmuir* **1998**, *14*, 248-251.
(73) Li, J.; Thielemann, C.; Reuning, U.; Johannsmann, D. *Biosens. Bioelectron.* **2005**, *20*, 1333-1340.
(74) Richter, R. P.; Brisson, A. *Langmuir* **2003**, *19*, 1632-1640.
(75) Richter, R. P.; Him, J. L. K.; Brisson, A. *Materials Today* **2003**, *6*, 32-37.
(76) Seantier, B.; Breffa, C.; Felix, O.; Decher, G. *Nano Lett.* **2004**, *4*, 5-10.
(77) Richter, R. P.; Maury, N.; Brisson, A. R. *Langmuir* **2005**, *21*, 299-304.
(78) Heinrich, F.; Ng, T.; Vanderah, D. J.; Shekhar, P.; Mihailescu, M.; Nanda, H.; Lo sche, M. *Langmuir* **2009**, *25*, 4219-4229.
(79) Boubour, E.; Lennox, R. B. *Langmuir* **2000**, *16*, 4222-4228.
(80) Wiesendanger, R. *Scanning probe microscopy and spectroscopy: methods and applications*; Cambridge Univ Pr, 1994.
(81) Cappella, B.; Dietler, G. *Surface Science Reports* **1999**, *34*, 1-104.

2. Supported Lipid Bilayer Membranes: Platforms for Studying Biomolecular Interactions

2. Supported Lipid Bilayer Membranes: Platforms for Studying Biomolecular Interactions

Supported Lipid Bilayer (SLB) membranes have to date proved to be quite successful as models in mimicking the cell membrane. Their innate features, like the 2-D fluidity of the phospholipids, the amphiphilic environment of the membrane, their ease of preparation (see section 1.3.3) and handling, have taken SLBs from being mere supramolecular architectures into a technology offering various applications.[1-4] This system has evolved not only as a model for the incorporation of membrane/transmembrane proteins (bearing small outer membrane domains) and their studies with their receptors,[5,6] but has also proved to be a useful platform for studying biomolecular interaction events. The inertness of the bare phospholipids bilayers to almost all biomolecules makes them an excellent support for studying processes like immune recognition and cell adhesion.[7-10] This inertness of SLBs has been demonstrated to be arising due the structure and organization of phospholipids in the SLB. Among various other lipids and phospholipids, 1-palmitoyl-2-oleoyl-*sn*-glycero-3-phosphocholine (POPC) is the most commonly used lipid in designing supported lipid bilayers. POPC is also a major component of the cell membrane. As shown in Figure 2.1, POPC possesses a zwitterionic phosphorylcholine head group that is linked to the glycerol backbone to a fully saturated palmitoyl (16:0) chain and an unsaturated oleyl (18:1) chain. Various groups have suggested that it is this zwitterionic (phosphorylcholine) headgroup in phospholipids that confers to the bilayers a non-fouling nature as well as a resistance to non-specific interactions with biomolecules.[9]

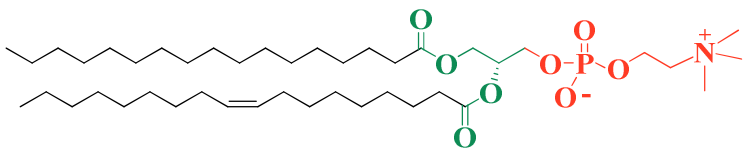

Figure 2.1 Structure of 1-palmitoyl-2-oleoyl-sn-glycero-3-phosphocholine (POPC), the oleyl and the palmitoyl chains are colored black, the glycerol backbone is shown in green and the phosphatidyl choline part is indicated in red.

One suggested factor, which contributes to this property, is that the attractive electrostatic interaction between proteins and the phosphorylcholine surface diminishes because the zwitterionic surfaces are neutral. A second contributing factor might be the high fraction of bound water of hydration associated with phosphorylcholine headgroups, which creates a barrier for unwanted protein–surface interactions. Thus, these factors such as electrical neutrality, strongly bound water of hydration and fluidity are likely to contribute cooperatively to the inherent resistance of bare SLBs toward proteins and cells.[7] Furthermore, the ease in introducing cell adhesion ligands in controlled quantities and the ability of providing these incorporated ligands with a lateral mobility within the bilayer is another striking feature that makes SLBs quite appealing as model system for studying cell adhesion.[11]

The present chapter will thus describe the applications of supported lipid bilayers exploited for two different kinds of studies:

1. Cell adhesion processes on ligand doped SLBs
2. Incorporation of an *E. coli* outer membrane protein, namely FhuA, in SLBs and its recognition by a T5 phage protein, namely pb5.

2.1. cRGD Induced Cell Adhesion of HEK-β3 Cells on Supported Lipid Bilayers

2.1.1. Introduction

Cell adhesion is a process of binding of a cell to a surface, which can be the extracellular matrix or another cell, using cell adhesion molecules. It is a phenomenon of considerable importance in living beings, as it triggers a wide range of cellular processes. For example, the adhesion of blood-borne cells to the vascular surface occurs in the inflammatory response, cancer cell metastasis[12], and the homing of lymphocytes to Peyer's patches and lymph nodes.[13,14] The interest in understanding cell adhesion in vivo has led to the design of many in vitro experiments in order to understand the physical

and chemical processes that control adhesion. In vivo cell adhesion is known to be promoted by cell adhesion molecules (CAMs) such as selectins[15], cadherins[16,17] and integrins[18,19]. Among these CAMs, the integrins constitute an important group of receptors that bind to the proteins of the extracellular matrix[18]. Integrins, which are a class of transmembrane proteins, are large heterodimeric receptors on cell surfaces. Besides playing a very crucial role in cell adhesion, tumor cell metastasis, differentiation and proliferation, integrins are also involved in several cellular functions such as signal transductions or immune dysfunctions osteoporosis (see section 1.2.2).[20,21] Considering the various extracellular matrix (ECM) proteins that recognize integrins, the RGD (Arg-Gly-Asp) tripeptide sequence was found to be the sequence most often involved in the active recognition site of these ECM proteins.[22] Later, it was demonstrated by the group of H. Kessler that the cyclic analogue (*c*RGD) of this peptidic sequence showed much more affinity and specificity towards the integrins over its linear analogue.[23,24] Consequently, various materials and substrates have been functionalized with the *c*RGD-bearing peptide sequence for studying its interactions with the integrins.[18,25]

It was demonstrated by our group in the laboratoire "Ingénierie et Interactions Biomoléculaires (I2BM)" that multivalent *c*RGD ligands presented on a cyclodecapeptide scaffold (Figure 2.2) exhibited quite interesting properties like targeted delivery[26], localisation of the molecule in tumour cells[27]and imaging of tumour cells[28] etc. Moreover, this scaffold presents two independent regioselective functional domains where one domain contains the *c*RGD ligand and the other domain can be addressed with various groups of interest. This scaffold presenting 4 *c*RGD units has been demonstrated to have an improved affinity for $\alpha_v\beta_3$ integrin (K_D of 3.9 nM) as opposed to the *c*RGD monomer (K_D of 41.7 nM).[27] Encouraged by these promising properties shown by this molecule, we were further driven to explore the adhesive properties of this clustered *c*RGD presenting ligand on HEK β3 cells. HEK β3 cells were chosen because they overexpress the $\alpha_v\beta_3$ integrin.

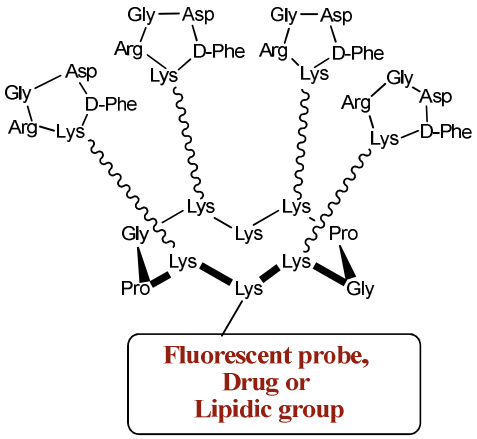

Figure 2.2 Structure of the cyclodecapeptide scaffold presenting four cRGD ligands on one side of its structure, whereas various groups can functionalize the other side of the structure.

Thus, to be able to incorporate this scaffold in SLBs and to study the cell adhesion properties of this clustered *c*RGD ligand incorporated in the SLBs, the two-lysine groups of the cyclodecapeptide scaffold were functionalized with palmitoyl chains (Figure 2.3). The synthesis of this lipopeptide **1** bearing 4 *c*RGDs is described in our earlier publication.[29]

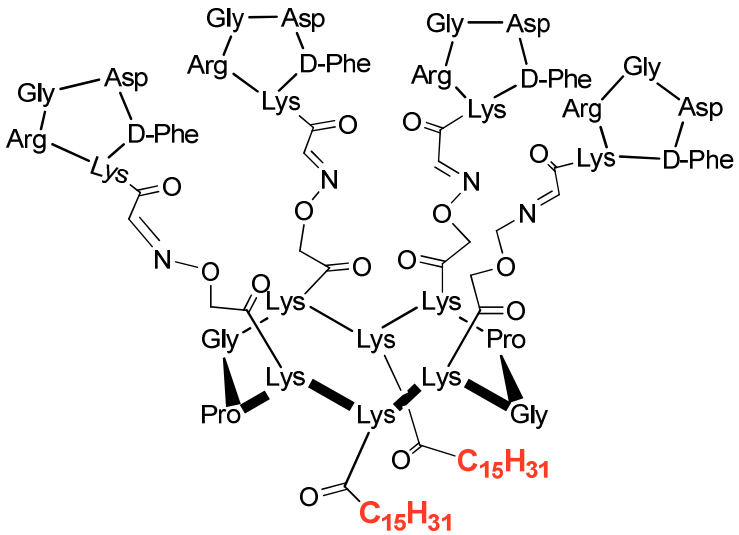

Figure 2.3 Structure of Lipopeptide 1 bearing four cRGD on one side of the functional domain and palmitoic acid chains on the other side of the functional domain.

2.1.2. Preparation of lipopeptide 1 doped small unilamellar vesicles

Small unilamellar vesicles bearing lipopeptide **1** were prepared by mixing an appropriate volume of a chloroform solution of lipopeptide **1** with an appropriate volume of a chloroform solution of POPC in a glass vial. Following evaporation of chloroform under a mild stream of nitrogen, a thin film of lipids was obtained on the surface of glass. This film of lipids was then hydrated by addition of Tris buffer (containing Tris HCl 50 mM, NaCl 150 mM, $MgCl_2$ 1mM, $MnCl_2$ 1mM at pH 7.4) and probe sonicated for 30 minutes, using a 5-second pulse cycle at 10 ºC. This dispersion was then centrifuged at 137,000*g* for 4 hours at 4 ºC and the intermediate fraction bearing monodispersed small unilamellar vesicles was collected from the tube. The vesicles were then diluted to a working concentration of 0.2 mg/ml and stored at 4 ºC for until 3 weeks. Lipopeptide 1 doped vesicles were monodispersed in size with a mean hydrodynamic radius (R_h) of 40 nm as determined by a Zetasizer Nano device.

2.1.3. Formation of Supported Lipid bilayers from Lipopeptide 1 doped vesicles

2.1.3.1 QCM-D measurements

The formation of Supported Lipid Bilayer from vesicles bearing the Lipopeptide **1** was followed by QCM-D. Since the cell adhesion experiments needed to be monitored close to physiological conditions *i.e.* at 37 ºC, the SLB formation was also monitored at the same temperature. The vesicles were injected at 0.2 mg/ml on a QCM-D chamber containing previously cleaned SiO_2 coated quartz at a constant flow of 50 μL/min. Upon completion of the process, the chamber was rinsed with buffer. Figure 2.4 shows the QCM-D profile for the fusion of pure POPC vesicles and for the fusion of POPC vesicles containing 1% of the lipopeptide 1.

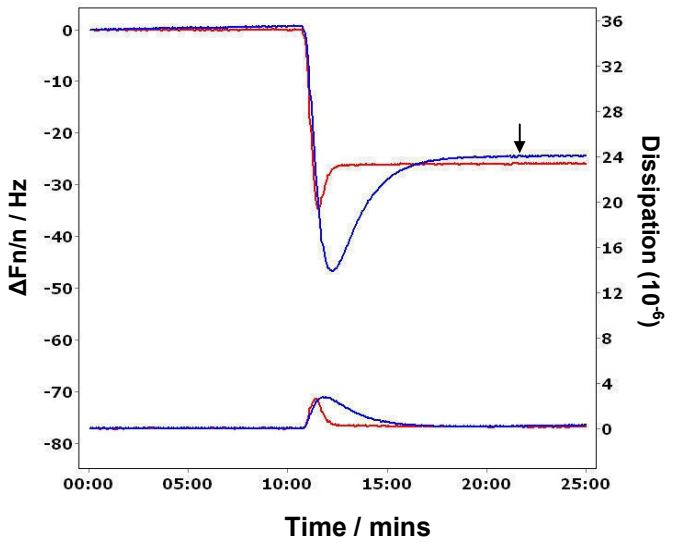

Figure 2.4 Fusion of vesicles made from pure POPC (blue curve) and POPC with 1% lipopeptide 1 (red curve) on a SiO_2 surface as observed on the 7th harmonic by QCM-D. The left axis represents the normalized frequency and the right axis represents the Dissipation. The arrow indicates the rinsing with buffer.

As observed in Figure 2.4, the QCM-D profiles for the fusion of both the doped and undoped vesicles follow the characteristic phenomenon of initial adsorption of intact vesicles indicated by a sharp decrease in frequency and increase in dissipation reaching a ΔF_{min} and ΔD_{max}. This was followed by rupture and fusion of vesicles as indicated by an increase in frequency and decrease in dissipation to reach stable values ($\Delta F_n/n = -24.5$ Hz and $\Delta D_n = 0.12\times10^{-6}$ for POPC SUVs and $\Delta F_n/n = -25.9$ Hz and $\Delta D_n = 0.23\times10^{-6}$ for 1% lipopeptide containing SUVs). Moreover, interestingly, the presence of the lipopeptide did not seem to have a drastic affect on the fusion behavior of the vesicles. The small difference, however, in the transition states (ΔF_{min} and ΔD_{max}) of the fusion of the pure and doped vesicles could be eventually a result of small difference in the size/dispersity of vesicles as it was demonstrated by Reimhult *et* al.[30]

2.1.3.2 AFM characterization of the pure and doped SLBs

AFM measurements were carried out on SLBs prepared from pure POPC and from lipopeptide **1** doped POPC vesicles. We performed these experiments to investigate into the homogeneity of the bilayer in the presence of lipopeptide **1**. For this purpose experiments, freshly cleaved mica was used as a substrate. It was mounted into the liquid cell of AFM that was previously cleaned with SDS followed by abundant rinsing and drying. The SUVs at 0.2mg/ml were then added to this substrate and allowed to incubate for 1 hour, which was followed by gentle yet generous rinsing of the substrate with buffer and then imaging in buffer.

The interaction of POPC SUVs with mica clearly led to a flat, featureless topography (Figure 2.5A) with a rms of 0.25 ± 0.05 nm, whereas the rms measured for a bare mica substrate was found to be 0.10 ± 0.05 nm (image not shown). It was demonstrated by Richter *et al.*[31] that SUVs upon interaction with mica in the presence of a divalent cation (Ca^{2+}) lead to the formation of a SLB quite rapidly (5 minutes) at high coverage of vesicles. In the present case, the experiments were done in a buffer containing Mg^{2+} and Mn^{2+} (see section 2.1.2) and the SUVs were used at a concentration of 0.2 mg/ml. Thus taking into account, the present experimental conditions which are close to that demonstrated by Richter *et al.*[32] and the small but clear increase in rms of the substrate after interaction with SUVs as compared to that for bare mica, we concluded the formation of a SLB on mica with pure POPC SUVs.

The situation seemed rather different, for SUVs bearing 5% lipopeptide **1,** (Figure 2.5B and C). The SUVs upon incubation with mica (1 hour) followed by rinsing and imaging showed the presence of objects of clearly distinguishable sizes (green and blue arrows on Figure 2.5B). These smaller objects (green arrow) show an average diameter of 55 nm and the larger objects (blue arrow) display an average diameter of about 500 nm (see profile Figure 2.5C). Moreover, the larger objects show a height of ~ 4.5 nm (see profile in Figure 2.5C), indicating that these patches correspond to patches of bilayers formed on the surface.[32] This observation was however noteworthy, as the vesicles doped with 5% of lipopeptide **1** did not have the same interactions with mica as those of pure POPC. To rule out the effect of the absence of Ca^{2+}, the substrate (after interaction with doped SUVs and imaging) was incubated for 30 minutes in the working buffer where 2 mM Ca^{2+} was added, followed by imaging in the same buffer. Seemingly, no change in the

topology was observed (image not shown) and the bilayer patches were still present. This observation indicated that the interaction of 5% lipopeptide **1**-doped SUVs with mica was not altered by the presence of Ca^{2+} ions in the medium. It is rather the presence of the peptide head group, which could have altered its fusion properties from that of pure POPC.

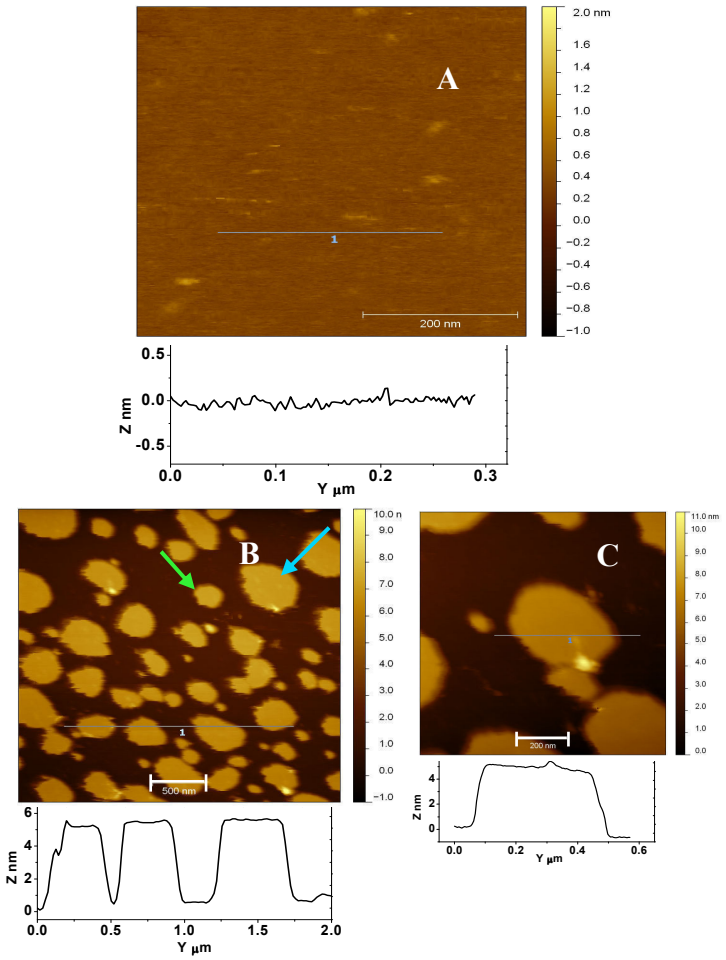

Figure 2.5 Topography AFM imaging in buffer of A) SLB of POPC formed on mica after interaction with POPC SUVs and rinsing with buffer, (B) bilayer patches observed on mica after interaction with 5% lipopeptide 1 doped POPC SUVs, followed by rinsing, (C) zoom on image B to image a single bilayer patch. Images were done in a magnetically driven acoustic mode (Top-MAC mode) using a MAC lever type VI cantilever having a spring constant k = 0.292 N/m and a resonant frequency in buffer = 17.8 kHz. The scan rate was set to 1.0 Hz and the images were flattened and analyzed using the Gwyddion 2.1 software. Below each image are their respective profiles in terms of Z vs Y traced on white line drawn on the image.

Nevertheless, QCM-D suggested that SUVs bearing lipopeptide **1** fused quite normally on a surface of SiO_2 (cf. section 2.1.3.1). Hence, we carried out the same experiment

using a Si wafer, which was cleaned using 1% SDS solution, and oxidized by a UV-ozone treatment.

To this Si/ SiO_2 silicon wafer surface, were then added vesicles made up of either pure POPC or 5% lipopeptide **1** containing POPC vesicles. The vesicles were allowed to remain in contact with the surface for about one hour, which was followed by rinsing with buffer and imaging in buffer. It is important to note here, that the fusion of SUVs made from zwitterionic phospholipids on a Si wafer has been shown by Richter *et al.* to be a process independent of the presence of Ca^{2+} ions in the medium.[32] The fusion of these SUVs leading to the formation of SLB was also demonstrated to be an instantaneous process. Accordingly, we observed (Figure 2.6A) that the interaction of pure POPC SUVs with the Si wafer lead to the formation of SLB, as represented by the topography images (Figure 2.6A), which showed a flat and homogenous surface (rms = 0.22 ± 0.06 nm). The scenario was not very different in the case of SUVs doped with 5% lipopeptide **1**, here too, the substrate after interaction with SUVs showed a flat, featureless topology (Figure 2.6B).

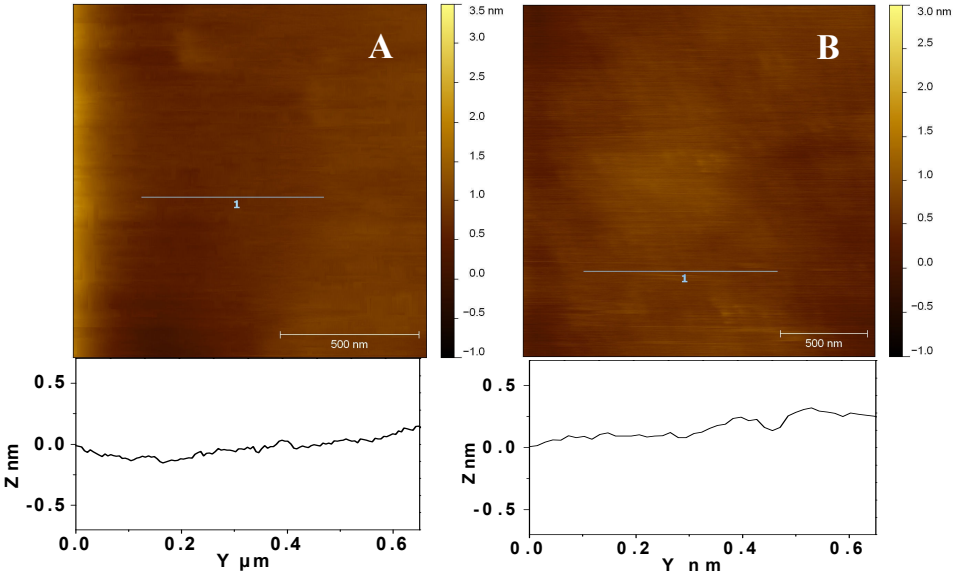

Figure 2.6 Topography AFM imaging in buffer of SLBs prepared from (A) POPC SUVs and (B) 5% lipopeptide 1 doped POPC SUVs. Images were done in a magnetically driven acoustic mode (Top-MAC mode) using a MAC lever type VI cantilever having a spring constant k = 0.292 N/m and a resonant frequency in buffer = 17.8 kHz. The scan rate was set to 1.0 Hz and the images were flattened and analysed using Gwyddion 2.1. Below each image are their respective profiles in terms of Z vs. Y traced on white line drawn on the image.

In the structure of lipopeptide **1**, the length of the cyclodecapeptide headgroup was calculated to be around 4.5 nm (using ChemDraw 3D Pro), while the length of the phosphorylcholine head group is known to be 1 nm. This would indicate that the aggregates formed (if any) would be roughly of about 3.5 nm. However, the profile traced over Figure 2.6B varied over less than 0.2 nm (peak to height). Moreover, phase segregated aggregates of heights ~ 2 nm (on a mixed SAM of different thiol lengths) are quite easily discernible by AFM and have been determined by us (section 3.3.4). Hence, this observation could suggest that the lipopeptide **1** did not phase segregate in the SLB.

2.1.4. Cell adhesion tests on SLBs presenting different ratios of lipopeptide 1

We were then intrigued into testing the cell adhesion onto SLBs decorated with different ratios of the lipopeptide **1**. To assess the influence of the lipopeptide on cell adhesion we prepared SLBs from vesicles bearing increasing concentration of lipopeptide **1**, *i.e.* 0.01%, 0.1%, 1% and 5% of the lipopeptide **1**.

The cell adhesion experiments were carried out using human embryonic kidney HEK-293 (β3) cells that overexpress $\alpha_v\beta_3$ integrin. For a negative control, HEK-293 (β1) cell line overexpressing the $\alpha_v\beta_1$ integrin (which has almost no affinity for *c*RGD) was used. The specificity of cell adhesion to the *c*RGD groups in the SLB was analyzed by carrying out another control experiment of HEK-293 (β3) cells on a pure POPC SLB.

2.1.4.1 QCM-D measurements to follow cell adhesion

The QCM-D experiments were carried out in a Q-sense window module, which was coupled to an optical microscope. This set up permitted us to not only to measure the cell adhesion by means of following the frequency and dissipation changes but also to understand the morphology of the adhered cells. To this end, DMEM (Dulbecco's Modified Eagle Medium) was injected over the formed SLBs to have a stable base line. Successively, cell suspension of 100,000 cells/mL in DMEM (Dulbecco's Modified

Eagle Medium) was continuously injected at a flow of 100 μL/min. Cell adhesion was monitored for about half an hour after the injection of cells.

Figure 2.7 presents the QCM-D monitoring of cell adhesion processes performed on SLBs doped with increasing concentrations of the lipopeptide **1**.

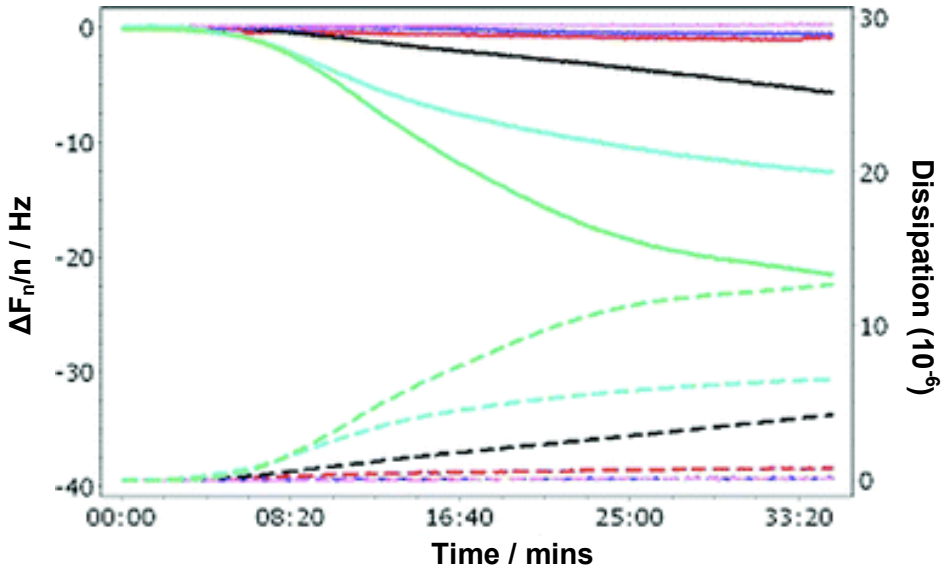

Figure 2.7 QCM-D profile for the adhesion of HEK-β3 cells on SLBs made from 5% lipopeptide 1 (green), 1% lipopeptide 1 (cyan), 0.1% (black), 0.01% (dark pink) and 0% (purple). In pink is the response of HEK- β1 cells on a SLB of 1%lipopeptide. The solid lines represent the frequency shift (left axis) and the dashed line represent the shift in dissipation (right axis) as measured on the 9th harmonic. Cell suspension (100,000cells mL^{-1}) in DMEM was injected at 100 µL/min.

As it can be observed on the purple profiles in Figure 2.7, a SLB of pure POPC does not induce any non-specific interaction with the HEK-β3 cells. Similarly, the interaction of HEK-β1 cells with a SLB presenting 1% lipopeptide **1** did not cause any significant shift in both frequency and dissipation (see the pink profile), indicating that the β1 cells had no affinity for the *c*RGD groups.

On the contrary, the HEK-β3 cells showed clear interactions with SLBs bearing 0.1%, 1% and 5% of lipopeptide 1 (black, cyan and green profiles respectively) as indicated by a strong shift in frequency and dissipation. This observation signifies that the cRGD motif in the SLB triggers $\alpha_v\beta_3$ integrin mediated cell adhesion. Moreover, the response in frequency and dissipation of the adhered cells varied directly as the mole fraction ratio of lipopeptide **1** in the SLB. In addition, it was curious to observe that a SLB bearing 0.01% of lipopeptide **1** (dark pink profile) did not generate any cell adhesion under our experimental conditions.

Although QCM-D is a technique very sensitive to changes in mass adsorbed on the surface of the sensor, the calculation of the mass uptake on the sensor using both Sauerbrey and Voinova modeling has certain limitations. In that, the sensitivity of the measured Δf versus the calculated Δm (by Voinova model) depends on the thickness of the adsorbed bilayer. In general, the higher the harmonic number, the shorter the decay length of the resonating wave, e.g. being around 250 nm in water for the 5MHz frequency f_1, it is no more than 100 nm for f_7.[33,34] Accordingly, for an entire cell attached to a surface, the height of the protuberant cell nucleus (typically in the micrometer range) greatly exceeds the penetration depths of the resonating waves of the quartz crystal.[35] Thus, estimation of the mass of the adhered cells by application of the Voinova model is frequently avoided as it can lead to significant errors.

2.1.4.2 Optical Microscopy to visualize the adhered cells

Optical microscopy done in parallel to the QCM-D measurements revealed that cells interacting with a bilayer bearing 0.1 % of the lipopeptide **1**, clearly adhered to the surface and adopted spheroid morphology with no filapoidal extensions. Thus, at this ratio of lipopeptide **1** in the bilayer, the cells adhered, while having a diameter of 15 to 20 μm but did not spread as seen in Figure 2.8.

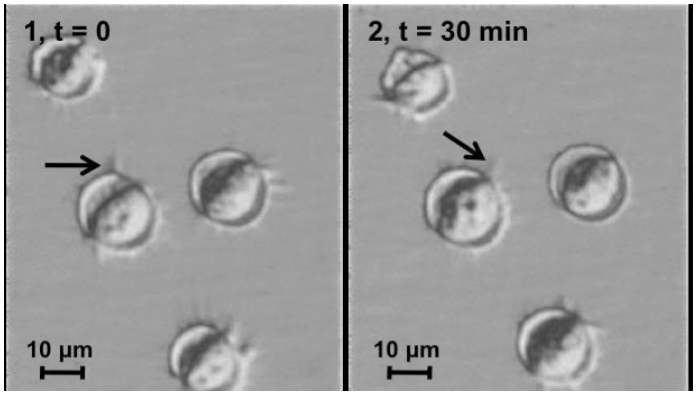

Figure 2.8 Optical microscopy images of cells adhered on a SLB prepared from 0.1% lipopeptide **1** bearing vesicles.

The cell adhesion process on a 0.1% lipopeptide bearing SLB can thus be envisaged as demonstrated in Figure 2.9.

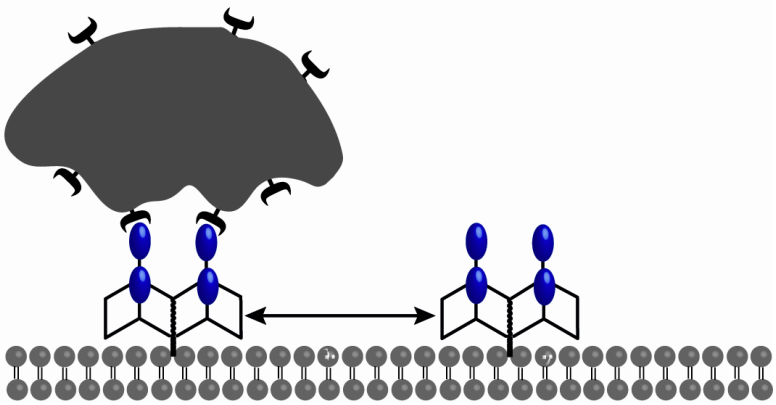

Figure 2.9 Cartoon representation of the cell-adhesion process on a 0.1% lipopeptide 1 bearing SLB. The black protrusions coming out of the cell are representing the $\alpha_v\beta_3$ integrins.

A completely different behavior was observed when testing cell adhesion onto a SLB displaying 1% of lipopeptide **1**. In this case, the β3 cells not only adhered but also assumed a flattened morphology with a diameter of about ~ 40 μm with filapoidal extensions (Figure 2.10). Moreover, the cells were able to move on the fluid surface. These results indicate that the adhesion of cells to a 1% lipopeptide **1** bearing SLB leads to the formation of actin stress fibers in the cells and strongly suggest that the *c*RGD motifs induce integrin-mediated tyrosine phosphorylation.[36]

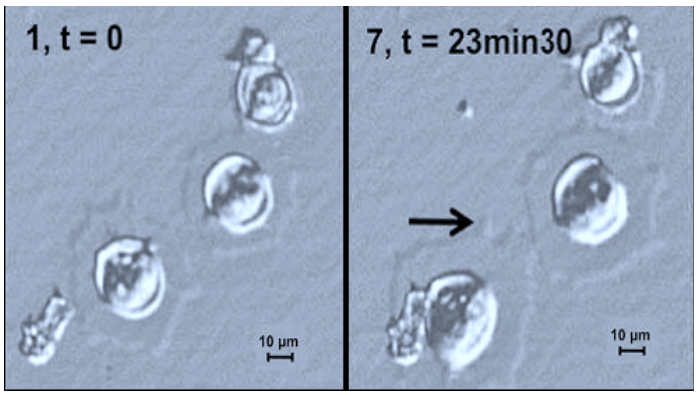

Figure 2.10 Optical microscopy images of cells adhered and on a SLB presenting 1% of the lipopeptide **1**.

The cell adhesion process on a 1% lipopeptide bearing SLB can be best illustrated by the cartoon presented in Figure 2.11.

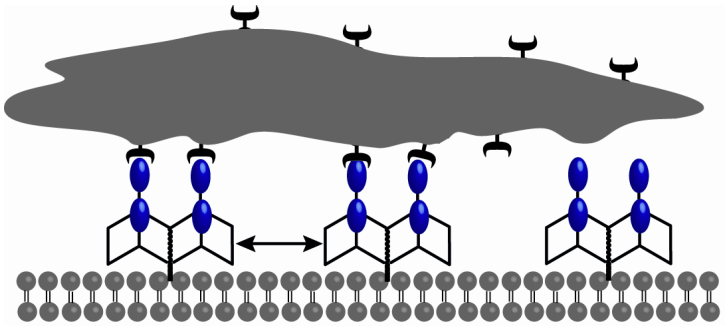

Figure 2.11 Cartoon representation of the cell-adhesion process on a 1 % lipopeptide 1 bearing SLB. The black protrusions coming out of the cell are representing the αvβ3 integrins.

To investigate this difference in the cell adhesion pattern between SLBs displaying increasing concentrations of the lipopeptide **1**, we estimate the interligand spacing of the lipopeptide **1** in these SLBs.

To estimate this, knowing that lipopeptide **1** is fully mixed in the SLBs (from AFM imaging, section 2.1.3.2), we assume that each molecule is organized in such a way that it can be envisaged to be placed at the centre of a square having sides L as described in Figure 2.12.

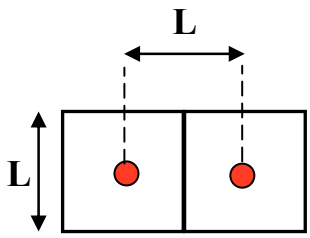

Figure 2.12 Diagram representing the ligand in red dots placed at the center of a square having sides L.

In this case, L (the interligand spacing) would then be defined as $\mathbf{L = (\sigma/R)^{1/2}}$

Where, L = sides of the square (interligand spacing), σ = surface occupied by one molecule of phospholipids and R = the concentration ratio between the two species (for a 1% lipopeptide bilayer R will be 0.01).

The ligand density would be defined as **D = 1/A**, where A = area of the square which is L^2

Thus, $\mathbf{D = 1/(\sigma/R) = R/\sigma}$

The area occupied by a molecule of phospholipids in its fluid state is known to be 0.7 nm^2.[37]

Thus for a 1% lipopeptide bilayer, R will be = 0.01, and the interligand spacing L will be 8.4 nm whereas the ligand density will be 14 300 ligands μm^{-2}. Similarly, the values of L and D estimated for other SLBs doped with different ratios of lipopeptide **1** are listed in Table 2.1.

Thus, it is worth concluding that in a SLB bearing 0.01 % lipopeptide where no cell adhesion is observed, the interligand spacing of 84 nm is too distant to induce cell adhesion. Similarly, for a 0.1% and 1% lipopeptide **1** bearing SLBs the interligand spacing is ~26 nm and ~8.4 nm respectively. It appears that the 26 nm interligand distance in bearing 1430 ligands μm^{-2} (0.1%) was sufficient to induce cell adhesion but rather too spaced out or insufficient to trigger the formation of filapoidal extensions or actin stress fiber formation. Whereas, an interligand spacing of ~8.4 nm with a ligand density of 14 300 ligands μm^{-2} (1% lipopeptide **1**) could induce both cell adhesion and cell spreading.

Table 2.1 Indicating the interligand spacing L and the ligand density D for SLBs doped with various ratios of lipopeptide 1, and the cell adhesion response observed for each SLB.

% Lipopeptide **1** in the SLB	Interligand spacing L (nm)	Ligand density D (ligands μm^{-2})	Cell adhesion
0.01	~84	143	No cell adhesion
0.1	~26	1430	Adhesion, no spreading and actin fiber formation
1	~8.4	14300	Adhesion with spreading and actin fiber formation

It is worth noting that the ligand spacing where we observe this effect 8.4 nm), is significantly smaller than those reported for solid surfaces (~20–140 nm).[38-42] For instance, a ligand-to-ligand spacing of 140 nm was necessary for $\alpha_v\beta_3$ integrin -mediated actin stress fiber organization in human foreskin fibroblasts.[42] Our result is not entirely

surprising since the differences in the physical properties of a rigid and a fluid surface (out-of-plane mobility, membrane tension) affect cell adhesion.[43] The RGD ligand is not covalently bound to the substrate surface, therefore receptor mediated removal of adhesion ligands from the substrate surface is possible. In this context, formation of focal contacts *via* extensive stress fiber formation required higher RGD ligand concentration. Others parameters such as the cell line used and the peptide ligand could also influence the cell response. We also investigated cell adhesion for a lower ligand concentration (molar ratio of 0.1% and interligand spacing of ~ 26 nm). In these conditions, the HEK cells adopted spheroid morphology (~15–20 μm in diameter) with no filapoidal extensions. This result indicates that at this low concentration, ten fold lower than that necessary for cell spreading, the RGD-containing lipopeptide **1** solely promotes cell attachment on the surface.

2.1.5. Design and synthesis of phospholipid cRGD conjugate.

As seen in Figure 2.13 the phospholipid *c*RGD conjugate (PL-*c*RGD) is composed of, besides the *c*RGD unit, a phosphate group that is negatively charged and linked through a glycerol backbone to two palmitoic acid groups. A phospholipid was chosen here as opposed to the lipopeptide **1** where simple palmitoyl chains were used for two principal reasons. The first one being an anticipation of better incorporation of the conjugate in POPC vesicles, due to the similarity in their head groups. Secondly, the PL-*c*RGD conjugate as compared to the lipopeptide **1** has only one cyclopentapeptide group. Consequently, this conjugate is less polar in its peptide region and hence, adding a phospholipid would ease its solubility in polar solvents.

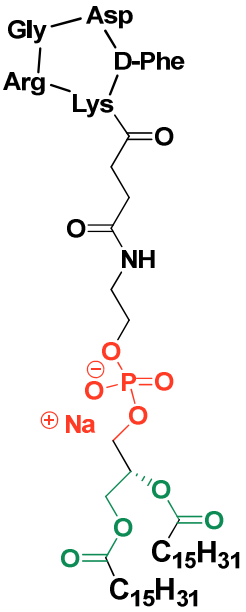

Figure 2.13 Structure of the phospholipids cRGD conjugate (PL-cRGD). The phosphate group is colored red, the glycerol backbone green.

The synthesis of the *c*RGD pentapeptide sequence was effectuated by solid phase peptide synthesis (SPPS) as described in scheme 2.1. The linear peptide sequence was constructed on an acid labile 2-chlorotritylresin®, the use of this resin for SPPS permitted the protection of amino acids by groups such as Pmc, O*t*Bu, Alloc and amino acids side chains such as arginine, aspartic acid and lysine. The functionalization of the resin was initiated using an achiral amino acid like glycine at its C-terminal to avoid epimerization during cyclization. The linear peptide sequence **2** was then cyclised in DMF under diluted conditions (5×10^{-4} M) in the presence of PyBOP giving the protected cyclic pentapeptide **3**.

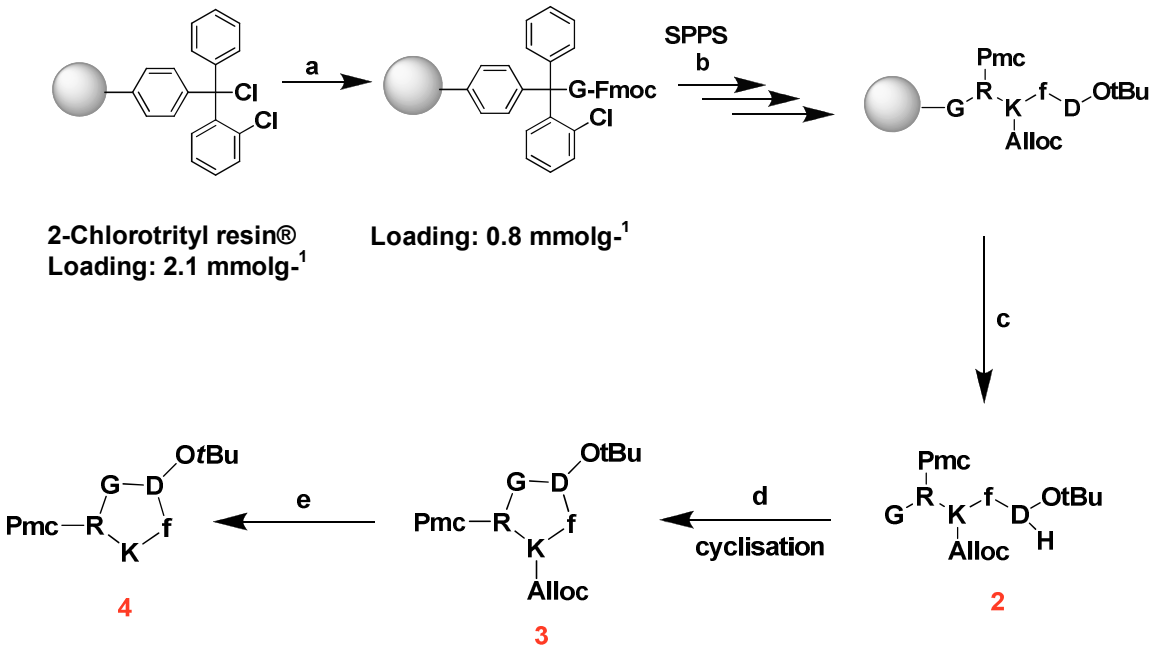

Scheme 2.1 Scheme of the solid phase peptide synthesis of the protected cRGD unit: (a) 0.6 equiv of Fmoc-Gly-OH, DIPEA, anhyd. DCM;
(b) SPPS: (i) Piperidine: DMF (1:4); (ii) 2 equiv. of Fmoc-Xaa-OH, 2 equiv. PyBOP, 3-4 equiv. DIPEA, DMF;
(c) (1) Piperidine: DMF (1:4); (2) TFA: CH_2Cl_2 (1:99)
(d) 1.2 equiv PyBOP, 3-4 equiv, of DIPEA, DMF
(e) $Pd(PPh_3)_4$, $PhSiH_3$, CH_2Cl_2

To now access the lysine group of the cyclo peptide **3**, the Alloc group was reductively deprotected using Pd^0 as a catalyst. The reaction was carried out using $Pd(PPh_3)_4$ along with a large excess of phenylsilane which acts as a hydride donor and also helps in trapping the π-allyl-palladium adduct which is an intermediate in the reaction. The reaction typically lasts for an hour, after which the volatiles were evaporated and the peptide was precipitated in ether to give **4**. Besides washing the precipitate repeatedly with ether, the molecule was not purified any further at this step.

The coupling of **4** with a succinyl derivative of 1,2-dipalmitoyl-*sn*-glycero-3-phosphoethanolamine **(5)** was effectuated using PyBOP as described in scheme 2.2; the protected intermediate thus obtained was precipitated in ether and washed several times with ether to remove the unreacted reactants. This protected intermediate was then deprotected in one pot using trifluoroacetic acid and product **1** was purified on a preparative TLC. The detailed protocol of the complete synthesis and characterization of the intermediates is described in detail in the experimental section 2.1.9.

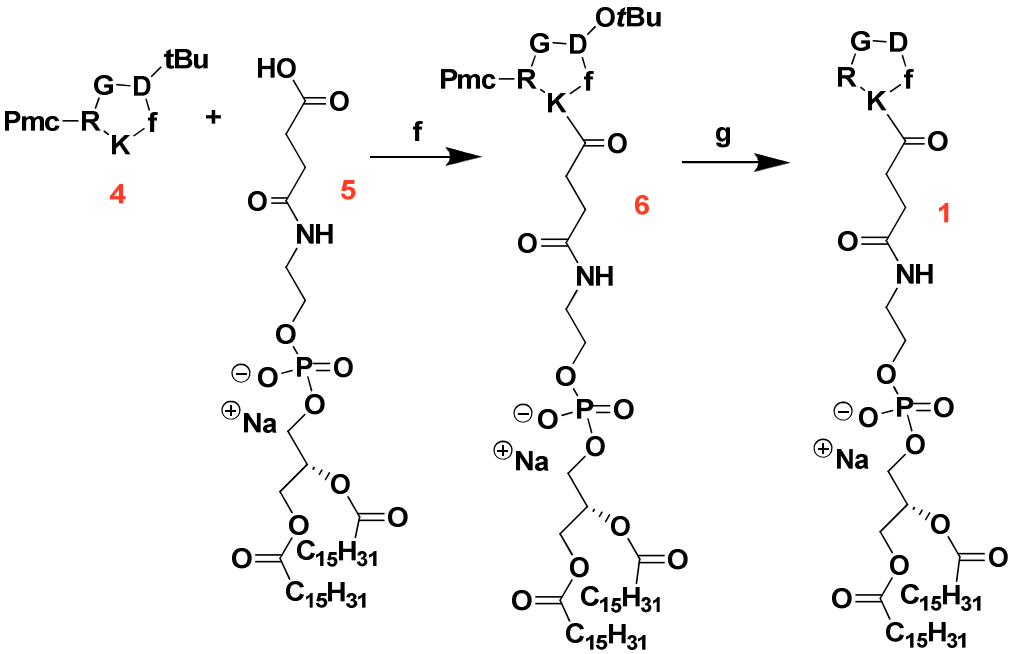

Scheme 2.2 Scheme of synthesis of phospholipid *c*RGD (PL-*c*RGD) conjugate. (f) 2 equiv. of PyBOP, 3-4 equiv. of DIPEA, DMF; (g) TFA: H_2O: TIS 95: 2.5: 2.5.

2.1.6. Preparation of SUVs bearing PL-*c*RGD and formation of SLB

Small unilamellar vesicles containing PL-*c*RGD were prepared as described earlier in section 2.1.2. Monodispersed vesicles of size 30 nm as measured by DLS were obtained. These vesicles were diluted to a working concentration of 0.2 mg/ml, and stored at 4 ºC for until about 3 weeks.

The SLB formation of vesicles bearing 1% PL-*c*RGD was followed by QCM-D as shown in Figure 2.14. The fusion behavior of 1% PL-*c*RGD containing vesicles was similar to that observed for pure POPC vesicles indicating that the presence of the negatively charged PL-*c*RGD at this particular concentration did not influence the fusion behavior of the vesicles.

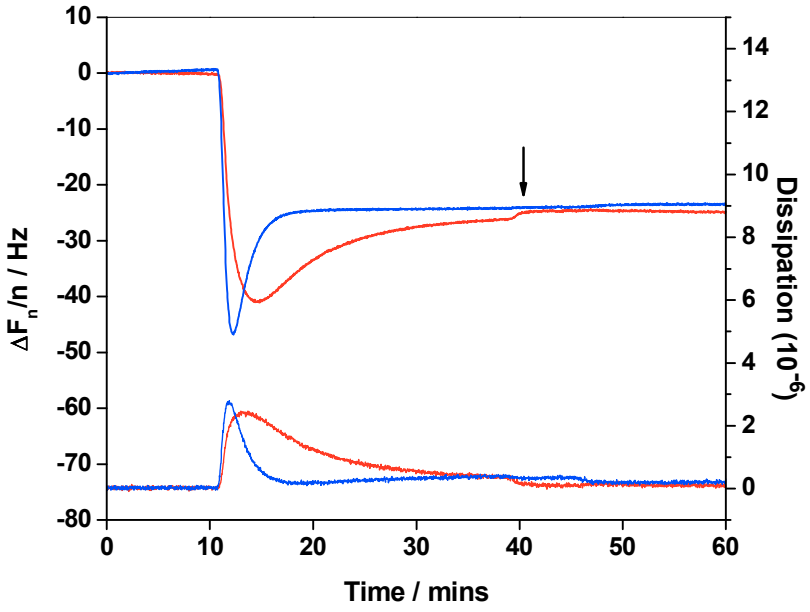

Figure 2.14 Fusion of vesicles made from pure POPC (blue curve) and 1% PL-cRGD (red curve) on a SiO_2 surface as observed on the 7th harmonic by QCM-D. The left axis represents the normalized frequency and the right axis represents the Dissipation. The arrow indicates the rinsing with buffer.

Figure 2.14 shows the fusion profile of POPC vesicles (blue) and 1%PL-*c*RGD doped vesicles (red). The final shifts in frequency and dissipation after rinsing were found to be $\Delta F_n/n = -23.5$ Hz and $\Delta D_n = 0.18 \times 10^{-6}$ for POPC SUVs and $\Delta F_n/n = -24.6$ Hz and $\Delta D_n = 0.12 \times 10^{-6}$ for 1%PL-*c*RGD containing SUVs. These values clearly indicate the formation of a perfect SLB with both POPC and 1%PL-*c*RGD containing POPC vesicles. Moreover, the SLBs obtained from both pure and doped SUVs are quite rigid in nature as suggested by the small shift in dissipation.

2.1.7. Test of cell adhesion of HEK-β3 cells on a SLB bearing PL-*c*RGD.

Cell adhesion studies were performed with HEK-β3 cells on both SLBs of pure POPC and of POPC doped with 1% PL-*c*RGD. Clearly, no interactions (non-specific) of cells was observed on SLB made of pure POPC, however a clear decrease in frequency and increase in dissipation was observed on 1% PL-*c*RGD doped SLB, as seen in Figure

2.15. This signifies that the presence of monovalent cRGD functionalized phospholipids within the SLB was capable of inducing $\alpha_v\beta_3$ integrin mediated cell adhesion.

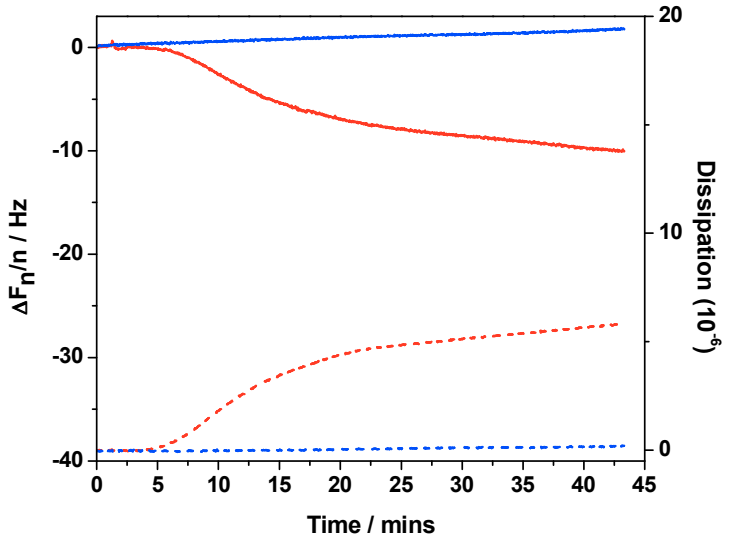

Figure 2.15 QCM-D profile for the adhesion of HEK-β3 cells on SLBs made from 1% PL-*c*RGD (red curve), and pure POPC (blue). The solid lines represent the frequency shift (left axis) and the dashed line represent the shift in dissipation (right axis) as measured on the 9th harmonic. Cell suspension (100 000cells mL^{-1} were injected at 100 µL/min.

Moreover, it is interesting to observe that the shifts in frequency and dissipation observed for adhesion of cells to a 1% PL-*c*RGD bearing SLB are quite comparable to that observed for a 1% lipopeptide **1** bearing SLB **(***cf.* cyan curve in Figure 2.7 and red curve in Figure 2.15). This observation could be explained by the fact that the diameter of a *c*RGD ligand is about 3 nm, whereas that of the $\alpha_v\beta_3$ integrin is approximately 10 nm. Thus by geometric/steric constraints each lipopeptide **1,** although being multivalent, can bind to only one $\alpha_v\beta_3$ integrin. Hence, the cell adhesion induced by a SLB bearing 1% PL-*c*RGD is comparable to that by 1% lipopeptide **1.**

Further studies by optical microscopy to reveal the morphology of the adhered cells on SLBs bearing varied concentrations of the PL-*c*RGD are still underway. Hence, it would be a bit too early to comment further on the influence of the PL-*c*RGD in the bilayer on the morphology of the adhered cells. Nevertheless, upon comparison of these initial results described for both lipopeptide **1** and PL-*c*RGD, they are quite indicative of a 1:1 interaction between both a single *c*RGD unit as in PL-*c*RGD or multiple *i.e.* 4- *c*RGDs as in the case of lipopeptide **1**.

2.1.8. Conclusion and Perspectives

In the present work, we successfully demonstrate the use of SLBs for studying cell adhesion of HEK-293 (β3) cells induced by *c*RGD based ligands. The inertness of bare SLBs to cells or proteins served as a great asset to the present study. Moreover, the use of two complementary techniques like QCM-D and optical microscopy helped distinguishing between round cells with no filapoidal extensions and spread (flattened) cells with the formation of actin stress fibers. An interesting trend in the cell adhesion behavior was observed at increasing concentrations of the lipopeptide **1**. This phenomenon helped us in estimating the critical RGD concentration required for cell attachment and for cell spreading upon attachment. While cell attachment required ~1430 ligands μm^{-2}, cell spreading was found to occur at a concentration of ~14,300 ligands μm^{-2}. This value corresponding to an interligand spacing of ~10 nm is found to be remarkably low as compared to that reported earlier for non-fluid systems. We also demonstrate here that the *c*RGD ligand is specific to HEK-293 (β3) cells, *i.e.* the $\alpha_v\beta_3$ integrin and does not interact with HEK-293 (β1) *i.e.* $\alpha_v\beta_1$ integrin.

To deconvolute, if any, the effects of multivalency presented by the lipopeptide **1** bearing 4 *c*RGD ligands, we synthesized a phospholipid- *c*RGD conjugate (PL-*c*RGD). Very preliminary results of cell adhesion with this molecule reveal that the interactions are essentially 1:1 *i.e.* each integrin can bind only 1 ligand in both cases. Nevertheless, the effect of this PL-*c*RGD ligand on the morphology of the adhered cells still needs to be evaluated. The present results suggest that SLBs bearing 1% of RGD bearing ligands can serve as potential model systems for further exploiting cell adhesion studies.

2.1.9. Synthetic protocols

2.1.9.1 General procedure for synthesis of linear protected peptides by SPPS

Assembly of all linear protected peptides was performed manually by solid-phase peptide synthesis (SPPS) using the standard 9-fluorenylmethoxycarbonyl/tertiary-butyl (Fmoc/*t*Bu) protection strategy. The device consisted of a glass reaction vessel fitted

with a sintered glass. The latter allowed elimination of excess reagents and solvents under the pressure of compressed air. Before use, the glass vessel was treated (typically overnight) with $(CH_3)_2SiCl_2$ to render the glass hydrophobic and prevent the resin beads from sticking to the walls of the container during the synthesis. It was then carefully washed with CH_2Cl_2 until complete removal of acid. At the beginning of the synthesis and after each wash with ether, the resin was washed and swollen twice with DCM (20 mL/g resin) for 15 min and once with DMF (20 mL/g resin) for 15 min. DMF used for the synthesis was degassed under argon for 1 h.

2.1.9.2 Coupling of the N^{α}-Fmoc-protected amino acids.

Coupling reactions were performed using, relative to the resin loading, 1.5-2 equiv. of N^{α}-Fmoc-protected amino acids which where activated in situ with 1.5-2 equiv. of PyBOP and 3-4 equiv. of DIPEA in DMF (10 mL/g resin) for 30 min. The resin was then washed twice with DMF (20 mL/g resin) for 1 min and twice with DCM (20 mL/g resin) for 1 min.

2.1.9.3 Cleavage of the N^{α}-Fmoc-protecting group

N^{α}-Fmoc protecting groups were removed by treatment with piperidine/DMF (1:4) (10mL/g resin) for 10 min. The process was repeated three times and the resin was then washed five times with DMF (10 mL/g resin) for 1 min. The completeness of the deprotection was checked by UV measurement. The release of Fmoc groups afforded dibenzofulvene whose adduct with piperidine absorbs light in the UV range (λ = 299 nm, ε = 7800 $M^{-1}cm^{-1}$). Cleavage and washing solutions were thus collected together and the volume of the solution was adjusted to a known value (V) with MeOH. Quantification of the absorbance of this solution at 299nm gave the number of Fmoc protecting groups released from the cleavage according to the Beer-Lambert relation.

$$\mathrm{nFmoc} = \frac{\mathrm{OD}(299\mathrm{nm}) \times \mathrm{V}}{\varepsilon(299\mathrm{nm}) \times \mathrm{l}} \quad \text{(l: length of the optical path)}$$

This method was employed before each coupling of an amino acid to follow the SPPS and to determine, in an indirect manner, the loading of the resin.

2.1.10. Cleavage of the peptide sequence from the resin

Synthetic linear peptide sequence was recovered directly upon repeated acid cleavage of the resins according to the following conditions: 1% TFA in DCM with the volume adjusted to10 mL/g resin for 5 min. This procedure was repeated 3 times

The combined washings were concentrated under reduced pressure and the crude linear peptide sequence was obtained by precipitation and triturating from ether. The peptides were analyzed by RP-HPLC and, if necessary, purified on a preparative column.

2.1.10.1 Cyclization reactions of linear peptides in solution

C- and N-termini deprotected linear peptides were dissolved in DMF (at a concentration of 0.5 mM) and the pH of the solution was adjusted to 8-9 by addition of DIPEA. PyBOP (1.2 eq.) was added and the solution was stirred at r.t. for at least 1 h. The solvent was removed under reduced pressure and the residue dissolved in the minimum of CH_2Cl_2. Ether was added to precipitate the peptide. The latter was triturated and washed three times with ether affording crude material, which was used without additional purification.

2.1.10.2 Deprotection of the Alloc group

N^{ε}-Alloc protecting groups were removed by dissolving the peptide in anhydrous DCM and anhydrous DMF (3:1) followed by the addition of phenylsilane (25 eq.) and $Pd(PPh_3)_4$ (0.25 eq.) and stirring for 1 h at r.t under argon. The mixture was then treated with methanol before evaporation of the solvents under reduced pressure. The product was washed with ether and used as such without further purification.

Synthesis of H-D(O*t*Bu)-f-K(Alloc)-R(Pmc)-G-OH (2)

The linear peptide **2** which was assembled on a 2-chlorotritylchloride® resin (1.005 g, loading of 2.1 mmol.g-1). The anchoring of the first amino acid (Fmoc-Gly-OH) through nucleophilic substitution was performed following the procedure given by Advanced ChemTech as described in 2.1.9.2 and yielding to a convenient resin loading of 0.8 mmol g^{-1}. The peptide was released from the resin following the protocol described in 2.1.10. The free linear protected peptide was obtained as a white solid powder (980.4 mg) after precipitation, triturating and washing in ether. This crude material was used without additional purification.

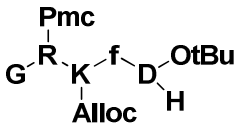

2

RP-HPLC: RT = 11.1 min (C18, 214 nm and 250nm, 5-100% B in 15 mins)

$C_{49}H_{73}N_9O_{13}S$

Calcd MW = 1027.5 g.mol-1

Synthesis of c[-R(Pmc)-G-D(O*t*Bu)-f-K(Alloc)-] (3)

The cyclization reaction was carried out on the linear peptide **2** (980.4 mg) as described in section 2.1.10.1 The cyclic peptide **3** was obtained as a white solid powder (1162.5 mg) after precipitation in ether. The crude material was further used without additional purification.

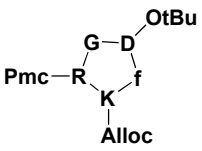

3

RP-HPLC: RT = 11.9 min (C18, 214 nm and 250 nm, 5-100% B in 15 mins)

$C_{49}H_{71}N_9O_{12}S$

Calcd MW = 1009.5 $g.mol^{-1}$

Synthesis of c[-R(Pmc)-G-D(O*t*Bu)-f-K(H)-] (4)

Alloc group was removed from the cyclic peptide **3** (1162.5 mg) following protocol 2.1.10.2. The peptide **4** was obtained as a slightly brown solid powder (819.8 mg) after precipitation in ether. The crude material was used without purification.

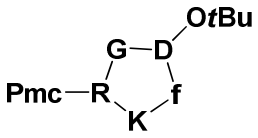

4

RP-HPLC: RT = 10.0 min (C18, 214 nm and 250 nm, 5-100% B in 15 min)

$C_{45}H_{67}N_9O_{10}S$

Calcd MW = 925.5 g.mol-1

Synthesis of 1,2-dipalmitoyl-*sn*-glycero-3-phosphoethanolamine-N-c[-R(Pmc)-G-D(O*t*Bu)-f-K(H)-]-succinamide (6)

The partially deprotected cyclopeptide **4** (10 mg, 0.011 mmol) was added to a DMF: CH_2Cl_2 2:1 solution of **5** (8.78 mg, 0.011 mmol) containing PyBOP (11.45 mg, 0.022 mmol) and DIPEA (2.84 mg, 0.033 mmol). The reaction was allowed to stir overnight followed by evaporation of DMF under reduced pressure. The product **6** was purified by precipitation using a solvent mixture of hexane:ethylacetate 95:5 by gentle heating and gradual cooling.

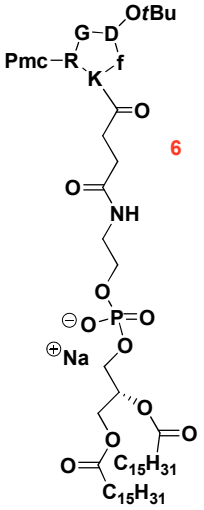

6

Yield : 12 mg, 63%

$C_{86}H_{144}N_{10}O_{21}PNaS$

Calcd. MW = 1721

Found MW (negative mode)= 1698.5 [M-Na^-]

Synthesis of 1,2-dipalmitoyl-*sn*-glycero-3-phosphoethanolamine-N-c[-R-G-D-*f*-K(H)-]-succinamide sodium salt (1)

The Pmc and *t*Bu groups were removed by treating a DMF: CH_2Cl_2 3:1 solution of **6** (10 mg) with a mixture of TFA: TIS: H2O 95:2.5:2.5. The reaction was stirred for 3 hours after which the solvents were removed under reduced pressure. The crude product was purified on a preparative TLC using $CHCl_3$: MeOH: CH_3COOH (80: 10: 10) to afford **1**.

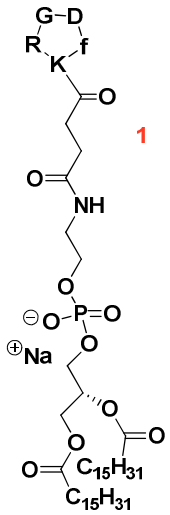

Yield : 3 mg, 37%

$C_{86}H_{144}N_{10}O_{21}PNaS$

Calcd. MW = 1398

Found MW (negative mode)= 1375.9 [M-Na^-]

2.2. Incorporation of FhuA in SLBs to Monitor its Interaction with pb5 by QCM-D

The study of transmembrane/membrane proteins in controlled non-native environments is a subject of intense scientific interest that researchers have explored over the past few decades.[44,45] Towards this goal, artificial lipid bilayers have always stood out as the most consistent models for the study of membrane proteins.[46,47] Incorporation of a membrane protein to these systems imparts a lateral mobility to the protein, which is favorable as it renders environments similar to that of the cell membrane. [48,49] Although, between a solid supported lipid bilayer (SLB) and a tethered bilayer lipid membrane (tBLM), the latter is found to be well suited for the incorporation and study of membrane proteins bearing large extra-membranous domains. Nevertheless, SLBs have still demonstrated to be useful systems for studying proteins bearing rather small extra-membrane domains.[50-53]

In the present work, we describe our attempts towards the incorporation of FhuA (an *E.coli* outer membrane protein, *cf.* section 1.2.2) into SLBs of POPC on SiO_2. FhuA as described in section 1.2.2 is a ferrichrome transporter in *E.coli*. Its crystal structure was first solved by Ferguson *et al.* in its bound state with LPS (an outer membrane lipid *cf.* section 1.2.2) and later in its unliganded (free) state by Locher *et al.*, both these structures demonstrated that FhuA possesses a hydrophobic domain of 2.5 nm thick.[54-56] As can bee seen in Figure 2.16, the crystal structure of FhuA suggests that the periplasmic part of FhuA is quite small (>1 nm) as compared to the hydrophilic part or the extracellular loops. Furthermore, the thickness of a SLB obtained from POPC at room temperature is found to be 4 nm.[57,58] Hence, the incorporation of FhuA within bilayers made of POPC could be envisaged considering the small periplasmic domain of the protein. One could also assume that the periplasmic domain would not be hugely hindered by interactions with the surface, as the hydration layer of the SLB (1-2 nm) would eventually be big enough to accommodate it.

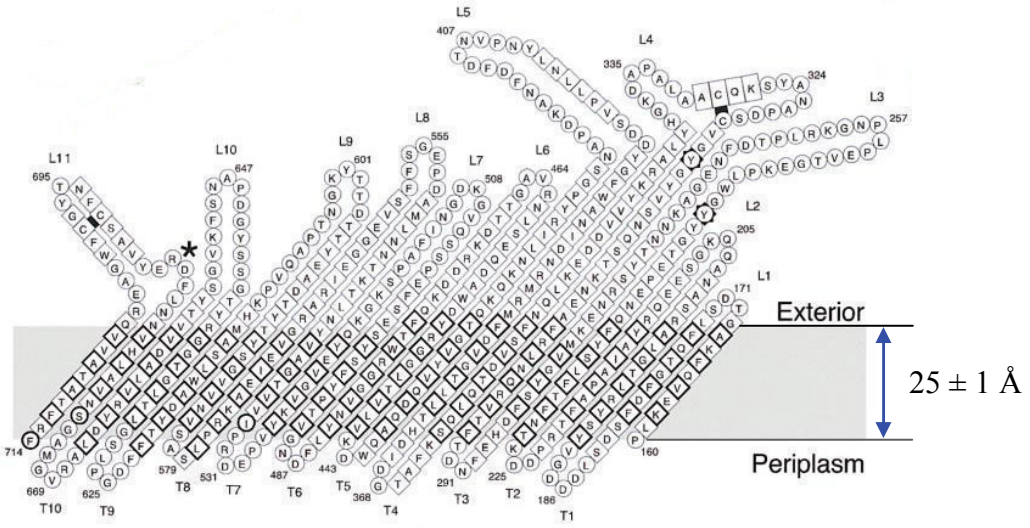

Figure 2.16 Topology of the β-barrel porin FhuA as described by Locher et al.[56] The grey region represents the hydrophobic domain. L and T have been referred to extracellular loops and periplasmic turns, respectively. Residues are framed according to their secondary structure: β strands (diamonds), α helices (rectangles), loops or turns (circles); thick frames indicate residues that are exposed to the lipid bilayer (gray shading). The two disulfide bridges (in L4 and L11) are shown in black.

As discussed in section 1.2.2, the infections of the gram-negative bacteria like *E.coli* by the bacteriophage T5 is initiated by the recognition of the host receptor, the outer membrane protein FhuA by the receptor binding protein of the phage pb5. Although, most of the binding properties of FhuA with its ligands (Ferrichrome, TonB) have been extensively studied, little is known still about its molecular interactions with the phage proteins.

Studies involving the incorporation of purified FhuA into liposomes and its interaction with the phage T5 by cryo-electron microscopy and fluorescence measurements clearly demonstrated the transfer of the phage DNA into the liposomes. [59-61] This suggested that FhuA incorporated in liposomes was still active and interacted with the phage. Further, the structural analyses done by J. Böhm *et al.* ice-embedded T5 phages docked on FhuA containing liposomes were studied by cryo-electron microscopy. Because of their results, they concluded on a plausible mechanism of the interaction of phage T5 with membrane embedded FhuA as shown in Figure 2.17. The accepted mechanism of phage infection is the interaction of pb5 (located at the distal end of the straight fiber of the phage) with FhuA. This interaction would induce conformational changes, transmitted along the tail- by pb2 (pb2 is the tape measure protein of the phage) up to the capsid, allowing its opening and the release of the DNA. Simultaneously, the distal domain of pb2, probably forming most of the straight fiber would perforate the cell wall, constituting a channel

allowing the DNA into the cell cytoplasm.[62] This proposition was reinforced by earlier observations by Bonhivers *et. al.* which showed that the FhuA channel is still accessible to transport ferrichrome even after binding to the phage T5.[63] This indicates that the T5 straight fiber would not be inserted into the channel of FhuA but rather penetrates through the bilayer. They thus describe the straight fiber strand (bearing the pb2) to be like a "DNA injection needle".

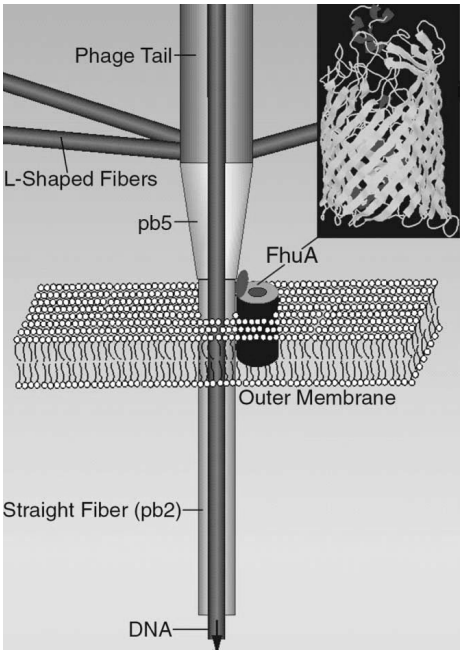

Figure 2.17 Cartoon illustrating the mechanism of phage T5 interacting with FhuA in a liposome as proposed by Böhm *et al.*[61]

Enticed by these interesting results of the initial interaction studies, we were keenly inquisitive to pursue these interaction studies. Thus, in collaboration with Dr. Cécile Breyton (Institut de Biologie Structurale, Grenoble) who provided us with both FhuA and pb5, we ventured upon investigating the interactions between FhuA and pb5. Our approach to these studies was from perspectives of physical chemistry; In that our pursuit was oriented towards quantifying the affinity between FhuA and pb5, using physico-chemical techniques like QCM-D, AFM and Impedance spectroscopy.

However, the results presented in this chapter are an outcome of one of the most recent activities in the group. Hence, this chapter will describe the rather initial, yet well-characterized results towards the incorporation of FhuA into SUVs, their characterization

by DLS, their fusion behavior on SiO_2 substrates and the interactions of the bilayers bearing FhuA with pb5.

2.2.1. Preparation of proteoliposomes containing FhuA

FhuA bearing proteoliposomes were prepared by slow evaporation of 10 μL of a chloroform solution of POPC (10 mg/ml) in a glass vial using a gentle stream of nitrogen. Upon complete evaporation of chloroform, the glass vial was kept under reduced pressure for 1 hour to remove the traces of chloroform. This was followed by the addition of an appropriate volume of FhuA (from a 41.3 μM stock solution containing 2.2 μM LDAO) and the final volume was made up to 50 μL with a 2 mM LDAO solution in buffer containing 10 mM HEPES, 150 mM NaCl, 1 mM $MgCl_2$ at pH 7.4. LDAO (Lauryldimethylamine *N*-oxide is a zwitterionic surfactant of cmc_{H2O} ~ 1mM). Vigorous vortexing of this dispersion gave an almost clear suspension indicating the formation of mixed micelles of POPC and LDAO. This was confirmed by DLS measurements section 2.2.2.

This was followed by the addition of 0.5 mg of Biobeads (SM2 BioRad) and agitation for 3 hours. (Detailed protocol on the use of Biobeads is described in the experimental section 2.2.6). After this period, the biobeads were renewed in the solution and 50 μL of the buffer was added to dilute the LDAO close to its cmc and to have a concentration of 0.1 mg/ml of liposomes. This mixture was agitated overnight at 4 ºC. The solution, at this concentration was observed to be turbid after this time. It was further diluted to have a concentration of 0.03mg/ml for DLS measurements.

These proteoliposomes were extruded through a 50 nm polycarbonate membrane on a mini extruder (Avanti Polar) at a concentration of 0.1 mg/ml. The detailed procedure adopted for extrusion is described at the end of this chapter.

2.2.2. Dynamic Light Scattering (DLS) measurements to characterize the proteoliposomes formation

DLS measurements were performed to follow the vesicle formation by the biobeads method. The measurements were done on sample with a protein: lipid ratio 1:750 as well as with POPC liposomes, both before and after the addition of biobeads. The DLS data are represented as double Y axis plots, where the time-intensity correlation is plotted on the left axis, whereas the decay time distribution is plotted on the right axis (both as functions of time). The decay time constant was calculated using the Contin software.[64] Figure 2.18A shows the DLS data for the FhuA containing sample before treatment with Biobeads. From this curve, it is clearly observed that the correlation function (asterix symbols) shows two decorrelations, indicating the presence of two sized species. This observation is confirmed in the decay time distribution curve (circle symbols), which clearly showed the presence of two peaks (maxima) with very different time constants (Γ^{-1}).

These time constants were then transformed into the diffusion coefficient using equation (1.11) in section (1.4.3). From these diffusion coefficients, the hydrodynamic radii (R_h) corresponding to each peak can be estimated using the Stokes-Einstein equation as shown in equation (1.13) in section 1.4.3. The time constants associated with each peak and the corresponding calculated R_h values are listed in Table 2.2 Among the two peaks observed here the one corresponding to the smaller time constant (R_h = 3.34 nm) was found to be the major one.

Similar measurements were done on this sample after treatment with biobeads, the single decorrelation (Figure 2.18B, asterix symbols, left axis) as well as a single decay time constant (red peak, circle symbols) are suggestive of the dominance of single sized species. Moreover, the decay time (Γ_3^{-1}) observed after treatment with biobeads was found to increase significantly from that of the major peak observed (Γ_1^{-1} before biobead treatment as compared in Figure 2.18A and B). This peak observed (Γ_3^{-1}), although quite broad was found to be a single peak. The hydrodynamic radius calculated for this peak (Table 2.2) was found to be 114 nm. This drastic increase in R_h upon treatment with biobeads suggested the successful formation of proteoliposomes.

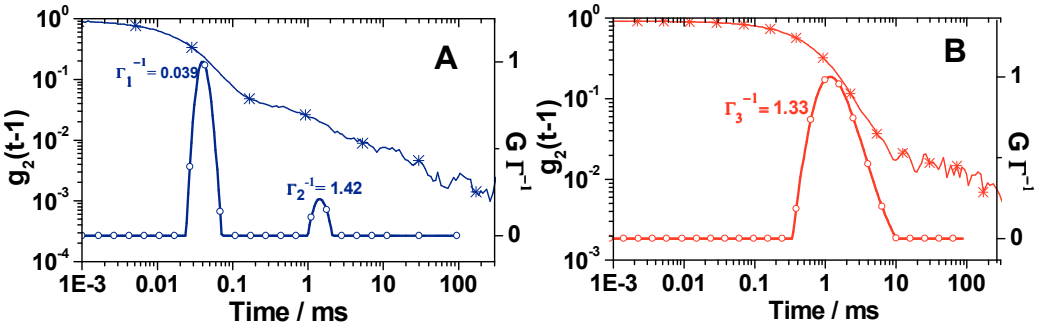

Figure 2.18 DLS measurements performed on a sample containing lipid: protein ratio 1: 750 before (A) and after interaction with biobeads (B). The left axis denotes the time intensity correlation functions and the right axis presents the decay time distributions. The curves with asterix symbols correspond to the correlation function for the samples measured. The curves with circle symbols represents the correlation function for sample measured. All the samples were measured at a concentration of 0.03 mg/ml of POPC. The dispersions were transparent at this concentration.

Table 2.2 Table indicating the measured decay time and the calculated hydrodynamic radius Rh for the sample mixtures before and after treatment with biobeads.

Sample	Decay time Γ^{-1} (ms)		Hydrodynamic Radius R_h (nm)	
FhuA : POPC 1:750 Before Biobeads	Γ_1^{-1} = 0.039	Γ_2^{-1} = 1.42	3.34	121
FhuA : POPC 1:750 After Biobeads	Γ_3^{-1} = 1.33		114	
Pure POPC after biobeads	Γ_4^{-1} = 0.84		72	

Similar measurements were done on POPC liposomes, prepared by treatment with Biobeads method (data plots not shown). These measurements showed the presence of a single peak (Γ_4^{-1}) for the decay time constant (Table 2.2). This peak was found to be also quite broad as for the proteoliposomes, and the calculated R_h was 72 nm.

Thus, in summary for a mixture of POPC: FhuA and LDAO (before treatment with Biobeads) a major peak (narrow) corresponding to a calculated R_h = 3.34 nm was obtained.

This small R_h value is suggestive of the formation of mixed proteomicelles composed of POPC, LDAO and FhuA (see Figure 2.19). Besides this major peak, a small peak giving

a R_h = 122 nm was observed. This peak could be attributed to the spontaneous formation of larger vesicular structures/aggregates of POPC.

Consequently, upon treatment of this mixture with Biobeads, a single, relatively broad distribution peak corresponding to R_h = 114 nm was obtained. This increase in size from R_h = 3.34 nm to 114 nm upon treatment with biobeads strongly suggests the formation of proteoliposomes (see Figure 2.19).

Also, the absence of any smaller or larger structures here is indicative of the successful removal of micelles of LDAO by the biobeads and the absence of protein aggregates respectively. These results thus affirm that the FhuA is successfully inserted in the bilayers of the liposomes (*cf.* Figure 2.19)

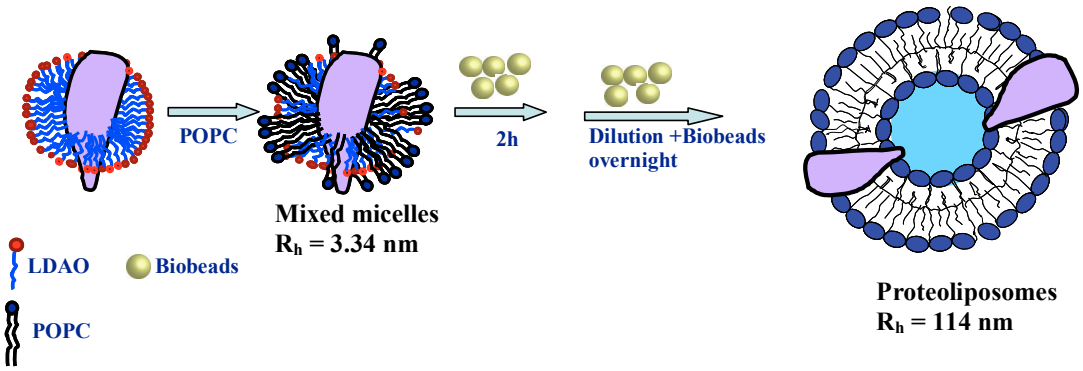

Figure 2.19 Schematic representation showing the steps involved in the formation of proteoliposome containing FhuA from LDAO micelle stabilized FhuA. Note that for simplicity, the biobeads are drawn much smaller here, although they are much bigger objects (a few mm) than the proteomicelles or proteoliposomes.

The liposomes of pure POPC as well as the proteoliposomes bearing FhuA, obtained by treatment with biobeads were then extruded over a 50 nm polycarbonate membrane (protocol described in section 2.2.6.2). After extrusion, the liposome/proteoliposome solution was found to become transparent. DLS measurements were then performed with a dispersion of 0.03 mg/ml concentration.

Figure 2.20 indicates the intensity correlation (left axis) as a function of time for pure POPC liposomes (red dashed curve) and proteoliposomes (blue solid curve). These correlation functions clearly showed a single decorrelation for both pure POPC liposomes and FhuA containing proteoliposomes, suggesting the presence of single average sized species in both cases. These correlation functions were then analysed using

the Contin software package and the decay time distribution was obtained. The decay time distribution for both POPC liposomes and FhuA bearing proteoliposomes were then plotted (right axis) as a function of time in Figure 2.20. Quite interestingly, the decay time constants observed for POPC liposomes (red peak, circular symbols) was found to be the same as that for FhuA bearing proteoliposomes (blue peak, square symbols).

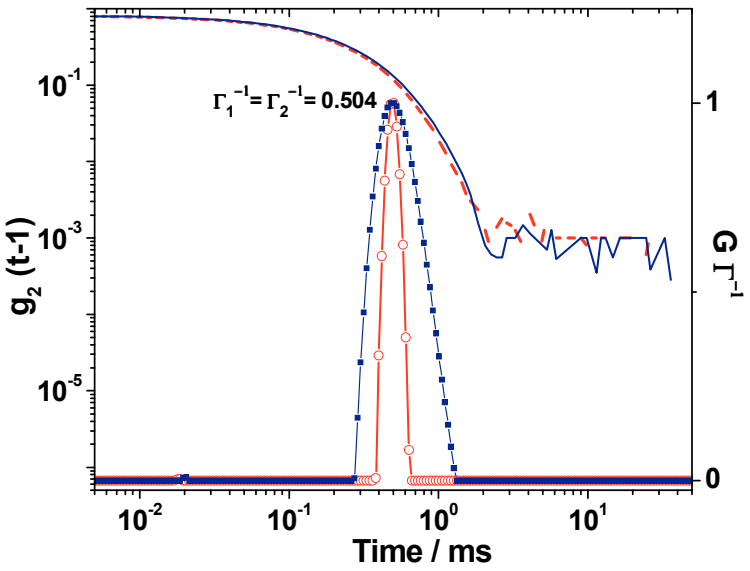

Figure 2.20 DLS measurements performed on proteoliposomes containing lipid: protein ratio 1: 750 (blue curves) and of liposomes of pure POPC (red curves) after extrusion over 50 nm meambranes. The left axis denotes the time intensity correlation functions, the blue solid line corresponds to the correlation function for the proteoliposomes and the red dashed line represents the correlation function liposomes of pure POPC. The right axis presents the decay time distributions, the blue curve (square symbols) denotes the decay times for the proteoliposeomes, the red curve (circlular symbols) shows the decay time for liposomes of POPC. All the samples were measured at a concentration of 0.03 mg/ml of POPC.

This fact suggests that the hydrodynamic radii (R_h) for both POPC liposomes and FhuA bearing proteoliposomes were the same for both pure and FhuA containing POPC liposomes. A similar R_h of 43 nm, calculated using the method described above, was found for both POPC liposomes and FhuA bearing proteoliposomes. Albeit, the similar sizes observed for both liposomes and proteoliposomes, it is important to observe in the Figure 2.20, that the decay time distribution in the case of FhuA bearing proteoliposomes is much broader (blue peak, square symbols) than that for pure POPC liposomes (red peak, circular symbols). The above results can thus be summarized as follows: the incorporation of FhuA in the bilayer of POPC liposomes does not alter the size of the liposomes. Nonetheless, the proteoliposomes containing FhuA were found to be rather polydispersed as compared to the pure POPC liposomes as suggested by the broad

distribution peak. In order to understand these observations, it is important to reiterate here that the size of FhuA is quite small, the extracellular part being about 39 Å, as compared to the liposomes of POPC obtained here (43 nm). Hence, the presence of a few FhuA molecules in the liposomes would not be expected to reflect a drastic change on the average size measured. The polydispersity induced by the presence of FhuA could however be explained by imagining a scenario where the proteoliposomes are not identical *i.e.* the number of FhuA molecules present in each liposome may not be the same. This situation, would then lead to a distribution function that would rather resemble a Gaussian-like peak, as seen in Figure 2.20 (blue peak, square symbols) for the proteoliposomes bearing FhuA.

2.2.3. Monitoring the fusion behavior of proteoliposomes by QCM-D

The fusion behavior of proteoliposomes bearing increasing concentrations of the protein (FhuA) was studied by QCM-D. To have a set of experimental results that could be directly compared, we choose to work with a fixed concentration of POPC *i.e.* at 0.1 mg/ml of POPC, which is equivalent to 1.32 mM of POPC. The ratios of FhuA incorporated in the liposomes were thus varied to obtain proteoliposomes bearing increasing concentrations of FhuA. All the experiments were carried out in the buffer described in section 2.2.1, and in ambient conditions of temperature and pressure.

At the outset, we looked at the fusion of proteoliposomes that were prepared as described in section 2.2.1 without extruding them. The size of these proteoliposomes with a protein: lipid ratio of 1:750 was found to be 114 nm (see Table 2.2)**.** The fusion of liposomes of extruded liposomes having a radius of 50-100 nm has been demonstrated by Reimhult *et al.*[30] These liposomes were shown to follow a classical fusion behavior as discussed in section 1.3.3.

From our observations, the vesicles of POPC prepared by treatment with biobeads (without extrusion) were found to fuse quite instantly upon interaction with the SiO_2 surface (Figure 2.21, blue curve). It can be seen in this figure that the fusion followed the classic "signature" transition of initial adsorption of intact liposomes to fusion and SLB

formation. The final shifts in frequency and dissipation are found to be $\Delta F_7/7$ = -27.7 Hz and $\Delta D_7 = 0.9 \times 10^{-6}$ respectively.

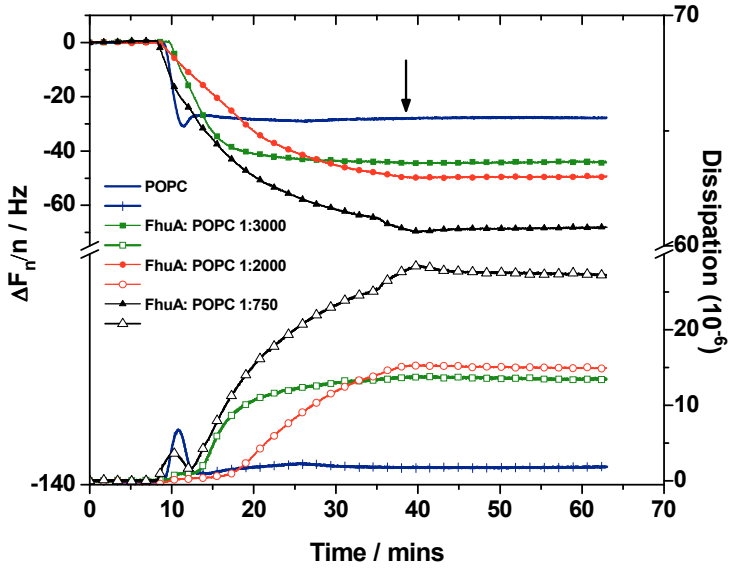

Figure 2.21 QCM-D plots for the interaction with a surface of SiO_2 of proteoliposomes of POPC containing 0 μM FhuA (blue curve), 0.44 μM FhuA (green curve, square symbols), 0.66 μM FhuA (red curve, round symbols) and 1.32 μM FhuA (black curve, triangle symbols). The curves with filled symbols represent the shift in normalized frequency (left axis), while the curves with hollow symbols represent the shift in dissipation (right axis). The measurements shown here were recorded on the 7th harmonic of a 5 MHz SiO_2 coated quartz crystal. The breaks on the axes are introduced for better clarity. The arrow indicates the rinsing with buffer.

This trend was observed to change however, in the case of proteoliposomes containing increasing concentrations of FhuA. It can be seen from Figure 2.21 that the presence of FhuA in the proteoliposomes severely altered the fusion behavior. In all of the preparations demonstrated above bearing FhuA: POPC at ratios 1:3000 (green curve), 1:2000 (red curve) and 1:1000 (black curve) respectively, the transition from liposomes to SLB was distinctly absent. The QCM-D profiles for each case were marked by an initial decrease in frequency and increase in dissipation until saturation, which was followed by their stabilization. These profiles were rather suggestive of the adsorption of a highly dissipative film, as indicated by a remarkable dissipation shift in each case. Further, the final values in the normalized frequency and dissipation shift were found to be increasing in proportion with the increase in the quantity of FhuA present in the proteoliposomes (*cf.* Figure 2.21 and Table 2.3).

Hence, these results were indicative of the adsorption of intact liposomes, which is apparently favored in the presence of FhuA in the liposomes. Two principal factors could

explain this unusual behavior of proteoliposomes interactions with the SiO_2 surface. The first one is a marked difference in the size of the proteoliposomes (R_h = 114 nm) as compared to pure liposomes of POPC (R_h = 72 nm) which would alter the adsorption and fusion kinetics of the proteoliposomes with the substrate. The second factor concerns the interaction of the incorporated FhuA with the substrate, which alters the rupture and fusion of the proteoliposomes. Both these factors have previously been shown to be important in the SLB formation with proteoliposomes.[52,65,66] The first one in particular, was demonstrated by S. Evans and co workers where they studied the fusion of isolated *E.coli* inner membrane (100 nm diameter) and that of Egg PC vesicles (30 nm diameter). They observed that while Egg PC vesicles fused with the "signature" fusion profile, the proteoliposomes from the *E.coli* inner membrane remained adsorbed intact on the substrate.[65]

To examine further on this effect, the fusion behavior of extruded proteoliposomes were then studied. The interactions of extruded liposomes of pure POPC and extruded proteoliposomes bearing FhuA: POPC at ratios 1:3000, 1:2000, 1:750 and 1:500 were looked at by QCM-D. As observed in Figure 2.22 (left panel: shift in normalized Frequency, right panel: shift in Dissipation) the interactions of proteoliposomes has drastically changed from that observed for non-extruded proteoliposomes (Figure 2.21). In this case, the liposomes from POPC (blue curves) and proteoliposomes made from a ratio 1:3000 (green curves, square symbols) showed not only similar fusion behaviors, but also gave almost the same final shifts in final frequency and dissipation (see Table 2.3).

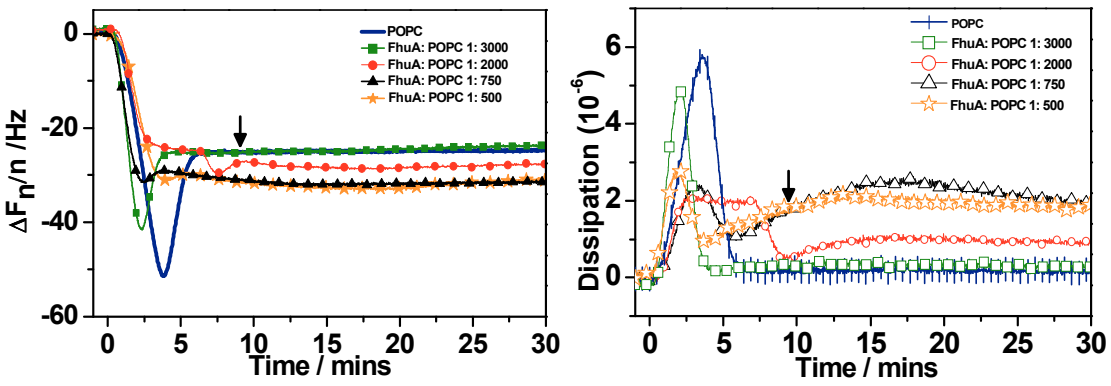

Figure 2.22 QCM-D plots for the interaction on a surface of SiO_2 with extruded proteoliposomes of POPC containing 0 µM FhuA (blue curve), 0.44 µM FhuA (green curve, square symbols), 0.66 µM FhuA (red curve, round symbols), 1.76 µM FhuA (black curve, triangle symbols) and 2.64 µM FhuA (orange curve, star symbols). The curves with filled symbols represent the shift in normalized frequency (left panel), while the curves with hollow symbols represent the shift in dissipation (right panel). The measurements shown here were recorded on the 7th harmonic of a 5 MHz SiO_2 coated quartz crystal. The arrow indicates the rinsing with buffer.

However, this situation was different in the case of proteoliposomes bearing increasing concentration ratios of FhuA. As it can be seen, in the case of proteoliposomes having ratios of FhuA 1: 2000, 1:750 and 1: 500 (red, black and orange curves in Figure 2.22 respectively) the "signature" two step fusion profiles was observed to be almost masked in the frequency plot, whereas hugely diminished in the dissipation plot.

Moreover, upon careful observation of the profile of dissipation shifts for the FhuA ratios 1:750 and 1:500 (black and orange curves) the frequency is found to decrease slightly and dissipation is found to increase clearly after the transition step. This shift seems to continue for a few minutes after the rinsing step, after which the profiles seem to stabilize.

To explain these results where the fusion profile of proteoliposomes with increased concentrations of the protein tends to go away from the "signature" two-step fusion process, it is remember to reiterate that the fusion pathways of liposomes on a substrate are shown to be dependent on various factors. [30,67] One of the most important one, being the liposome-substrate interaction. It is clear from Figure 2.21, that the presence of the protein altered the interactions between the liposomes and the substrate. This effect still seems to be operational in the case of extruded proteoliposomes. Nonetheless, upon observing the final shifts in frequency and dissipation (Table 2.3), a significant difference is observed upon extrusion of the proteoliposomes.

Table 2.3 Consolidation of the final shifts in frequency and dissipation (measured on the 7th harmonic) as observed for the interaction of proteoliposomes bearing increasing concentrations of FhuA.

FhuA:POPC ratio	Before extrusion		After extrusion	
	$\Delta F_7/7$ (Hz)	ΔD_7	$\Delta F_7/7$	ΔD_7
0	– 27.7	0.9	-24.1	0.10
1:3000	– 46.2	13.7	-24.1	0.25
1:2000	– 49.7	15.1	-28.3	0.94
1:750	– 68.3	27.6	-31.7	1.85
1:500	nd	nd	-32.4	2.07

On comparing the values of the normalized frequencies and dissipation for the interaction of proteoliposomes, before and after extrusion, it is clear that in the case of ratios FhuA: POPC 1:3000 and 1:2000, intact proteoliposomes were adsorbed before extrusion, whereas a SLB is obtained upon extrusion of these liposomes.

However, for higher ratios of FhuA in the proteoliposomes such as 1:750, while the values before extrusion clearly indicate the adsorption of intact liposomes, the values after extrusion are suggestive of the presence of few intact proteoliposomes on a formed SLB (transition in Figure 2.22). The same remark can be made for the proteoliposomes of FhuA ratios 1:500. This fact is reinforced by the observation that the frequency continued to decrease slightly and the dissipation increased clearly after the "signature" transition step in these two cases.

A similar scenario was observed by F. Höök and co workers[52], where they studied the fusion behavior of tyrosine hydrogenase containing proteoliposomes.

This observation can be arguably a result of protein-protein interactions between the SLB bound FhuA and the proteoliposomes bound FhuA. Although, further investigations need to be made to support this argument, nevertheless, the increasing values of frequency and dissipation upon increasing concentrations of FhuA in the proteoliposomes are in coherence with the argument.

2.2.4. Interaction of pb5 with FhuA embedded SLBs

The activity of the Supported Lipid Bilayers made of proteoliposomes bearing FhuA was now tested to understand, to what extent the SLBs retain the function of the incorporated FhuA. This was performed by checking the interaction of FhuA bearing SLBs with the phage protein pb5 (see section 2.2). The measurement was done by injecting a solution of pb5 of known concentration onto the SLBs described above (Figure 2.22). pb5 is known to be most stable at slightly acidic pH, while it can precipitate at neutral to alkaline pH. The experiments were thus performed in 0.1 M PBS buffer containing 150 mM NaCl at pH 6.0. The SLBs bearing FhuA were thus equilibrated in this buffer to have stable baselines before the injection of pb5. Figure 2.23 shows the QCM-D profiles for the interaction of pb5 with FhuA containing SLBs. It can be seen from the blue lines in the plots that pb5 did not interact with SLB of pure POPC, indicating the absence of non-specific interactions.

Further, it was observed that SLB made from FhuA:POPC at 1:3000 ratios, did not show any recognition with pb5 (data not shown). However, SLBs made of FhuA:POPC at 1:2000 (orange curve), 1:750 (maroon curve) and 1:500 showed clear interactions as suggested by the decrease in frequency and the increase in dissipation.

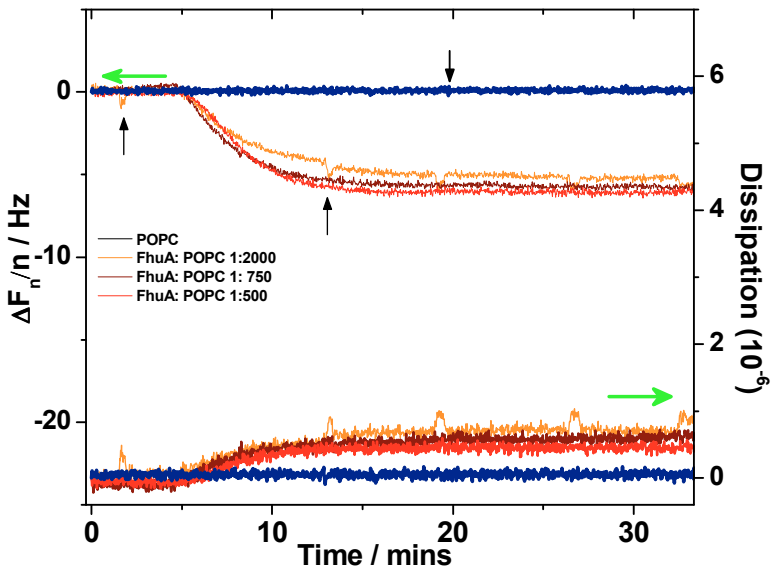

Figure 2.23 QCM-D profiles for the interaction of pb5 with SLBs containing pure POPC (blue line), FhuA: POPC 1:2000 (orange curve), 1:750 (maroon curve) and 1:500 (red curve). The first upward arrow from left, indicates the injection of 10 nM pb5, the second upward arrow indicates the injection of 15 nM pb5 while the third downward arrow indicates the rinsing with buffer. The left axis indicates the shift in frequency, while the right axis indicates the shift in dissipation (shown by green arrows) as measured on the 7th harmonic. The injections were made at a constant flow of 20 µl/min.

The injection of 10 nM of pb5 (first arrow from the left) induced a negative shift in frequency on SLBs containing FhuA. Another injection of 15 nM of pb5 led only to a small decrease in frequency (*cf.* Figure 2.23 and Table 2.4). It was quite interesting to observe that the interaction of FhuA immobilized in SLBs with pb5 in solution was irreversible as the signals remain stable even after rinsing with pure buffer.

Table 2.4 Indicating the relative shifts in normalised frequency and dissipation upon interaction of pb5 with SLBs bearing increasing concentrations of FhuA

FhuA: POPC ratio in SLB	Response			
	10 nM pb5		15 nM pb5	
	$\Delta F_7/7$	ΔD_7	$\Delta F_7/7$	ΔD_7
0	0	0	0	0
1:2000	–3.9	0.39	-1.3	0.62
1:750	–4.2	0.44	-1.5	0.55
1:500	–5.6	0.48	-0.9	0.57

However, the shifts in frequency and dissipation were rather small for the first injection of 10 nM pb5, and even slender upon the second injection of 15 nM pb5 (see Table 2.4). This indicated that almost all the binding sites of FhuA in the SLB were saturated with 10 nM pb5, which suggest a strong affinity of the interaction between FhuA and pb5. Further, the shifts in frequencies were found to be in proportion with the concentration of FhuA in the SLB, but the shifts in dissipation had almost no clear correlation with the amount of FhuA present in the SLB. It is also important to note here that the affinity constants of the FhuA-pb5 interactions are still unknown. However, the present experiments suggest that the affinity constant of FhuA is about 10 nM when immobilized in a POPC SLB.

2.2.5. Conclusions and Perspectives

In the present piece of work, we were not only successful in demonstrating the formation of proteoliposomes with FhuA, but we could clearly characterize the steps involved in the proteoliposomes formation. We could also probe in to the effects like size of the proteoliposomes, concentration of FhuA present in the proteoliposomes which actually seemed to critically govern the liposome to SLB transformation.

With the present studies, we could determine both the advantages and the disadvantages of Supported Lipid Bilayers for the incorporation and studies of the small membrane proteins like FhuA. With the help of this model system, we could clearly understand that the interaction between FhuA and the phage protein is irreversible and stable after rinsing and occurs with a high affinity (K_D in the order of 10 nM). This observation helped us confirm that the irreversible interactions of FhuA with the phage T5 are pb5 mediated.

These results open up doors to the next level of investigation, which would involve impedance spectroscopy to study the transfer of phage DNA across the bilayer into the aqueous space, high resolution AFM imagining to understand the conformation of FhuA in the SLB and QCM-D to determine the affinity constants between the protein and the phage/pb5.

2.2.6. Experimental protocols

POPC (1-Palmitoyl-2-oleoyl-sn-glycero-3-phosphocholine) was obtained from Avanti Polar (Alabaster, AL) and used as supplied. Milli-Q grade water of resistivity 18 MΩ·cm was used for all physical measurements.

2.2.6.1 Biobeads treatment

The Biobeads obtained from BioRad were treated with ethanol and water prior to use as per the protocol developed by JL Rigaud *et al.*[68] 20 mg of wet Biobeads were added for each mg of LDAO.

2.2.6.2 Extrusion of liposomes/proteoliposomes.

The extrusion of proteoliposomes were done at a concentration of 0.1 mg/ml of POPC, the mini extruder equipped with a 1 ml Hamilton syringe was precleaned using 1% SDS, water and ethanol and well dried before use. A polycarbonate membrane of 50 nm pore size was mounted into the Teflon extruding compartment, which was adjusted with filters on both sides. A single turn of working buffer was passed through the extruding compartment and the syringes to minimize the dead volume in the extruding system. The proteoliposomes were extruded by passing them 21 times through the membrane. After which they were recovered and used immediately.

2.2.6.3 Dynamic Light scattering

DLS measurements were done with liposomes at a dilute concentration (0.03 mg/ml of POPC) to ensure that the solution measured was transparent. The measurements were done on an AVL device. The measurement tubes (internal diameter of 13 mm) were filled with 0.7 ml of the liposome/proteliposome dispersion. The tube in the measurement chamber was immersed in a toluene bath with a temperature regulator. All measurements were done at 21 ºC.[51]

2.2.6.4 QCM-D measurements

All the QCM-D measurements described in this chapter were performed on a E4 QCM-D device. The SiO_2 coated quartz crystals were precleaned with 1% SDS, followed by generous rinsing with water and drying. They were activates in UV-ozone just before use.

2.3. References

(1) Jensen, T. W.; Hu, B. H.; Delatore, S. M.; Garcia, A. S.; Messersmith, P. B.; Miller, W. M. *J. Am. Chem. Soc.* **2004**, *126*, 15223-15230.
(2) Wolny, P. M.; Banerji, S.; Gounou, C.; Brisson, A. R.; Day, A. J.; Jackson, D. G.; Richter, R. P. *J. Biol. Chem.*, *285*, 30170.
(3) Marchi-Artzner, V.; Lorz, B.; Hellerer, U.; Kantlehner, M.; Kessler, H.; Sackmann, E. *Chem. Eur. J.* **2001**, *7*, 1095-1101.
(4) Stroumpoulis, D.; Zhang, H.; Rubalcava, L.; Gliem, J.; Tirrell, M. *Langmuir* **2007**, *23*, 3849-3856.
(5) Milhiet, P. E.; Gubellini, F.; Berquand, A.; Dosset, P.; Rigaud, J. L.; Le Grimellec, C.; Lévy, D. *Biophys. J.* **2006**, *91*, 3268-3275.
(6) Chiantia, S.; Ries, J.; Chwastek, G.; Carrer, D.; Li, Z.; Bittman, R.; Schwille, P. *Biochim. Biophys. Acta-Biomembranes* **2008**, *1778*, 1356-1364.
(7) Andersson, A. S.; Glasmästar, K.; Sutherland, D.; Lidberg, U.; Kasemo, B. *Journal of Biomedical Materials Research Part A* **2003**, *64*, 622-629.
(8) Kam, L.; Boxer, S. G. *J. Biomed. Mater. Res.* **2001**, *55*, 487-495.
(9) Groves, J. T.; Dustin, M. L. *J. Immunol. Methods* **2003**, *278*, 19-32.
(10) Ananthanarayanan, B.; Little, L.; Schaffer, D. V.; Healy, K. E.; Tirrell, M. *Biomaterials*.
(11) Dillow, A. K.; Ochsenhirt, S. E.; McCarthy, J. B.; Fields, G. B.; Tirrell, M. *Biomaterials* **2001**, *22*, 1493-1505.
(12) Nicolson, G. L. *Biochim. Biophys. Acta* **1982**, *695*, 113.
(13) Butcher, E. C.; Scollay, R. G.; Weissman, I. L. *Eur. J. Immunol.* **1980**, *10*, 556-561.
(14) Chin, Y. H.; Rasmussen, R.; Cakiroglu, A. G.; Woodruff, J. J. *J. Immunol.* **1984**, *133*, 2961-2965.
(15) McEver, R. P.; Zhu, C. *Annu. Rev. Cell Dev. Biol.*, *26*, 363-396.
(16) Thuault, S.; Plutoni, C.; Comunale, F.; Gauthier-Rouviere, C. *Bull. Cancer (Paris). 97*, S35-S35.
(17) Soler, A. P.; Kindel, S. E.; McCloskey, G.; Burchette, J. L. *Rare Tumors*, *2*, e43.
(18) Hersel, U.; Dahmen, C.; Kessler, H. *Biomaterials* **2003**, *24*, 4385-4415.
(19) Ruoslahti, E. *Advances In Cancer Research, Vol 76* **1999**, *76*, 1-20.
(20) Hynes, R. O. *Cell* **2002**, *110*, 673-687.
(21) Desgrosellier, J. S.; Cheresh, D. A. *Nat. Rev. Cancer*, *10*, 9-22.
(22) Rouslahti, E.; Pierschbacher, M. D. *Cell* **1988**, *44*, 517-518.

(23) Aumailley, M.; Gurrath, M.; Muller, G.; Calvete, J.; Timpl, R.; Kessler, H. *FEBS Lett.* **1991**, *291*, 50-54.
(24) Gurrath, M.; Muller, G.; Kessler, H.; Aumailley, M.; Timpl, R. *Eur. J. Biochem.* **1992**, *210*, 911-921.
(25) Arnold, M.; Cavalcanti-Adam, E. A.; Glass, R.; Blummel, J.; Eck, W.; Kantlehner, M.; Kessler, H.; Spatz, J. P. *ChemPhysChem* **2004**, *5*, 383-388.
(26) Boturyn, D.; Coll, J. L.; Garanger, E.; Favrot, M. C.; Dumy, P. *J. Am. Chem. Soc* **2004**, *126*, 5730-5739.
(27) Sancey, L.; Garanger, E.; Foillard, S.; Schoehn, G.; Hurbin, A.; Albiges-Rizo, C.; Boturyn, D.; Souchier, C.; Grichine, A.; Dumy, P.; Coll, J. L. *Mol. Ther.* **2009**, *17*, 837-843.
(28) Razkin, J.; Josserand, V.; Boturyn, D.; Jin, Z.; Dumy, P.; Favrot, M.; Coll, J. L.; Texier, I. *ChemMedChem* **2006**, *1*, 1069-1072.
(29) Sandrin, L.; Coche-Guérente, L.; Bernstein, A.; Basit, H.; Labbé, P.; Dumy, P.; Boturyn, D. *Org. Biomol. Chem.***2010**, *8*, 1531.
(30) Reimhult, E.; Höök, F.; Kasemo, B. *J. Chem. Phys.* **2002**, *117*, 7401.
(31) Richter, R. P.; Bérat, R.; Brisson, A. R. *Langmuir* **2006**, *22*, 3497-3505.
(32) Richter, R.; Mukhopadhyay, A.; Brisson, A. *Biophys. J.* **2003**, *85*, 3035-3047.
(33) Rodahl, M.; Höök, F.; Fredriksson, C.; Keller, C. A.; Krozer, A.; Brzezinski, P.; Voinova, M.; Kasemo, B. *Faraday Discuss.* **1997**, *107*, 229-246.
(34) Voinova, M. V.; Rodahl, M.; Jonson, M.; Kasemo, B. *Phys. Scr.* **1999**, *59*, 391.
(35) Modin, C.; Stranne, A. L.; Foss, M.; Duch, M.; Justesen, J.; Chevallier, J.; Andersen, L. K.; Hemmersam, A. G.; Pedersen, F. S. *Biomaterials* **2006**, *27*, 1346-1354.
(36) Burridge, K.; Turner, C. E.; Romer, L. H. *J. Cell Biol.* **1992**, *119*, 893.
(37) Purrucker, O.; Gönnenwein, S.; Förtig, A.; Jordan, R.; Rusp, M.; Bärmann, M.; Moroder, L.; Sackmann, E.; Tanaka, M. *Soft Matter* **2007**, *3*, 333-336.
(38) Huang, J.; Gra ter, S. V.; Corbellini, F.; Rinck, S.; Bock, E.; Kemkemer, R.; Kessler, H.; Ding, J.; Spatz, J. P. *Nano Lett.* **2009**, *9*, 1111-1116.
(39) Kuhlman, W.; Taniguchi, I.; Griffith, L. G.; Mayes, A. M. *Biomacromolecules* **2007**, *8*, 3206-3213.
(40) Tugulu, S.; Silacci, P.; Stergiopulos, N.; Klok, H. A. *Biomaterials* **2007**, *28*, 2536-2546.
(41) Cavalcanti-Adam, E. A.; Volberg, T.; Micoulet, A.; Kessler, H.; Geiger, B.; Spatz, J. P. *Biophys. J.* **2007**, *92*, 2964-2974.
(42) Massia, S. P.; Hubbell, J. A. *J. Cell Biol.* **1991**, *114*, 1089.
(43) Oliver, A. E.; Ngassam, V.; Dang, P.; Sanii, B.; Wu, H.; Yee, C. K.; Yeh, Y.; Parikh, A. N. *Langmuir* **2009**, *25*, 6992-6996.
(44) Diaz, A. J.; Albertorio, F.; Daniel, S.; Cremer, P. S. *Langmuir* **2008**, *24*, 6820-6826.
(45) Merzlyakov, M.; Li, E.; Gitsov, I.; Hristova, K. *Langmuir* **2006**, *22*, 10145-10151.
(46) Kiessling, V.; Domanska, M. K.; Murray, D.; Wan, C.; Tamm, L. K.; Wiley Encyclopedia of Chemical Biology.
(47) Castellana, E. T.; Cremer, P. S. *Surf. Sci. Rep.* **2006**, *61*, 429-444.
(48) Erb, E. M.; Tangemann, K.; Bohrmann, B.; Muller, B.; Engel, J. *Biochemistry* **1997**, *36*, 7395-7402.
(49) Sprong, H.; van der Sluijs, P.; van Meer, G. *Nat. Rev. Mol. Cell Biol.* **2001**, *2*, 504-513.
(50) Schmitt, E. K.; Vrouenraets, M.; Steinem, C. *Biophys. J.* **2006**, *91*, 2163-2171.

(51) Salafsky, J.; Groves, J. T.; Boxer, S. G. *Biochemistry* **1996**, *35*, 14773-14781.
(52) Granéli, A.; Rydström, J.; Kasemo, B.; Höök, F. *Langmuir* **2003**, *19*, 842-850.
(53) Zagnoni, M.; Sandison, M. E.; Marius, P.; Lee, A. G.; Morgan, H. *Lab Chip* **2007**, *7*, 1176.
(54) Ferguson, A. D.; Hofmann, E.; Coulton, J. W.; Diederichs, K.; Welte, W. *Science* **1998**, *282*, 2215.
(55) Lee, A. G. *Biochim. Biophys. Acta-Biomembr.* **2003**, *1612*, 1-40.
(56) Locher, K. P.; Rees, B.; Koebnik, R.; Mitschler, A.; Moulinier, L.; Rosenbusch, J. P.; Moras, D. *Cell* **1998**, *95*, 771-778.
(57) Chen, R.; Poger, D.; Mark, A. E. *J. Phys. Chem. B*, *115*, 1038-1044.
(58) Rawicz, W.; Olbrich, K. C.; McIntosh, T.; Needham, D.; Evans, E. *Biophys. J.* **2000**, *79*, 328-339.
(59) Plançon, L.; Chami, M.; Letellier, L. *J. Biol. Chem.* **1997**, *272*, 16868.
(60) Lambert, O.; Plançon, L.; Rigaud, J. L.; Letellier, L. *Mol. Microbiol.* **1998**, *30*, 761-765.
(61) Böhm, J.; Lambert, O.; Frangakis, A. S.; Letellier, L.; Baumeister, W.; Rigaud, J. L. *Curr. Biol.* **2001**, *11*, 1168-1175.
(62) Boulanger, P.; Jacquot, P.; Plançon, L.; Chami, M.; Engel, A.; Parquet, C.; Herbeuval, C.; Letellier, L. *J. Biol. Chem.* **2008**, *283*, 13556.
(63) Bonhivers, M.; Ghazi, A.; Boulanger, P.; Letellier, L. *The EMBO Journal* **1996**, *15*, 1850.
(64) Provencher, S. W. *J. Chem. Phys.* **1976**, *64*, 2773-2777.
(65) Dodd, C. E.; Johnson, B. R. G.; Jeuken, L. J. C.; Bugg, T. D. H.; Bushby, R. J.; Evans, S. D. *Biointerphases* **2008**, *3*, FA59-FA67.
(66) Granéli, A.; Rydström, J.; Kasemo, B.; Höök, F. *Biosens. Bioelectron.* **2004**, *20*, 498-504.
(67) Reimhult, E.; Höök, F.; Kasemo, B. *Langmuir* **2003**, *19*, 1681-1691.
(68) Rigaud, J. L.; Levy, D.; Mosser, G.; Lambert, O. *Eur. Biophys. J.* **1998**, *27*, 305-319.

3. Design and Characterization of tBLMs based on mixed SAMs: Influence of the SAM composition on bilayer formation

3. Design and Characterization of tBLMs based on mixed SAMs: Influence of the SAM composition on bilayer formation

3.1. Introduction

Although Supported Lipid Bilayers (SLBs) are undoubtedly one of the simplest and most convenient approaches towards designing cell membrane-mimic models, these architectures present a major drawback when it concerns transmembrane proteins. Since these supported lipid bilayers retain a very thin layer (ca. 10 Å)[1] of hydration between the substrate and the proximal layer of lipids, incorporation of transmembrane proteins possessing a considerable intracellular domain becomes restrictive as the interaction of the protein with the substrate can lead to loss of activity of the protein.[2]

To overcome this problem, tethered bilayer lipid membranes (tBLMs) have been developed. In these assemblies the bilayer is separated from the substrate by a soft, flexible, hydrophilic layer. This layer acts as the aqueous or ionic reservoir between the substrate and the membrane, therefore providing ample space and enhanced mobility to the inserted protein. In this context, several entities like polymer cushions,[3-8] self-assembled monolayers of polar peptides,[9] or self assembled monolayers of oligoethylene glycol bearing thiols [10-12] have been used as the hydrophilic spacers (see Figure 3.1). These spacers however are usually bifunctional in nature, in that they are often conjugated with a hydrophobic moiety such as cholesterol, [13-19] alkane[10,11] or phytanyl chains.[20-22] These hydrophobic domains act as an anchor to the bilayer by forming the proximal leaflet of the bilayer.

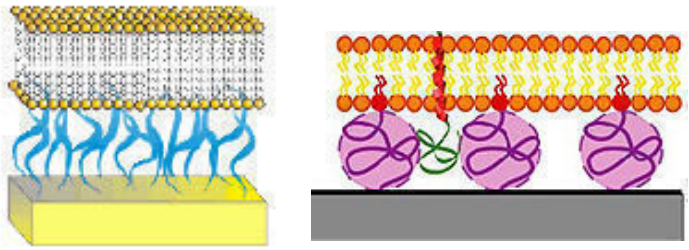

Figure 3.1 Cartoon representations of tethered bilayer lipid membranes based on (left) a self-assembled monolayer and (right) polymer cushion.

Although several substrates like SiO_2[23] or zirconated surfaces,[24] have been employed, the substrate of choice is often gold, essentially due to its ease of functionalization via the Au–S bond formation. Gold is also an electrically conducting substrate which facilitates the investigation by various techniques such as electrochemistry, Quartz Crystal Microbalance or Surface Plasmon Resonance. The fabrication of a tBLM is in most cases a two step process where the first step involves the formation of a self assembled monolayer followed by the formation of the phospholipid bilayer. The latter step can be effectuated in several ways such as the well known Langmuir Blodgett technique,[6] rapid solvent exchange of an organic solution of phospholipids,[10,11,25] applying an osmotic shock to preformed vesicles in order to drive their fusion[3,23] or by self directed fusion of vesicles upon interaction with the substrate.[18,20,26] The last mentioned is the more commonly used technique as it is the best suited to handle protein containing vesicles. One of the most well studied and well applied tBLM system to date is the diphytanyl-ethylene glycol thiol (DPTL) based SAM initially developed by Knoll and coworkers.[21] While these authors demonstrated the formation of a very resistive bilayer by using a SAM of pure DPTL (anchoring) molecule, it was observed by them and by other groups that such tBLMs obtained from pure anchoring thiol based SAMs were inefficient in the incorporation of large peptides/membrane proteins such as gramicidin and mellitin.[6,14] Therefore, a lot of attention has been given in developing tethered lipid bilayer systems by dilution of the hydrophobic oligoethylene based thiol with a small hydrophilic thiol.[6,9,27] Despite these numerous attempts on developing such diluted/sparsely tethered bilayers, only a very few reports detail the impact of the composition of the SAM on the formation process and on the properties of the phospholipid membrane. [10,11]

Interesting results by Heinrich *et al.*[10] and McGillivray *et al.*[11] described the effect of backfilling with small hydrophilic thiols on the hydration, electrical and structural

properties of the tBLM. They also derived from these two studies the effect of chain length of the anchoring thiol on resistivity of the bilayer to ion transfer. However, in both these reports the bilayer formation was effectuated by a rapid solvent exchange as opposed to auto/self directed fusion. Other promising results by Jeuken *et al*. highlighted the vesicle fusion on a cholesterol based SAM where they successfully demonstrated the presence of phase segregation in the SAM and its impact on the formation of a bilayer.[15] Nevertheless, detailed studies illuminating the effects of the composition and structure of the SAM on the kinetics and fusion behavior of vesicles still needs attention.

We were thus keenly interested in understanding the effects of dilution of the hydrophobic anchoring moiety in the SAM on the fusion process, and in probing into the threshold dilution ratio of this hydrophobic moiety. The present chapter is essentially dedicated to studies involving the design and study of bilayers tethered on self-assembled monolayer modified gold. The SAMs were obtained using either a dipalmitoyl terminal TEG thiol or an ethylene glycol terminal thiol and a specific mixture of both these thiols. These SAMs were then treated with preformed small unilamellar vesicles (SUV) and the fusion process was chosen to be self directed. We observe here for the first time, that it is the composition of the SAM that determines and governs the fusion kinetics of vesicles to form a tethered bilayer. A multipronged approach was used to characterize both the SAMs and the bilayers involving techniques like Quartz Crystal Microbalance with Dissipation (QCM-D) to follow the phase transition from vesicles to bilayer, Electrochemical Impedance Spectroscopy (EIS) to understand the impact of dilution of the lipidic thiol on both the SAM and bilayer resistance properties and Atomic Force Microscopy (AFM) to have insights upon the phase segregation of the mixed SAM and also on the formation of a bilayer.

3.2. Design and Synthesis of Thiols

In the design of the TEG-DP thiol (Figure 3.2), dipalmitoyl chains were chosen as anchoring elements for the bilayers. A tetra ethylene glycol moiety was used to define the hydrophilic part and act as a vertical spacer between the gold surface fixing thiol group and the hydrophobic palmitoyl chains. TEG thiol presenting a similar tetraethylene glycol part was used to dilute the anchoring TEG-DP molecules in the SAM as seen in Figure 3.2.

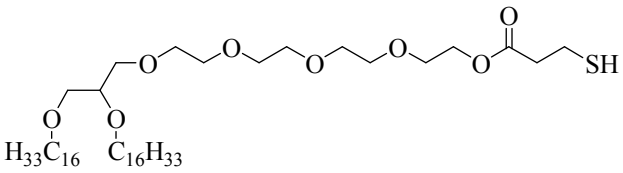

TEG-DP thiol (**1**)

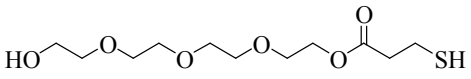

TEG thiol (**2**)

Figure 3.2 Structures of TEG-DP and TEG thiols.

3.2.1. Synthesis of TEG-DP Thiol

For the synthesis of TEG-DP (Scheme 3.1), isopropylidene glycerol was first activated as a tosyl group to obtain molecule **4,** this tosylate enabled the introduction of the tetraethylene glycol moiety by a nucleophilic substitution furnishing molecule **5**. Protection of the TEG hydroxy group as a benzyl function yielded **6** which in turn facilitated the selective etherification of the glycerol hydroxy groups, obtained upon ketal deprotection **7**, by palmitoyl chains to furnish **8**. This dipalmitoyl product was then debenzylated to obtain **9**. The intermediate **9** upon esterification with trityl protected mercaptopropanoic acid yielded **10**. Acid deprotection of the trityl group of **10** gave the final molecule **1**. The detailed synthetic procedures for each step in the scheme and the

spectral characterizations of every intermediate are described at the end of this chapter in the experimental section.

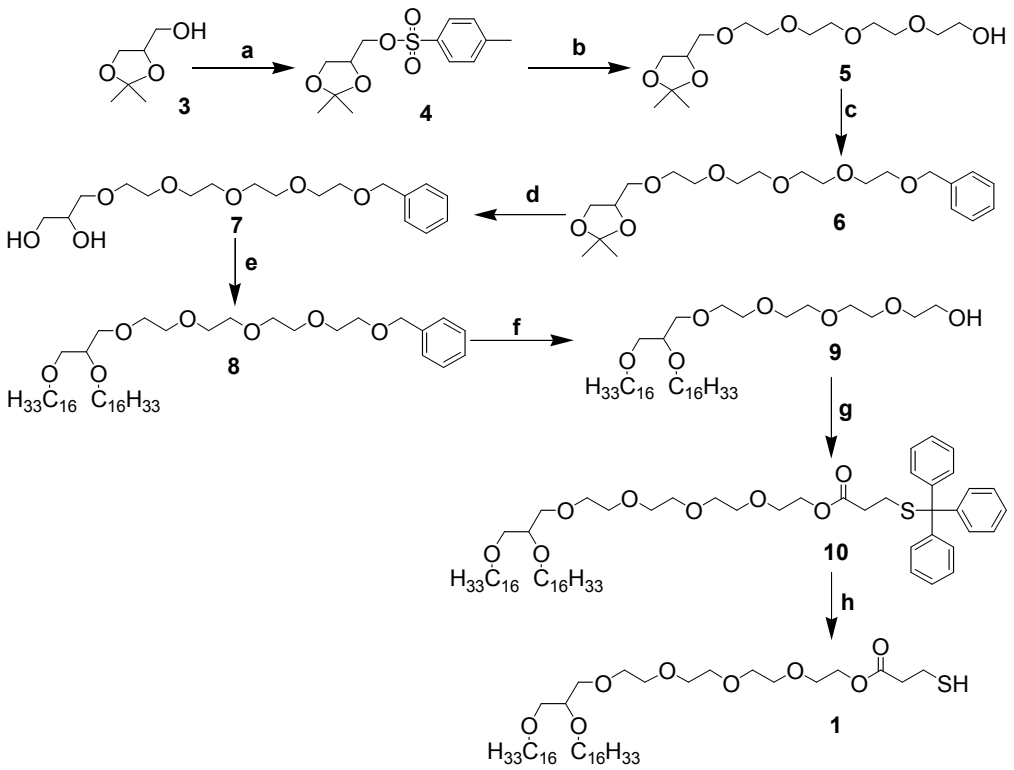

Scheme 3.1 Synthesis of thiol TEG-DP: (a) 1.5 equiv. of TsCl, CH_2Cl_2, rt, overnight, 86%; (b) 2 equiv. of tetraethylene glycol, 3 equiv. of NaH, THF, reflux, 3 days, 83%; (c) 1.5 equiv. of NaH, 1.5 equiv. of BnBr, TBAB (cat.), THF, rt, 2 h, 72%; (d) 5M HCl, CH_2Cl_2/MeOH, overnight, rt, quantitative; (e) 6 equiv. of NaH, 3 equiv. of hexadecyl bromide, TBAI (cat.), THF, reflux, 3 days, 56%; (f) 5% Pd/C (cat.), H2 (1atm), EtOH, 3 h, rt, 90%; (g) 1.5 equiv. of DCC, 1 equiv.. of DMAP, 1.5 equiv. of Trt-propanoic acid (synthesised from propanoic acid), CH_2Cl_2, 12 h, rt, 76%; (h) 5 equiv. of TFA, 5 equiv. of triisopropylsilane, CH_2Cl_2, rt, 4h, 80%. TsCl = tosyl chloride, BnBr = benzyl bromide, TBAB = tetrabutylammonium bromide, TBAI = tetrabutylammonium iodide, DCC = dicyclohexylcarbodiimide, DMAP = 4-dimethylaminopyridine, Trt = trityl.

3.2.2. Synthesis of TEG thiol

The synthesis of the TEG thiol (Scheme 3.2) was carried using tetraethylene glycol as the starting material. A selective TBDMS protection of one of the hydroxyl groups of tetraethylene glycol furnished the intermediate **12**, this intermediate was then esterified with trityl protected mercaptopropanoic acid to obtain intermediate **13**. This product after acid deprotection in one pot furnished the final molecule **2**.

The detailed synthetic procedures for each step in the scheme and their characterizations are described at the end of this chapter in the experimental section.

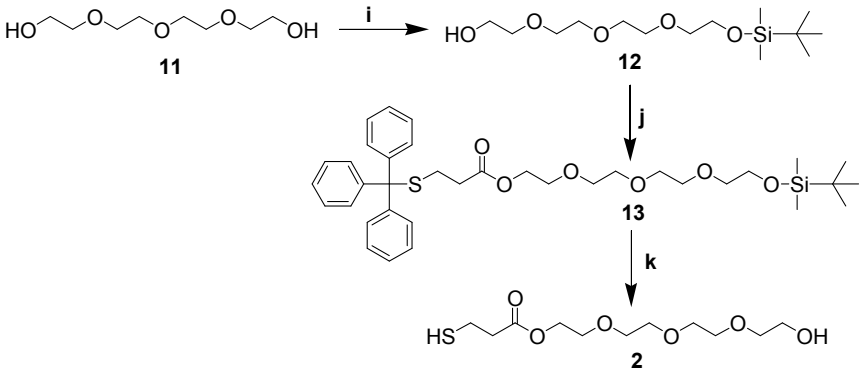

Scheme 3.2 Synthesis of thiol TEG: (i) 1 equiv. of TBDMS, 1.1 equiv. of imidazole, DMAP (cat.), CH_2Cl_2, DMF, rt, overnight, 76% (j) 1.5 equiv. of DCC, 1 equiv. of DMAP, 1.5 equiv. of Trt-propanoic acid (synthesised from propanoic acid), CH_2Cl_2 , 12 h, rt, 76%; (k) 5 equiv of TFA, 5 equiv of triisopropylsilane, CH_2Cl_2, 4 h, rt 78%. TBDMS = ***tert***-butyldimethylsilyl chloride, DCC = dicyclohexylcarbodiimide, DMAP = 4-dimethylaminopyridine, Trt= trityl.

3.3. Preparation and Characterizations of SAMs

Self assembled monolayers were prepared from 0.2 mM ethanolic solutions of either pure TEG-DP thiol or TEG thiol or with particular ratios of both thiols. While their formation was once followed by QCM-D, they were henceforth prepared ex-situ and characterized using several techniques like contact angle measurements, ellipsometry, AFM and electrochemical reductive desorption. The SAM formation followed by QCM-D and their detailed characterizations are described in the present section, which is sub-divided on the basis of the techniques used for measurements.

3.3.1. Quartz Crystal Microbalance with Dissipation (QCM-D)

The adsorption of a freshly prepared 0.2 mM solution of thiols in ethanol onto the surface of gold coated quartz was followed by QCM-D. As seen in Figure 3.3 both adsorption of TEG and TEG-DP were very rapid, indicated by a sharp decrease in frequency upon injection. However, this initial adsorption was followed by a slight negative drift in the frequency which could be indicative of a slow reorganization between the molecules to form a well packed monolayer on the surface.[28] After subsequent rinsing with ethanol, $\Delta F_5/5$ and ΔD_5 values for both SAMs reached stable values, i.e. – 17.0 Hz and 0.17×10^{-6} for TEG-DP and – 7.0 Hz and 0.08×10^{-6} for TEG monolayers respectively.

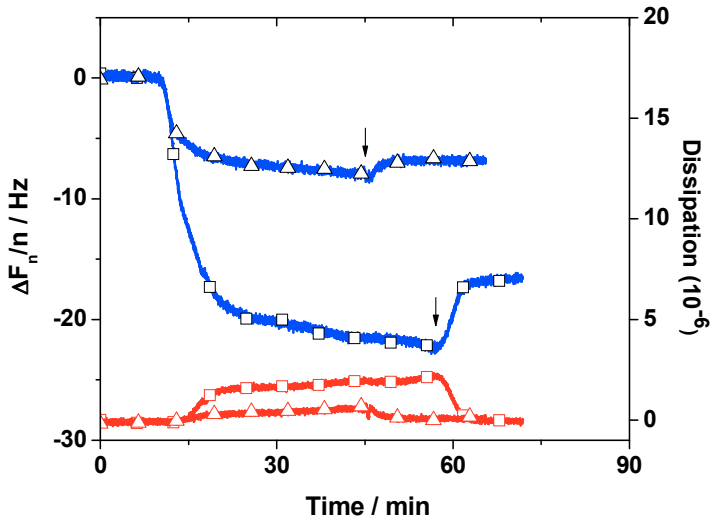

Figure 3.3 QCM-D profiles recorded for the adsorption of 0.2 mM ethanolic solutions of TEG-DP thiol (squares) and TEG thiol (triangles) on gold coated Quartz as measured on the 5th harmonic. In blue is the normalised shift in frequency (Δfn/n) (left axis) and in red is the Dissipation (ΔDn) (right axis). The arrow indicates the rinsing step with ethanol.

Considering the relatively low values of dissipation, the Sauerbrey equation was applied to determine the acoustic masses which were found to be 301 ng/cm^2 for the TEG-DP SAM and 124 ng/cm^2 for the TEG SAM. The values of the Sauerbrey mass density obtained for TEG-DP are quite in agreement with those reported by Vockenroth *et al*. for the adsorption of a structurally similar DPTL molecule (300 ng/cm^2).[29] Once the adsorption of the thiol was followed by QCM-D, the SAMs were henceforth prepared by overnight adsorption in an ethanolic solution of either pure or specific mixtures of the

two thiols. All the experiments discussed in this chapter deal with SAMs obtained by overnight adsorption of the thiols.

3.3.2. Contact Angle Measurements

The two thiols being quite different in their structure (OH and CH_3 terminated) their monolayers would exhibit a measurable difference in wettability. Contact angle (CA) made by water was thus used to characterize the difference in the hydrophobicity of the SAM. Monolayers prepared from pure TEG-DP thiol was hydrophobic and made a contact angle of 104 ± 2^o, whereas that formed from TEG thiol was hydrophilic and made a contact angle of 36 ± 2^o as seen in Figure 3.4. The uncertainties in the contact angle values are standard deviations of typically five measurements on individual samples prepared.

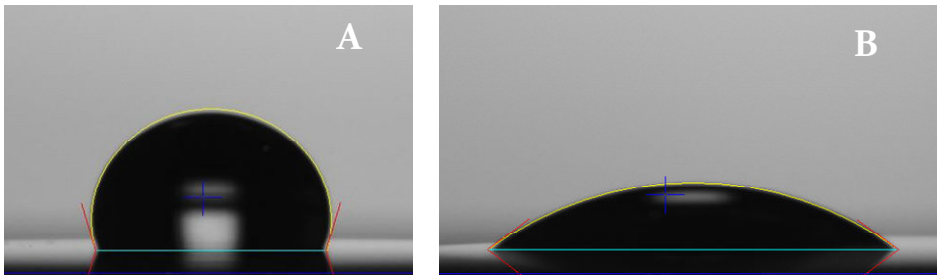

Figure 3.4. Photo of a water droplet in contact with a self-assembled monolayer of (A) TEG-DP thiol and (B) TEG thiol. The contact angles are measured between the solid-liquid interface (blue line) and the tangent drawn (red line) from the edge of the water droplet at the liquid-vapor interface.

Mixed SAMs of TEG-DP: TEG thiols obtained by varying molar ratios in solution of TEG-DP between 0 and 1 were studied by CA. It was observed that with successive increase in concentration of TEG-DP thiol in the adsorption solution the contact angle values increased linearly as seen in Figure 3.5. However, this increase, reached saturation for a SAM obtained from an equimolar mixture of the thiols in solution where a contact angle value of 102 ± 2^o was recorded. It was inferred from the group of G. M. Whitesides that coadsorption of two thiols of different chain lengths from a solution would lead to the preferential adsorption of the longer chain thiol as the attractive van der Waals forces between the hydrocarbon chains favor its adsorption.[30,31]

The consonance of our results by CA measurements, with the XPS characterization described for thiol adsorption from a solution mixture[31] clearly elucidates the preferential adsorption of the longer hydrophobic TEG-DP over the shorter hydrophilic TEG thiol. In addition, in the present system the TEG-DP thiol is expected to have dominating van der Waals interactions between the hydrophobic palmitoyl chains and form a more compact and dense SAM, thus favoring its adsorption over the smaller TEG thiol.

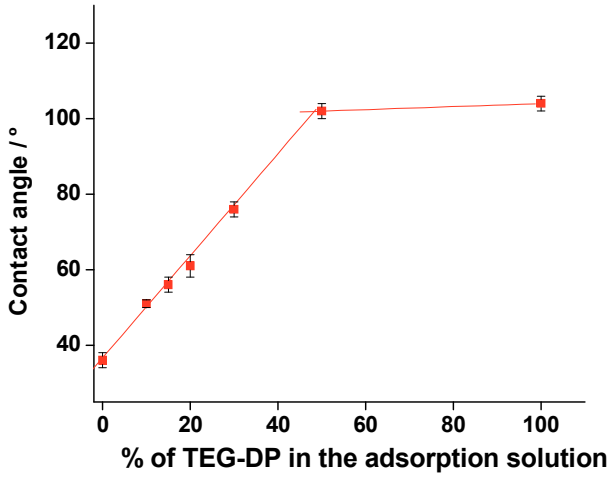

Figure 3.5. Plot of contact angle values made by water on the SAM against the percentage of TEG-DP thiol in solution. The standard error bars were estimated by contact angle measurement on five individual samples. The lines joining the data points are presented as guides to the eye and have no physical significance.

Thus, in summary, the hydrophobicity of the SAMs could be adjusted by varying the solution ratio of TEG-DP thiol in the range of 0 to 0.5.

3.3.3. Nulling Ellipsometric

Ellipsometric measurements was performed on SAMs, which were prepared ex-situ by overnight adsorption of 0.2 mM ethanolic thiol solutions followed by rinsing and drying under a stream of nitrogen gas. Their thickness were evaluated by fitting on a model of substrate/monolayer/air, where the refractive index 'n' of the thiol was taken as 1.45.[32] The measured thickness of the SAM of TEG-DP was found to be 3.68 ± 0.16 nm with a mean square error (MSE) of 1.5 and that of the TEG SAM was 1.86 ± 0.12 nm with a

MSE of 0.85. These thickness values conformed to the molecular dimensions of the thiols obtained by gas phase molecular modeling using CS Chem3D Pro, Cambridge Soft Corporation, Version 5 see Figure 3.6. Here the length of the TEG-DP thiol was found to be 3.7 nm (measured between the sulphur atom and the methyl hydrogen atom) and 1.9 nm for TEG thiol (measured between the sulphur atom and the hydroxy hydrogen atom) as seen in Figure 3.6. Furthermore, ellipsometric measurements of the SAM obtained from equimolar mixture of thiols gave a thickness of 3.5 ± 0.14 nm (MSE = 0.76), which confirmed its closer resemblance to that of SAM of pure TEG-DP as previously discussed with contact angle measurements.

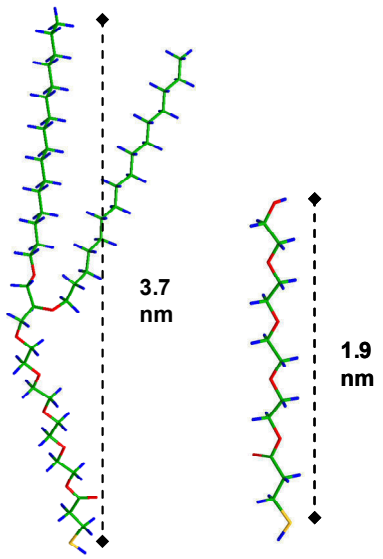

Figure 3.6. Gas phase modelled structures of TEG-DP thiol (left) and TEG thiol (right), indicating their molecular dimensions. The carbon atom is depicted in green, the hydrogen atoms blue, the oxygen atoms red and the sulphur atom yellow. CS Chem Draw 3D Pro version 5 was used for modelling.

3.3.4. AFM measurements

Atomic Force Microscopy was performed in the working buffer (Tris-HCl 50 mM, NaCl 150 mM, $MgCl_2$ 2 mM and $MnCl_2$ 1 mM at pH 7.4) on SAMs prepared on Template Stripped Gold (TSG) surfaces. The preparation of Template Stripped Gold surface has been described in detail in section 3.6.2 of the experimental protocols. The SAM modified TSG surface was placed in the liquid cell and the cell was then filled with the buffer. Imaging was performed in Top-MAC mode with a cantilever of spring constant

0.292 N/m. Topography images obtained were flattened and analyzed using Gwyddion 2.1.

A template stripped gold surface was imaged initially to analyze its morphology and roughness. An essentially flat surface was observed (Figure 3.7A) with a root mean square roughness of 0.25 nm. Similarly, the SAM of pure TEG thiol prepared on a TSG surface (Figure 3.7B) displayed a featureless topography with a root mean square roughness of 0.29 nm. However a SAM from 30% TEG-DP thiol solution showed regular arrangements of white spots, all through a surface of 1 × 1 μm^2 (Figure 3.7C).

It has been concluded by several groups that coadsorption at room temperature of two thiols from a solution can lead to phase segregation if the two thiols are quite different in their structure and lengths. As discussed in the preceding sections, we observed a marked preference in adsorption of the TEG-DP thiol over the TEG thiol. Since the TEG-DP thiol is longer by several carbon atoms (>16 carbon atoms), phase segregation would be quite obvious. These white spots (higher height) in topography images have previously been demonstrated to be corresponding to the aggregates/domains of the longer chain thiols as studied for a system of C8/C16 or C18 thiols.[33]

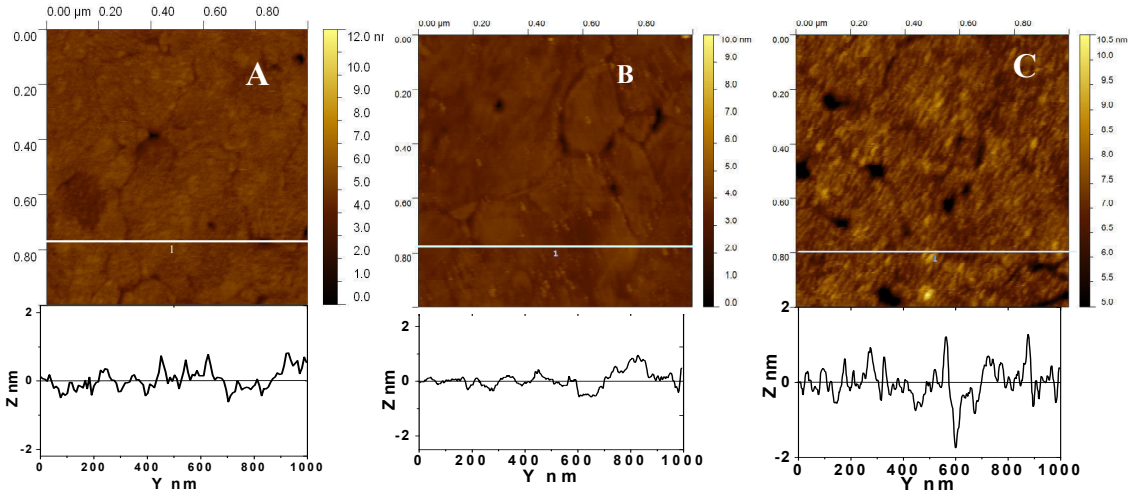

Figure 3.7. Topography AFM imaging in buffer of A) bare gold and B) SAM of pure TEG thiol and C) SAM of 30% TEG-DP thiol done in a magnetically driven acoustic mode (Top-MAC mode) using a MAC lever type VI cantilever having a spring constant k = 0.292 N/m and a resonant frequency in buffer = 17.8 kHz. The scan rate was set to 1.0 Hz and the images were flattened and analysed using Gwyddion 2.1. Below each image are their respective profiles in terms of Z vs Y traced on white line drawn on the image.

3.3.5. Electrochemical Reductive Desorption

Electrochemical Reductive Desorption by Cyclic voltammetry was employed to study the phase segregation in binary SAMs. This technique in which by application of a negative potential, electrochemical reduction of the Au-thiol bond takes place is a one-electron reduction process as described in reaction (1) leading to the detachment of the reduced species, alkane thiolate from the electrode surface.

$$Au-SR_{(ads)}+e^{-} \rightarrow Au+^{-}SR_{(soln)} \qquad (1)$$

It has previously been demonstrated that reductive desorption profiles of mixed/binary SAMs can throw insights on phase segregated SAMs.[15] When SAMs of a mixture of thiols are reductively desorbed, one can expect two very different situations.[34-37] In the case of SAMs where the thiols are randomly mixed on the surface and do not present phase separated domains, a single reductive desorption peak is expected at a potential that is dependent on the SAM composition. [36] However, when the SAM is largely phase segregated, the reductive desorption is expected to yield two peaks corresponding to their individual components where the surface area of these peaks would be proportional to the surface concentrations of the individual components. [15,35]

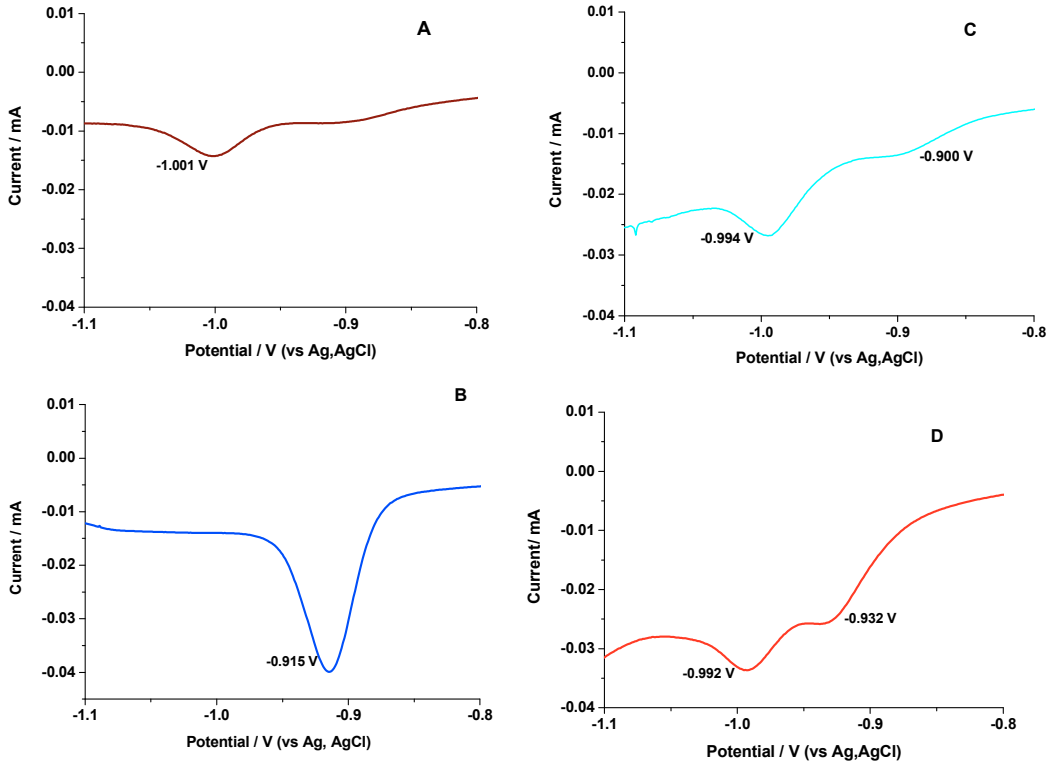

Figure 3.8 Cyclic voltammograms in 0.1 M NaOH (as an electrolyte) of self-assembled monolayers prepared from (A) 100% TEG-DP thiol (red curve), (B) 100% TEG thiol (blue curve), (C) 50% TEG-DP thiol (orange curve) and (D) 30% TEG-DP thiol (brown curve) recorded at 20 mV/s using Ag,AgCl as a reference electrode.

Figure 3.8 shows the reductive desorption of the various pure and binary SAMs prepared. On comparing Figure 3.8A and Figure 3.8B it can be seen that the SAM of pure TEG-DP thiol desorbs at more negative potentials (– 1.001 V) than the TEG SAM which desorbs at – 0.916 V. This fact has been previously reported to be a result of strong lateral interactions due to van der Waals forces between the alkane chains thus shifting the electrochemical desorption signal to more negative potentials.[15,38] We also observe that the peak area of the TEG-DP thiol desorption is smaller than that of the TEG thiol desorption peak, which corresponds to the fact that the TEG-DP thiol occupies a larger surface area per molecule than the TEG thiol. However, a more quantitative analysis by integrating the peaks of the voltammogram is not possible since the desorption peaks are essentially a combination of both Faradaic currents due to the reduction of the Au-S bonds and transient capacitance-charging currents due to a sudden increase in the capacitance caused by the detachment of the SAM from the surface.[38] Moreover, since these experiments were performed on gold coated quartz crystals as opposed to a template stripped gold surface, contributions/peaks arising from the

possible crystalline planes of the gold surface besides the most abundant (111) plane cannot be neglected.[39] Nevertheless, a purely qualitative picture of the homogeneity of the mixed SAMs can be obtained by comparing their reductive desorption profiles with that of their pure components.

As observed in Figure 3.8C, the reductive desorption of a SAM obtained from an equimolar mixture of TEG-DP and TEG thiols essentially leads to a single peak at about –0.994 V with the presence of a negligibly small peak at –0.900 V indicating that TEG-DP and TEG are rather randomly/completely mixed in the SAM. However, for a SAM prepared from 30% TEG-DP thiol in solution two clearly distinguishable reductive desorption peaks were observed. Interestingly, the peak at more negative potential (contribution from TEG-DP thiol) showed a less significant shift in peak potential (–0.992 V) as opposed to the peak at less negative potential (contribution from TEG thiol) which shifted to – 0.932 V, indicating that the domain in the SAM consisting TEG-DP thiols are almost exclusive with very less amounts of TEG thiols, while the domains of TEG thiols could have the presence of TEG-DP thiols. These results however, are quite in congruence with the AFM results, where a SAM made from 30% TEG-DP shows discernable patches or domains of the longer chain TEG-DP thiol.

3.3.6. Electrochemical Impedance Spectroscopy

Electrochemical Impedance Spectroscopy was used to characterize the self-assembled monolayers of different compositions containing decreasing amounts of TEG-DP thiol. These self-assembled monolayers were prepared on TSG surfaces to avoid surface inhomogeneities.

The Electrochemical Impedance (EI) spectrums of the various SAMs were analyzed as Complex-capacitance-plane plots (Figure 3.10). These plots display semicircular shapes at high frequencies and 'tails' at low frequencies. To extract the electric and dielectric parameters of the SAMs from impedance measurements, the EI spectrums of the SAMs were fitted using an Equivalent Circuit Model (ECM) as described in Figure 3.9. This circuit has previously been used by other groups to fit EIS data recorded for both pure and mixed SAMs[6,9-11] in the absence of a redox probe in solution.

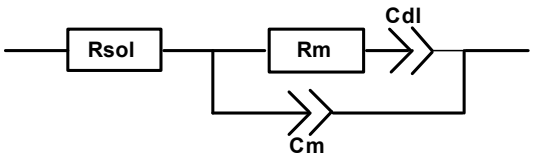

Figure 3.9 Equivalent circuit model (ECM) used to fit the Electrochemical Impedance Spectroscopy data.

Moreover, it takes into account all the parameters that best define the systems. The circuit consists of a solution resistance R_{sol} in series with parallel elements of the membrane (R_m // C_m) constituted of resistance and capacitance respectively and also in series with the electrical double layer capacitance C_{dl}. It is important to note here, that the order in which the elements are placed in the circuit are decided by their response on the time scale *i.e.* frequency and not on their physical arrangement in the measuring device. For example, in the ECM described in Figure 3.9, the solution resistance R_{sol} is obtained from the high frequency zones in the EIS spectrum shown in Figure 3.10 and hence it is placed first, the R_m, C_m in turn are characterised at moderate frequencies, whereas the C_{dl} appears at lower frequencies, defining their order in the ECM.

The equivalent circuit uses constant phase elements (CPE) instead of capacitances, to account for imperfections of the membrane due to surface inhomogeneities in the SAMs. The impedance of a CPE is given by $Z_{CPE} = Q^{-1}(j\omega)^{-\alpha}$ where Q is the amplitude of the CPE, ω is the angular frequency and α is the exponent which is a real number that varies between 0 and 1.

When $\alpha = 1$, purely capacitive behaviour is observed (i.e. Q = C).

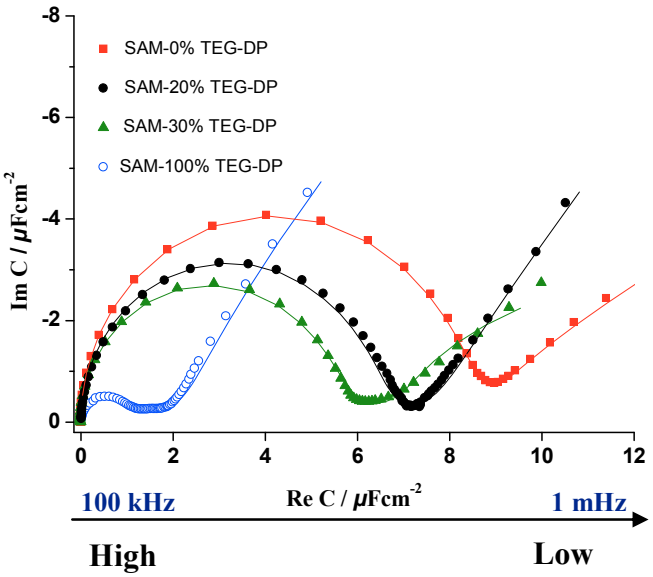

Figure 3.10 EIS data in Complex-Capacitance-plane representation recorded on SAMs of 100% TEG-DP (blue points), 30% TEG-DP (green points), 20%TEG-DP (black points) and 0% TEG-DP (red points). The lines through the points are the fits on the experimental data.

The lines passing through the data points in Figure 3.10 correspond to the fit using the equivalent circuit. The superposition of these lines on the data points demonstrates the perfect match between the experimental data (dots) and the electrical model. The values of resistance, capacitance and α parameter obtained by fitting are given in Table 3.1

Figure 3.10 represents the EI spectra measured for various SAMs with varying mol fractions of TEG-DP. Following the Helmholtz theory where the capacitance of a monolayer is inversely proportional to the layer thickness,[40] the SAM of the longer TEG-DP thiol exhibited lower capacitance (smaller semicircle) whereas the SAM of the shorter TEG thiol showed higher capacitance (bigger semicircle). Moreover, a systematic progression from spectra of smaller radius i.e. lower capacitance to spectra of higher capacitance was observed for SAMs obtained by successive dilution from 100% TEG-DP to 0% TEG-DP respectively. This increase in capacitance upon mixing the TEG-DP thiol with TEG thiol could be attributed to two principal factors, the first one being the mean thickness of the monolayer decreasing upon introduction of the shorter TEG thiol, thus increasing the capacitance and secondly the decrease in hydrophobicity of the monolayer as observed by contact angle measurements. The latter was explained by Bard *et al*. and others[41,42] that the interfacial capacitance of a hydroxy terminal SAM would be

higher than a similar length methyl terminated SAM due to increased hydrophilicity of the monolayer, thus influencing the dielectric properties of the layer.

Further, the introduction of the TEG thiols in a TEG-DP SAM would increase the 'disorder' in the SAM due to the presence of rather less well packed structures of TEG thiol in the SAM compared to the relatively denser or well packed TEG-DP thiols with van der Waals associated palmitoyl chains. The introduction of these disordered/less well packed zones of TEG thiol would facilitate the transport of ions across the membrane and thus decrease the resistance of the SAM.

It is worthwhile to note that the values of R_{sol}, does not vary much with different SAMs. This parameter, as explained in section 1.4.2 depends on the ionic strength of the electrolyte. Since in our experiments the same electrolyte was used for all the measurements, the R_{sol} remains invariant.

A similar remark can be made for the CPE_{dl}, values however, with the exception of a SAM of pure TEG thiol (0% TEG-DP thiol). This parameter (electrical double-layer capacitance) is dependent on various factors, the most important ones being the electrode potential, the ionic strength, the interfacial properties of the electrode (hydophobicity etc.). Thus, the closely similar values of CPE_{dl} obtained for the SAMs bearing the TEG-DP thiol and a distinct difference for a SAM bearing pure TEG thiol could be attributed to the fact that the interfacial properties are rather in close resemblance in SAMs bearing the TEG-DP thiol, whereas they hugely differ in its absence.

Table 3.1 Indicating the solution resistance (Rsol), the membrane resistance (Rm),, the membrane capacitance (Cm), and the double layer capacitance (Cdl) along with their α parameters for SAMs obtained from various compositions of TEG-DP thiols.

SAM	R_m MΩ cm^2	C_m $\mu F/cm^2$ (Q)	α_m	R_{sol}	CPE_{dl} $\mu F/cm^2$ $s^{(\alpha-1)}$	α_{dl}
100% TEG-DP	1.5 ± 0.2	2.68 ± 0.02	0.92 ± 0.01	20.4 ± 0.5	0.10± 0.02	0.77 ± 0.01
30% TEG-DP	1.2 ± 0.1	7.71 ± 0.04	0.97 ± 0.01	20.6 ± 0.4	0.14± 0.01	0.50 ± 0.01
20% TEG-DP	1.0 ± 0.3	8.32 ± 0.05	0.97 ± 0.01	19.2 ± 0.1	0.11± 0.03	0.50 ± 0.01
0% TEG-DP	0.035 ± 0.004	9.7 ± 0.1	0.97 ± 0.01	21.2 ± 0.2	0.36± 0.04	0.60 ± 0.01

3.4. Interaction of Small Unilamellar Vesicles (SUVs) with the SAMs

Small unilamellar vesicles of a hydrodynamic radius of 25 nm were allowed to interact with the preformed SAMs in the presence of buffer. These interactions of SUVs with various SAM compositions were studied by techniques like QCM-D, AFM and EIS. Each of these techniques highlights or points towards different aspects of these interactions with various SAMs. The present section is thus divided into sub-sections as per the technique used for the characterization of the interaction of SUVs with the SAMs. The preparation of small unilamellar vesicles is described in section 3.6.1 in the experimental protocols.

3.4.1. Quartz Crystal Microbalance with Dissipation (QCM-D)

Quartz Crystal Microbalance with Dissipation has been a technique extensively used for studying the adsorption events in real-time on the surface. QCM-D can not only determine the mass of very thin surface bound layers by following the frequency of oscillation, but it can also provide information on their viscoelastic properties, by the simultaneous measurements of Dissipation as a parameter.[43] The synchronous measurements of these two parameters help in understanding structural details of the adsorbed film. Thus, besides the various other applications offered by this technique, one of the most discussed application in literature is the formation of lipid bilayers on hydrophilic substrates and more precisely on a SiO_2 surface.[44-46] Several years ago, it was shown by Keller and Kasemo that QCM-D is one of the distinct techniques useful in measuring the different pathways of lipid vesicle adsorption on varied substrates. Besides being useful in clearly distinguishing the presence of intact adsorbed vesicles and the formation of a mono/bilayer of lipids, it also permits the real-time observation of a vesicle-to-bilayer phase transition. To this date, this technique has been extensively exploited to follow the formation of SLB, however its application to tBLM has been rather less investigated. We utilized this technique as a means to understand the interaction of vesicles with SAMs prepared from both pure TEG and TEG-DP thiols and subsequently with their various mixtures, which involved successive dilution of the anchoring TEG-DP thiol.

Vesicles upon interaction with a SAM of pure TEG thiol adsorbed quite instantly as indicated by a sharp shift in values (Figure 3.11 A) of normalized frequency reaching saturation within less than an hour of injection. As seen in Figure 3.11 A, the frequency and dissipation values were quite stable to further injection and rinsing ($\Delta F_9/9 = -75$ Hz) and ($\Delta D_9 = 5.8\times10^{-6}$) (Table 3.2).

These high shifts in both frequency and dissipation were suggestive of the adsorption of intact vesicles on the polar OH group by electrostatic interactions. Moreover, the frequency shift being dependent on the harmonic number was indicative of the presence of viscoelastic intact vesicles. Such high shifts in frequency and dissipation ($\Delta F_n/n = -90$ Hz) and $\Delta D_n = 3\times10^{-6}$) were obtained by Keller and Kasemo upon adsorption of intact vesicles on oxidized gold surface.[45] The presence of intact vesicles on a SAM of TEG thiol was later confirmed by AFM measurement (see Figure 3.19A).

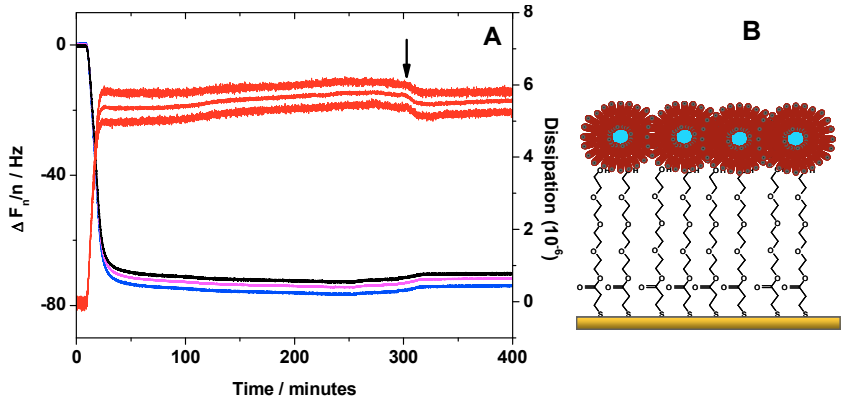

Figure 3.11 (A) QCM-D profile of vesicle interaction with a SAM of pure TEG thiol. On the right axis is the Dissipation (red for all harmonics) and on the left axis is the normalized frequency shift over several harmonics, depicted as blue for the 7th harmonic, magenta for the 9th harmonic and black for the 11th harmonic. The arrow indicates the rinsing with buffer and (B) a cartoon representation of the vesicles adhered on a TEG SAM.

As anticipated though, the interactions of vesicles with the hydrophobic TEG-DP SAM lead to the attachment of a phospholipid monolayer (Figure 3.12A). The process followed a one step pathway as previously reported where adsorption and rupture of vesicles occurred simultaneously[45]. The final shift in frequency ($\Delta F_9/9 = -11$ Hz) was close to that observed for the fusion of vesicles on a hydrophobic octadecane thiol SAM ($\Delta F_9/9 = -13$ Hz).[45] However the dissipation ($\Delta D_9 = 1.7\times10^{-6}$) was found to be slightly

high compared to the value reported for the attachment of a monolayer of lipid on a hydrophobic SAM.

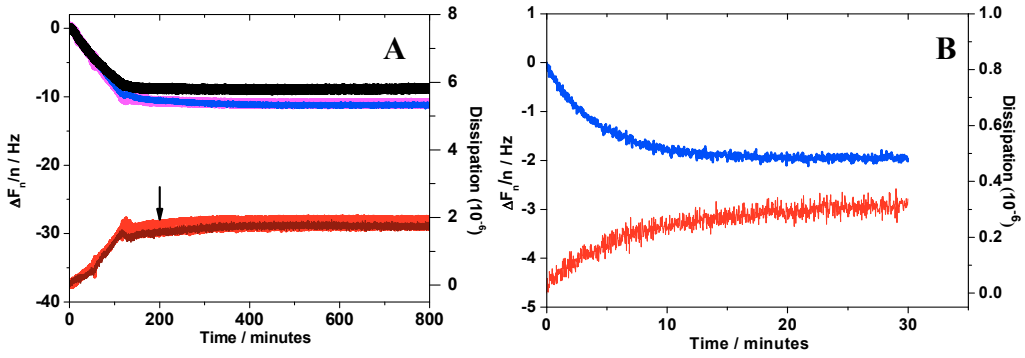

Figure 3.12 QCM-D profiles of (A) the interaction of vesicles with a TEG-DP SAM. On the right axis is the Dissipation (red for all harmonics) and on the left axis is the normalized frequency shift over several harmonics, depicted as blue for the 7th harmonic, magenta for the 9th harmonic and black for the 11th harmonic. The arrow indicates the rinsing with buffer (B) the swelling/hydration of the TEG-DP monolayer when exposed to buffer solution. In blue is the normalized frequency and red is the dissipation as measured on the 9th harmonic.

We observed in our experiments, that the SAMs underwent an initial hydration and/or swelling upon contact with the aqueous buffer. This process was marked by a small and gradual change in frequency and dissipation which stabilised after a few minutes (Figure 3.12 B). Vockenroth *et al*. reported this phenomenon to be the swelling of the ethylene glycol moieties [29] in the DPhyTL molecule upon hydration to form a layer which is more dissipative than the unhydrated SAM.

Therefore, this slightly higher dissipation value could be attributed to the swelling of the ethylene glycol moiety rather than to the presence of unfused vesicles.[20] However, besides the slightly higher dissipation, the variation of normalised frequencies for different harmonic numbers was quite small, which also supports the absence of highly dissipative unfused vesicles. Application of the Voinova model to calculate the mass of the film adsorbed gave a value of 238 ng/cm^2, which is in good agreement with that expected for the attachment of half a bilayer of phospholipids (Figure 3.13).

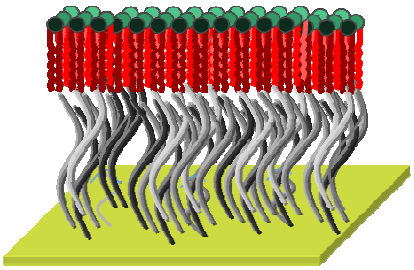

Figure 3.13 Cartoon representation showing the attachment of half a bilayer formed on a TEG-DP SAM.

We now probed into the interaction of vesicles with mixed SAMs where the hydrophobic thiol was successively diluted to investigate its threshold concentration required to induce the fusion of vesicles. Quite interestingly, we observed that the fusion of vesicles on a SAM obtained from a solution of 30% of TEG-DP thiol, continued to follow a similar trend (Figure 3.14A), as in the case of 100% TEG-DP (Figure 3.12A). The vesicles fused upon adsorption. It is important to notice here though that a SAM of 30% TEG-DP made a contact angle of 76°, implying that there is a significant decrease in hydrophobicity of the surface as compared to the pure TEG-DP SAM (CA= 104°).

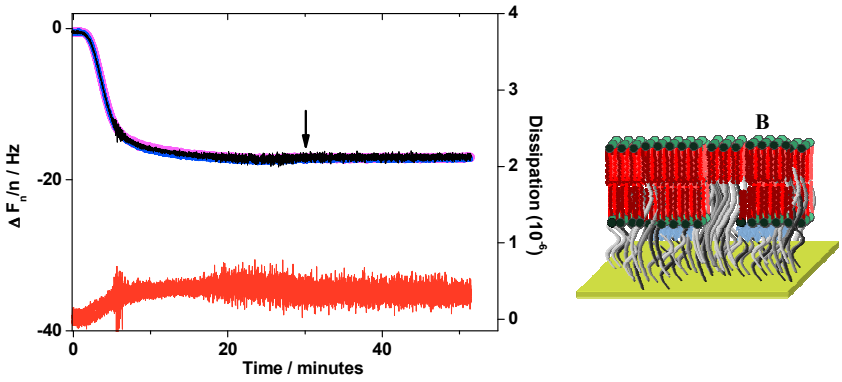

Figure 3.14 (A) QCM-D profile for the interaction of vesicles with a SAM made from 30% TEG-DP thiol On the right axis is the Dissipation (red for all harmonics) and on the left axis is the normalized frequency shift over several harmonics, depicted as blue for the 7th harmonic, magenta for the 9th harmonic and black for the 11th harmonic. The arrow indicates the rinsing with buffer. (B) A cartoon representation of a tBLM formation on a SAM made from 30% TEG-DP thiol.

Nevertheless, apparently the hydrophobic forces that govern the fusion still continued to be dominant at this mixture ratio. It is also worthwhile to note that the final shift in frequency ($\Delta F_9/9$ = –17 Hz) after the completion of the process and rinsing is intermediate to that one would expect for the attachment of a complete bilayer ($\Delta F_9/9$ = –

26 Hz) and a half of a bilayer ($\Delta F_9/9$ = –13 Hz).[45] However, the total mass of the film attached was found to be 401 ng/cm^2, a value rather close to as demonstrated for a Supported Lipid Bilayer (468 ng/cm^2).[45] This could be explained by the fact that the SAM possesses significant TEG thiol molecules which would lead to the attachment of phospholipid molecules in the proximal layer. Thus besides the attachment of the distal monolayer of phospholipids on the anchoring TEG-DP part of the SAM by hydrophobic interactions, the phospholipids would also be expected to adsorb as a bilayer on the TEG part (Figure 3.14B). This would then lead to the formation of a compact defect free bilayer as also confirmed by AFM (see Figure 3.19B). One could also envisage a hydration layer between the OH terminal of TEG part of the SAM and the phospholipids head groups of the proximal layer, which would contribute to this rather increased mass values. The presence of this hydration layer on sparsely tBLMs formed on mixed SAMs has previously been reported.[10]

On the other hand, a spectacular difference in the fusion pattern was observed upon further dilution of the TEG-DP thiol in the SAM. In the case of a SAM of 20% TEG-DP, the vesicles were found to initially adsorb as marked by a sharp decrease in frequency and increase in dissipation, followed by a gradual transition marked by an increase in frequency and decrease in dissipation until they reached a stable point (see Figure 3.15). The values of frequency upon stabilization of the signal were higher ($\Delta F_9/9$ = –19 Hz) than that obtained on a 30% TEG-DP SAM.

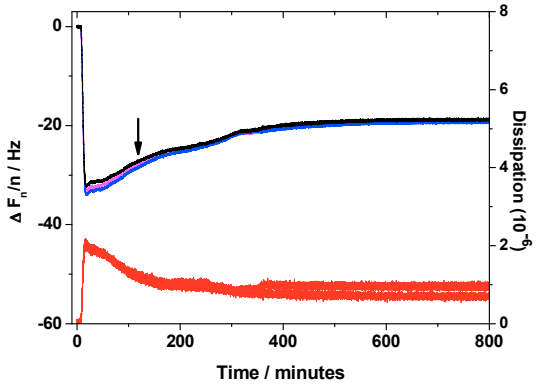

Figure 3.15 QCM-D profile for the interaction of vesicles with a SAM made from 20% TEG-DP. On the right axis is the Dissipation (red for all harmonics) and on the left axis is the normalized frequency shift over several harmonics, depicted as blue for the 7th harmonic, magenta for the 9th harmonic and black for the 11th harmonic. The arrow indicates the rinsing with buffer.

Application of the Voinova calculation revealed a mass of (440 ng/cm^2). This higher mass value upon dilution of TEG-DP from 30% to 20% TEG-DP thiol is in agreement with our argument that the phospholipids are included as a bilayer in the proximal layer, with hydration water molecules infixed between the TEG part of the SAM and phospholipid head groups. On careful observation of Figure 3.15, it is clear that vesicles after initial adsorption underwent a transition which was not perturbed by rinsing with buffer. This QCM-D profile is similar to a two-step process as observed for a supported lipid bilayer formation on SiO_2, where the first step (decrease in frequency) corresponds to the adsorption of intact vesicles until a critical surface coverage and the second step (increase of frequency) corresponds to the bilayer formation by fusion of vesicles and the release of entrapped water.[46] Moreover, the frequency appeared to stabilize to a constant value only after a few hours suggesting that after an initial deposition, vesicles underwent a rather slow re-organisation on the surface before their rupture.

It was proposed by Jenkins *et al* that adsorbed vesicles on a mercaptoethanol/octadecanethiol micro-patterned SAM could have some surface mobility and by "random walk" they could migrate to the hydrophobic edges which induce their rupture.[47] This proposition, if extended to our system, where the SAM could exist as discrete phase segregated patches of TEG-DP thiol, the vesicles initially adsorb intact on the TEG domains. Then these vesicles slowly traverse/travel to the hydrophobic TEG-DP patches, where their rupture and fusion to a bilayer occurs (see Figure 3.16).

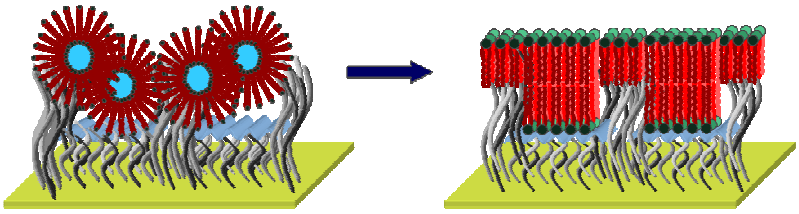

Figure 3.16 Cartoon representation of the fusion process on a 20%TEG-DP TEG-DP SAM, the vesicles could initially adsorb on the TEG part of the SAM and then undergo fusion to form a tBLM.

Upon further dilution of the TEG-DP thiol to 15% in the SAM (CA = 56°) this transition was even more marked and prolonged and the signal stabilised only after about 16 hours (see Figure 3.17). This retarded transition from vesicles to tBLM formation could be attributed to the lower density of the anchoring TEG-DP thiol in the SAM. This two step

fusion process of vesicles to form a bilayer has been usually observed on solid hydrophilic substrates like SiO_2, Si_3N_4,[48] or on a polymer coated solid substrate.[49,50] However to the best of our knowledge, this observation of a two step fusion process by QCM-D on a tethered architecture has never been discussed.

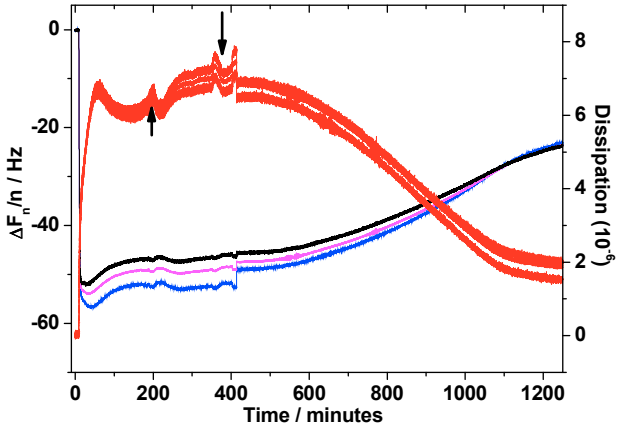

Figure 3.17 QCM-D profile for the interaction of vesicles with a SAM made from 15% TEG-DP thiol. On the right axis is the Dissipation (red for all harmonics) and on the left axis is the normalized frequency shift over several harmonics, depicted as blue for the 7th harmonic, magenta for the 9th harmonic and black for the 11th harmonic. The upward arrow indicates the increase in flow of vesicles to 50 µL/min and the downward arrow indicates the rinsing with buffer.

Additionally, on a SAM obtained by further dilution of TEG-DP thiol i.e. 10%, the vesicles ceased to form a bilayer and remained intact on the surface as observed for a pure TEG SAM. This fact reinforces our suggestion that in SAMs containing rather dilute concentrations of the anchoring thiol, vesicles initially adsorb intact on the TEG domain and fuse by migrating towards the hydrophobic TEG-DP domains. Since in this case, the anchoring group is overly diluted in the SAM, this restricts the fusion of the vesicles. We can thus infer from the above results that a critical concentration of the hydrophobic anchoring thiol is essential in the SAM to induce rupture and fusion of the vesicles (Figure 3.18 and Table 3.2) and also that the concentration of the hydrophobic thiol on the surface governs the kinetics of vesicle fusion.

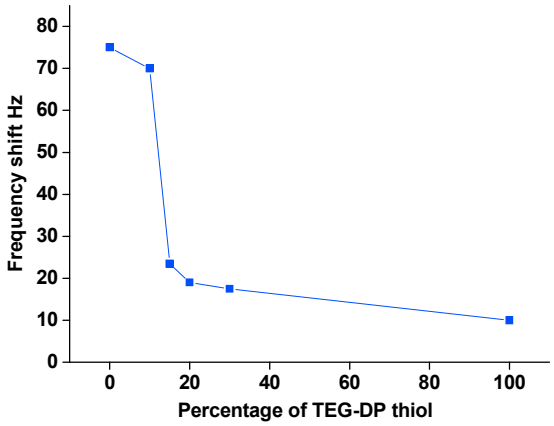

Figure 3.18 Plot of final shift in frequency vs percentage of TEG-DP thiol in the process of interaction with vesicles. The abrupt increase below 15 % indicates the critical conc. of TEG-DP thiol required for fusion of vesicles to a bilayer.

Table 3.2 Final shifts in frequency as measured on the ninth harmonic observed for the interaction of vesicles with various SAMs. The Voinova model was applied to the frequency and dissipation to calculate the final mass uptake.

Fraction of TEG-DP in solution ($\chi_{TEG\text{-}DP}$- mol %)	**$\Delta F_9/9$ (Hz)**	**Mass uptake (ng/cm^2)**
100	–11	238
30	–17	401
20	–19	440
10	–70	4100
0	–75	3150

3.4.2. AFM measurements

AFM imaging was carried out to distinguish between unfused vesicles and the formed tBLM. As discussed earlier, a SAM of TEG thiol was almost featureless as seen in Figure 3.7A and thus the presence of the unfused vesicles upon interaction with this SAM was quite clearly discernable *cf.* Figure 3.19A. Upon careful analysis of the profiles traced on the images (Figure 3.19A), the root-mean-square (RMS) roughness of the SAM-TEG was observed to be 0.29 nm with a maximum peak to valley height of <1 nm. However, upon interaction with vesicles followed by rinsing and imaging, this peak

to valley height was found to increase to around 25-30 nm (Figure 3.19A). It was reported recently by Wang *et al.* by AFM observations that pristine TSG surface had almost no affinity for vesicles as opposed to plasma treated TSG surfaces where vesicles adsorbed intact.[51] This observation helps us to comment that the intact vesicles observed by AFM are a result of the interaction of vesicles with the TEG SAM as observed by QCM-D and not with the gold substrate itself.

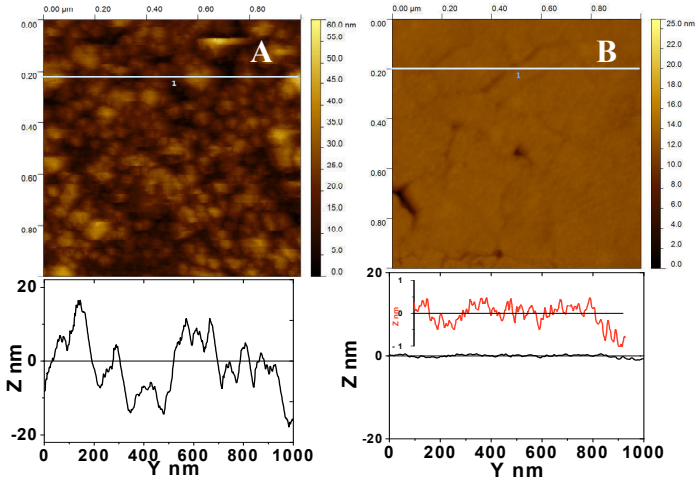

Figure 3.19 Topography AFM imaging in buffer of (A) SAM of pure TEG thiol upon interaction with vesicles and rinsing and (B) SAM of 30% TEG-DP after interaction with vesicles and rinsing. Imaging was done in a magnetically driven acoustic mode (Top-MAC mode) using a MAC lever type VI cantilever having a spring constant k = 0.292 N/m and a resonant frequency in buffer = 18 kHz. The scan speed was set to 1Hz. Below each image are their respective profiles in terms of Z vs Y traced on the white line drawn on the image. The inset in figure 3.19 B shows a zoom on the Z axis of its profile.

The tBLM formation on a phase segregated SAM of 30% TEG-DP was also interesting to observe by AFM measurements. The domains previously observed on the segregated SAM appeared to be covered/masked upon the formation of the bilayer by fusion of vesicles (Figure 3.19B). The bilayer appeared to be free of patches, islands or discontinuities and defects over several zones of surface $1 \times 1\ \mu m^2$.

3.4.3. Electrochemical Impedance Spectroscopy

EIS was used to analyze the interactions of vesicles with various SAMs. The self-assembled monolayers were treated with vesicles for typically 4 hours, during which the vesicles were renewed in the electrochemical cell every few minutes; the EIS were then recorded in buffer. The EIS spectra presented in Figure 3.20 were recorded on various SAMs after interaction with vesicles.

It was observed in the case of a SAM of pure TEG thiol that interaction with vesicles leads to an insignificant decrease in membrane capacitance (compare red curves in Figure 3.10 and Figure 3.20). The values of the membrane resistance R_m, capacitance C_m and α parameters for membrane capacitance α_m, as well as the solution resistance R_{sol}, the double layer capacitance CPE_{dl} and double layer capacitance α_{dl} for this curve were obtained by fitting using the ECM described in Figure 3.9. The values obtained by fitting for the vesicle interaction with a TEG-SAM are described in Table 3.3. The rather insignificant increase in R_m and negligible decrease in C_m, confirmed our earlier observations by QCM-D and AFM that vesicles remained intact and did not form a bilayer on this SAM.

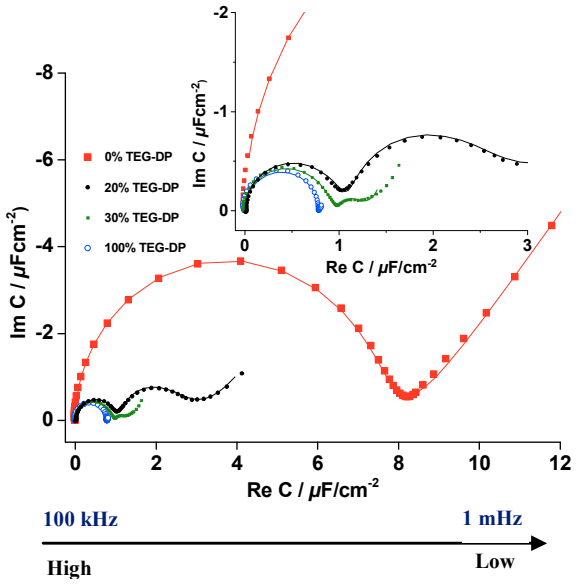

Figure 3.20 EIS data in Complex-Capacitance-plane representation as recorded after vesicles interaction with SAMs made from 100% TEG-DP (blue points), 30% TEG-DP (green points), 20% TEG-DP (black points), 0% TEG-DP (red points). The lines through the points are the fits on the experimental data. The data represented here are after 4 hours of interaction with vesicles except for 20% TEG-DP where it is represented after 24 hours interaction with vesicles.

However, in the case of a 100% TEG-DP SAM, a remarkable increase in membrane resistance (~ 180 fold) and a decrease in membrane capacitance (by a factor of ~ 3.3) was observed upon interaction with vesicles as compared to the SAM (fitted with the ECM described in Figure 3.9). This significant increase in membrane resistance and decrease in the capacitance clearly indicated the formation of a tBLM on a SAM of 100%TEG-DP (*cf.* Figure 3.20 and Table 3.3). Also, notably the value of α_m was found to be nearly equal to 1, indicating the formation of a perfect, homogenous tBLM.

Similarly, in the case of a 30% TEG-DP SAM upon interaction with vesicles for 4 hours, a clear decrease in capacitance was observed (compare green curves in Figure 3.10 and Figure 3.20). However, on careful examination of Figure 3.20, another phenomenon marked by the presence of a second very small semicircle appears.

Further, for a SAM of 20% TEG-DP, the interaction of vesicles with the SAM for 4 hours showed no significant decrease in capacitance (data not shown). However, another measurement after 24 hours of interaction with vesicles led to a drastic decrease in the capacitance as seen in Figure 3.20.

The presence of a second semicircle is also observed here, although it is much more pronounced than that for the vesicle interaction on a 30% TEG-DP SAM.

This second semicircle, on both 20% and 30% TEG-DP SAM, is different/well separated in terms of frequency from the first semicircle which corresponds to the capacitance of the tBLM formed on all the 3 SAMs i.e. 100, 30 and 20% TEG-DP.

The presence of this second semicircle could eventually be attributed to the presence of unfused vesicles/vesicular aggregates on the formed bilayer. These unfused vesicles/aggregates observed here could be a result of ineffective rinsing due to the absence of a continuous flow as opposed to QCM-D measurements. To account for this additional phenomenon, the EI spectra for these two substrates (30 and 20% TEG-DP) were thus fitted by adding, in series, a parallel resistance/capacitance element (Rv // Cv) (Figure 3.21) to the ECM described in Figure 3.9.

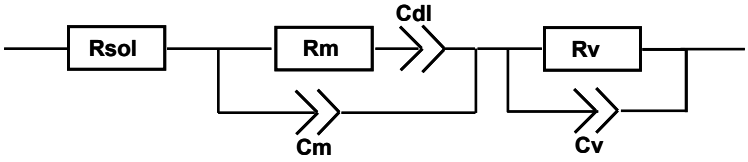

Figure 3.21 Equivalent circuit model used to fit the EIS spectrum for measurements on vesicle interaction with a SAM of 30% TEG-DP thiol (measured after 4 hours) and a SAM of 20% TEG-DP thiol (measured after 24 hours)

Albeit, the contribution of this second semicircle (values of Rv = 10,500 Ω and 22,000 Ω for 20% and 30% TEG-DP SAM respectively) was midget as compared to the Resistance (Rm) of the first semicircle (*cf.* Table 3.3), we still chose to take these additional components into account to obtain better precision on the fitting of the first semicircle which appeared to be characteristic of the membrane.

By comparing the values of R_m and C_m of the SAMs of both 30% and 20% TEG-DP, before and after interaction with vesicles (Table 3.1 and Table 3.3) a clear increase in membrane resistance and decrease in membrane capacitance confirmed the formation of bilayers on these two SAMs. Also, it is interesting to note that α_m values decrease with increasing dilutions of the TEG-DP thiol, indicating that among the various tBLMs formed, the one formed on pure TEG-DP SAM is the most homogenous while the 20% TEG-DP is the least homogenous/ordered. It was also interesting to observe that the tBLM on a pure TEG-DP SAM was ten times more resistive than that on a 30 % mixed SAM, and that the tBLM on a 30 % TEG-DP mixed SAM was ten times more resistive than that of a 20 % TEG-DP mixed SAM. This decrease in resistance with dilution of the TEG-DP in the SAM is coherent with earlier observations.[10,15]

Furthermore, upon observation of Table 3.3 it can be seen that the double layer capacitances parameters (CPE_{dl} and α_{dl}) of tBLMs formed on both 20% and 30% TEG-DP SAMs were not determined, but rather they were fixed to a certain value. This approach was adopted, as the determination of these parameters by fitting leaded to a rather poor determination of the membrane parameters (R_m, C_m and α_m). Moreover, since the electrolyte used for all the experiments is the same, the double layer charging capacitance are not expected to vary much from one substrate to another.

Moreover, as observed previously in section 3.3.6, the CPE_{dl} remained invariant for SAMs bearing the TEG-DP thiol and thus they were not expected to vary much upon the formation of a tBLM. Further, this parameter was secondary to our interests of measurements and data exploitation. The principal parameters that we were keen in observing were that of the membrane (R_m, C_m and α_m), and thus fixing the CPE_{dl} to constant values (for 30 and 20% TEG-DP bearing SAM) was an attempt to determine the membrane parameters with precision.

Table 3.3 Indicating the membrane resistance (Rm), solution resistance (Rsol), membrane capacitance (Cm), double layer capacitance (Cdl) and their α parameters (α_m and α_{dl}) for SAMs obtained from various compositions of TEG-DP thiols after interaction with vesicles.

SAM	R_m MΩ cm^2	C_m $\mu F/cm^2$	α_m	R_{sol}	CPE_{dl} $\mu F/cm^2\ s^{(\alpha-1)}$	α_{dl}
100% TEG-DP	280 ± 70	0.81 ± 0.01	0.99 ± 0.01	21.4 ± 0.2	0.12 ±0.04	0.68 ± 0.01
30% TEG-DP	22 ± 4	1.50 ± 0.01	0.97 ± 0.01	22.6 ± 0.4	0.12[b] (fixed)	0.50[b] (fixed)
20% TEG-DP [a]	2.4 ± 0.7	4.5 ± 0.2	0.92 ± 0.01	24.2 ± 0.1	0.12[b] (fixed)	0.70[b] (fixed)
0% TEG-DP	0.05 ± 0.02	8.9 ± 0.1	0.97± 0.02	24.2 ± 0.2	0.64 ± 0.02	0.60 ± 0.02

[a] Measured after 24 hours of vesicle interaction followed by rinsing. [b] The values were fixed and not determined.

Likewise, an increase in capacitance of the tBLM was observed upon dilution of the TEG-DP in the SAM from 100% TEG-DP to 20% TEG-DP in the SAM, however this increase appears to be rather prominent between 30% to 20% of TEG-DP thiol. A plausible explanation to this prominent increase would be the presence of increased hydration molecules between the SAM and the phospholipid head groups which would influence the dielectric properties of the bilayer. These results however need further investigations using other complementary techniques like Neutron Reflectivity to evaluate the structure and packing of the bilayer.

3.5. Conclusion and Perspectives

Self Assembled Monolayers were used as platforms for the design of Tethered Lipid Bilayers (tBLMs). To this end SAMs were prepared by using pure hydrophobic TEG-DP thiol or by mixing it in different ratios with a hydrophilic TEG thiol. A complex trend in the SAM formation was observed upon mixing the two thiols. The hydrophobic TEG-DP thiol showed higher propensity in adsorption over the hydrophilic thiol. It was observed by AFM that a mixed SAM containing moderate concentration of TEG-DP thiol, showed phase segregated patches of the hydrophobic thiols.

While the formation of tBLM on hydrophobic SAMs by fusion of vesicles is known to be a spontaneous one step process, correspondingly vesicles fused upon interaction with a SAM made from 100% TEG-DP. The tBLM formation continued to follow the same trend for TEG-DP dilutions up to 30%. However, we identified by QCM-D, that for SAMs prepared by further dilution of the TEG-DP to 20 or 15%, the tBLM formation process followed a two step pathway where vesicles first adsorb intact and then rupture and fuse to form a bilayer. It was also observed that upon further dilution of the TEG-DP in the SAM below 10%, the vesicles adsorb intact and cease to form a bilayer. The results were also complemented by EIS measurements. We also demonstrate by EIS measurements that although the electrical sealing properties of the tBLMs decrease with decrease in TEG-DP thiol in the SAM, the tBLM formed on a 30% TEG-DP is still fairly resistive.

Thus, we successfully demonstrate that the kinetics of fusion of vesicles depends on the composition of the SAM. Furthermore, a critical concentration of the hydrophobic thiol is vital in inducing the rupture and fusion of vesicles to form a bilayer. While the dilution of the anchoring hydrophobic thiol in the SAM is the interest of this paper, we observed that below a certain concentration, the tBLM formation is either too slow or the tBLM thus formed is less homogenous. Hence, an optimum in terms of the formation kinetics and the bilayer properties is observed at moderate dilutions of the anchoring thiol.

3.6. Experimental Protocols

POPC (1-Palmitoyl-2-oleoyl-sn-glycero-3-phosphocholine) was obtained from Avanti Polar (Alabaster, AL) and used as supplied. Milli-Q grade water of resistivity 18 MΩ·cm was used for all physical measurements. Buffer containing Tris-HCl 50 mM, NaCl 150 mM, $MgCl_2$ 2 mM and $MnCl_2$ 1 mM at pH 7.4 was used for all experiments unless otherwise specified.

3.6.1. Preparation of Small Unilamellar Vesicles (SUVs)

Small unilamellar vesicles were prepared using a 200µl POPC solution from a 10 mg/ml stock solution in chloroform. The chloroform was evaporated under a continuous flow of Nitrogen to form a thin, uniform lipid film and then the remaining traces of chloroform were removed keeping under vacuum for 1 hour. This dried lipid film was then hydrated with 2 ml of buffer and vortexed vigorously for 60 seconds. The resulting multilamellar vesicles/ aggregates were probe sonicated for 30 min at 10 ^{o}C followed by ultracentrifugation at 150,000g at 4 ^{o}C for 4.5 hours to separate small unilamelllar vesicles (SUVs) from titanium particles and larger lipid structures. These vesicles were finally diluted to a working concentration of 0.1 mg/ml and their size distribution was immediately characterized using a Zetasizer Nano series (Malvern, USA). Vesicles of size 25 nm were obtained with a polydispersity index (PDI) of 0.15. The PDI being inferior to 0.25 indicated that the vesicles were monodisperse. These vesicles were stored at 4 °C for until 3 weeks after their preparation.

3.6.2. Preparation of Template Stripped Gold (TSG)

Template stripped gold substrates were prepared using commercially available (Ssens, Netherlands) slides of mica onto which a ~200 nm thick gold was deposited. The gold side of this slide was then glued to an appropriately sized glass using EPO-TEK 377 and cured for 90 min at 150 °C. After cooling, the slides were detached from mica and used immediately for the preparation of the SAM.

3.7. Synthetic Protocols

Synthesis of 4.

Isopropylidene glycerol **3** (800mg, 6.05 mmol) was taken in 5 ml of dry dichloromethane. To this solution was added anhydrous pyridine (5 ml) and the solution was cooled to 0 ^{o}C. To this cooled solution was added

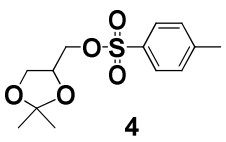

4

p-toluene sulfonyl chloride (1.7 g, 9.084 mmol) and stirred overnight at room temperature. The volatiles were then removed in vacuo and dichloromethane (50 ml) was added. The organic layer was washed with water (2x 10 ml), $NaHCO_3$ (2x 15 ml) and 0.5 M HCl (1x 5 ml) and brine solution (1x 10 ml). The organic layer was dried over anhydrous Na_2SO_4 and concentrated to give a solid which was recrystallized in a mixture of ethyl acetate and hexane to afford pure product as white crystals.

Yield : 1.5 g, 86 %

^{1}H NMR, ($CDCl_3$, 300 MHz) δ 1.31 (s, 3H), 1.34 (s, 3H), 2.45 (s, 3H), 3.74- 3.9 (series m, 4H), 4.03-4.3 (m, 1H), 7.34 (d, 2H, J = 8.4 Hz), 7.79 (d, 2H, J = 7.53 Hz).

ESI-MS $C_{13}H_{18}O_5S$

Calcd MW= 286

Found MW = 309 [M+ Na^+] 287 [M+H^+]

Synthesis of 5.

NaH (125 mg, 5.22 mmol) was taken in 5 ml of dry THF and allowed to stir at 0 ^oC for 5 minutes in an argon atmosphere. To this was added dropwise a solution of tetraethylene glycol (680mg, 3.5mmol) in dry THF. After the evolution of hydrogen gas ceased, a solution of 4 (500 mg, 1.75 mmol) in dry THF was added dropwise. This mixture was gradually allowed to attain room temperature and was then refluxed for 3 days in an inert atmosphere. On completion, the solvent was removed by evaporation and $CHCl_3$ (75 ml) was added. The organic layer was washed with water (2x10 ml) and brine (1x 10 ml). The organic layer was dried over anhydrous Na_2SO_4 and the crude product was purified by column chromatography on silica using CH_2Cl_2: MeOH (97:3) as colourless oil.

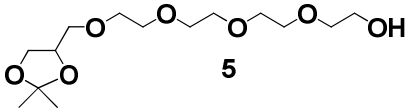

5

Yield : 450 mg, 83%

^{1}H NMR, ($CDCl_3$, 300 MHz) δ 1.33 (s, 3H), 1.40 (s, 3H), 3.47-3.61 (m, 20H), 4.2-4.25 (m, 1H)

ESI-MS $C_{14}H_{28}O_7$

Calcd MW= 308

Found MW = 331 [M+Na^+]

Synthesis of 6.

NaH (16 mg, 0.68 mmol) was taken in 2 ml of dry THF and allowed to stir at 0 ^{o}C for 5 minutes in an argon atmosphere. To this was added a solution of **5** (140 mg, 0.455 mmol) in dry THF dropwise. After stirring for 15 mins, catalytic amount of tetrabutyl ammonium bromide and a solution of benzyl bromide (116mg, 0.68mmol) in dry THF were slowly added. The reaction was allowed to warm to room temperature and stirred for 2 h. On completion of the reaction as monitored by TLC, THF was evaporated and $CHCl_3$ added. This was then washed with water (2 x 10 ml) and brine (1 x 10ml). Organic layer was dried over anhydrous Na_2SO_4 and the product was purified by column chromatography on silica using CH_2Cl_2: MeOH (9:1) to afford **3** as clear oil

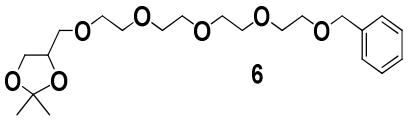

Yield : 135 mg, 72%

^{1}H NMR, ($CDCl_3$, 300 MHz δ 1.35 (s, 3H), 1.41 (s, 3H), 3.38-3.65 (m, 19H), 3.64-3.91 (br, s, 2H), 4.49 (s, 2H), 7.17-7.26 (m, 5H).

ESI-MS $C_{21}H_{34}O_7$

Calcd MW = 398

Found MW = 421 [*M*+Na^+]

Synthesis of 7.

Compound **6** (135 mg, 0.339mmol) was dissolved in a 1:1 mixture of CH_2Cl_2: MeOH. To this was added 2-3 drops of 5M HCl and the reaction allowed to stir overnight. Evaporation of the solvents under reduced pressure afforded pure product as a colorless oil.

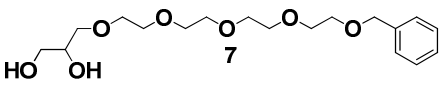

Yield : 450 mg, 83%

^{1}H NMR, ($CDCl_3$, 300 MHz) δ 1.33 (s, 3H), 1.40 (s, 3H), 3.47-3.61 (m, 20H), 4.2-4.25 (m, 1H)

ESI-MS $C_{14}H_{28}O_7$

Calcd MW = 308

Found MW = 331 [*M*+Na^+]

Synthesis of 8.

NaH (48 mg, 2.01 mmol) was taken in 3 ml of dry THF and stirred at 0 ^{o}C. To this was added **7** (120 mg, 0.335 mg) in 3 ml of THF dropwise at 0 ^{o}C over a period of 20 minutes. The solution was allowed to stir till the evolution of hydrogen gas ceased. To this was then added a solution of hexadecyl bromide in dry THF dropwise and a catalytic amount of tetrabutyl ammonium iodide, on completion of addition, the reaction was refluxed for 3 days. After this period the solvent was removed by evaporation and 75 ml of $CHCl_3$ added. The organic layer was washed with water (2 x 10 ml) and brine (1 x 10 ml). The organic layer was dried over anhydrous Na_2SO_4, and evaporated to dryness. The crude product obtained was purified by column chromatography on silica using $CHCl_3$ as the eluent.

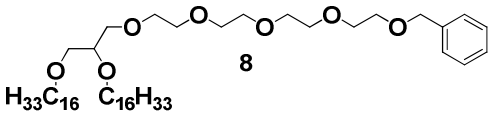

8

Yield : 150 mg, 56 %

^{1}H NMR, ($CDCl_3$, 300 MHz) δ 0.87 (t, 6H, *J*= 6.6 Hz), 1.25 (s, 52H), 1.58- 1.61 (m, 4H), 3.39-3.66 (m, 25H), 4.52 (s, 2H) 7.24 (s, 1H), 7.33-7.35 (m, 4H).

ESI-MS $C_{50}H_{94}O_7$

Calcd MW = 806

Found MW = 829 [*M*+Na^+]

Synthesis of 9.

A solution of **8** (150 mg, 0.186 mmol), catalytic amount of 5% Pd/C and ethanol (5 mL) was stirred under hydrogen atmosphere at room temperature. The reaction progress was monitored by TLC. When the reaction was complete after 3 hrs, the reaction mixture was diluted with CH_2Cl_2 and the catalysts were removed by celite filtration. The filtrate was evaporated under reduced pressure and

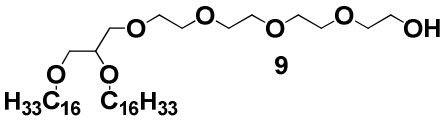

9

Yield : 120 g, 90%

^{1}H NMR, ($CDCl_3$, 300 MHz) δ 0.87 (t, 6H, *J*= 6.6 Hz), 1.25 (s, 52H), 1.58-1.61 (br, s, 4H) 2.09 (br, s, 1H), 3.39-3.41 (m, 4H),

the crude product was purified by column chromatography on silica with the MeOH/$CHCl_3$ (3:97) to give **9**, as a waxy solid

3.54-3.66 (m, 21H).

ESI-MS $C_{43}H_{88}O_7$

Calcd MW = 716

Found MW = 739 [*M*+Na^+]

Synthesis of 10.

To a solution of **9** (40 mg, 0.069 mmol) and DMAP (1.22 g, 10 mmol) in dichloromethane (5 ml) was added dicyclohexylcarbodiimide (22 mg, 0.11 mmol) and the mixture was stirred for 30 min. Trityl protected mercaptopropanoic acid (36 mg, 0.1046 mmol) was then added and the resulting suspension was stirred for 12 h. The solid was removed by filtration, and the filtrate was concentrated under reduced pressure. Purification by column chromatography on SiO_2 with MeOH/$CHCl_3$ (1.5:98.5) gave **10**.

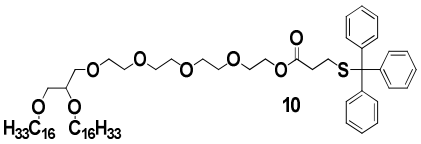

Yield : 55 mg, 76%

^{1}H NMR, ($CDCl_3$, 300 MHz δ 0.88 (t, 6H, *J*= 6.9 Hz), 1.25 (s, 52H), 1.54-1.56 (m, 4H), 2.275 (t, 2H, *J*= 6.9 Hz), 2.45 (t, 2H, *J*= 6.9 Hz), 3.39- 3.66 (m, 23H), 4.16 (m, 2H), 7.17-7.42 (m, 15H).

ESI-MS $C_{65}H_{106}O_8S$

Calcd MW = 1046

Found MW = 1069 [*M*+Na^+]

Synthesis of 1.

To a solution of **10** (5 mg, 0.008 mmol) in dichloromethane, trifluoroacetic acid (4.46 mg, 0.04 mmol) and triisopropyl silane (6.3 mg, 0.04 mmol) was added and stirred for 4 hrs at room temperature. On completion of the reaction as observed by TLC,

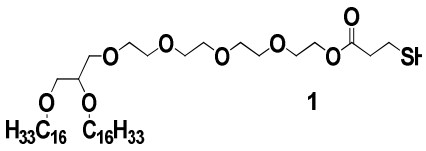

Yield : 80%

^{1}H NMR, ($CDCl_3$, 300 MHz δ

the volatiles were removed under reduced pressure and product purified by column chromatography on SiO_2 with MeOH/$CHCl_3$ (2:98) gave 1 with 80% yeild.

0.87 (t, 6H, *J*= 6.9 Hz), 1.25 (br, s, 52H), 1.54-1.59 (m, 4H), 2.65 (m, 2H), 2.75 (m, 2H), 3.31-3.65 (series of m, 23H), 4.26 (m, 2H).

ESI-MS $C_{46}H_{92}O_8S$

Calcd MW = 804

Found MW = 827 [*M*+Na^+]

Synthesis of 12.

To a stirred solution of tetraethylene glycol **11** (500 mg, 2.57 mmol), imidazole (192 mg, 2.83 mmol), and catalytic amount of 4-dimethylaminopyridine in CH_2Cl_2: dimethylformamide (20 ml: 2 ml) at 0 ^oC was added dropwise tert-butylchlorodimethylsilane (388 mg, 2.57 mmol) over 30 minutes. The resulting mixture was stirred at room temperature overnight and quenched with water (3 mL). The organic phase was collected and the aqueous phase was extracted with ethyl acetate. The combined organic phase was dried over anhydrous magnesium sulfate. After concentrating under vacuum, the residue was purified by chromatography on silica gel (methanol/CH_2Cl_2 = 2/98) to give alcohol **1** as a light yellow oil

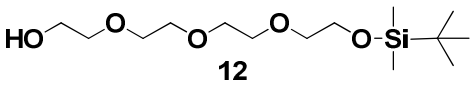

12

Yield : 600 mg, 76%

^{1}H NMR, ($CDCl_3$, 300 MHz) δ 0.06(s, 6H), 0.89 (s, 9H), 2.34 (br, s, 1H), 3.53–3.78 (m, 16H)

ESI-MS $C_{14}H_{32}O_5Si$

Calcd MW = 308

Found MW = 331 [*M*+Na^+]

Synthesis of 13.

To a solution of **12** (75 mg, 0.243 mmol) and DMAP (29 mg, 0.243 mmol) in dichloromethane (5 ml) was added dicyclohexylcarbodiimide (75.2 mg, 0.36 mmol) and the mixture was stirred for 30 min. Trityl protected mercapto propanoic acid (85 mg, 0.243 mmol) was then added and the resulting suspension was stirred for 12 h. The solid was removed by filtration, and the filtrate was concentrated under reduced pressure. Purification by column chromatography on SiO_2 with ethyl acetate/ hexane (15: 85) gave **13**

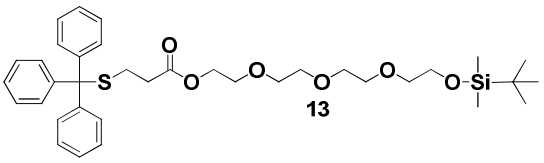

Yield : 95 mg, 61%

^{1}H NMR, ($CDCl_3$, 300 MHz) δ 0.02 (s, 6H), 0.83 (s, 9H), 2.25 (t, 2H, *J*= 6.6 Hz), 2.43 (t, 2H, *J*= 6.9 Hz), 3.48-3.61 (m, 12H), 3.71 (t, 2H, *J* = 5.4 Hz), 4.13 (m, 2H), 7.12-7.24 (m, 15H).

ESI-MS $C_{36}H_{50}O_6SSi$

Calcd MW = 638

Found MW = 661 [*M*+Na^+], 677 [*M*+K^+].

Synthesis of 2.

To a solution of **13** (5 mg, 0.008 mmol) in dichloromethane, trifluoroacetic acid (4.46 mg, 0.04 mmol) and triisopropyl silane (6.3 mg,

0.04 mmol) was added and stirred for 4 hrs at room temperature. On completion of the reaction as observed by TLC, the volatiles were removed under reduced pressure and product purified by column chromatography on SiO_2 with MeOH/$CHCl_3$ (4:96) gave **2** in 78% yields

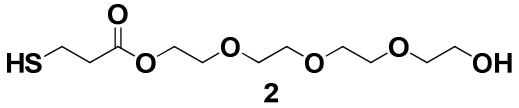

Yield : 78%

^{1}H NMR, ($CDCl_3$, 300 MHz) δ 2.63 (t, 2H, *J*= 6.6 Hz), 2.82 (t, 2H, *J*= 6.9 Hz), 3.48-3.61 (m, 12H), 3.71 (t, 2H, *J* = 5.4 Hz), 4.13 (m, 2H)

ESI-MS $C_{11}H_{22}O_6S$

Calcd MW = 282

Found MW = 283 [*M*+H^+], 321 [*M*+K^+].

3.8. References

(1) Koenig, B. W.; Kruger, S.; Orts, W. J.; Majkrzak, C. F.; Berk, N. F.; Silverton, J. V.; Gawrisch, K. *Langmuir* **1996**, *12*, 1343-1350.
(2) Salafsky, J.; Groves, J. T.; Boxer, S. G. *Biochemistry* **1996**, *35*, 14773-14781.
(3) Munro, J. C.; Frank, C. W. *Langmuir* **2004**, *20*, 10567-10575.
(4) Theato, P.; Zentel, R. *Langmuir* **2000**, *16*, 1801-1805.
(5) Tanaka, M.; Sackmann, E. *Nature* **2005**, *437*, 656-663.
(6) He, L. H.; Robertson, J. W. F.; Li, J.; Karcher, I.; Schiller, S. M.; Knoll, W.; Naumann, R. *Langmuir* **2005**, *21*, 11666-11672.
(7) Kaufmann, S.; Papastavrou, G.; Kumar, K.; Textor, M.; Reimhult, E. *Soft Mattet* **2009**, *5*, 2804-2814.
(8) Ye, Q.; Konradi, R.; Textor, M.; Reimhult, E. *Langmuir* **2009**, *25*, 13534-13539.
(9) Naumann, R.; Baumgart, T.; Graber, P.; Jonczyk, A.; Offenhausser, A.; Knoll, W. *Biosens. Bioelectron.* **2002**, *17*, 25-34.
(10) Heinrich, F.; Ng, T.; Vanderah, D. J.; Shekhar, P.; Mihailescu, M.; Nanda, H.; Losche, M. *Langmuir* **2009**, *25*, 4219-4229.
(11) McGillivray, D. J.; Valincius, G.; Vanderah, D. J.; Febo-Ayala, W.; Woodward, J. T.; Heinrich, F.; Kasianowicz, J. J.; Losche, M. *Biointerphases* **2007**, *2*, 21-33.
(12) Knoll, W.; Koeper, I.; Naumann, R.; Sinner, E.-K. *Electrochim. Acta* **2008**, *53*, 6680.
(13) Anderson, N. A.; Richter, L. J.; Stephenson, J. C.; Briggman, K. A. *J. Am. Chem. Soc.* **2007**, *129*, 2094-2100.
(14) Kendall, J. K. R.; Johnson, B. R. G.; Symonds, P. H.; Imperato, G.; Bushby, R. J.; Gwyer, J. D.; van Berkel, C.; Evans, S. D.; Jeuken, L. J. C. *ChemPhysChem* **2010**, *11*, 2191-2198.
(15) Jeuken, L. J. C.; Daskalakis, N. N.; Han, X. J.; Sheikh, K.; Erbe, A.; Bushby, R. J.; Evans, S. D. *Sens. Actuators, B* **2007**, *124*, 501-509.
(16) Sheikh, K. H.; Christenson, H. K.; Bushby, R. J.; Evans, S. D. *J. Phys. Chem. B* **2007**, *111*, 379-386.
(17) Spencelayh, M. J.; Cheng, Y. L.; Bushby, R. J.; Bugg, T. D. H.; Li, J. J.; Henderson, P. L. F.; O'Reilly, J.; Evans, S. D. *Angew. Chem., Int. Ed.* **2006**, *45*, 2111-2116.
(18) Baumgart, T.; Kreiter, M.; Lauer, H.; Naumann, R.; Jung, G.; Jonczyk, A.; Offenhausser, A.; Knoll, W. *J. Colloid Interface Sci.* **2003**, *258*, 298-309.
(19) Han, X. J.; Achalkumar, A. S.; Bushby, R. J.; Evans, S. D. *Chem. Eur. J.* **2009**, *15*, 6363-6370.
(20) Naumann, R.; Schiller, S. M.; Giess, F.; Grohe, B.; Hartman, K. B.; Karcher, I.; Koper, I.; Lubben, J.; Vasilev, K.; Knoll, W. *Langmuir* **2003**, *19*, 5435-5443.
(21) Schiller, S. M.; Naumann, R.; Lovejoy, K.; Kunz, H.; Knoll, W. *Angew. Chem., Int. Ed.* **2003**, *42*, 208-211.
(22) Dorvel, B. R.; Keizer, H. M.; Fine, D.; Vuorinen, J.; Dodabalapur, A.; Duran, R. S. *Langmuir* **2007**, *23*, 7344-7355.
(23) Atanasov, V.; Atanasova, P. P.; Vockenroth, I. K.; Knorr, N.; Koper, I. *Bioconjugate Chem.* **2006**, *17*, 631-637.
(24) Fabre, R. M.; Talham, D. R. *Langmuir* **2009**, *25*, 12644-12652.
(25) Cornell, B. A.; BraachMaksvytis, V. L. B.; King, L. G.; Osman, P. D. J.; Raguse, B.; Wieczorek, L.; Pace, R. J. *Nature* **1997**, *387*, 580-583.

(26) Robertson, J. W. F.; Friedrich, M. G.; Kibrom, A.; Knoll, W.; Naumann, R. L. C.; Walz, D. *J. Phys. Chem. B* **2008**, *112*, 10475.
(27) Raguse, B.; Braach-Maksvytis, V.; Cornell, B. A.; King, L. G.; Osman, P. D. J.; Pace, R. J.; Wieczorek, L. *Langmuir* **1998**, *14*, 648.
(28) Dubacheva, G. V.; Van der Heyden, A.; Dumy, P.; Kaftan, O.; Auzely-Velty, R.; Coche-Guerente, L.; Labbe, P. *Langmuir* **2010**, *26*, 13976-13986.
(29) Vockenroth, I. K.; Rossi, C.; Shah, M. R.; Koper, I. *Biointerphases* **2009**, *4*, 19-26.
(30) Love, J. C.; Estroff, L. A.; Kriebel, J. K.; Nuzzo, R. G.; Whitesides, G. M. *Chem. Rev.* **2005**, *105*, 1103-1169.
(31) Folkers, J. P.; Laibinis, P. E.; Whitesides, G. M.; Deutch, J. *J. Phys. Chem.* **1994**, *98*, 563.
(32) Devillers, C. H.; Boturyn, D.; Bucher, C.; Dumy, P.; Labbe, P.; Moutet, J. C.; Royal, G.; Saint-Aman, E. *Langmuir* **2006**, *22*, 8134-8143.
(33) Chen, S. F.; Li, L. Y.; Boozer, C. L.; Jiang, S. Y. *Langmuir* **2000**, *16*, 9287-9293.
(34) Cabrita, J. F.; Abrantes, L. M.; Viana, A. S. *Electrochim. Acta* **2005**, *50*, 2117.
(35) Hobara, D.; Ota, M.; Imabayashi, S.-i.; Niki, K.; Kakiuchi, T. *J. Electroanal. Chem.* **1998**, *444*, 113.
(36) Kim, Y.-K.; Koo, J. P.; Huh, C.-J.; Ha, J. S.; Pi, U. H.; Choi, S.-Y.; Kim, J. *Appl. Surf. Sci.* **2006**, *252*, 4951.
(37) Munakata, H.; Kuwabata, S.; Ohko, Y.; Yoneyama, H. *J. Electroanal. Chem.* **2001**, *496*, 29.
(38) Kakiuchi, T.; Usui, H.; Hobara, D.; Yamamoto, M. *Langmuir* **2002**, *18*, 5231.
(39) Walczak, M. M.; Alves, C. A.; Lamp, B. D.; Porter, M. D. *J. Electroanal. Chem.* **1995**, *396*, 103-114.
(40) Porter, M. D.; Bright, T. B.; Allara, D. L.; Chidsey, C. E. D. *J. Am. Chem. Soc.* **1987**, *109*, 3559-3568.
(41) Finklea, H. O. In *Electroanal. Chem.*; Dekker: 1996; Vol. 19, p 109.
(42) Chidsey, C. E. D.; Loiacono, D. N. *Langmuir* **1990**, *6*, 682-691.
(43) Dixon, M. C. *Journal of Biomolecular Techniques* **2008**, *19*, 151-158.
(44) Boudard, S.; Seantier, B.; Breffa, C.; Decher, G.; Felix, O. *Thin Solid Films* **2006**, *495*, 246-251.
(45) Keller, C. A.; Kasemo, B. *Biophys. J.* **1998**, *75*, 1397-1402.
(46) Richter, R. P.; Berat, R.; Brisson, A. R. *Langmuir* **2006**, *22*, 3497-3505.
(47) Jenkins, A. T. A.; Bushby, R. J.; Evans, S. D.; Knoll, W.; Offenhausser, A.; Ogier, S. D. *Langmuir* **2002**, *18*, 3176-3180.
(48) Reimhult, E.; Hook, F.; Kasemo, B. *Langmuir* **2003**, *19*, 1681-1691.
(49) Satriano, C.; Edvardsson, M.; Ohlsson, G.; Wang, G.; Svedhem, S.; Kasemo, B. *Langmuir* **2010**, *26*, 5715-5725.
(50) Tang, Y. C.; Wang, Z. N.; Xiao, J. W.; Yang, S. H.; Wang, Y. J.; Tong, P. G. *J. Phys. Chem. B* **2009**, *113*, 14925-14933.
(51) Wang, X.; Shindel, M. M.; Wang, S.-W.; Ragan, R. *Langmuir* **2010**, *26*, 18239.

4. Amphipols – Molecular toolkits for manipulating membrane proteins

4. Amphipols – Molecular toolkits for manipulating membrane proteins

Transmembrane/membrane proteins, due to their distinct structural features (discussed in section 1.2.1), which comprise prominent hydrophobic domains are not soluble in water. Thus, they are classically stabilized in aqueous media as detergent/surfactant complexes. However, this method of stabilization has shown to present several disadvantages, some of them being the easy dissociation of the surfactant micelles from the proteins, the need to have an excess of surfactant *etc.* These disadvantages are demonstrated to pose severe threats to the stability and activity of membrane proteins and also lead to their denaturation.[1,2] To shun these barriers or disadvantages in dealing with membrane proteins, varied systems were developed.[3-5] However, among these systems, the most promising and consistent one to-date are the macromolecular systems called Amphipols (Apols). Apols were introduced almost a decade ago by C. Tribet, R. Audebert and J-L. Popot, were demonstrated by them as an efficient toolkit to entrap membrane proteins owing to their amphipathic nature, and were also found to be much more potent than surfactants or any other systems.[6,7] Although, initially different molecular structures were tested by the above mentioned authors, the most efficient Apol was found to be the "A8-35" in terms of the stability that it offered to Bacteriorhodopsin (BR). Since their inception, the Apols, and more precisely the "A8-35" has been demonstrated to be triumphant in dealing with membrane proteins. The applications of Apols are not just restricted to the domain of solubility and stability of membrane proteins, they are also found to be useful in the functional studies of the membrane protein that they trap. Some examples of these applications include their efficiency in providing a medium for folding GPCRs (membrane proteins that are responsible for various biological processes like signaling in senses for sight, smell, taste etc.),[8] delivering membrane proteins into preformed bilayers *etc.*.[9]

However, in the present context of this thesis, the most exciting application of amphipols was demonstrated by the group of J-L.Popot. In one of their recent articles, they demonstrated the use of a biotin tagged amphipol (A8-35) for immobilizing a wide variety of membrane proteins onto streptavidin-coated surfaces. These studies not only permitted the surface fixation of amphipol stabilized proteins, but also their interaction

studies with their antibodies by Surface Plasmon Resonance (SPR). The use of amphipols in these studies seemed advantageous over systems like SLBs or tBLMs for the following various reasons, the first one being that the biotin labeled amphipol when fixed on streptavidin coated substrates, were distant enough from the surface (CM5 substrates are substrates of gold functionalized with carboxymethyldextran of lengths about 100 nm from the surface). This is advantageous from the point of view of minimizing the interactions of the hydrophilic domains of the proteins with the substrate. This interaction as discussed earlier is often the cause of denaturation of membrane proteins. Secondly, in bilayer systems (SLBs or tBLMs) the quantity of membrane protein inserted in the bilayer is limited by various factors. As we have seen in section 2.2.3, the fusion of proteoliposomes to obtain SLBs was severely hindered due to increased quantity of protein inserted in the proteoliposomes. Moreover, it is also demonstrated in section 2.2.4 that the response of the protein immobilized in the SLB to its partner (pb5) was quite small.

Thus, artificial bilayers although being advantageous on certain aspects like their ease of preparation and handling etc. have certain inherent drawbacks which can be envisaged to overcome by the use of Amphipols.

Although, the "A8-35" is historically the oldest and hitherto one of the best characterized amphipol*, its structure in which the polar groups constitute a carboxylic acid (see Figure 4.1) is shown to be detrimental in certain studies which require high salt concentration, low pH and divalent cations such as Ca^{2+}.[10,11] This problem, however was found to be alleviated by replacing this carboxylic group by phosphorylcholine groups.[11] This phosphorylcholine based amphipol developed in the group of F. Winnik (see Figure 4.1) is structurally similar to the A8-35, except for its polar group, which is comparatively bigger than the A8-35 and that it bears phosphorylcholine groups instead of the carboxylate group in A8-35.[12]

* A8-35 is now also commercially available.

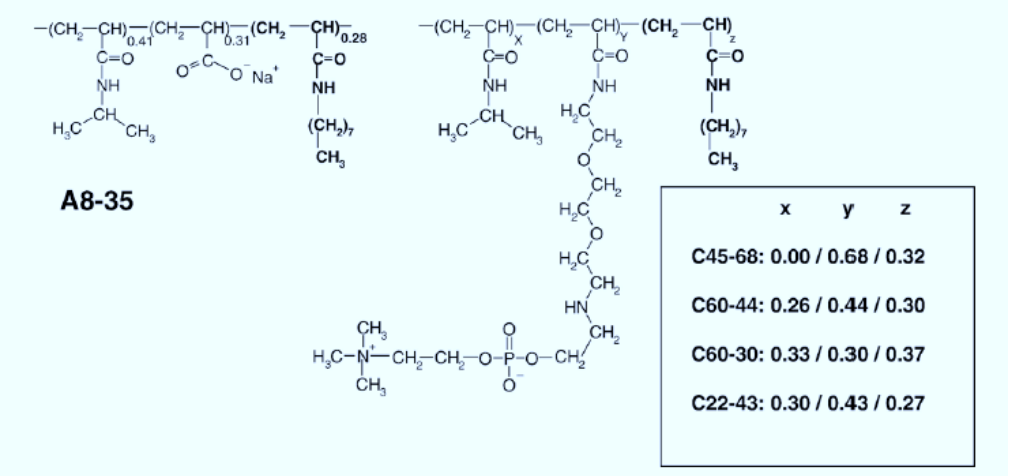

Figure 4.1 Stucture of A8-35 (left) and the different phosphorylcholine based amphipols (right). Both the structures present a polyacrylamide backbone.

A study comparing the properties of the two Apols (*i.e.* A8-35 and the above described phosphorylcholine based Apols) were done jointly by the groups of F. Winnik and J-L. Popot.[11] In this study, they demonstrated that while A8-35 was slightly more efficient in trapping and solubilizing Bacteriorhodopsin (BR), nonetheless, the phosphorylcholine based Apols had a winning edge over the A8-35 in terms of its stability in the presence of high concentration of salts like NaCl, Ca^{2+} and at acidic pH. Moreover, later by ITC measurements they observed that the energetics of transfer of BR from the surfactant to both A8-35 or C22-43 (one of the above described phosphorylated Apols) were nearly identical despite the difference in their structures.[13] This observation suggested that the interactions between the hydrophobic regions of both the Apol with the hydrophobic regions of the membrane proteins were identical despite of the difference in their polar groups.

Given the above mentioned features of amphipols, which describe consistent promise to membrane chemists, we were inclined towards studying its applications to the membrane proteins of our interests. In view of the objective of the present thesis, we were curious to test the viability of Amphipols in not only solubilizing membrane proteins, but also mediating the functionalization of these proteins to sensor surfaces. Thus, through a formal collaboration with Prof. Françoise M. Winnik (Université de Montréal, Canada) who provided us the phosphorylated amphipols, we ventured into this system for studying the immobilization and activity of the membrane proteins of our interest *i.e.* $\alpha_v\beta_3$ integrin and FhuA (see section 1.2.2)

4.1. Structure and self-assembling properties of Biotinylated-phosphorylcholine Apol (B-PCApol)

4.1.1. Synthesis and spectral characterization of B-PCApols

The biotinylated phosphorylcholine based Amphipol was synthesized in the group of Prof. Françoise M. Winnik in Canada. The structure of B-PCApol shown in Figure 4.2 is based on a backbone of Poly (N-isopropylacrylamide).

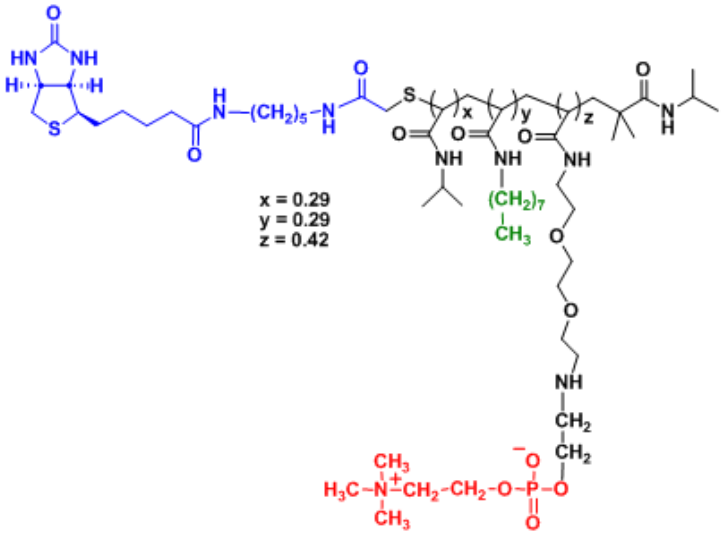

Figure 4.2 Structure of the biotinylated phosphorylcholine based Amphipol **(B-PCApol)** used in the present study. The Poly (N-isopropylacrylamide) backbone is shown in black, the hydrophobic octyl chains are shown in green, the phosphorylcholine group is shown in red and the biotin group is shown in blue.

The initial steps in the synthesis of B-PCApol were already reported by F. Winnik *et al.* in their earlier publications.[12] However, the biotin functionalisation was done as the final step in the synthesis of B-PCApol. The ^{1}H NMR spectra of this B-PCApol is shown in Figure 4.3.

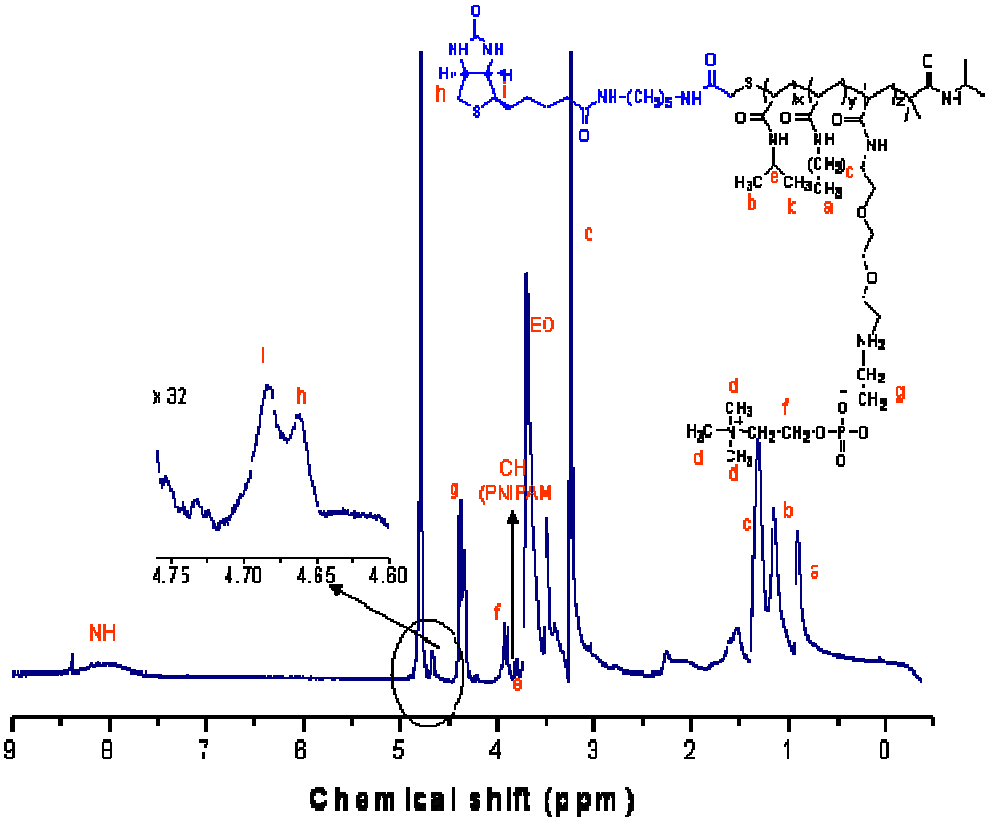

Figure 4.3 ^{1}H NMR spectra of B-PCApol in D_2O at 298 K (64 scans), M_n = 18.4 x 10^3 g mol^{-1} by comparing the peak assignment of Biotin proton (δ = 4. 67 ppm) to the methyl proton of n-C_8H_{17} (δ = 0.92 ppm), PNIPAM (δ = 1.2 ppm), and phosphorylcholine (δ = 1.2 ppm).

The integration of characteristic protons of the various groups present in the B-PCAPol molecule was done to confirm the structure of the polymer. GPC analysis was done to determine the number average molecular weight (M_n) of the polymer, which was found to be 18,400 g mol^{-1}. The infrared (IR) spectrum of the B-PCApol see Figure 4.4, besides clearly indicating the presence of amide functions, confirmed the presence of the phosphoryl and the choline groups as their characteristic asymmetric stretching bands were present at 1100 and 970 cm^{-1} respectively.

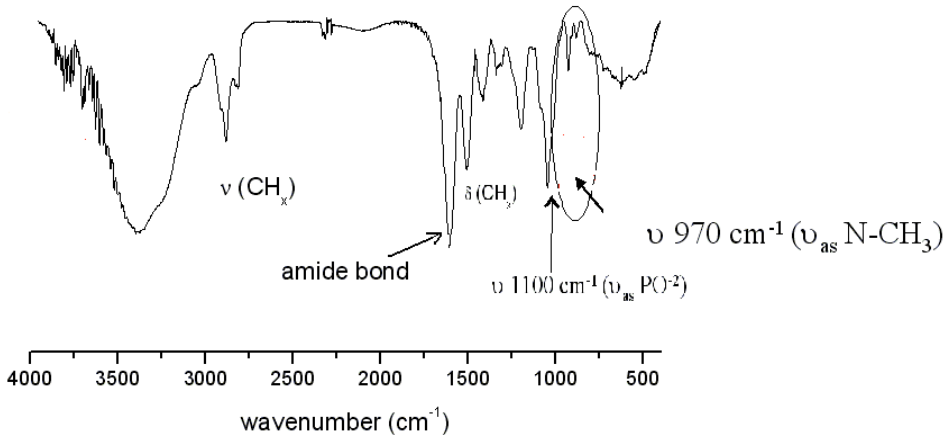

Figure 4.4 Infra red (IR) spectroscopy of B-PCApol indicating the presence of the amide function at 1650 cm-1, the phosphoryl group at 1100 cm-1 and the choline groups at 970 cm-1

4.1.2. Dynamic Light Scattering (DLS) measurements

Dynamic Light Scattering measurements were carried out to characterize the size of the aggregates formed by the B-PCApol. The B-PCApol was solubilized in 0.1 M PBS buffer at pH 7.0 by overnight agitation at 4 ^{o}C to have a solution of 1 mg/ml of B-PCApol in solution. This clear solution was filtered through a PVDF membrane of pore size 0.22 μm and DLS measurements were performed at 2 different temperatures. Figure 4.5 represents the DLS data measured at 29 ^{o}C (red curve with star symbols) and 32 ^{o}C (black curve with triangles) respectively.

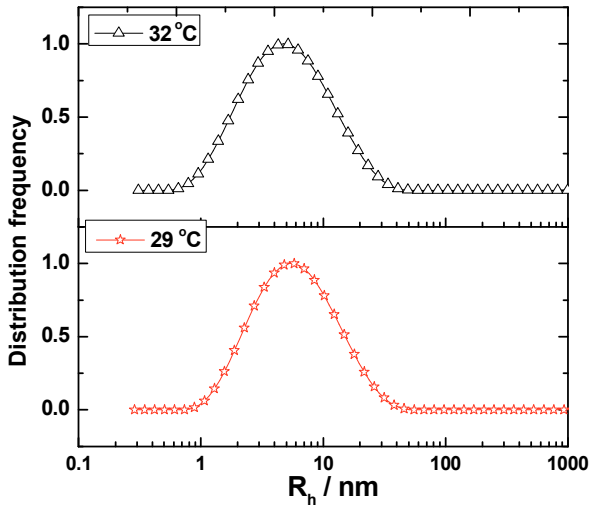

Figure 4.5 DLS measurements on a 1mg/ml solution of B-PCApol in PBS buffer (pH 7.0). The red curve (star symbols) represents the measurements done at 29 ^{o}C and the black curve with triangle symbols represents the measurements done at 32 ^{o}C.

The B-PCApol at 29 ^{o}C (red curve) showed a broad, yet single peak corresponding to a hydrodynamic radius of 5.2 nm. Upon a slight increase of temperature to 32 ^{o}C, this peak was found to become slightly broader and the hydrodynamic radius was found to decrease slightly to a value of 4.9 nm. This phenomenon of a slight decrease in the hydrodynamic radius with the increase in temperature could be attributed to the dehydration of the micellar aggregates of the B-PCApols. However, the most important aspect to note here is the presence of a single (broad) peak corresponding to a radius R_h of 5.2 nm at 29 ^{o}C which is close to the ambient temperature, indicating that the B-PCApol forms particles of an average size of 5.2 nm sizes. Moreover, the broad distribution of the peak indicates the presence of other sized particles, which are quite close to the average size measured.

4.2. Surface Plasmon Resonance (SPR) studies to measure the interaction of pb5 with Amphipol entrapped FhuA

FhuA as discussed in detail in section 1.2.2a is an outer membrane protein of *E.coli*. Besides being a ferrichrome transporter, it is a key receptor involved in the viral infection of *E.coli* with the bacteriophage T5. Its interactions with the viral phage T5 is characterized by the "injection" of the phage DNA into bacterial cell. This process of the phage T5 infection, essentially deals with the irreversible binding of a phage protein pb5 to FhuA (detailed in section 2.2). In the chapter 2.2, we successfully demonstrated the formation of FhuA bearing proteoliposomes and their fusion on a SiO_2 substrate to obtain FhuA bearing SLBs. The incorporation of FhuA into SLBs although being quite facile in terms of the preparation, suffered from a drawback, in that very small amounts of the protein could be incorporated in a conformation where the recognition site would be exposed to the flowing solvent.

Hence, in the present section we exploit the use of biotinylated-PC-amphipol (B-PCApol) for immobilizing FhuA onto a SPR chip. Our approach was to first determine the optimum conditions for the efficient trapping of FhuA into the Apols, followed by the immobilization of the B-PCApol in the optimum conditions to a streptavidin functionalized SPR chip and finally the determination of the affinity constants of the FhuA-pb5 binding.

4.2.1.a Complexing FhuA with B-PCApol; determination of the optimum FhuA: B-PCApol ratio

FhuA (80 kDa) was obtained from Dr. Cécile Breyton (IBS, Grenoble) as a 3.3 mg/ml solution in 2.2 mM LDAO (Lauryldimethylamine *N*-oxide is a zwitterionic surfactant having a cmc_{H2O} ~1mM). The molar absorptivity of FhuA is $\varepsilon = 103690\ M^{-1}cm^{-1}$

The B-PCApol solution was used at a working concentration of 2.5 mg/ml in a buffer containing 10 mM HEPES, 150 mM NaCl and 1 mM $MgCl_2$.

It is important to note here though, that 'n' the number of Amphipol molecules in each Amphipol particle is not known for this particular B-PCAmphipol, however the 'n' *i.e.*

the number of Apols associated in a particle for structurally similar Amphipols have been shown to be close to 4. Thereby, to calculate the ratio of the Protein: Apol required for trapping the membrane protein in the B-PCApol-particles, we assume the number of B-PCApol present in a single particle to be 4. Thus the molecular weight of each Apol particle made up of 4 B-PCApol molecules would be 73,600 g mol^{-1}

As in the case of FhuA which is a small protein bearing several transmembrane helices, one FhuA molecule is expected to be associated with 1 B-PCApol particle. *i.e.* 80,000 g of FhuA will associate with 73,600 g of B-PCApol (or 8 mg FhuA with 7.36 mg B-PCApol) thus accounting for nearly a 1:1 wt/wt ratio of FhuA: B-PCApol.

Thus, the mass ratios described in the following sections are reasoned in the same way as described above.

In all these mixtures the concentration of FhuA was fixed to 2.2 μM. Care was taken to maintain the concentration of LDAO at 2 mM in all the mixtures to be at a concentration well above the cmc of LDAO. These mixtures were then treated with Biobeads (20 mg wet weight of biobeads was added for 1 mg of LDAO) for 3 hours, followed by renewal of the biobeads and dilution to twice the volume. These mixtures containing Biobeads were agitated overnight at 4 ^{o}C

After this period, UV-visible spectrum at wavelength 280 nm was recorded on a Nanodrop device to determine the concentration of FhuA in solution. To determine the ratio at which maximum trapping of FhuA in the B-PCApol is achieved, the sample mixtures were centrifuged at 200,000×g for 10 mins. The supernatant from each tube was collected and UV-visible spectrum at 280 nm was measured. Measurement of 2.2 μM of FhuA in 2 mM LDAO was done as a control experiment. Figure 4.6 shows the UV-absorption measurements for the various mixtures containing increasing amounts of Apol. The hollow bars in the figure represent the measurement done before centrifugation, while the solid bars represent the measurements done after centrifugation. It can be seen in this figure, that precipitation or a small loss of the protein occurs by mere dilution in LDAO as shown by the small difference in the absorbance value after centrifugation. This phenomenon is quite well known and has been observed earlier.[11] As expected, it can also be seen that almost complete loss of protein occurs upon dilution in buffer, below the cmc of the LDAO.

However, it is suggested from Figure 4.6 that precipitation of the protein is favored at low FhuA: Apol ratios (1:1 and 1:2). This fact can be explained by considering the

reduced hydrophobic groups surrounding the hydrophobic region of the membrane protein, thus causing it to aggregate within itself. The situation however, improves drastically for high FhuA: B-PCApol ratios, starting from a ratio of 1: 3 (wt/wt) of FhuA: B-PCApol, where about 80-90% of FhuA is soluble in the presence of B-PCApol.

C. Tribet *et al.* demonstrated that the solubility of a membrane protein by Apols is attributed to the formation of protein/Apol complexes, where the hydrophobic region of the protein is well covered by the hydrophobic pockets of the Apols.[6]

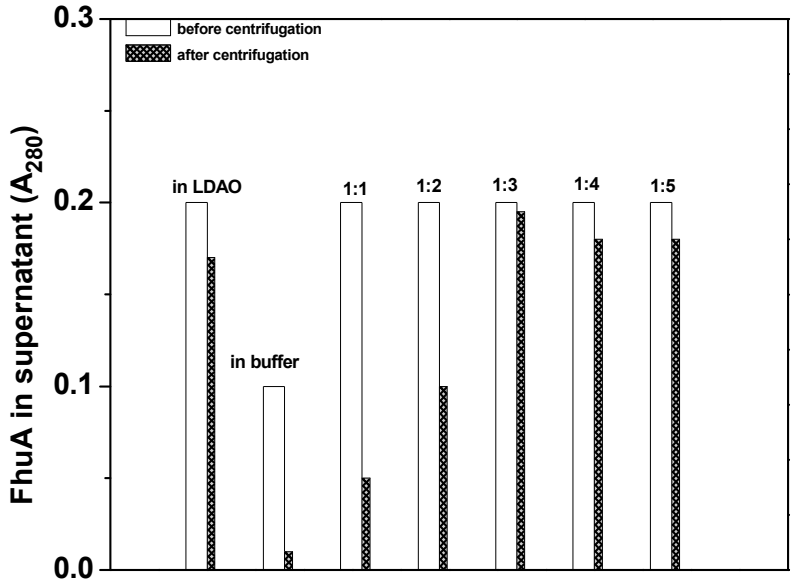

Figure 4.6 Solubility of FhuA upon trapping with B-PCApols. The hollow bars correspond to the measurements done before centrifugation whereas the filled bars correspond to the measurements done after centrifugation. All the samples were treated with Biobeads (3h followed by dilution, renewal of Biobeads and overnight agitation).

Hence, to summarize the above results, it would be appropriate to suggest that at low ratios of FhuA: Apol, only about 20-50% of the protein remains soluble after centrifugation. However, starting from ratios 1: 3 (wt/wt of FhuA: B-PCApol), the solubility of the FhuA is improved drastically. These results also suggest that a FhuA: Apol ratio of 1:3 (g/g) would be an appropriate ratio to keep FhuA soluble in solution.

4.2.1.b Immoblization of the FhuA: Apol complex to a streptatvidin functionalized SPR chip

The fixation of the Amphipol with and without FhuA, on a SPR chip was mediated via the very strong affinity interaction between streptavidin and biotin. To effectuate this, a CM5 chip of Biacore was functionalized with streptavidin. Herein, the carboxylate groups in the carboxymethyl dextran matrix (CM5) were activated by a 10 minute injection of freshly mixed NHS (50 mM) and EDC (200 mM) to form the NHS activated ester. To this NHS ester activated chip, a 15 min injection of streptavidin (0.5 mg/ ml in acetate buffer at pH 4.5) resulted in the formation of amide bonds with the amino groups of streptavidin. The functionalization was carried out to have 8000 RU of immobilized streptavidin. This was followed by blocking the remaining active sites with a 5 minute injection of 1 M ethanolamine.

Since the optimum ratio for keeping most of the FhuA soluble in B-PCApol was observed to be 1: 3 (wt/wt of FhuA: B-PCApol), all further experiment were done at this ratio.

Figure 4.7 represents the adsorption profile of the FhuA: B-PCApol complex (red curve) on the active channel and the B-PCApol alone on the reference cell (black curve). In both cases, the B-PCApol concentrations were 3.75 μM and in the case of the FhuA: B-PCApol complex, the concentration of FhuA was 2.23 μM. Upon careful observation of these adsorption profiles, it can be seen that the adsorption behavior of the smaller Apol alone was much different as compared to the Apol-FhuA complex. Indeed, the adsorption of B-PCApol alone seemed to be a spontaneous process (red curve) marked by a sharp increase in the SPR response, stabilizing after the rinsing step to a value of 1886 RU. In contrast, the adsorption of FhuA: B-PCApol was marked by a slightly higher value i.e. 2204 RU, and the adsorption profile of the complex showed a rather different response. In that, the initial adsorption of the FhuA: B-PCApol complex was characterized by an initial sharp increase in the SPR signal, followed by a regular linear increase suggesting that adsorption of the complex was controlled by a diffusion process. This phenomenon can be explained by taking into account the difference in the molecular weights and dimensions between the complex and the Apol alone. The adsoprtion of this rather big complex of FhuA: B-PCApol onto a streptavidin coated chip, although initially being a rapid process could lead to the formation of a first layer

(exposed) of the adsorbed complex, whereas, the further adsorption of the FhuA: B-PCApol complex would now require diffusion into this layer, and this step will definitely be slower than the adsorption of an initial layer of the complex. Moreover, the slightly higher shift in the final values for the FhuA bearing complex is in correlation with the added mass due to FhuA.

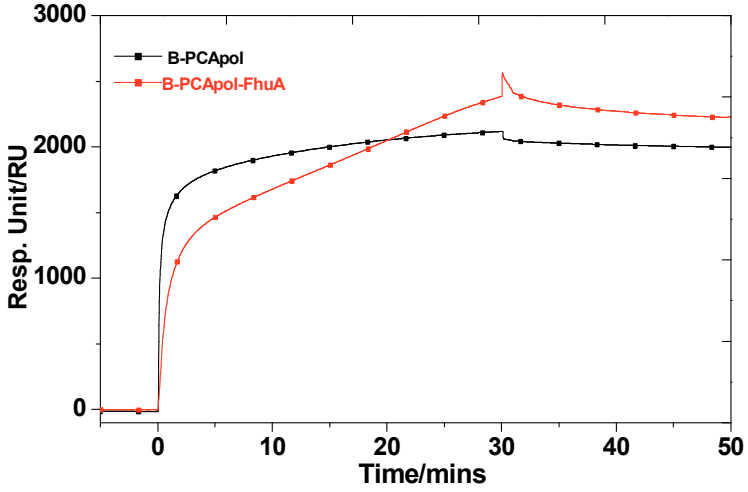

Figure 4.7 Sensorgram showing the immobilization of the Apol alone (black curve) and Apol-FhuA complex (red curve) to a Streptavidin functionalised CM5 surface.

4.2.1.c "Testing the waters" Interaction studies of surface immobilized FhuA (Apol: FhuA complex) with pb5.

To validate the efficiency of B-PCApol in maintaining the FhuA active upon immobilization on the streptavidin coated surface, we now tested the interactions of FhuA with pb5. While pb5 is known to be most stable at slightly acidic pH, it tends to precipitate at neutral to alkaline pH. Thus, all the experiments were performed in 0.1 M PBS buffer containing 150 mM NaCl at pH 6.0. Further, the flow channels containing the Apol alone and the Apol: FhuA complex were first equilibrated in this buffer to have a stable baseline.

It is known from literature that the interaction between FhuA and pb5 is irreversible, i.e. the complex once formed cannot be dissociated.[14] This feature of the present system, almost totally ruled out the classical kinetic measurements, which requires a regeneration step in between each binding cycle of the analyte on the same ligand. Withal, for such systems, where regeneration is not achievable, another method of analysis classically

called the "equilibrium analysis" or lately referred to as "single-cycle kinetics" has been used. [15-17] This method entails sequential injections of increasing concentrations of the analyte, without any regeneration steps. Accordingly, we carried out a series of 11 injections of pb5 (see section 4.5.2 for protocol) from a carefully chosen concentration range (Figure 4.8).

The reference channel in this case showed no response for the injections of pb5, whereas, clear binding of irreversible nature was observed exclusively on the active flowcell containing FhuA, starting from 10 nM concentration. This result indicated that the response obtained was exclusively arising from the active flowcell bearing FhuA, and thus the effects of non-specific interactions could be ruled out. Further, the increase in the SPR signal with increased concentration of pb5 in solution indicated that the immobilized FhuA retained its activity in the present architecture.

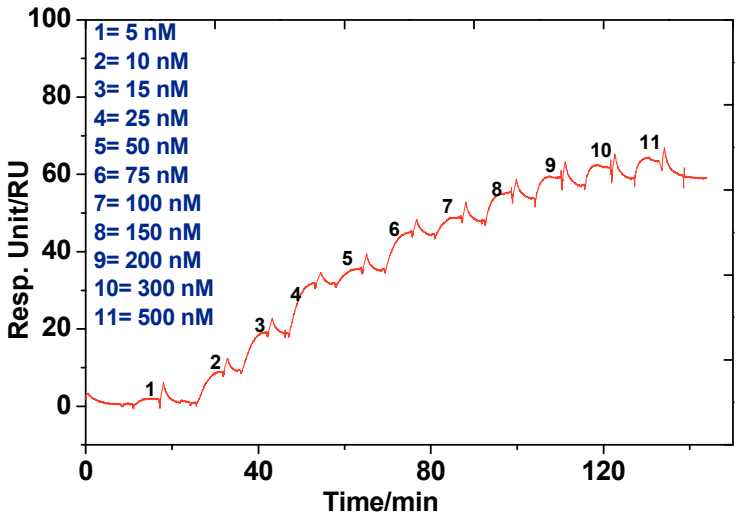

Figure 4.8 Adjusted sensorgram indicating the irreversible interaction of 10 nM (first step) and 25 nM (second step) pb5 with B-PCApol embedded FhuA immobilized on the surface.

The reference subtracted equilibrium response values obtained during the association cycle was then plotted as a function of the concentration of pb5 injected (Figure 4.9). The dissociation constant, K_D= 31.1 ± 0.9 nM was obtained by fitting the data to a single-site Langmuir isotherm in Kaleidagraph 3.5 as indicated in Table 4.1.

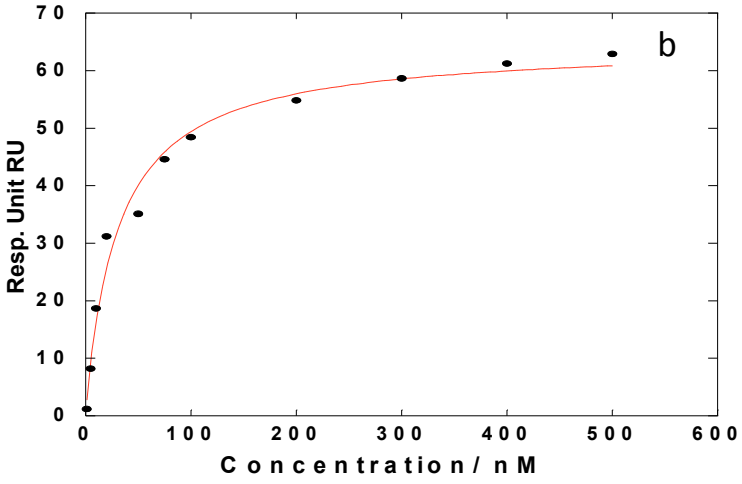

Figure 4.9 Langmuir 1:1 binding isotherm fitted on the data obtained from the single-cycle kinetics data depicted in figure 4.8.

This value obtained is of the same order as that has been previously reported for systems that show an irreversible biding/association.[15,17] In these reports, where the single cycle kinetic data was analyzed as both Langmuir 1:1 analysis and kinetic 1:1 modeling, the irreversibility of the system is attributed to the very small dissociation rate constant (k_{off}).[15]

Table 4.1 Parameters obtained by fitting the data of figure 4.9 into a Langmuir 1:1 model

Analyte	Rmax	K_D (nM)	χ^2
pb5	65.2 ± 0.5	31.1 ± 1	1.63

The above described results present the first ever quantification measurements done on an amphipol stabilized and surface immobilized-membrane protein. We have for the first time, successfully determined the dissociation constant of the FhuA-pb5 complex by SPR measurements. Thus, these results indicate a promise not only in the field of label-free detection of viral proteins but also in the field of studying membrane protein-protein interactions using amphipols.

As a second aspect of this work, we also studied the immobilization, surface fixation and receptor binding properties of $\alpha_v\beta_3$ Integrin entrapped in Amphipols.

4.3. Trapping of $\alpha_v\beta_3$ Integrin with B-PCApol, surface immobilization of the complex and interaction studies with vitronectin

Integrins which are a class of transmembrane proteins are responsible for myriads of functions at the cellular level (discussed in section 1.2.2 and 2.1). Almost all of the integrins are receptors of the peptidic sequence Arg-Gly-Asp (R-G-D), which is present in the active site of their natural ligand. In particular, the $\alpha_v\beta_3$ integrin has been "under the telescope" of various research groups as it has been identified to be one of the key factors in tumor angiogenesis.[18] Since then, research in designing artificial ligands that can occupy the active binding site of the $\alpha_v\beta_3$ integrin, thereby blocking its interaction with the natural ligand, has been on the surge. The interests of our group towards studying the $\alpha_v\beta_3$ integrin dates back to almost a decade.[19,20] In the process, it has been demonstrated that ligands bearing multivalent presentations of the Arg-Gly-Asp sequence are much more efficient than monomeric ligands.[21,22]

Nevertheless, in the above studies the $\alpha_v\beta_3$ integrin was studied by overexpression in cells. Our approach was thus inclined towards studying the activity of the isolated/purified $\alpha_v\beta_3$ integrin after its incorporation within reconstituted artificial bilayer mimics, in order to study its interactions with both the natural ligand (vitronectin) and the artificial multimeric Arg-Gly-Asp ligands. Towards this approach, in the present chapter we discuss the viability of amphipols in handling the $\alpha_v\beta_3$ integrin, while keeping it stable in its active form.

4.3.1. Trapping of αvβ3 integrin by the B-PCApol particles, determination of the experimental conditions.

$\alpha_v\beta_3$ integrin (237,000 g mol^{-1}) was purchased from Millipore as a 50 µg aliquot at 0.35 mg/ml in a 100 mM Octyl glucoside (*n*-octyl-β-D-glucoside) solution. Octyl glucoside (OG) is a non ionic surfactant having a cmc of 17 mM.

This stock solution had a concentration of 750 nM of $\alpha_v\beta_3$ integrin. At this concentration of the protein, UV-visible spectrum recorded at a wavelength of 280 nm showed no characteristic absorbance of the protein.

This fact was quite limiting, as now the trapping of the $\alpha_v\beta_3$ integrin by the B-PCApol particles could not be followed by UV-visible spectroscopy.

To alleviate this situation, a technique called Dot-blot was applied for the detection of the $\alpha_v\beta_3$ integrin. Dot-blot is a technique commonly used in molecular biology to detect biomolecules. The procedure involves spotting of the sample containing the protein on a localized area like a "dot" on a membrane (nitrocellulose, PVDF, nylon etc.), which is followed by blocking the remaining protein binding sites by incubation with a solution of 5% milk. This spotted membrane is then treated with a specific antibody for the protein for about one hour followed by rinsing with buffer. Then the membrane bearing the protein-antibody complex is treated with a secondary antibody. This secondary antibody recognizes a specific region of the first antibody. It is important in this case, for the second antibody to be coupled with an enzyme such as HRP (horse radish peroxidasein our case). After treatment with this secondary antibody the membrane is rinsed with buffer and contacted with a solution containing hydrogen peroxide and luminol in equal quantities. The role of this enzyme present on the secondary antibody is to catalyse the hydrolysis of the peroxide bond. This hydrolysis in presence of luminol can be described by the following reaction:

$$\text{luminol} + H_2O_2 \xrightarrow{HRP} \text{3-APA}[\Diamond] \rightarrow \text{3-APA} + \text{light},$$

Where, 3-APA [◊] is the excited state of the aminophthalate, which slowly deactivates to the APA molecule in the fundamental state, giving rise to luminescence.

This luminescence is then transferred to a photographic film, which is then developed using a developing agent (see section 4.5.3) in order to obtain photography of the fluorescing spots of the membrane. This process of chemiluminescence can be described as follows in Figure 4.10.

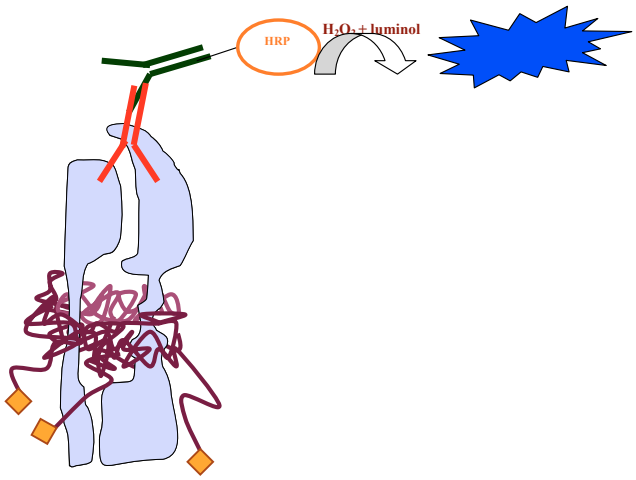

Figure 4.10 Cartoon illustrating the chemiluminescence reaction with B-PCApol entrapped integrin

4.3.2. Detection of $\alpha_v\beta_3$ integrin and $\alpha_v\beta_3$ integrin B-PCApol complex.

A dot blot assay performed on OG stabilized $\alpha_v\beta_3$ integrin is presented in Figure 4.11. Here, the $\alpha_v\beta_3$ integrin was spotted at a concentration of 0.1 mg/ml on a nitro cellulose membrane. LM 609 (1mg/ml solution), the primary antibody that interacts specifically with the $\alpha_v\beta_3$ integrin was diluted 500 times in buffer containing 5 % milk, and was then allowed to interact with the nitro cellulose membrane bearing the $\alpha_v\beta_3$ integrin spots.
After this period, the membrane was washed carefully with buffer, and was treated with an anti-mouse-HRP (a secondary antibody specific towards LM 609) in a 5% milk containing buffer. After this period, the membrane was carefully rinsed with buffer and treated with the luminol-peroxide mixture. Upon treatment with this mixture, the membrane was then isolated and kept in contact with a photographic plate (in an absolutely dark room). The exposed photographic film was then developed to observe the transfer of luminescence (Figure 4.12).

Figure 4.11 Dot blot assay performed on a nitrocellulose membrane where a solution of OG stabilized $\alpha_v\beta_3$ integrin at a concentration of 0.1 mg/ml (spot on the right) and 0.05 mg/ml (spot on the left) was spotted. LM609 was used as the primary antibody.

After examining the clear detection of $\alpha_v\beta_3$ integrin as seen in Figure 4.11, we then studied the trapping of the $\alpha_v\beta_3$ integrin by the B-PCApols using the dot blot technique.

As described in section 4.2.1a, the calculation of the B-PCApol was done by taking into account the structure of the protein and the number of amphipol particles that would associate with it. Although, the structure of the membrane domain of the $\alpha_v\beta_3$ integrin is still unknown, it is considered in general that each of the two subunits, that is, the 'α' and the 'β' subunits, possess one transmembrane helix each.

As in the case of FhuA, we observed that each FhuA molecule bearing one transmembrane helix was found to be stable only in the presence of 3 B-PCApol particles. Hence, to start with we designed our experiments, taking into account the association of each transmembrane helix with 3 amphipol particles.

And thus, 1 $\alpha_v\beta_3$ integrin 237,000 g would associate with 6 × 73,600 = 441600 g of Apol. In short 2.37 g of $\alpha_v\beta_3$ would be associated to 4.47 g of B-PCApol for a massic ratio (1:6) of $\alpha_v\beta_3$: B-PCApol.

The recognition of the $\alpha_v\beta_3$ integrin as described in section 1.2.2, is situated on both the subunits, moreover the right conformation of these subunits are an important feature in the activation of the protein. This conformation has been shown to be dependent on the presence of bivalent cations (Mn^{2+}). Hence, the buffer used in the present studies, by rule should have Mn^{2+} in sufficient quantities. The buffer was thus composed of HEPES 10 mM, NaCl 150 mM, $MgCl_2$ 2 mM and $MnCl_2$ 1 mM.

Moreover, in all the mixtures prepared, care was taken to have the OG concentration above its cmc, *i.e.* around 33 mM, in order to avoid precipitation of the protein.

It was important to evaluate in the trapping measurements, the exchange time required for complete removal of OG by biobeads. This was done by preparing 2 mixtures of $\alpha_v\beta_3$: B-PCApol particles at 1:6 ratio. One of these mixtures was treated just once with biobeads (20 mg wet weight/mg of OG) followed by overnight agitation, this mixture

being called mixture 1. Whereas the other mixture was treated with biobeads for 3 hours, after which the beads were renewed and agitated for 90 mins, followed by another step of renewal of beads and dilution to twice the volume (to be below the cmc of OG) and agitated overnight. This mixture was called mixture 2.

It is important to understand here, that to evaluate the presence of the protein in the Apol particles by dot-blot technique, it was essential to separate the free B-PCApol particles from the protein-Apol complex. This step was envisaged by a density based separation as the complex of the $\alpha_v\beta_3$ integrin (237 kDa) with Apol particles would be much heavier than the Apol particles themselves. Hence, sucrose gradient based density separation was resorted to separate the Apol- $\alpha_v\beta_3$ integrin complex from the free Apol particles. Sucrose gradient separations usually involve the formation of a continuous gradient of sucrose in a narrow centrifuge tube. The gradients are made in such a way, so that the highest density gradient is at the bottom, whereas the lowest density gradient is on the top of the tube. The samples are placed on top of the lowest density gradient and the tube is centrifuged at very high speeds for several hours.

In our case, after a few trial measurements, we found that a gradient ranging from 60% sucrose to 10% sucrose in 7 steps of 10% (*i.e.* 60%, 50%. 40%, 30%, 20%, 10% and 0%) was appropriate to effectuate a good separation. To these tubes containing the gradients was then added the mixtures (1 and 2) in two different tubes. As control experiments, the Apol alone was also loaded on two such similar gradients. After preparation of these gradients, the tubes were centrifuged at 250,000×g for 5h at 4 ^{o}C.

After centrifugation, each gradient percentage was recovered as two different fractions and collected in separate eppendorf tubes. Hence, for each mixture (1 and 2), 14 fractions were collected from each tube. Since the fractions were collected from top to bottom, the numbering was done denoting the 0% fraction to be 1.

Each of these fractions was then spotted on nitro cellulose membranes and the detection of the protein was carried out by interactions with the antibodies as described above. However, the biotin tag in the B-PCApol was also detected by a streptavidin-dot blot assay. In this assay, instead of the two antibodies, streptavidin coupled to HRP was treated for 15 minutes with the membrane; this was followed by rinsing and treatment with peroxide and luminol reagent.

The development of the luminescence on the photographic film was done in the same way as described above. A photo of the dot blot assay is shown in figure 4.12 and 4.13

Figure 4.12A shows the LM 609 dot blot assays for the mixture 1, whereas figure 4.13A shows the streptavidin assay for the mixture 1. As it can been seen in Figure 4.12 A, the integrin in this case is dispersed almost all along the gradient, however in figure 4.13A the B-PCApols are present only in the few initial fractions (3,4,5 and 6). This indicates that among the various spots of integrin seen in figure 4.12A, only the fraction 3,4,5 and 6 correspond to the integrin-Apol complex. The rest of the spots from fraction 6-12 do not contain the Apol. The presence of these spots can be plausibly explained to be corresponding to OG-$\alpha_v\beta_3$ integrin complexes or aggregates of the protein with insufficient amount of the surfactant.

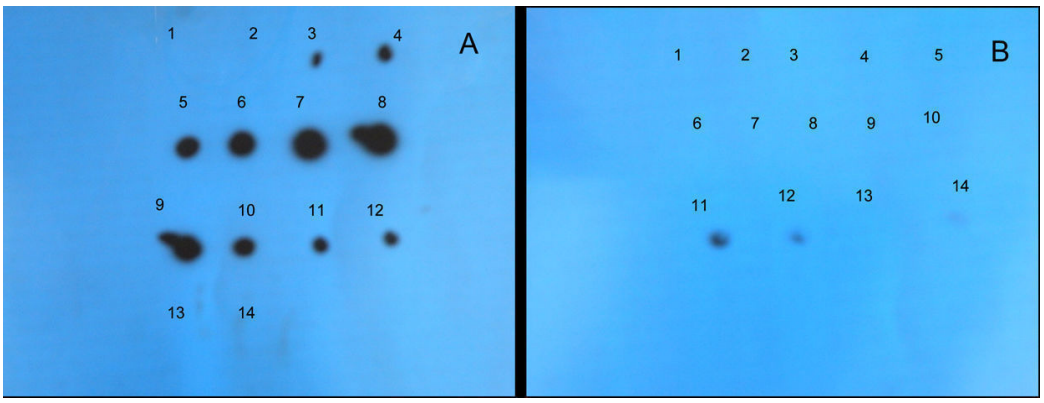

Figure 4.12 Dot blot assays for detection of integrin using LM 609 of (A) mixture 1, notice the protein present in all the fractions and (B) mixture 2 integrin present only in fraction s 10, 11 and 12

However, the situation seems quite different in the case of mixture 2, the blots as shown in figure 4.12B (LM 609 assay) and Figure 4.13 B shows the presence of integrin in fraction 10,11 and 12, similarly in the streptavidin assay corresponding fractions shows spots corresponding to the presence of Apol. Moreover, in the case of Figure 4.13 B, the Apol was also found to be present in the initial fraction (2-6); these spots can be attributed to the presence of free Apol in the mixture.

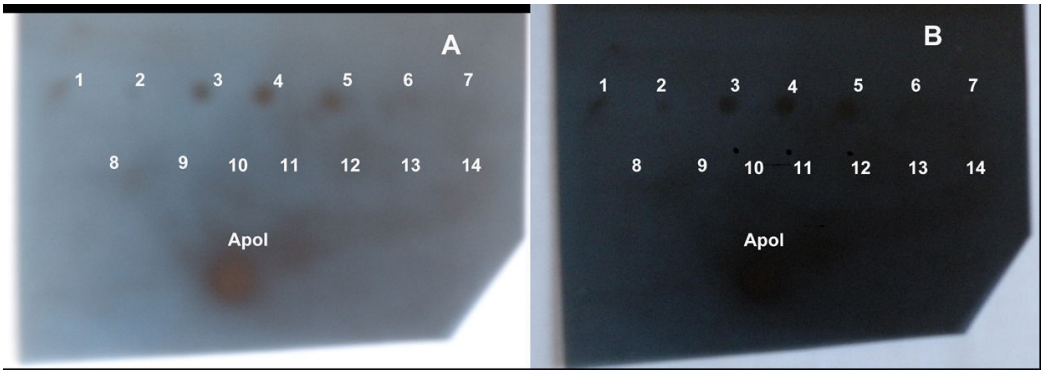

Figure 4.13 Dot blot assays for the detection of the amphipol using a streptavidin assay of (A) mixture 1, notice the B-PCApol Apol present only in fraction 3,4,5 and 6 and (B) of mixture 2, notice the Apol fractions present in fractions 3,4,5,6 and 10,11,12.

This explanation is also in coherence with the difference in the molecular weights of the free Apol and the Apol-$\alpha_v\beta_3$ integrin complex. Since the free Apol particles are much lighter than the complex, they would be present in the low density gradients, whereas the complex being much heavier would descend down to the higher density gradients.
Moreover, the presence of the Apol in the higher density gradient in the case of mixture 2 (Figure 4.13B) is also a strong indication that it is complexed with the integrin. Because only upon complexation, can the Apol be heavy enough to be present in the high density gradient zone. Thus, on comparing figures (4.12B) and (4.13B) it can be concluded that both $\alpha_v\beta_3$ integrin and the Apol are present in fractions 10, 11 and 12 of the sucrose gradient. These results also indicate that the procedure adapted for trapping of Apol described for mixture 2 (renewal of biobead twice, followed by dilution and overnight treatment with biobeads) was efficient in the formation of the Apol- $\alpha_v\beta_3$ integrin complex. In contrast, the procedure used for the formation of mixture 1 lead to the presence of largely uncomplexed protein.

4.3.3. Immobilization of the B-PCApol- $\alpha_v\beta_3$ integrin complex on a SPR chip

A SPR (CM5) chip which was functionalized with streptavidin at a fictionalization level of 8000 RU using the same protocol as described in section 4.2.1b. To these streptavidin coated flow cells, the reference flow cell was functionalized with the B-PCApol alone.

To the active flow cells were injected the combined fractions 10, 11 and 12 of the mixture describe above. Quite strangely the adsorption of these fractions on a Strepavidin coated chip showed no fixation of the Apol as seen in Figure 4.14. This unexpected result could be the effect of highly viscous sucrose in the medium which prevented the diffusion and thus the adsorption of the Apol-integrin complex to the surface.

To understand this effect, the experiment was repeated and the fractions collected from sucrose gradient tube were filtered through an Amicon ultrafiltration device (3,000 MWCO). This step, expected to ensure the removal of the sucrose, did not help in the adsorption of the Apol-integrin complex, as even after removal of the sucrose, no fixation was observed (data not shown).

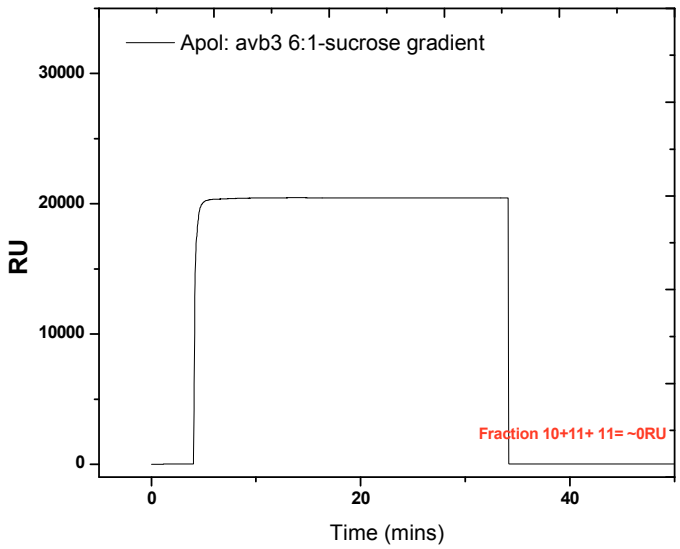

Figure 4.14 Sensorgram indicating the interaction of fraction collected from sucrose gradient onto a streptavidin immolised chip.

Although, we are unable to provide a clear explanation for this fact, we suspect that the B-PCApol precipitates in the presence of sucrose. However, this argument cannot be made with complete confidence as these results need to be verified.

Thus, to rule out the effect of sucrose on the stability of the system, we then attempted to immobilize the $\alpha_v\beta_3$ integrin-B-PCApol complex simply prepared at a ratio of 1:6 without the sucrose gradient separation step. Figure 4.15 shows the sensorgram obtained for the 30 min immobilization of $\alpha_v\beta_3$ integrin-B-PCApol (black curve asterix symbols) and Apol alone (red curve with star symbols). On observation of the adsorption profile of

the B-PCApol alone, a rapid binding followed by a saturation plateau at 3300 RU is observed after about 10 minutes of injection. The signal remains stable to further injection and rinsing with pure buffer. In contrast the binding of integrin-Apol complex appears as a much slower process, indicated by a slow linear increase after a short initial rapid binding of about 700 RU after 5 min of injection. During the following 20 minutes of injection the observed linear increase of the SPR signal suggests that binding of the integrin-Apol complex is controlled by a diffusion limiting process. After rinsing a signal of about 1900 RU is obtained which slowly decreases with time and then stabilizes at 1850 RU after extensive rinsing with pure buffer. This slow binding of the integrin-Apol complex can be explained by the significant size of the integrin-Apol complex, which induces diffusion constraints within the streptavidin-dextran matrix and slows down its binding to dextran immobilized streptavidin. Nonetheless, the difference in the adsorption profiles of the integrin-Apol complex from the FhuA-Apol complex is quite suggestive of the adsorption of a bigger complex than that of FhuA-Apol.

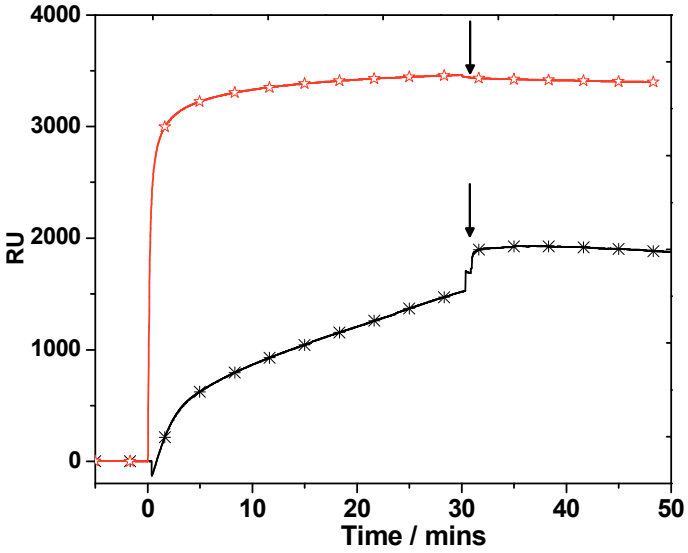

Figure 4.15 Sensorgram showing the immobilization of the Apol (red curve with star symbols) and Apol-integrin complex (black curve with asterix symbols) to a Streptavidin functionalised CM5 surface. The arrows indicate the rinsing step with pure buffer.

4.3.3.a Interaction studies of surface immobilized αvβ3 integrin (Apol: integrin complex) with vitronectin.

Vitronectin is a 75 kDa glycoprotein circulating in the serum. Vitronectin is a multifunctional protein. In vitro, Vitronectin upon binding with the $\alpha_v\beta_3$ integrin promotes the adherence, spreading, and migration of many different cell types including tumor cells in serum-free medium.[18] Under some conditions, vitronectin also promotes the proliferation and differentiation of some cell types. The interactions of vitronectin with its receptor the $\alpha_v\beta_3$ integrin have been thus a topic of investigation for the past few years.

We use this system to test the activity of the Apol-entrapped $\alpha_v\beta_3$ integrin on the biacore chip. As a first step, we carry out a manual injection of a 50 nM solution of vitronectin in the running buffer onto both flow cells containing Apol alone and $\alpha_v\beta_3$-Apol complex. Figure 4.16 represents the response obtained on both the reference and the active cell. Quite encouragingly the reference cell did no show significant binding with vitronectin. In contrast, a strong increase in the SPR signal is observed upon interaction of vitronectin with the active cell bearing Apol-immobilized integrin.

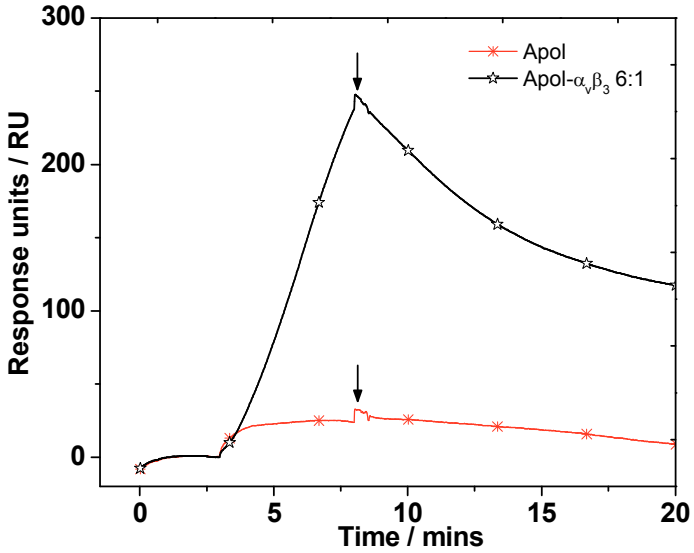

Figure 4.16 Adjusted sensorgram indicating the irreversible interaction of 50 nM vitronectin with B-PC-Apol embedded integrin immobilized on the surface. The arrows indicate the rinsing step with pure buffer.

These results, not only confirm the presence of integrin in the Apol-immobilised surface but also indicate that the immobilised integrin is active in its natural form is able to interact with its natural vitronectin receptor. Also the binding profile of the vitronectin injection is suggestive of a relatively fast adsorption, but rather slow dissociation of the complex. These results are in coherence of results demonstrated earlier (where the integrin was chemically coupled to the surface).[23]

Nonetheless, complete dissociation of the complex is not achieved by rinsing with buffer. Regeneration was tested using chemical agents such as EDTA at both pH 4.5 and pH 8.0, that are commonly used for regeneration of the integrin-vitronectin complex, seemed in our case to be harmful not only to the protein, but also to the integrity of the integrin-B-PCApol. A huge loss in the SPR signal was observed upon injection of such agents (data not shown) which indicated a significant loss of the adsorbed material. Moreover, the reproducibility of the present system was also under question, as two different experiments, hardly led to similar recognition response with vitronectin.

4.4. Conclusions and Perspectives

The present chapter demonstrates the use of Amphipols in stabilizing and surface immobilizing membrane proteins. With the help of the two proteins of our interest i.e FhuA and the $\alpha_v\beta_3$ integrin, we could quite successfully demonstrate that Amphipols present an interesting alternative to the study of membrane proteins. More particularly, in the case of FhuA we demonstrated that Apols are not just a convenient medium for stabilizing and fixing membrane proteins on the surface, but also that they provide an interference free substrate for quantifying interactions between FhuA and its phage protein pb5. These results are not only novel in the domain of the contemporary research in amphipols, but it is for the first time that the FhuA-pb5 interactions are quantified to obtain their affinity constants.

The case of $\alpha_v\beta_3$ integrin, however, is a bit more delicate than that of FhuA. In the present case, the extremely small quantity of the protein limits the detection by a simple UV-visible method. Rather it requires the long time consuming dot-blot technique for the determination of the optimum trapping conditions. Moreover, this technique although

being an excellent means of detection is not a quantitative method. Hence, using this technique the determination of appropriate ratios of effective trapping could not be clearly established.

Hence, to conclude it would be appropriate to comment that besides, the constraints offered by the $\alpha_v\beta_3$ integrin, the use of amphipols in general is truly one of the most convenient and efficient methods of handling and analyzing membrane proteins. In view of the contemporary interest in developing platforms for studying membrane proteins, we believe that our present results take the understanding on amphipols a step further on the global scenario.

4.5. Experimental Protocols

B-PCAPol solutions in buffer were prepared by overnight agitation at 4 ^{o}C and stored for about one week. Milli-Q grade water of resistivity 18 MΩ·cm was used for all physical measurements.

4.5.1. Biobeads

The Biobeads obtained Bio-Beads SM2 (20-50 mesh) polystyrene beads were purchased from Bio-Rad. As per the protocol developed by JL Rigaud *et al.* they were treated with methanol for about half an hour and washed several times with water, followed by overnight incubation in water prior to their use. 20 mg of wet Biobeads were added for each mg of LDAO or OG.[24]

4.5.2. Protocol for the single-cycle kinetic measurement of B-PCApol-immobilized FhuA with pb5 by SPR

pb5 was purified according to the procedure described elsewhere.[14] Aliquots of increasing concentrations of pb5 ranging from 5 nM to 500 nM were prepared in PBS buffer at pH 6.0, from its stock solution of 5 μM concentration.

After functionalization of the SPR chip with the FhuA: B-PCApol (1:3 wt/wt) complex on the active flowcell and the B-PCApol alone on the reference flowcell, the surface was

allowed to stabilize in PBS buffer, pH 6.0 for a period of 30 minutes. After this period, when the signal was found to be sufficiently stable, a few injections of the PBS buffer were performed to condition the surface. This was followed by a series of 11 injections of aliquots of increasing concentration of pb5 (of the above mentioned concentration range) at a flow rate of 20 µL/min on both the active and reference flowcells. The association or binding time of each injection was 300s whereas, in between each injection, a stabilization time of 180s was given. The reference-subtracted sensorgrams were then extracted and the data obtained were treated using a Langmuir single-site binding model using Kaleidagraph 3.5.

4.5.3. Dot blot assays

Dot blot assays were done by blotting the sample solutions (2 μl-3 times) on a spot on a nitrocellulose membrane. These nitrocellulose membranes of 0.45 μm were obtained from Whatmann and used without any pretreatment. These membranes after spotting the samples were treated with 5% milk solution, which was prepared by freshly dissolving powdered milk (full cream, available in supermarkets) in buffer.

The luminol and peroxide mixture was prepared by mixing equal volumes of the two solutions from a luminol reagent kit obtained from ThermoFisher scientific.

The transfer of the chemiluminescence was done on photographic films obtained from Kodak® Biomax, these films were developed in a dark room using the Kodak® processing chemicals for autoradiography films.

4.5.4. Surface Plasmon Resonance (SPR) measurements

SPR measurements were performed on a Biacore T100 (GE Healthcare) operated by the Biacore T100 Control software. The CM5 chip from Biacore was appropriately functionalized with streptavidin for the experiments. All the measurements were performed at 25 ^{o}C. The recorded sensorgams were analysed using the Biacore T100 Evaluation software and Origin 8.0.

4.6. References

(1) Brotherus, J. R.; Jost, P. C.; Griffith, O. H.; Hokin, L. E. *Biochemistry* **1979**, *18*, 5043-5050.

(2) Breyton, C.; Tribet, C.; Olive, J.; Dubacq, J. P.; Popot, J. L. *J. Biol. Chem* **1997**, *272*, 21892–21900.

(3) Yu, S. M.; McQuade, D. T.; Quinn, M. A.; Hackenberger, C. P. R.; Gellman, S. H.; Krebs, M. P.; Polans, A. S. *Protein Sci.* **2000**, *9*, 2518-2527.

(4) Theisen, M. J.; Potocky, T. B.; McQuade, D. T.; Gellman, S. H.; Chiu, M. L. *Biochim. Biophys. Acta, Prot. Proteom.* **2005**, *1751*, 213-216.

(5) Chae, P. S.; Wander, M. J.; Bowling, A. P.; Laible, P. D.; Gellman, S. H. *ChemBioChem* **2008**, *9*, 1706-1709.

(6) Tribet, C.; Audebert, R.; Popot, J. L. *Proc. Natl. Acad. Sci. U. S. A.* **1996**, *93*, 15047.

(7) Tribet, C.; Audebert, R.; Popot, J. L. *Langmuir* **1997**, *13*, 5570-5576.

(8) Dahmane, T.; Damian, M.; Mary, S.; Popot, J. L.; Bane res, J. L. *Biochemistry* **2009**, *48*, 6516-6521.

(9) Nagy, J. K.; Kuhn Hoffmann, A.; Keyes, M. H.; Gray, D. N.; Oxenoid, K.; Sanders, C. R. *FEBS Lett.* **2001**, *501*, 115-120.

(10) Picard, M.; Dahmane, T.; Garrigos, M.; Gauron, C.; Giusti, F.; le Maire, M.; Popot, J. L.; Champeil, P. *Biochemistry* **2006**, *45*, 1861-1869.

(11) Diab, C.; Tribet, C.; Gohon, Y.; Popot, J. L.; Winnik, F. M. *Biochim. Biophys. Acta, Biomembr.* **2007**, *1768*, 2737-2747.

(12) Miyazawa, K.; Winnik, F. M. *Macromolecules* **2002**, *35*, 2440-2444.

(13) Tribet, C.; Diab, C.; Dahmane, T.; Zoonens, M.; Popot, J. L.; Winnik, F. M. *Langmuir* **2009**, *25*, 12623-12634.

(14) Plançon, L.; Janmot, C.; le Maire, M.; Desmadril, M.; Bonhivers, M.; Letellier, L.; Boulanger, P. *J. Mol. Biol.* **2002**, *318*, 557-569.

(15) Abdiche, Y.; Malashock, D.; Pinkerton, A.; Pons, J. *Anal. Biochem.* **2008**, *377*, 209-217.

(16) Karlsson, R.; Katsamba, P. S.; Nordin, H.; Pol, E.; Myszka, D. G. *Anal. Biochem.* **2006**, *349*, 136-147.

(17) Glück, J. M.; Koenig, B. W.; Willbold, D. *Anal. Biochem.*

(18) Hynes, R. O. *Cell* **2002**, *110*, 673-687.

(19) Boturyn, D.; Coll, J. L.; Garanger, E.; Favrot, M. C.; Dumy, P. *J. Am. Chem. Soc* **2004**, *126*, 5730-5739.

(20) Garanger, E.; Boturyn, D.; Jin, Z.; Dumy, P.; Favrot, M. C.; Coll, J. L. *Molecular Therapy* **2005**, *12*, 1168-1175.

(21) Garanger, E.; Boturyn, D.; Coll, J. L.; Favrot, M. C.; Dumy, P. *Org. Biomol. Chem.* **2006**, *4*, 1958-1965.

(22) Jin, Z. H.; Josserand, V.; Foillard, S.; Boturyn, D.; Dumy, P.; Favrot, M. C.; Coll, J. L. *Molecular Cancer* **2007**, *6*, 41.

(23) Petrie, T. A.; Raynor, J. E.; Reyes, C. D.; Burns, K. L.; Collard, D. M.; García, A. J. *Biomaterials* **2008**, *29*, 2849-2857.

(24) Rigaud, J. L.; Levy, D.; Mosser, G.; Lambert, O. *European Biophysics Journal* **1998**, *27*, 305-319.

5. SPR Studies of Lectin Recognition by Small Multivalent Carbohydrate Ligands

5. SPR Studies of Lectin Recognition by Small Multivalent Carbohydrate Ligands

5.1. Introduction

Carbohydrate – protein interactions play a central role in a wide variety of biological recognition processes. These interactions are involved in inflammation processes, in cell-cell recognition, signal transduction and immune response.[1-5] Despite weak affinity between lectin and monosaccharides (K_D in the 0.1-1 mM range), sugar-protein interactions are very efficient and specific. To enhance the binding affinity and thus improve the biological response, carbohydrate binding proteins (namely lectins) are multimeric and usually engaged in multivalent interactions with the recognition systems. This interaction process is commonly known as the "glycoside cluster effect" and is defined as "the affinity enhancement achieved by multivalent ligands over monovalent ones that is greater than that would be expected from a simple effect of concentration increase".[6,7] Multivalent carbohydrate derivatives which can simultaneously interact with several binding sites of a multivalent lectin (chelate effect) are relevant for medicinal interest. In this context, synthetic polyvalent ligands, presenting the possibility to bind to several receptors can act as inhibitors of pathological processes or as effectors of signal-transduction pathways.[8,9] A large variety of glycoclusters displayed by low molecular weight (LMW) scaffolds,[8,10,11] dendrimers,[12-14] calixarenes[15] or polymers[16-21] has emerged in order to understand, mimic and try to control carbohydrate-lectin interactions.[22] Indeed, understanding the parameters that govern the carbohydrate-lectin interaction would be useful from a fundamental point of view as well as for drug design.

While LMW glycoclusters are too small to span two binding sites on a single lectin,[23] it is well known that such ligands allow a significant enhancement of the sugar-lectin affinity. However, the understanding of the interaction mechanisms which could be responsible of this phenomenon is difficult to analyse.[11,24,25]

In the present studies, we develop a direct Surface Plasmon Resonance (SPR) based binding assay to identify and quantify the fundamental mechanisms involved in recognition of LMW glycoclusters towards a multimeric lectin. The interactions between

Concanavalin A (ConA) and mannosyl residues grafted on a LMW scaffold was studied as a model and SPR was chosen as the technique which allowed easy assessment of the kinetic and thermodynamic parameters of sugar-protein interactions.[26]

5.1.1. Individual Mechanisms Operating in Multivalent Recognition

The glycoside cluster effect as defined previously is "the affinity enhancement achieved by multivalent ligands over monovalent ones that is greater that would be expected from a simple effect of concentration increase".[6] As suggested by this general definition, the sum of the contribution of several individual effects should be taken into account in recognition through multivalent ligands. In contrast to monovalent compounds which only allow 1:1 interaction (Figure 5.1A), multivalent ligands can bind to receptors in three specific ways,[8,27,28] as depicted on Figure 5.1.

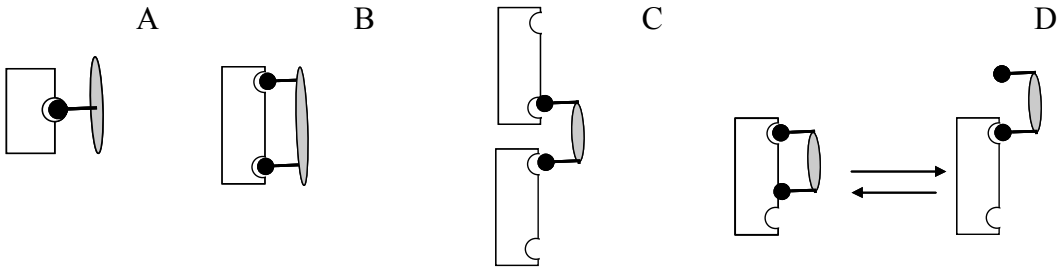

Figure 5.1. Schematic representation illustrating the interactions in solution of a divalent receptor with A) a monovalent ligand (1:1 interaction) B,C,D) with a divalent ligand B) chelate effect C) clustering effect and D) proximity/statistical effect.

The chelate effect refers to the simultaneous multiple interactions of a multivalent ligand to a single oligomeric lectin (Figure 5.1B). It is observed when the size of the ligand is sufficient enough to span multiple binding site of a single receptor.[29] In this binding mode, the nature, the length and the flexibility of the linker between the epitope have a great importance in the resulting interactions.[9]

The clustering effect corresponds to several 1:1 interactions engaged by one glycocluster towards several individual lectins to form cross-linked complexes (Figure 5.1C).[11,30,31] This effect has been observed to be independent of the ligand size. In some cases, this effect is also responsible for aggregation/precipitation when it occurs in solution.[23]

Another binding mode is the proximity/statistical effect,[24,32] also know as recapture or statistical rebinding effect[18] (Figure 5.1D). This effect appears when the inter-binding site distance of the lectin is significantly higher than the inter-epitope distance of the ligand. In this case, the close proximity of several carbohydrates on the scaffold favours the rebinding of a second moiety with the receptor just after its dissociation from a first one. In fact, the high effective epitope concentration on the ligand increases the possible binding permutation of its epitopes with one lectin binding site. This effect has been evidenced for different kinds of multivalent structures,[33] polymers,[21] or dendrimers[24].

Knowledge of the participation of each effect in the globally enhanced affinity is crucial to orient the conception and synthesis of optimized glycoclusters. While the characterization of a monovalent interaction is relatively simple, the case of multivalent interactions is more complex since it is difficult to unambiguously ascribe the enhanced affinity to the specific effects occurring simultaneously. However, the quantification of these different binding mechanisms requires their isolation and still remains arduous to investigate.

5.1.2. Study of Multivalent Recognition at Interfaces

As depicted in Figure 5.1, even for small multiple molecules which do not lead to chelation, the dissociation of the two other processes namely statistical/proximity and clustering effect is quite difficult. In order to control the individual mechanisms participating in the recognition, studies at interfaces appear to be a promising route. Indeed, by adjusting the density of the immobilized ligands, the phenomena involved in the recognition could be adjusted.

Moreover, techniques such as SPR appear to be apt to study such interactions, as it can provide direct information on the affinity of the interactions as well as on its kinetics. Another advantage of this technique is that no labelling of the partners is necessary (see section 1.4.4) In order to optimize the detection signal, which is directly related to the molecular weight of the analyte interacting with the surface, immobilization of the smallest partner in weight is preferred. Indeed, several SPR studies involving the surface fixation of the carbohydrate and the detection of lectins in solution can be found in the literature.[26] However, among these various examples, only a few reports demonstrate a systematic investigation of the recognition of the lectin based on the density of the sugar

exhibited by the surface.[33-36] Our group has previously described the impact of each process (1:1 interaction, chelating effect, proximity/statistical effect and clustering effect) that could occur during the recognition between a model lectin in solution and a multivalent sugar surface as a function of the surface composition, *i.e.* the ligand structure (mono or multivalent) and its surface density (see Figure 5.2).[25]

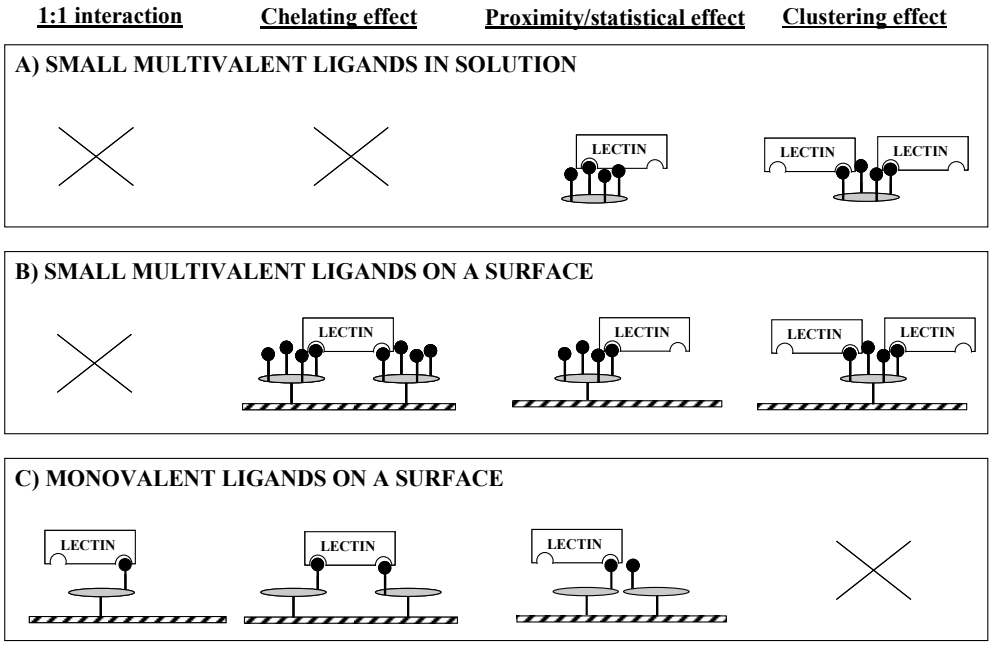

Figure 5.2. Schematic representation of the three main effects at the origin of the "glycoside cluster effect", illustrated by the interaction of a bivalent lectin with small multivalent ligands which cannot span to multiple sites of a single lectin (A) in solution, (B) immobilized on a surface, and (C) comparison with the interaction of a bivalent lectin with monovalent ligands immobilized on a surface: "1:1 interaction", "chelating" effect, "proximity/statistical" effect and "clustering" effect. Figure from ref [25].

The chelate effect induced by the surface presentation of the carbohydrate could be a factor responsible for the enhancement of the affinity observed for recognition of a lectin in solution towards both mono and multivalent ligands. Efficient reduction of the surface density of the immobilised sugar has helped to rule out the chelate effect for both surfaces modified with mono and multivalent ligands as well as the proximity/statistical binding occurring with the monovalent ligand present at the surface. While we have succeeded in providing evidence on the impact of clustering and proximity/statistical effects induced by LMW multivalent carbohydrate ligands on the enhanced affinity, quantification of both effects couldn't be evaluated independently.

To succeed in the total dissociation of the statistical rebinding from the cross-linking process, the immobilization of the lectin on the surface appears to be a favorable approach (see Figure 5.3).

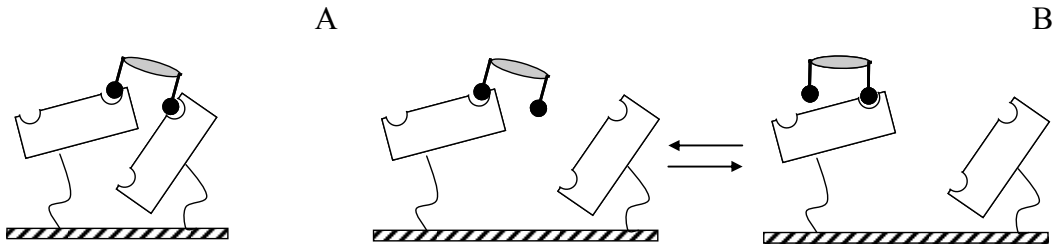

Figure 5.3. Schematic representation of the interaction of multivalent small ligands (which cannot span to multiple sites of a single lectin) with a multivalent lectin immobilized on a surface A) clustering effect and B) proximity/statistical effect

This strategy of lectin immobilization, presents greater advantage in ruling out the chelate effect that is induced in the opposite configuration, by immobilizing either mono or multivalent carbohydrate ligands on the transducing surface. It could also be anticipated that dilution of immobilized protein will prevent a clustering effect. However, the main disadvantage of this approach lies in the low detection limit of small carbohydrates.

The use of the improved version *i.e.* the latest SPR device, the direct measurement of the binding of low molecular weight molecules are now attainable.[37,38] However, due to the low affinity of the lectin-carbohydrate interactions, direct observation of low molecular weight mono or multivalent carbohydrate ligand still remains a challenge. To the best of our knowledge, to date, only four studies have demonstrated the direct investigation of small carbohydrates in solution interacting with surface immobilized lectins.[39-42]. Among these reports, the one by Beccati *et al.* have resolved the problem of low detection signal of LMW monocarbohydrate by using organoplatinum(II) complexes.[42] The advantage of platinum here was that, upon interacting with the evanescent field it resulted in a large signal enhancement, thus facilitating the interaction studies. However, this approach of labelling, eventually gave rise to the overestimation of the affinity constants. Another report by Murthy *et al.* describes the study of the interactions of amphiphilic mono and multivalent carbohydrates to ConA (immobilized at a single surface density) by SPR.[39] In their studies, besides identification of the kinetic rate constants by SPR, they have

used complementary techniques like DLS and TEM to characterize the cross-linked complexes formed between their ligand and ConA.

In the two above mentioned papers, the individual mechanisms involved in the recognition were not treated. The work of Gomez-Garcia *et al.* is focussed on the cyclodextrin-centered glycoclusters where they compared SPR, ELLA and ITC results.[40] However, by SPR, reliable data could not be obtained with their low-density glycoclusters. Another interesting piece of work by Munoz *et al*. provides evidence on the impact of clustering effect in the recognition by studying the interaction of glycodendrimers with ConA immobilized at low and high surface coverages.[41] These authors have suggested that the reliability of results of surface-based measurement of lectin/carbohydrate recognition is based on the control of the lectin surface densities used in the assay. However, in their studies proximity/statistical effects induced by the multivalent glycoclusters have not been taken into consideration.

Thus, to summarize it would be appropriate to comment that any successful study of the multivalent interactions at an interface will be dependent on multiple assays based on variation of the ligand surface density. This procedure should allow the separation of the different effects involved in the recognition.

5.1.3. The Lectin

Concanavalin A (ConA) is a plant lectin isolated from the jack bean, *Canavalia ensiformis*. ConA exists as a homotetramer at pH 7 and as a homodimer at acidic pH (below 5).[43,44] Each monomer unit (26.5 kDa) presents one binding site for α-mannosides. In the tetramer, the four binding sites are presented in a tetrahedral arrangement which facilitate its ability to bind several multivalent ligands and to form 3-D aggregates. ConA binds specifically to mannose (Man) or mannose containing oligosaccharides. Being one of the most characterized lectin, ConA is extensively used as a model for multivalent carbohydrate –protein recognition studies.

5.1.4. Multiple-Carbohydrate Presentations on a Cyclodecapeptide Scaffold

Our group has been for years, devoted in the study of cyclodecapeptide based scaffolds called Regioselectively Addressable Functionalized Template (RAFT). These scaffolds present two distinct functional domains which can be functionalised individually with various groups (see section 2.1).

The RAFT scaffold was also used in this study, to assemble a cluster of sugar moieties.[45-47] Figure 5.4, describes the structures of the two RAFT molecules, used in this study. The structure shown in Figure 5.4A displays four mannose residues and are hence called RAFT-$(Man)_4$ where as the one in Figure 5.4B demonstrates the RAFT bearing one mannose and is thus called RAFT-$(Man)_1$. In both these structures the mannose group was functionalised through the lysine groups (K) present on the upper addressable domain of the RAFT.

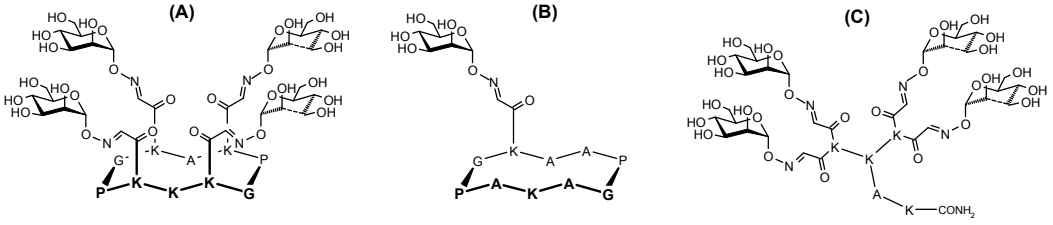

Figure 5.4. Structures of (A) RAFT-$(Man)_4$ (B) RAFT-$(Man)_1$ and (C) MAP-$(Man)_4$. Their molecular weights are respectively 1082, 1953 and 1532 $g.mol^{-1}$.

It has previously been demonstrated that clusters of carbohydrate based ligands present on the surface of RAFT molecules ensure the specific recognition and a significantly enhanced affinity for lectins through multivalent interactions.[45,46,48-50]

It is important to note here, that this RAFT template based LMW tetramannosyl glycoconjugate presents mannose residues with an intermolecular distance of ~ 25 Å, as estimated from molecular modelling. This distance is much lower than the distance between two binding sites of Con A (~70 Å).[51-53] In consequence, simultaneous binding of RAFT molecules to multiple sites of a same lectin (chelate effect, Figure 5.1) can be ruled out. Another molecule called the Multiple Antigenic Peptide (MAP) as shown in Figure 5.4C was also tested as another LMW tetravalent ligand. This molecule also displays multiple presentations of carbohydrate groups, however through a different template structure.

In the present chapter, we discuss the comparative SPR studies of the mono and tetravalent (RAFT/MAP based) carbohydrate molecule binding with ConA immobilized on the surface at both high densities (HD) and low densities (LD). Careful adjustments of experimental conditions have allowed the obtention of reliable data for the small carbohydrate ligands. As a first part of this study, comparative results for the interaction of the glycocluster with two surfaces differing in their density of immobilized lectin are discussed in relation to the binding processes involved. The design of RAFT-glycoclusters that exclude chelate effect, coupled with an adequate modulation of the surface density of ConA have provided an evaluation of the impact of proximity/statistical effect of our ligand in absence of any clustering effect. As a second part of this work, the defined procedure was extended to the determination of the thermodynamic parameters such as free energy, enthalpy and entropy involved in the binding of the molecules to ConA at low surface densities in order to have insights on the statistical rebinding phenomenon.

5.2. Experimental Section

5.2.1. Data Analysis

In the present study, we paid special attention to the interpretation of the data. In the following section, general notions on interaction model will be summarized and the approach used for the data analysis of our experiments will be described.

5.2.1.a Monovalent interactions – definition of the binding equilibrium constant.

• A monovalent interaction is characterized by the binding of two monovalent molecules A and L to form a complex LA as illustrated below:

$$\mathbf{L + A} \underset{k_{off}}{\overset{k_{on}}{\rightleftharpoons}} \mathbf{LA} \qquad \textbf{Scheme 1}$$

The interaction is characterized by an equilibrium between the formation of the complex and its dissociation. The binding force of the interaction is defined by the equilibrium association constant K_A or by the equilibrium dissociation constant K_D:

$$K_A = \frac{1}{K_D} = \frac{[LA]_{eq}}{[L]_{eq} \cdot [A]_{eq}} = \frac{k_{on}}{k_{off}} \qquad \textbf{Equation 5-1}$$

Where k_{on} is the association rate constant
k_{off} is the dissociation rate constant
[L], [A] and [LA] are the concentrations of L, A and LA at equilibrium respectively.

Through this equation, it appears that the equilibrium binding constant could be experimentally measured via two kind of analysis (i) by a kinetic analysis via determination of the association and dissociation rate constant or (ii) by a steady state analysis via the determination of the concentration of each substance at equilibrium.
Both these above mentioned analyses will be described in the context of our study considering that one partner is immobilized on a surface (Figure 5.5).

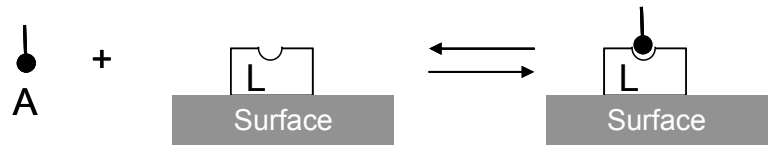

Figure 5.5. Schematic representation of a monovalent interaction between A in solution and L immobilized on a surface.

The molecule in solution (A) is usually called analyte while the molecule immobilized on the surface (L) is named ligand. To perform any analysis, the concentration of the partner at equilibrium has to be expressed as a function of the experimental parameters for example the concentration of A injected $[A]_{inj}$ and the response (R) of the device are the two parameters that are used to follow the interactions.
In SPR experiments, the concentration of the free analyte is maintained constant throughout an injection, by the help of a flow system. Thus, in this case $[A]_{inj} = [A]_{eq}$. For simplification, the concentration of A injected is denoted as [A]. The SPR response is proportional to the quantity of A bound to the surface at equilibrium. The concentration of A bound is equal to the concentration of the complex formed: R = [LA].

The concentration of the free ligand [L] is obtained by subtracting its total concentration from the concentration of its bound form (complex LA). The total concentration $[LA]_{total}$ of LA is the response (R_{max}) measured when the surface is saturated with A : $[L] = [LA]_{total} - [LA] = R_{max} - R$.

By including these considerations in Equation 5.1, we obtain:

$$K_A = \frac{1}{K_D} = \frac{R_{eq}}{(R_{\max} - R_{eq}) \cdot [A]} = \frac{k_{on}}{k_{off}}$$ **Equation 5-2**

5.2.1.b Steady state analysis for determination of equilibrium constants

- The simplest steady state model for a monovalent interaction occurring at interface (Langmuir model) assumes that the analyte (A) is both monovalent and homogenous in solution, that the ligand (L) is homogeneous, and that all binding events are independent and equivalent. Under these conditions data should conform to the Langmuir binding isotherm corresponding to equation 5.2, also expressed as:

$$R_{eq} = \frac{K_A[A] \cdot R_{\max}}{1 + K_A[A]}$$ **Equation 5-3**

R_{max} and K_A can be extracted by non-linear curve fitting of the experimental adsorption isotherm (R_{eq} as a function of [A]) on the basis of the Langmuir model.

- The Scatchard representation is a linearization of the Langmuir equation, which produces a simple graphical analysis of the data collected during the interaction between an immobilized ligand and an analyte in solution. The advantage of this procedure is a rapid validation of the model used to fit the data. The Scatchard equation is given by:

$$\frac{R_{eq}}{[A]} = K_A R_{\max} - K_A R_{eq}$$ **Equation 5-4**

This method of analysis consists of plotting the (R_{eq}/[A]) variation as a function of R_{eq} (See Figure 5.6). A linear plot obtained is a confirmation of a 1:1 interaction occurring between the analyte and the ligand.

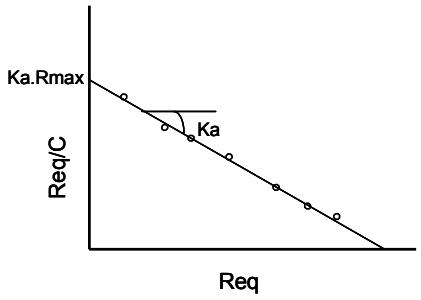

Figure 5.6. Scatchard plot obtained through linearization of the Langmuir equation corresponding to a 1:1 interaction

While in principle these diagrams should allow the determination of the K_A and R_{max}, they were not really used in this manuscript for determination of these parameters. This is because, these plots place inappropriate weight on the data obtained with the lowest concentrations of the analyte, which are generally the least reliable.

As described above, Scatchard plots are quite relevant for identification of the type of interactions: Indeed, in function of the various interactions involved in the recognition namely, 1:1 interactions, bivalent interactions, 1:1 interactions with heterogeneous ligand binding sites and so on (negative or positive cooperativity, etc), Scatchard plots present different profiles. A linear Scatchard plot indicates that the data conform to the Langmuir model while non linear plot exclude data analysis by a one binding site model and more complex models should be considered (see Figure 5.7).

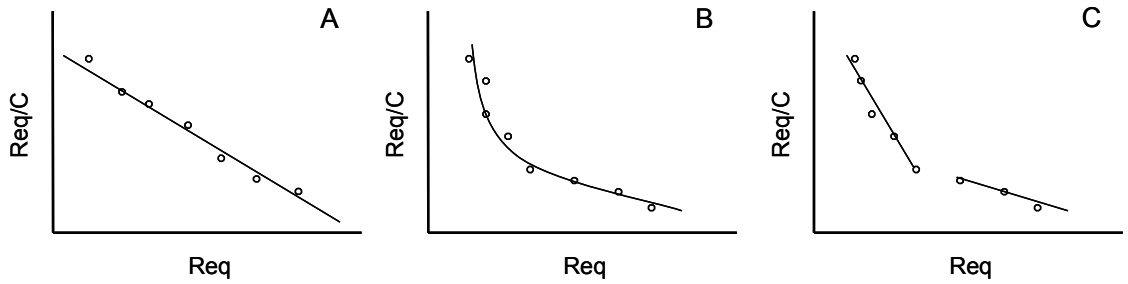

Figure 5.7. Three more common type of Scatchard plot: A) monovalent interaction B) multivalent analyte and C) heterogeneous ligand.

In consequence, in the present study, a Scatchard analysis was applied to all data collected at the steady state for all experiments in order to validate the model used for fitting the experimental curves.

5.2.1.c Kinetic analysis of the interactions

- The Langmuir kinetic model is based on the analysis of the kinetic parameters of a 1:1 interaction between an immobilized ligand and an analyte in solution In order to evaluate the kinetic parameters k_{on} and k_{off}, the association and dissociation part of the signal recorded during the interactions are fitted according to the following equation:

$$\frac{d[AB]}{dt} = k_{on}[A][L] - k_{off}[LA] \qquad \textbf{Equation 5-5}$$

Considering the reaction at interface, the equation could be rewritten under the following form:

$$\frac{dR}{dt} = k_{on}[A](R_{\max} - R) - k_{off}R \qquad \textbf{Equation 5-6}$$

Where, [A] is the injected concentration of analyte, R_{max} is the maximal response obtained for saturation of the surface and R stands for the response at time t.

- bivalent model. In the case of a divalent interaction between the analyte in solution and the ligand (L) immobilized on the surface, we have used the model of the bivalent analyte elaborated by R. Karlsson[54] according to the following scheme:

$$2L + A \underset{k_{off1}}{\overset{k_{on1}}{\rightleftharpoons}} LA + L \underset{k_{off2}}{\overset{k_{on2}}{\rightleftharpoons}} LLA \qquad \textbf{Scheme 2}$$

Where, k_{on1}, k_{off1} and k_{on2}, k_{off2} are the kinetic association and dissociation rate constants for the complexes LA and LLA respectively.

The analyte A will bind to two ligands L following two successive interactions. The equilibrium association constant corresponding to the formation of the complexes LA

and LLA in this case are thus defined as $K_{A1} = k_{on1}/k_{off1}$ and $K_{A2} = k_{on2}/k_{off2}$ respectively. The two binding sites of the analyte A are supposed to be independent and to react equivalently with the immobilized ligand L.

The equations corresponding to this reaction are expressed below:

$$\frac{dR_1}{dt} = k_{on1}[A]\times(R_{\max} - R_1 - 2R_2) - k_{off1}R_1 - k_{on2}\ R_1\times(R_{\max} - R_1 - 2R_2) + k_{off2}R_2 \qquad \textbf{Equation 5-7}$$

$$\frac{dR_2}{dt} = k^*_{a2}R_1\times(R_{\max} - R_1 - 2R_2) - k_{d2}R_2 \qquad \textbf{Equation 5-8}$$

$$\frac{dR_3}{dt} = -\frac{dR_1}{dt} \qquad \textbf{Equation 5-9}$$

Where, R_1, R_2 and R_3 correspond to the concentrations of species [LA], [LLA] and [L] respectively.

The second binding rate constant k_{on2} is expressed in $RU.s^{-1}$ since the second binding to the surface doesn't induce any change in the SPR response. This value could be expressed in $M.s^{-1}$ by using an adequate conversion factor which depends on the surface used as well as on the refractive index of the analyte in solution.

5.2.1.d Thermodynamic analysis

Affinity can also be expressed as the standard state molar free energy (ΔG°) which is deduced from the equilibrium association or dissociation constants as follows:

$$\Delta G^\circ = -RT\ln K_A = RT\ln K_D \qquad \textbf{Equation 5-10}$$

Where, T is the absolute temperature in Kelvin (298.15 K = 25 °C) and R is the Universal Gas Constant (1.987 $cal.K^{-1}.mol^{-1}$ or 8.314 $J.mol^{-1}.\ K^{-1}$)

The binding energy or affinity includes contributions from changes in enthalpy (heat absorbed or ΔH) and entropy (increased disorder or ΔS):

$$\Delta G^\circ = \Delta H^\circ - T\Delta S^\circ \qquad \textbf{Equation 5-11}$$

If it is assumed that ΔH° and ΔS° are temperature-independent, then the linear form of the van't Hoff equation can be used.

$$\ln K_D = \frac{\Delta H^\circ}{RT} - \frac{\Delta S^\circ}{R}$$ **Equation 5-12**

The value for ΔH° and ΔS° are deduced from the plot representing $\ln(K_D) = f(1/T)$ (Figure 5.8).

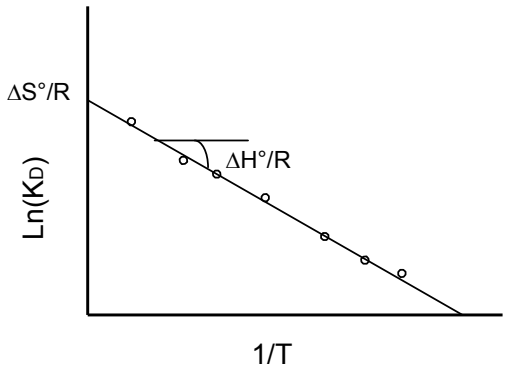

Figure 5.8. van't Hoff plot allowing the indirect determination of the enthalpy and entropy from the K_D values at different temperatures.

5.2.2. SPR experiments

SPR measurements were performed with a BIAcore T100 (Biacore AB, Sweden) operated with BIAcore T100 evaluation Software 1.1. All measurements were performed at 25°C, at 5 µL/min for ligand immobilization and 40 µL/min for kinetic measurements. Experiments are realized in working buffer (WB) consisting of HEPES Saline Buffer (HBS) (0.1 M HEPES, NaCl 0.1 M) pH 7.2 with 1 mM $CaCl_2$ 1 mM $MnCl_2$ and 0.05% P20 surfactant. The carboxymethylated dextran layer of a CM5 sensor chip was activated by a 7 min pulse of a 1:1 mixture of freshly prepared 50 mM N-hydroxysuccinimide and 200 mM N-ethyl-N'-(dimethylaminopropyl)-carbodiimide. *Peanut Agglutinin* (PNA) and ConA lectins in acetate buffer 10 mM pH 4.5 were bound to the activated surfaces during to the desired value. Blockage of the remaining N-hydroxysuccinimide esters was performed by a 7 min injection of 1.0 M ethanolamine hydrochloride pH 8.5. Curves obtained on the reference surfaces (PNA surfaces) are deduced from the curves recorded on the recognition surfaces, allowing elimination of refractive index changes due to

buffer effects. RAFT molecules were diluted in WB. The absence of mass transport effects on experiments was checked on each surface by running separately one injection of all analyte for 60 s at different flow rates (5, 15 and 75 µL/min). The curves obtained are able to be overlaid, confirming the absence of mass transport limitations (not shown). Regeneration is achieved by a 120 s injection of a 50 mM mannose solution. In order to control the stability of the functionalized surfaces, at least one analyte concentration solution was injected twice.

The kinetic parameters of the binding reactions were determined using BIAevaluation 2.0.1 software and statistically validated using the chi-square distribution (or $\chi 2$ distribution). The resonance signal is displayed in resonance units (RU) that is related to a specific biomolecules mass on the sensor chip surface.

Combined to the low detection limit of the device used in the present studies, the careful adjustment of the reference flowcell and the preparation of the mother solution of the injected analyte as well as its further dilutions in the working buffer are the successful key to obtained reliable data. Indeed, our system cumulated two unfavourable conditions for a SPR study of binding interaction, which are the low molecular weight of the analyte coupled to the low affinity of the interaction,

5.3. Clustering and proximity effect discrimination

The SPR experiments were carried out on Biacore T100 instrument (GE Healthcare, Uppsala) at 25°C. A carboxymethylated dextran sensorchip (CM5) was functionalized by amine coupling with ConA at two different surface coverages: at low density (LD) and at high density (HD) of ConA with an immobilized amount of the protein of respectively 3193 RU and 9670 RU. These conditions were designed to provide data able to distinguish the different binding mode of the compounds.

5.3.1. Study of the Interaction with ConA Immobilized at Low Surface Density

We considered first the experiments performed with ConA immobilized at low density (LD). As schematically represented in Figure 5.1, the clustering effect of the multiple ligand should in principle be suppressed and only a 1:1 interaction should be observed. Figure 5.9 shows sensorgrams recorded during the interaction of RAFT-$(Man)_1$, RAFT-$(Man)_4$ and MAP-$(Man)_4$ with the lectin immobilized at a low surface density. The sensorgrams depicted are double subtracted as explained in the experimental section (see paragraph 5.2.2). Initial examination of the sensorgrams suggests that the presence of the four mannose residues gave rise to the formation of more stable complexes compared to those formed with RAFT-$(Man)_1$; RAFT-$(Man)_1$ dissociated immediately upon rinsing while the multivalent RAFT exhibited slower dissociation phases. The off-rates for all mono and multivalent cycladecapeptides are rapid and baseline was reached almost immediately after the end of analyte injection indicating weak affinity interactions.

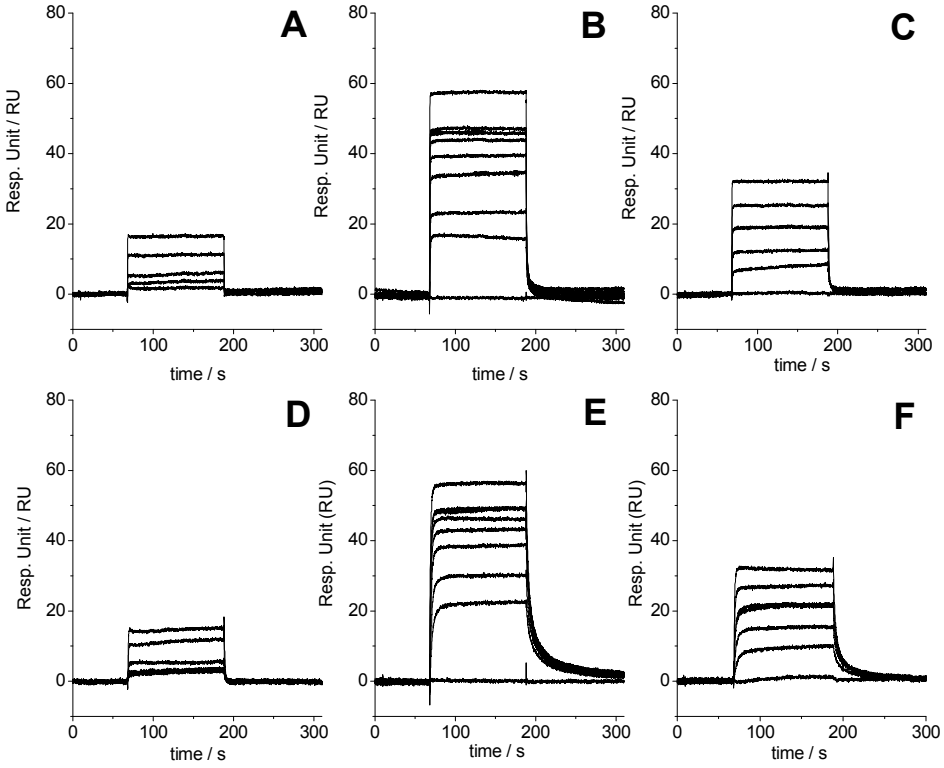

Figure 5.9. Sensorgrams recorded A) B) C) at 25°C, and D) E) and F) at 5°C during the interaction of A), D) RAFT-$(Man)_1$, B) E) RAFT-$(Man)_4$, C) F) MAP-$(Man)_4$ with ConA immobilized at low surface density (3193 RU). The reference flow cell is obtained by immobilization of PNA lectin at similar surface density. The flow rate is 40 µL/min. The concentration ranges are: 25 µM – 500 µM for RAFT-$(Man)_1$; 10 µM – 200 µM for RAFT-$(Man)_4$ and 5 µM – 100 µM for MAP-$(Man)_4$

Sensorgrams recorded at 25°C present squared profiles *i.e.*, fast steps of association and dissociation, ruling out any possibility for kinetic analysis of the curves (Figure 5.9A-C). The analysis temperature was then decreased in order to slow down the processes and to extract kinetics parameters from the sensorgrams. For the monovalent analyte at 5°C, the association and dissociation phases still exhibited too pronounced slopes to enable determination of kinetic constants (Figure 5.9D). However, slower association and dissociation phases are observed in the curves recorded for the multivalent ligands (Figure 5.9E, F). In consequence, at 5°C, kinetics parameters were only extracted for the interaction of the multivalent analytes with the LD ConA surface and will be discussed thereafter.

For the three molecules, the steady state is reached at the end of the injection of each concentration at both temperatures allowing a steady state analysis of the curves. The

responses obtained at equilibrium (Req) have been considered first for a Scatchard analysis. (See Figure 5.10 and paragraph 5.2.1).

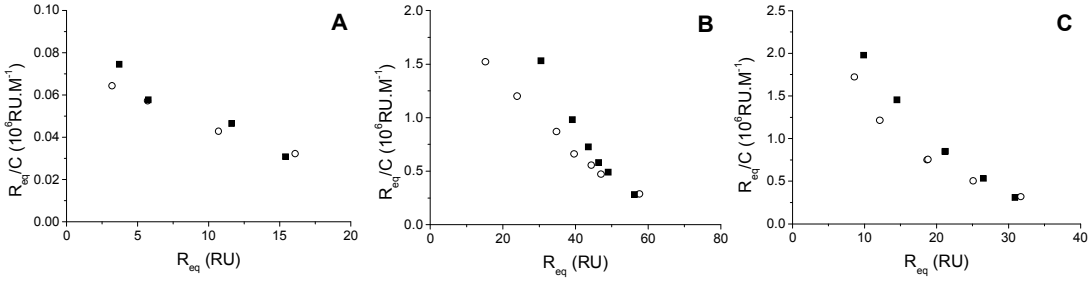

Figure 5.10. Scatchard plots for the interaction of ConA lectin immobilized at low surface density with (A) RAFT-$(Man)_1$, (B) RAFT-$(Man)_4$ and (C) MAP-$(Man)_4$. Analysis temperature is (■) 5°C and (○) 25°C.

For both mono- and multivalent molecules, Scatchard plots (Req/C as a function of Req, with C the glycocluster concentration in solution) obtained for both temperatures (Figure 5.10) are almost linear supporting a monovalent 1:1 interaction. A slight curvature is present on the plot corresponding to the multivalent ligand. Plausible interpretation could be that the proximity/statistic effect induced a more complex recognition that a 1:1 recognition or that, the lectin could be presented heterogeneously on the surface with shorted inter-lectin at some places. However, considering the lightness of the curvature and the small amount of immobilized protein, we considered that at this density, the mean distance between immobilized lectin was large enough to avoid the potential clustering effect of multivalent glycoclusters. Adsorption isotherms were fitted with a Langmuir model (Figure 5.11A) and data obtained are listed in Table 5.1.

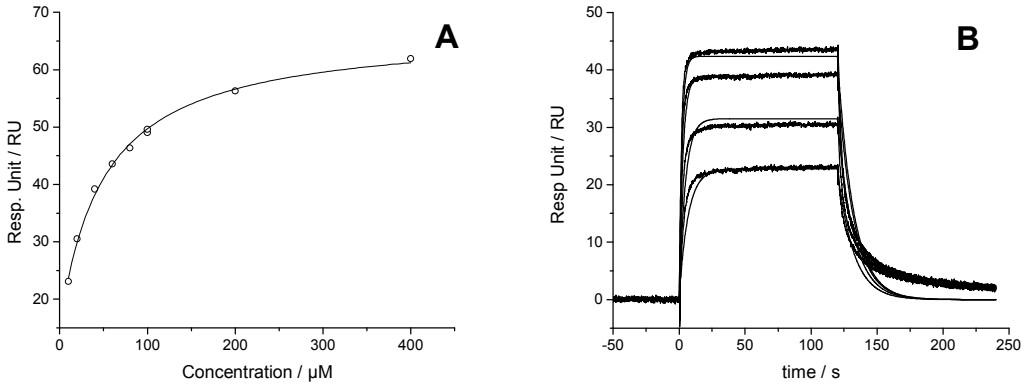

Figure 5.11. Steady state A) and kinetic analysis B) of the sensorgrams recorded at 5°C during the interaction of RAFT-$(Man)_4$ with ConA immobilized at low surface density (see Figure 5.9E).(A) fit (thin line) of the equilibrium responses of sensorgrams as a function of the concentration of the injected concentration with a 1:1 interaction model (B) Association and dissociation step of RAFT-$(Man)_4$ with ConA immobilized at low surface density at 5 °C (thick line) and its modelling (thin line) with a 1:1 model obtained with BIAcore® T100 evaluation software. For a better clarity of the figure, only few curves extracted from the experiment are shown.

Table 5.1. Dissociation constants (K_D) of the interaction between LMW carbohydrate ligands and ConA immobilized at a low surface density. Values are obtained by fitting the equilibrium responses of sensorgrams presented on Figure 5.9 versus the concentration of the injected analyte concentration with a Langmuir isotherm. The standard errors are presented in brackets.

Analyte	T (°C)	K_D (µM)	Rmax	χ^2
RAFT-$(Man)_1$	5	325.7 (60)	24.4 (2.4)	0.292
	25	nd	nd	nd
RAFT-$(Man)_4$	5	18.3 (2.0)	58.6 (1.6)	2.86
	25	36.7 (3.3)	65.05 (1.9)	1.80
MAP-$(Man)_4$	5	14.4 (0.14)	34.4 (1.1)	0.677
	25	23.1 (0.4)	37.8 (2.4)	1.79

nd: not determined

The low values of χ^2 obtained between the experimental data and the fitted value confirm the adequacy of the model. The high values of dissociation constant (K_D) obtained for RAFT-$(Man)_1$ (Table 5.1) confirm the weak affinity of the monovalent carbohydrate/lectin interaction and are in agreement with values reported in literature for monovalent sugar-lectin interaction.[13] Multivalent molecules RAFT-$(Man)_4$ and MAP-

$(Man)_4$ showed respectively a 8- and a 16-fold higher affinity for ConA as compared to RAFT-$(Man)_1$. Considering a constant concentration in sugar residues, the affinity is respectively increased by at least a factor 2. This enhanced affinity could thus be ascribed to a higher sugar local concentration (statistical/proximity effect, Figure 5.3B) offered by the multiple carbohydrate presentation in the multivalent ligands. The presence of close carbohydrate on the rigid cyclodecapeptide template favours its rebinding to the free binding site of the ConA from which it has been released.

In parallel, calculation of the kinetic rates by fitting the sensorgrams obtained for RAFT-$(Man)_4$ and MAP-$(Man)_4$ at 5°C to a 1:1 Langmuir binding profile produced association and dissociation binding rates constants (Figure 5.11B and Table 5.2).

Table 5.2. Kinetic parameters obtained for the fitting with a 1:1 interaction model of the association/dissociation curves obtained during the interaction of the analyte with ConA at 5°C. The standard deviations are indicated in bracket.

Analyte	k_{on} ($M^{-1}s^{-1}$)	k_{off} (s^{-1})	$K_{D,\ kin}$ (μM)	Rmax	χ^2
RAFT-$(Man)_4$	6595 (46)	0.0824 (0.0004)	12.5	51.2 (0.1)	4.19
MAP-$(Man)_4$	9209 (49)	0.1101 (0.0005)	12.0	32.0 (0.05)	0.898

For RAFT-$(Man)_4$ association and dissociation binding rates are respectively k_{on} 6595 $M^{-1}.s^{-1}$ and k_{off} 0.0824 s^{-1}, leading to a dissociation equilibrium constant $K_{D,kin}$ 12.5 μM. This value is close to the one obtained through the steady state analysis (18.3 μM). Similar results are obtained for MAP-$(Man)_4$ which confirms the adequacy of the 1:1 model used to model the data for the two multivalent ligands.

5.3.2. Study of the Interaction with ConA Immobilized at High Surface Density

To evaluate clustering effect of the multivalent ligands, the sugar/lectin recognition was studied with ConA immobilized at high surface density (9670 RU). At this average surface density, the proximity of lectin dimers should yield to clustering effect of the

multiple sugar ligand to the surface, meaning that the multiple analytes should have the ability to bridge between two adjacent proteins (Figure 5.3).[25,41] Sensorgrams recorded on this surface are represented in Figure 5.12. As previously observed sensorgrams recorded at 25°C for the three glycoclusters and especially for the monovalent one are not adequate for a kinetic analysis. Lowering the temperature to 5°C appeared again as an efficient way to slow down the recognition processes.

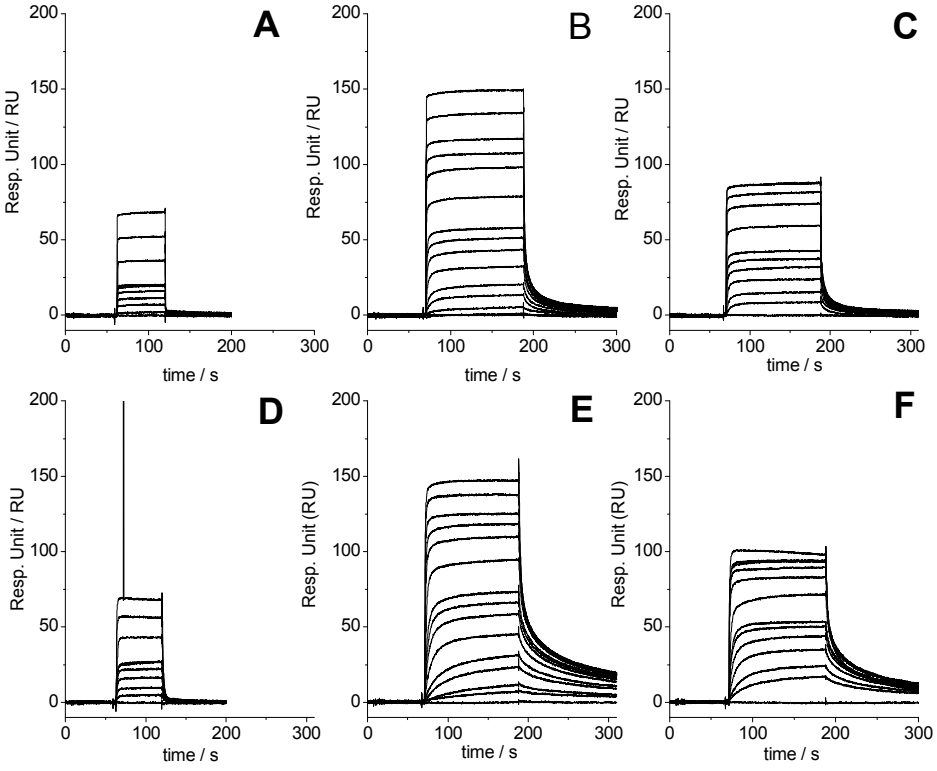

Figure 5.12. Sensorgrams recorded A) B) C) at 25°C, and D) E) and F) at 5°C during the interaction of A), D) RAFT-$(Man)_1$, B) E) RAFT-$(Man)_4$, C) F) MAP-$(Man)_4$with ConA immobilized at high surface density (9760 RU). The reference flow cell is obtained by immobilization of PNA lectin at similar surface density. The flow rate is 40 µL/min. The concentration ranges are: 10 µM–1000 µM for RAFT-$(Man)_1$, 50 nM–400 µM for RAFT-$(Man)_4$ and 500nM-200µM for MAP-$(Man)_4$.

The data were analysed using a similar procedure than the one applied to the sensorgrams obtained with the LD surface.

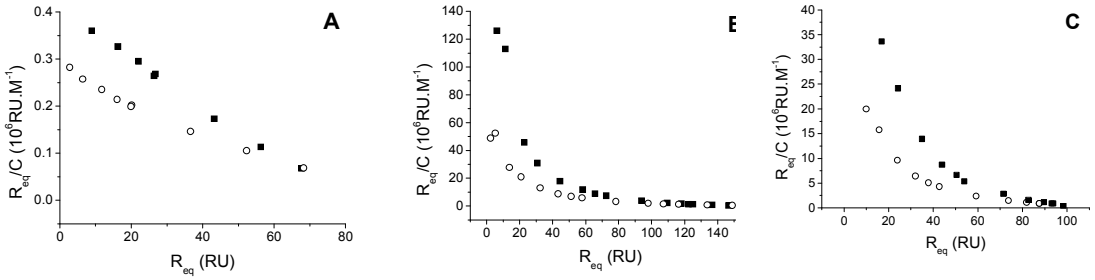

Figure 5.13. Scatchard plots for the interaction of ConA lectin immobilized at high surface density with A) RAFT-$(Man)_1$, B) RAFT-$(Man)_4$.and C) MAP-$(Man)_4$. Analysis temperature is (■) 5°C and (○) 25°C.

Scatchard plots of the interaction of RAFT-$(Man)_1$ with ConA still led to linear plots, characterizing a monovalent interaction (Figure 5.13A). As expected in the case of a 1:1 interaction between a monovalent carbohydrate ligand in solution and immobilized lectin, the density of the immobilized lectin has not influence. Langmuir analysis of adsorption isotherms gave K_D values of 368 µM at 25°C and 203.9 µM at 5°C for RAFT-$(Man)_1$. These results are in good agreement with those obtained on the lower ConA surface density (See Table 5.1). At 5°C a kinetic analysis was also possible (Table 5.3 and Figure 5.14). From the association and dissociation rate constants, respectively 2092 $M^{-1}.s^{-1}$ and 0.389 s^{-1}, the dissociation equilibrium constant RAFT-$(Man)_1$ was deduced to be 185.8 µM (see Table 5.3). The closeness of K_D value obtained by both kinetic and the steady state approaches attests for a 1:1 interaction model between ConA and RAFT-$(Man)_1$.

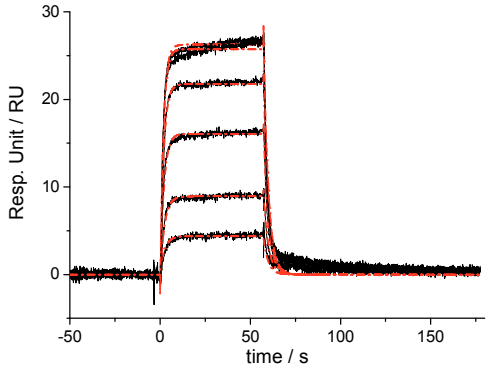

Figure 5.14. Association and dissociation step of RAFT-$(Man)_1$ with ConA immobilized with a high surface density at 5 °C (black solid line) and its modelling (red dash line) with a 1:1 model obtained with BIAcore® T100 evaluation software. For a better clarity of the figure, only few curves extracted from the experiment are shown.

Looking at the Scatchard plots obtained for the interaction of ConA with the tetravalent glycoclusters, dramatic changes occurred (Figure 5.13B, C). The non-linearity of the Scatchard plots demonstrates that a simple 1:1 model could not reflect the interaction anymore. A simple Langmuir model could not be applied for the steady state analysis. This analysis was thus not considered here and equilibrium association constant were extracted from a kinetic analysis of the sensorgrams. To this end, we hypothesis that at a high ConA coverage, immobilized lectin dimers are closed enough to allow multivalent RAFT ligands to interact with at least two distinct immobilized ConA dimers according to a clustering effect (Figure 5.3A). While the structural valency of RAFT-$(Man)_4$ and MAP-$(Man)_4$ is four, we considered in a first approximation their functional valency as two [55]. The tetravalent RAFT-$(Man)_4$ is assumed to interact with only two immobilized ConA, which corresponds to a bivalent analyte kinetic model

For both multivalent molecules, kinetics data could be extracted from the sensorgrams recorded at 5°C. Curves were fitted with a bivalent analyte model (χ^2=2.02 RU^2). It can be noticed (see Figure 5.15A) that as expected a 1:1 model leads to poor fit (χ^2=15.4 RU^2) as compared to the one obtained by using the bivalent analyte model (see Figure 5.15B). This observation supports our hypothesis on the clustering effect of RAFT-$(Man)_4$ and MAP-$(Man)_4$ with lectin immobilized on surface at a high density. Data are reported on Table 5.3.

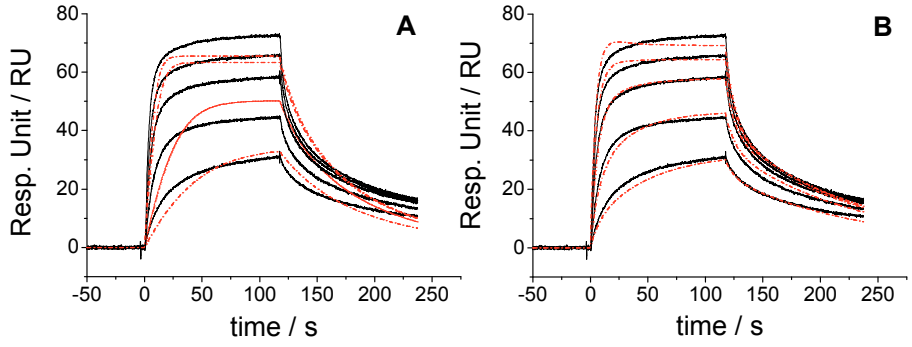

Figure 5.15. Kinetic analysis of the interaction of RAFT-$(Man)_4$ with ConA lectin immobilized at high surface density with A) a 1:1 interaction model and B) a bivalent analyte model. The black and red curves correspond respectively to experimental and fitted sensorgrams. The fit quality could be evaluated using the χ^2 value, which measures the average square residuals *i.e.*, the differences between the fitted curve and the experimental data. χ^2 value is 15.4 RU^2 for the 1:1 interaction model and 2.02 RU^2 for the bivalent model. For a better clarity of the figure, only few curves extracted from the experiment are shown.

Table 5.3. Kinetic parameters obtained for the fitting with a bivalent analyte model of the association/dissociation curves obtained at 5°C during the interaction of the glycoclusters with ConA immobilized at a high surface density.

Bivalent analyte model	k_{on1} ($M^{-1}s^{-1}$)	k_{off1} (s^{-1})	k_{on1}/k_{off1} (μM)	k_{on2} ($RU^{-1}s^{-1}$)	k_{off2} (s^{-1})	χ^2
RAFT-$(Man)_4$	6726	0.1123	16.7	0.00038	132.5	1.99
MAP-$(Man)_4$	7404	0.09322	12.6	0.00067	117.8	1.5
1:1 interaction model	k_{on} ($M^{-1}s^{-1}$)	k_{off} (s^{-1})	$K_{D,\,kin}$ (μM)	Rmax	χ^2	
RAFT-$(Man)_1$	2092 (42)	0.389 (0.002)	185.8	83.9 (1.3)	0.466	

Both multivalent molecules exhibit similar association and dissociation rate constants indicating that structures of both scaffolds are not different enough to influence in a significant way the interaction with the immobilized lectin. The comparison between the kinetics constants k_{on} obtained for mono and multivalent ligands during a 1:1 interaction is particularly interesting (Table 5.2 and Table 5.3). The association rate constants k_{on} for RAFT-$(Man)_4$ and MAP-$(Man)_4$ are about 3 to 4 time higher than those observed for k_{on} of RAFT-$(Man)_1$. This increase could undoubtedly be ascribed to the carbohydrate local concentration (relative to proximity/statistical effect) that is increased by 4 in the case of the tetravalent ligands. On the contrary, we observed a decrease in the dissociation rate

k_{off} in the same order. This decrease could also be explained by the proximity/statistical effect favouring a local rebinding of the LMW glycoclusters: as one carbohydrate dissociate from the protein, another one is already close enough to take its place. The increase of k_{on} and the decrease of k_{off} act complementary for a lower equilibrium dissociation constant for RAFT-$(Man)_4$ and MAP-$(Man)_4$ as compared to RAFT-$(Man)_1$. The coherence of our kinetic analysis is also well exemplified by comparing the kinetic rate constants obtained for RAFT-$(Man)_4$ and MAP-$(Man)_4$ with immobilized lectin at low and high surface densities. Indeed, k_{on1} and k_{off1} at high surface density (Table 5.3) are similar to k_{on} and k_{off} obtained at low ConA density (Table 5.2) meaning that, as expected, a similar proximity/statistical effect relative to one ConA binding site should operate whatever is the surface density.

5.3.3. Conclusion

In the present section, we present an original SPR study to identify and quantify the interaction processes between LMW multivalent ligands and a multimeric lectin. Compared to the surface immobilization of the carbohydrate, the choice of the lectin immobilization provides a simplification of the various processes that could be observed during the recognition events. By a simple adjustment of the surface density of the lectin, we demonstrate that both statistical/proximity effect and clustering effect induced by the multiple carbohydrate presentation could be evidenced and quantified. We have demonstrated that on LD surface the interaction of mono and multivalent molecules are conformed to a 1:1 interaction. These results have confirmed that the unique individual process observed on LD surface was the statistical rebinding as depicted in Figure 5.3B. The inter-lectin distance on the sensorchip was too high to allow multiple binding of one multivalent glycocluster towards several adjacent proteins. On HD surface, the interaction deviate from the 1:1 interaction which was correlated to the simultaneous participation of statistical as well as clustering effect

The method described above could be broadly applied to a wide variety of biologically relevant LMW ligands beyond the carbohydrate-lectin interaction studies shown here.

5.4. Thermodynamic Study of the Proximity/Statistical Effect by SPR

5.4.1. Introduction

In line with our previous results, we decide to enlarge this study to the determination of the thermodynamic parameters *i.e.* the Gibbs energy $\Delta G°$, the enthalpy $\Delta H°$ and the entropy $\Delta S°$ associated with the recognition of our glycoclusters toward immobilized ConA. In the previous part, we have shown that the proximity/statistical effects induced by LMW glycoclusters in the carbohydrate-lectin recognition could be isolated from the other effects, which has allowed its quantification. A new set of experiments was performed with the lectin immobilized at a similar density (2996 RU) as the one used in the previous part (3193 RU). PNA was also immobilized on the reference flowcell at a similar density. As low molecular weight glycoclusters for the present study, RAFT-$(Man)_4$ was evaluated and RAFT-$(Man)_1$ was taken as reference since it present the same cyclodecapeptide template bearing only one mannose moiety. The sensorgrams were recorded for the two molecules at temperatures ranging from 5°C to 45°C in order to extract thermodynamic parameters from the data. The affinity constants obtained will be first discussed, followed in a second part by the thermodynamic results obtained through a Van't Hoff analysis.

5.4.2. Thermodynamic Parameters Determination: SPR vs. ITC

A wide range of assays have been used to evaluate the binding parameters of lectin-carbohydrate interactions. Among them, the most popular are Inhibition of Hemagglutination (HIA), Enzyme-linked lectin assay (ELLA), Isothermal Titration Microcalorimetry (ITC) and SPR. While the two former assays allow measurement of inhibition concentrations (IC50), the two latter give direct accesses to affinity constants. ITC operates by evaluating the heat involved in during the binding of the ligand as a function of the titrant concentration. The binding enthalpy is thus directly measured and ITC is the unique technique allowing this direct analysis. However the amount of both protein and ligand required for the measurement is a serious limitation to this technique.

As seen in the previous section, SPR measurement allows the determination of the kinetic binding rates (association and dissociation) of recognition as well as the binding affinity. By collecting equilibrium constants at different temperatures, the enthalpy can be deduced by applying the van't Hoff relationship. While the measurement remains indirect, the low quantity of ligand and analyte required for SPR studies, as compared to ITC, have motivated comparable studies to validate this method.[56-58]

Moreover, in the context of our study, *i.e.* recognition involving multivalent ligands, subsequent limitation of ITC appears. The enthalpy recorded by ITC is the sum of all the processes occurring during the recognition. In consequence, data analysis becomes complex when dealing with multivalent ligands. As example, separation of the clustering effects from proximity/statistical effects of LMW ligand is difficult. Clustering effect could even lead to aggregation/precipitation which interfered with the measurement. Indeed, some ITC studies were tried with our glycoclusters and unfortunately, the experiments lead to aggregation of the compounds thought cross-linked complexes formation.

In the precedent section, we have presented a SPR methodology to enable the detection of our LMW as well as the characterisation of their interactions towards immobilized ConA. We succeed in evaluating the proximity/statistical effect occurring in the recognition between LMW glycoclusters and immobilized ConA. Motivated by our unsuccessful trial of ITC measurements, we have decided to extend our SPR approach to the determination of thermodynamic parameters and to particularly focus on the proximity/statistical effect.

5.4.3. Determination of the Equilibrium Dissociation Constants at Different temperatures

The interaction of monovalent RAFT-$(Man)_1$ as well as multivalent RAFT-$(Man)_4$ with ConA immobilized at low surface density was studied by SPR at different temperatures ranging from 5°C to 45°C leading to the sensorgrams represented on Figure 5.16.

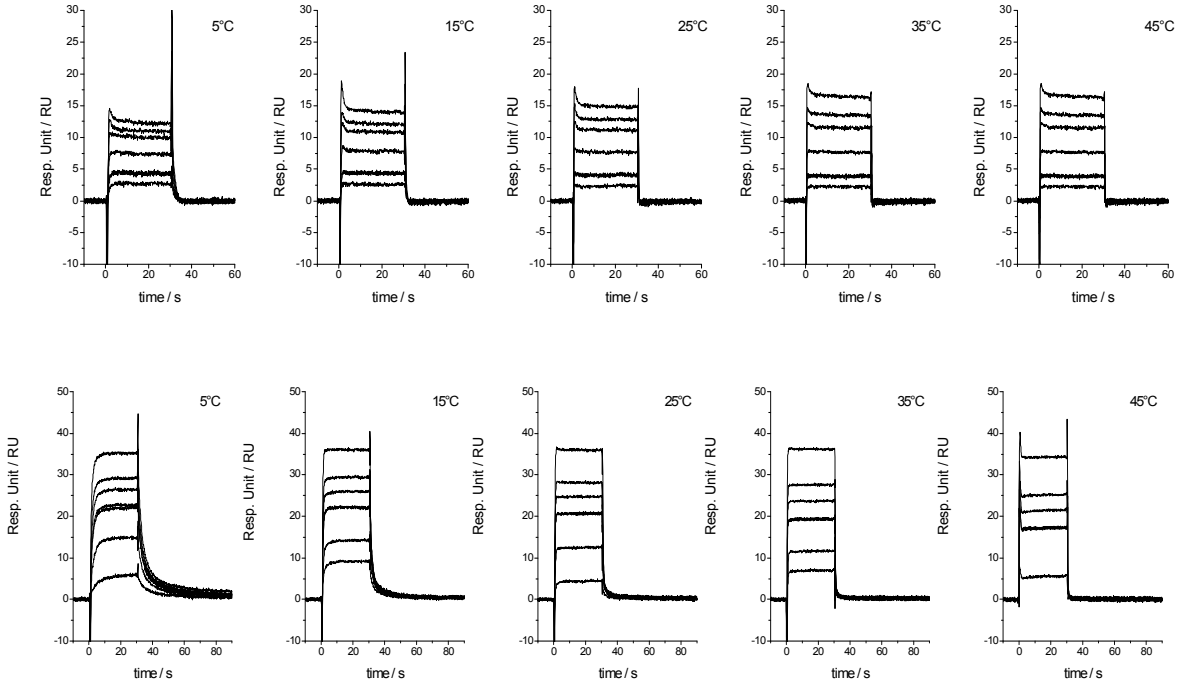

Figure 5.16. Sensorgrams recorded at 5°C, 15°C, 25°C, 35°C and 45°C for RAFT-$(Man)_1$ with concentration ranging from 50µM to 1142 µM (top panel) and RAFT-$(Man)_4$ with concentration ranging from 5 µM to 200µM (lower panel) with ConA immobilized at low surface coverage

The response recorded at the steady state for RAFT-$(Man)_4$ injected at 200µM was ~ 60 RU in the previous experiments whereas in the present one, it was ~ 35 RU. This value indicates that on the present surface, a lower amount of lectin is active as compared to the one used in the previous section. This result could be easily related to the use of a different batch of ConA, in the present case less active, or to the influence of the chemical immobilization step. As previously observed, the sensorgrams reached a stable signal at the end of the injection for all concentrations of analyte. A steady state analysis has been realized for the five temperatures. The raw SPR data were first analysed using Scatchard plots (Figure 5.17).

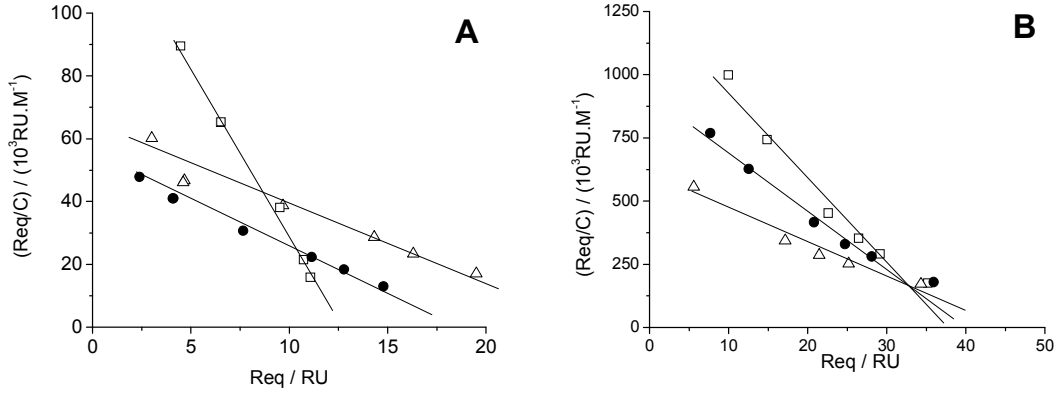

Figure 5.17. Scatchard analysis of the interaction of A) RAFT-$(Man)_1$ and B) RAFT-$(Man)_4$ with ConA immobilized ConA at low surface density (2996 RU) recorded at different temperatures: (□) 5°C, (●) 25°C and (Δ) 45°C. The data correspond to the sensorgrams presented in Figure 5.16.

As described in details in the previous section, on LD surface, the Scatchard plots are almost linear, supporting for RAFT-$(Man)_1$ and RAFT-$(Man)_4$ ligands a 1:1 interaction toward the immobilized lectin, in agreement with previous results. This result confirms our hypothesis that at low surface density, the inter-lectin distance should be large enough to prevent any clustering effect of the analyte. In other words, the surface is so diluted that our multiple analytes are not able to span several neighbouring lectins. The raw SPR data were fitted with a Langmuir isotherm (1:1 interaction model) and the collected values are summarized in Table 5.4. It should be noted that for RAFT-$(Man)_1$, the dissociation equilibrium constant is similar with those obtained in the previous section. This value was expected since RAFT-$(Man)_1$ could only be engaged in 1:1 interaction toward ConA (Figure 5.1A). RAFT-$(Man)_4$ exhibits a lower affinity than previously. It could be supposed that for the LD surface used in the previous set of experiments, the surface was not diluted enough and that clustering effect may have contributed to some extent in the recognition.

Table 5.4. Dissociation constants of RAFT-$(Man)_1$ and RAFT-$(Man)_4$ toward ConA immobilized at low surface coverage. The values are obtained by fitting the response recorded at the steady state in function of the concentration by a Langmuir isotherm. Standard Errors are presented in bracket.

	RAFT-$(Man)_1$			RAFT-$(Man)_4$		
T (°C)	K_D (μM)	Rmax	χ^2	K_D (μM)	Rmax	χ^2
5	244.7 (9.3)	14.78 (0.2)	0.0178	37.87 (4.5)	40.6 (1.7)	1.16
15	308.8 (10)	17.60 (0.23)	0.0155	43.30 (5.4)	42.5 (1.9)	1.17
25	386.7 (8.5)	19.80 (0.18)	0.00672	63.12 (5.8)	45.2 (1.7)	0.551
35	521.9 (1.9)	23.69 (0.39)	0.0176	70.36 (8.7)	47.8 (2.5)	1.00
45	682.2 (21)	25.14 (0.39)	0.00981	98.83 (1.0)	50.7 (2.4)	0.442

Looking on the equilibrium dissociation constants, it appears that a 6-fold enhancement in the binding affinity was obtained for RAFT-$(Man)_4$ as compared to the monovalent analyte. This value reported per sugar unit corresponds to about a 1.5-fold increase in affinity. While only a 1:1 interaction is engaged for the RAFT-$(Man)_4$ glycocluster, this increase in affinity could only be ascribed to proximity/statistical effect induced by the local increase in mannose residues offered by the template presentation.

For both mono and multivalent molecules, an increase in dissociation constants was observed upon increase in temperature, indicating negative enthalpy change. This fact suggested that the binding is exothermic in nature and driven by enthalpy.

5.4.4. Van't Hoff Analysis

The thermodynamic parameters, free energy ($\Delta G°$), enthalpy ($\Delta H°$) and entropy ($\Delta S°$) of binding, were then deduced from K_D at different temperatures, applying the van't Hoff equation (see paragraph 5.2.1 and Figure 5.18)

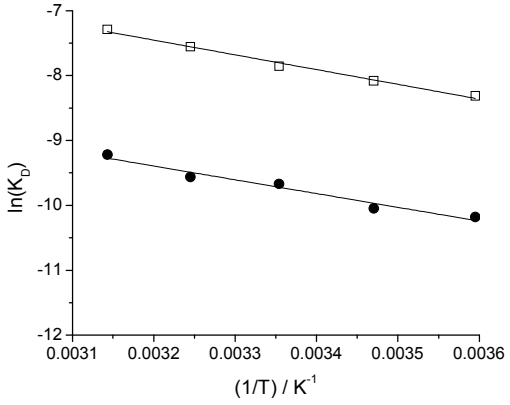

Figure 5.18. van't Hoff diagram for the interaction of (□) RAFT-$(Man)_1$ and (●)RAFT-$(Man)_4$ with ConA immobilized at low surface density.

The van't Hoff plots were linear for RAFT-$(Man)_1$ and RAFT-$(Man)_4$ in the temperature range studied, the parameters obtained are listed in Table 5.5.

Table 5.5. Thermodynamic parameters extracted from the Van't Hoff analysis of the SPR data

	ΔH° [kJ/mol]	ΔS° [J/(K.mol)]	χ^2	TΔS° [kJ/mol]	ΔG° [kJ/mol]
RAFT-$(Man)_1$	-18.89	1.5	0.019	0.45	-19.34
RAFT-$(Man)_4$	-17.64	21.6	0.006	6.44	-24.08

On the LD surface, the value of binding enthalpy ($\Delta H°$) obtained for the monovalent ligand is in well agreement with value obtained from ITC (around -20 kJ.mol-1)[59] for the binding of mannose toward ConA. However, ΔS° values are positive which is not in agreement with values measured by ITC. Usually, protein-carbohydrate interactions display negative entropic contributions.[55] However, the value here corresponds to the interaction of mannose linked to a scaffold. It could not be excluded that this scaffold participates to the interaction and induced positive entropic contribution. In fact, positive entropic contributions have been obtained by ITC for the interaction of ConA with amphiphilic monovalent and multivalent mannose ligands where the authors invoked hydrophobic contribution. [39]

The enthalpy for the multivalent LMW ligand is similar to the enthalpic contribution obtained for the monovalent one. This similar values are indicative of an equal interaction mode which in our conditions (low surface lectin density) is attributed to a

1:1 interaction.[60,61] Positive entropic contribution is increased in the recognition of RAFT-$(Man)_4$ as compared to RAFT-$(Man)_1$. By ITC, similar positive entropic contribution for the interaction of high density multivalent glycoclusters [40] has been reported and associated with a "bind and jump " process which could operate between multivalent lectins and large glycoclusters. Indeed, the "bind and jump" model reported by Brewer *et al.* allows a small fraction of bound lectin protein to dynamically moves from carbohydrate to carbohydrate epitope in multivalent glycoclusters, globular and linear glycoproteins.[18,62,63] This internal diffusion is reported to be entropically favourable. This phenomenon was also suggested for the enhanced affinity observed by SPR for the interaction of glycodendrimers to ConA immobilized at low surface density.[41] Considering the small size of RAFT-$(Man)_4$ compared to the inter-lectin binding site distance, this process is likely to be unfavourable in our case. However, by analogy, considering the proximity/statistical effect as an internal diffusion process, this process could be responsible of this favourable entropic contribution.

Finally, the difference in the affinity induced by proximity/statistical effects of the tetravalent molecules seems to be only due to entropic contribution. The present result is quite promising since it is highly difficult to experimentally isolate and study the statistical rebinding effect independently from the others phenomena induced by multivalent ligand. Cloninger et *al.* have attempted to assess the proximity/statistical effect by ITC by studying the interaction of glycodendrimers to monomeric and dimeric lectin. [24] However, while this elegant approach allowed removal of the chelate effect from the interaction, the clustering effect still remains present and has not been considered. This effect is indeed inevitably involved in solution measurements.

5.4.5. Conclusions

In the present section, we have investigated the binding thermodynamic parameters of the interaction of LMW with ConA by the mean of SPR. The equilibrium dissociation constants (K_D) values for the interaction between lectin immobilized with a low surface density and RAFT-$(Man)_4$ and RAFT-$(Man)_1$ molecules was determined from steady state analysis. Experiments realized at various temperatures followed by a van't Hoff analysis have enabled the calculation of free energy, enthalpy as well as entropy. At low surface density of immobilized lectin, a 1:1 interaction characterized by a similar enthalpic contribution is observed for both the monovalent and multivalent RAFT carbohydrate ligands. These results suggested that the statistical rebinding (the unique effect occurring under these conditions) leads to higher binding affinity only as a consequence of favourable entropic contribution. The method presented here should be applied to several series of multivalent ligands in order to be fully validated.

5.5. Overall Conclusion and Perspectives

This chapter focuses on an efficient SPR methodology to assess the specific interaction engaged during the recognition of low molecular weight glycoclusters with multimeric lectin. While this type of ligand is too small to bridge two binding sites of a unique receptor, they are known to provide an enhanced affinity to the interaction. This particularity could be induced by several individual phenomena, namely the proximity/statistical effect and/or the clustering effect. While both effects are hardly separable in solution, we proposed to take advantage of SPR surface-based experiments to investigate them separately. We found that the proximity/statistical effect could be discerned from the clustering effect by spacing out the receptors on the surface such a as the clustering effect became negligible. We also demonstrated that the close proximity of the epitopes grafted on the RAFT scaffold induced higher association rate constants and lower dissociation rate constants. The residence time of the glycoclusters is hence increased and a higher affinity is observed. The approach was then extended to the evaluation of thermodynamic parameters. Preliminary results strongly suggested that positive entopic contributions are induced by such effect. To generalize the present

study, further investigations are required on library of LMW ligands presenting different valencies. However, these results are quite promising since they are currently difficult to achieve in solution-based assays.

Experiments and analysis presented in this chapter could provide useful indication of the contribution of individual processes occurring in the whole LMW carbohydrate-lectin recognition event. Information on the impact of the parameters that can influence the ligand biological activity, *i.e.* its scaffold structure and flexibility, its epitope density or its valency are undoubtedly of high interest to orientate the synthesis of new multivalent ligands.

5.6. References

(1) Dwek, R. A. *Chem. Rev.* **1996**, *96*, 683-720.
(2) Varki, A. *Glycobiology* **1993**, *3*, 97-130.
(3) Bertozzi, C. R.; Kiessling, L. L. *Science* **2001**, *291*, 2357-2364.
(4) Lis, H.; Sharon, N. *Chem. Rev.* **1998**, *98*, 637-674.
(5) Sacchettini, J. C.; Baum, L. G.; Brewer, C. F. *Biochemistry* **2001**, *40*, 3009-3015.
(6) Quesenberry, M. S.; Lee, R. T.; Lee, Y. C. *Biochemistry* **1997**, *36*, 2724-2732.
(7) Lee, Y. C.; Lee, R. T. *Acc. Chem. Res.* **1995**, *28*, 321-7.
(8) Kiessling, L. L.; Gestwicki, J. E.; Strong, L. E. *Angew. Chem., Int. Ed.* **2006**, *45*, 2348-2368.
(9) Mammen, M.; Chio, S.-K.; Whitesides, G. M. *Angew. Chem., Int. Ed.* **1998**, *37*, 2755-2794.
(10) Renaudet, O. *Mini-Rev. Org. Chem.* **2008**, *5*, 274.
(11) Burke, S. D.; Zhao, Q.; Schuster, M. C.; Kiessling, L. L. *J. Am. Chem. Soc.* **2000**, *122*, 4518-4519.
(12) Roy, R. *Curr. Opin. Struct. Biol.* **1996**, *6*, 692-702.
(13) For a recent review; Niederhafner, P.; Sebestik, J.; Jezek, J. *J. Pept. Sci.* **2008**, *14*, 2.
(14) Woller, E. K.; Cloninger, M. J. *Org. Lett* **2002**, *4*, 7-10.
(15) For a recent review; Baldini, L.; Casnati, A.; Sansone, F.; Ungaro, R. *Chem. Soc. Rev.* **2007**, *36*, 254.
(16) Kanai, M.; Mortell, K. H.; Kiessling, L. L. *J. Am. Chem. Soc.* **1997**, *119*, 9931-9932.
(17) Gestwicki, J. E.; Cairo, C. W.; Mann, D. A.; Owen, R. M.; Kiessling, L. L. *Anal. Biochem.* **2002**, *305*, 149-155.
(18) Dam, T. K.; Brewer, C. F. *Biochemistry* **2008**, *47*, 8470.
(19) Yu, L.; Huang, M.; Wang, P. G.; Zeng, X. *Anal. Chem.* **2007**, *79*, 8979.
(20) Cairo, C. W.; Gestwicki, J. E.; Kanai, M.; Kiessling, L. L. *J. Am. Chem. Soc* **2002**, *124*, 1615-1619.

(21) Kanai, M.; Mortell, K. H.; Kiessling, L. L. *J. Am. Chem. Soc* **1997**, *119*, 9931-9932.
(22) Gestwicki, J. E.; Cairo, C. W.; Strong, L. E.; Oetjen, K. A.; Kiessling, L. L. *J. Am. Chem. Soc* **2002**, *124*, 14922-14933.
(23) Lundquist, J. J.; Toone, E. J. *Chem. Rev.* **2002**, *102*, 555-578.
(24) Mangold, S. L.; Cloninger, M. J. *Org. Biomol. Chem.* **2006**, *4*, 2458-2465.
(25) Wilczewski, M.; Van der Heyden, A.; Renaudet, O.; Dumy, P.; Coche-Guerente, L.; Labbe, P. *Org. Biomol. Chem.* **2008**, *6*, 1114.
(26) For a review see Duverger, E.; Frison, N.; Roche, A.-C.; Monsigny, M. *Biochimie* **2003**, *85*, 167-179.
(27) Pieters, R. J. *Org. Biomol. Chem.* **2009**, *7*, 2013-2025.
(28) Woller, E. K.; Walter, E. D.; Morgan, J. R.; Singel, D. J.; Cloninger, M. J. *J. Am. Chem. Soc* **2003**, *125*, 8820-8826.
(29) Kitov, P. I.; Sadowska, J. M.; Mulvey, G.; Armstrong, G. D.; Ling, H.; Pannu, N. S.; Read, R. J.; Bundle, D. R. *Nature* **2000**, *403*, 669-672.
(30) Dam, T. K.; Oscarson, S.; Roy, R.; Das, S. K.; Pagé, D.; Macaluso, F.; Brewer, C. F. *J. Biol. Chem.* **2005**, *280*, 8640.
(31) Ambrosi, M.; Cameron, N. R.; Davis, B. G.; Stolnik, S. *Org. Biomol. Chem.* **2005**, *3*, 1476-1480.
(32) Wolfenden, M. L.; Cloninger, M. J. *Bioconjugate Chem* **2006**, *17*, 958-966.
(33) Mann, D. A.; Kanai, M.; Maly, D. J.; Kiessling, L. L. *J. Am. Chem. Soc* **1998**, *120*, 10575-10582.
(34) Smith, E. A.; Thomas, W. D.; Kiessling, L. L.; Corn, R. M. *J. Am. Chem. Soc* **2003**, *125*, 6140-6148.
(35) Munoz, F. J.; Perez, J.; Rumbero, A.; Santos, J. I.; Can ada, F. J.; Andre, S.; Gabius, H. J.; Jime nez-Barbero, J.; Sinisterra, J. V.; Herna iz, M. J. *Bioconjugate Chem.* **2009**, *20*, 673-682.
(36) Suda, Y.; Arano, A.; Fukui, Y.; Koshida, S.; Wakao, M.; Nishimura, T.; Kusumoto, S.; Sobel, M. *Bioconjugate Chem* **2006**, *17*, 1125-1135.
(37) Shankaran, D. R.; Gobi, K. V.; Miura, N. *Sens. Actuators, B* **2007**, *121*, 158-177.
(38) Stenlund, P.; Frostell-Karlsson, Å.; Karlsson, O. P. *Anal. Biochem.* **2006**, *353*, 217-225.
(39) Murthy, B. N.; Sinha, S.; Surolia, A.; Indi, S. S.; Jayaraman, N. *Glycoconjugate J.* **2008**, *25*, 313-321.
(40) Gómez-García, M.; Benito, J. M.; Gutiérrez-Gallego, R.; Maestre, A.; Mellet, C. O.; Fernández, J. M. G.; Blanco, J. L. J. *Org. Biomol. Chem.* **2011**, *8*, 1849-1860.
(41) Munoz, E. M.; Correa, J.; Fernandez-Megia, E.; Riguera, R. *J. Am. Chem. Soc.* **2009**, *131*, 17765-17767.
(42) Beccati, D.; Halkes, K. M.; Batema, G. D.; Guillena, G.; Carvalho de Souza, A.; van Koten, G.; Kamerling, J. P. *ChemBioChem* **2005**, *6*, 1196-1203.
(43) McKenzie, G. H.; Sawyer, W. H.; Nichol, L. W. *Biochim. Biophys. Acta* **1972**, *263*, 283-293.
(44) Huet, M. *Eur. J. Biochem.* **1975**, *59*, 627-632.
(45) Renaudet, O.; Dumy, P. *Org. Biomol. Chem.* **2006**, *4*, 2628-2636.
(46) Renaudet, O.; BenMohamed, L.; Dasgupta, G.; Bettahi, I.; Dumy, P. *ChemMedChem* **2008**, *3*, 737.
(47) For a recent review; Boturyn, D.; Defrancq, E.; Dolphin, G. T.; Garcia, J.; Labbe, P.; Renaudet, O.; Dumy, P. *J. Pept. Sci.* **2008**, *14*, 224-240.
(48) Renaudet, O.; Dumy, P. *Org. Lett.* **2003**, *5*, 243-246.

(49) Razkin, J.; Josserand, V.; Boturyn, D.; Jin, Z.-h.; Dumy, P.; Favrot, M.; Coll, J.-L.; Texier, I. *ChemMedChem* **2006**, *1*, 1069-1072.
(50) Grigalevicius, S.; Chierici, S.; Renaudet, O.; Lo-Man, R.; Deriaud, E.; Leclerc, C.; Dumy, P. *Bioconjugate Chem.* **2005**, *16*, 1149-1159.
(51) Garanger, E.; Boturyn, D.; Renaudet, O.; Defrancq, E.; Dumy, P. *J. Org. Chem.* **2006**, *71*, 2402-2410.
(52) Singh, Y.; Renaudet, O.; Defrancq, E.; Dumy, P. *Org. Lett.* **2005**, *7*, 1359-1362.
(53) Schwarz, F. P.; Puri, K. D.; Bhat, R. G.; Surolia, A. *J. Biol. Chem.* **1993**, *268*, 7668.
(54) Müller, K. M.; Arndt, K. M.; Plückthun, A. *Anal. Biochem.* **1998**, *261*, 149-158.
(55) Dam, T. K.; Brewer, C. F. *Chem. Rev* **2002**, *102*, 387-430.
(56) Papalia, G. A.; Giannetti, A. M.; Arora, N.; Myszka, D. G. *Anal. Biochem.* **2008**, *383*, 255-264.
(57) Navratilova, I.; Papalia, G. A.; Rich, R. L.; Bedinger, D.; Brophy, S.; Condon, B.; Deng, T.; Emerick, A. W.; Guan, H. W.; Hayden, T. *Anal. Biochem.* **2007**, *364*, 67-77.
(58) Wear, M. A.; Walkinshaw, M. D. *Anal. Biochem.* **2006**, *359*, 285.
(59) Ambrosi, M.; Cameron, N. R.; Davis, B. G. *Org. Biomol. Chem.* **2005**, *3*, 1593-1608.
(60) Dam, T. K.; Roy, R.; Page, D.; Brewer, C. F. *Biochemistry* **2002**, *41*, 1351-1358.
(61) Dam, T. K.; Roy, R.; Page, D.; Brewer, C. F. *Biochemistry* **2002**, *41*, 1359-1363.
(62) Dam, T. K.; Gabius, H. J.; André, S.; Kaltner, H.; Lensch, M.; Brewer, C. F. *Biochemistry* **2005**, *44*, 12564-12571.
(63) Dam, T. K.; Gerken, T. A.; Brewer, C. F. *Biochemistry* **2009**, *48*, 3822-3827.

General Conclusions

Conclusion Générale

General Conclusions and Future Perspectives

The focus of this thesis entitled '**Functional Interfaces for Immobilizing Membrane Proteins: Concept, Characterization and Applications'** was centered on two principal objectives. The first objective was directed towards the design and characterization of functional interfaces which mimic the cell membrane, whereas the second objective was oriented towards studying the applications of these interfaces. Thus in this context, we were successfully able to develop three such interfaces namely Supported Lipid Bilayers (SLBs), Tethered Bilayer Lipid Membranes (tBLMs) and Amphipols.

With the Supported Lipid Bilayer systems, we were able to demonstrate that they can serve as excellent supports for studying the adhesion of HEK-β_3 cells when doped with both the monovalent and the clustered *c*RGD containing lipidic ligand. Further, a relation between the interligand spacing and the morphology of the adhered cells was clearly defined. Complementary techniques like QCM-D and Optical microscopy were found to be extremely useful in understanding the cell adhesion process.
We could also demonstrate the successful insertion of an *E.coli* outer membrane protein (FhuA) in the SLBs. A distinct feature in the fusion profile of the proteoliposomes was observed upon incorporating increasing amounts of FhuA in the SLBs. Moreover, the FhuA immobilized in the SLBs was found to be active and recognized (by irreversible binding) the phage protein pb5.

As a next step to this work, we studied the formation of Tethered Bilayer Lipid Membranes (tBLMs) on mixed SAMs. Towards this end, we synthesized a pair of two different thiols *i.e.* a hydrophobic anchoring thiol TEG-DP and a hydrophilic TEG thiol. The Self-Assembled Monolayers made up of both pure and specific mixtures of the two thiols were characterized using a multitude of techniques like QCM-D, contact angle measurements, AFM, electrochemistry and electrochemical impedance spectroscopy. A preference in adsorption of the hydrophobic TEG-DP thiol over the hydrophilic TEG thiol is

demonstrated. Moreover, a clear phase segregation in the mixed SAMs is also characterized by AFM and electrochemical reductive desorption.

Upon successful characterization of the SAMs, the interaction of Small Unilamellar Vesicles (SUVs) with these SAMs has been studied. Very interesting trends in the fusion behavior of the SUVs, observed upon varying the concentration of the anchoring TEG-DP thiol in the SAM are demonstrated. A threshold/critical concentration of the anchoring TEG-DP thiol in the SAM required to induce the fusion of SUVs is clearly defined. Moreover, the electrical properties of the tBLMs formed on the various SAMs were found to be dependent on the composition of the SAM. An excellent corroboration in the results obtained by different techniques such as EIS and QCM-D are remarkably encouraging. These results now describe that these tBLMs prepared on mixed SAMs can be used as a model for the insertion of transmembrane proteins and their investigations.

The final section dedicated to the study of transmembrane proteins, demonstrates the use of a biotin tagged phosphorylcholine based Amphipol. To this extent we demonstrate the use of such an amphipol called B-PCApol for studying two transmembrane proteins of our interest *i.e.* FhuA (the E.coli outer membrane protein) and $\alpha_v\beta_3$ integrin (an angiogenic factor in human cells). In the case of FhuA, an optimum ratio of FhuA: Apol required for effectively solubilizing a large part of the protein is determined. The FhuA: Apol complexes formed at this optimum ratio was thus immobilized on a SPR chip and the interactions of FhuA with pb5 were studied by single cycle kinetic measurements. This study, the first of its kind with amphipol based systems has been successfully demonstrated here.

Studies concerning the $\alpha_v\beta_3$ integrin, demonstrates the few preliminary results where the trapping of $\alpha_v\beta_3$ integrin by B-PCApol is studied as a function of time of interaction of B-PCApol with the $\alpha_v\beta_3$ integrin in the presence of Biobeads. These experiments, present a limitation in terms of detection of the $\alpha_v\beta_3$ integrin by UV-visible spectroscopy, as the $\alpha_v\beta_3$ integrin is present in dilute solutions of very small concentrations. Nonetheless, the use of an immune assay called dot-blot was found to alleviate this problem of detection of the $\alpha_v\beta_3$ integrin. The $\alpha_v\beta_3$ integrin-Apol complex formed was then immobilized on a SPR chip and the interaction of $\alpha_v\beta_3$ integrin with its natural receptor-protein vitronectin was studied.

These results on a global point of view were quite positive and thus are interesting for further pursuit.

The last section of this thesis, which does not essentially concern membrane proteins, is rather a section devoted to the study of biomolecular recognition events. To this effect we explore the interactions of a lectin (Concanavalin A (ConA)) with multivalent sugars presented on a RAFT scaffold. In this chapter through a direct SPR study we quite successfully distinguish between the proximity/statistical effect and/or the clustering effect. To this effect, two kinds of surfaces presenting high and low densities of immobilized lectin were studied with RAFT-based mannosyl derivatives. We successfully demonstrate, here, that the proximity/statistical effect could be discerned from the clustering effect by spacing out the receptors (ConA) on the surface such as the clustering effect became negligible. It is also described here, that close proximity of the epitopes grafted on the RAFT scaffold induced higher association rate constants and lower dissociation rate constants. The binding time of the glycoclusters is hence increased and a higher affinity is observed. The approach was then extended to the evaluation of thermodynamic parameters. Here, preliminary results probed into the entropic contributions to induce such effects.

Thus, in a general perspective, in this thesis we have been quite successful in our attempts to demonstrate the design characterization and applications of various functional interfaces. These functional interfaces were primarily designed to immobilize membrane proteins and study their interactions with their natural biological partners. Moreover, an extension to this work involving the study of lectin-sugar interactions throws useful insights on multivalent interactions prevalent in biological systems.

Conclusion Générale

L'objectif de cette thèse intitulée «**Interfaces Fonctionnelles pour L'immobilisation des Protéines Membranaires : Concept, Caractérisation et Applications**» se décline en deux axes principaux. Le premier objectif a été orienté vers la conception et la caractérisation d'interfaces fonctionnelles qui miment la membrane cellulaire, tandis que le deuxième objectif était orienté vers l'étude des applications de ces interfaces. Ainsi, dans ce contexte, nous avons été en mesure de développer trois interfaces, à savoir des bicouches lipidiques supportées (SLB), membranes de bicouches lipidiques suspendues (tBLM) et des Amphipols.

Avec le système de bicouches lipidiques supportées, nous avons démontré qu'elles peuvent servir d'excellents supports pour l'étude de l'adhésion des cellules HEK-β3 lorsque la membrane est dopée avec un ligand lipidique cRGD monovalent ou multivalent. De plus, une relation entre la distance inter-ligand et la morphologie des cellules adhérées a été clairement défini. Des techniques complémentaires comme la QCM-D et la microscopie optique ont ainsi été particulièrement utiles dans la compréhension du processus d'adhésion cellulaire.
Nous avons également démontré l'insertion réussie de FhuA, une protéine de la membrane externe d'E. coli, dans les SLB. Une tendance caractéristique dans les profils de fusion des protéoliposomes a été observée lors de l'incorporation de quantités croissantes de FhuA dans la SLBs. De plus, la protéine FhuA immobilisée dans les SLBs s'est avérée être active et capable de reconnaitre (de façon irréversible) son ligand, la protéine de phage pb5.

L'étape suivante de ce travail a été l'étude de la formation de membranes de bicouches lipidiques suspendues (tBLMs) sur des monocouches auto-assemblées (SAM) mixtes. À cette fin, nous avons synthétisé un couple de deux thiols à savoir, un thiol hydrophobe, TEG-DP, servant de point d'ancrage aux tBLMs et un thiol hydrophile, TEG. Les monocouches auto-assemblées composées soit des thiols purs soit de mélanges spécifiques des deux thiols ont été caractérisées par une série de techniques comme la QCM-D, la mesure d'angle de contact, l'AFM, l'électrochimie et la spectroscopie

d'impédance électrochimique. Une préférence de l'adsorption du thiol hydrophobe TEG-DP sur le thiol hydrophile TEG a été démontrée. De plus, une ségrégation de phases dans les SAMs mixtes a été clairement caractérisée par AFM et désorption électrochimique réductrice.

Apres leur caractérisation complète, l'interaction de petites vésicules unilamellaires (SUV) avec ces SAMs a été étudiée. Des tendances très intéressantes dans le processus de fusion des SUV ont été démontrées en fonction de la concentration en thiol d'ancrage TEG-DP dans les SAMs. Un seuil, ou concentration critique, en thiol d'ancrage TEG-DP dans la SAM requis pour induire la fusion de SUV a été clairement défini. De plus, les propriétés électriques des tBLMs formées sur les différentes SAM se sont avérées être dépendantes de la composition de la SAM. L'excellente concordance des résultats obtenus par différentes techniques telles que l'EIS et la QCM-D sont particulièrement encourageant. Ces résultats montrent désormais que ces tBLMs préparées sur des SAMs mixtes peuvent être utilisées comme modèle pour l'insertion et l'étude de protéines transmembranaires.

La deuxième section dédiée à l'étude des protéines transmembranaires, décrit l'utilisation d'un amphipol biotinylé à base de phosphorylcholine. Ainsi, nous avons démontré l'utilisation de cet amphipol, appelé B-PCApol, pour étudier nos deux protéines transmembranaires d'intérêt à savoir FhuA (protéine de la membrane externe d'E. coli) et l'intégrine αvß3 (un facteur de l'angiogénèse des cellules humaines). Dans le cas de FhuA, un ratio optimal FhuA: Apol, requis pour solubiliser efficacement une grande partie de la protéine, a été déterminé. Le complexe FhuA: Apol formé à ce rapport optimal a ensuite été immobilisé sur une puce SPR et les interactions de FhuA avec pb5 ont été étudiées par le biais de "single cycle kinetics". Cette étude, réalisée avec succès, est la première en son genre, *i.e*. en utilisant des systèmes basés sur des amphipols.

Les études concernant l'intégrine αvß3, sont quand à eux encore préliminaires. Le piégeage de l'intégrine αvß3 par B-PCApol a été étudié en fonction du temps d'interaction de B-PCApol avec l'intégrine αvß3, en présence de Biobeads. Toutefois, ces expériences présentent une limitation en termes de détection de l'intégrine αvß3 par spectroscopie UV-visible, l'intégrine αvß3 n'étant accessible que dans des solutions diluées de très faibles concentrations. Néanmoins, l'utilisation d'un test immunitaire, appelé dot-blot, a permis de pallier ce problème de détection de l'intégrine. Le complexe

intégrine αvß3-Apol formé a ensuite été immobilisé sur une puce SPR et l'interaction de l'intégrine αvß3 avec son récepteur protéique naturel, la vitronectine, a été étudiée. Ces résultats d'un point de vue global sont très positifs et sont donc intéressants à poursuivre.

La dernière section de cette thèse, qui ne concerne pas des protéines membranaires, est consacrée à l'étude d'événements de reconnaissance biomoléculaire. A cet effet, nous avons exploré les interactions d'une lectine (concanavaline A (ConA)) avec des sucres multivalents présentés sur un châssis moléculaire, RAFT. Dans ce chapitre, par une étude SPR directe, nous avons réussi à distinguer l'effet de proximité / statistique de l'effet cluster. Pour cela, deux types de surfaces, présentant des densités élevées ou faibles de lectine immobilisée, ont été étudiées avec des dérivés mannosyle greffés sur une plateforme RAFT. Nous avons ainsi réussi à démontrer que l'effet de proximité / statistique peut être distingué de l'effet cluster en espaçant suffisamment les récepteurs (ConA) sur la surface afin que l'effet cluster devienne négligeable. Ce chapitre démontre également que la proximité des épitopes greffés sur le châssis RAFT induit une augmentation des constantes de vitesse d'association et une diminution des constantes de vitesse de dissociation. Le temps de liaison du glycocluster est donc accru et une plus grande affinité est ainsi observée. L'approche a ensuite été étendue à l'évaluation des paramètres thermodynamiques. Ici, les résultats préliminaires sondent les contributions entropiques induites par un tel effet.

Ainsi, en conclusion générale de cette thèse, nous avons réussi à démontrer la caractérisation, la conception et les applications de diverses interfaces fonctionnelles. Ces interfaces fonctionnelles ont été principalement conçues pour immobiliser des protéines membranaires et étudier leurs interactions avec leurs partenaires biologiques naturels. En parallèle, une extension de ce travail impliquant l'étude des interactions sucre-lectine donne un aperçu utile sur les interactions multivalentes, particulièrement répandues dans les systèmes biologiques.

Functional Interfaces for the Immobilization of Membrane Proteins: Concept, Characterization and Interactions

Abstract: This thesis is dedicated towards the development of supramolecular assemblies, which are capable of mimicking the amphiphilic nature of the cytoplasmic cell membranes. To this effect, Supported Lipid Bilayers (SLB) was designed to incorporate FhuA (an *E.coli* outer membrane protein). The interaction of FhuA present in the SLB, with pb5 (the bacteriophage T5 protein), was then studied using QCM-D. Further, Tethered Lipid Bilayer Membranes (tBLM) were constructed on Self-Assembled Monolayers (SAMs) of a novel synthetic anchoring thiol. In this study, the tBLM formation was elaborately investigated using a host of techniques such as QCM-D, AFM and EIS, to infer upon the role of the anchoring thiol in the tBLM formation process. Further, a biotinylated Amphipol (B-PCApol) was employed to immobilize membrane proteins such as FhuA and the human $\alpha_v\beta_3$ integrin on streptavidin containing surfaces. Using their respective assemblies, the dissociation constant of the FhuA-pb5 complex was determined, whereas the interactions of integrin with its ligand vitronectin were studied by SPR. The last part of this thesis, deals with the study of biomolecular recognition events between a lectin (ConA) and multivalent sugars presented on a RAFT scaffold.

Keywords: supramolecular assemblies, bilayer, monolayer, thiol, amphipol

---

Interfaces Fonctionnelles pour l'immobilisation des Protéines Membranaires : Concept, Caractérisation et Applications

Résumé: Cette thèse est consacrée au développement d'assemblages supramoléculaires, qui miment la nature amphiphile des membranes cellulaires. A cette fin, des bicouches lipidiques supportées (SLB) ont été conçues pour l'insertion de la FhuA (protéine de membrane externe d'E. coli). L'interaction de FhuA présente dans la SLB, avec le pb5 (la protéine du bactériophage T5) a ensuite été étudiée par QCM-D. De plus, des bicouches lipidiques suspendues (tBLM) ont été construites sur des monocouches auto-assemblées (SAM) d'un nouveau thiol d'ancrage. Dans cette étude, la formation de tBLM a été minutieusement étudiée par différentes techniques telles que la QCM-D, l'AFM et l'EIS, afin de déduire le rôle du thiol d'ancrage dans le processus de formation de tBLM. En outre, un amphipol biotinylé (B-PCApol), a été employé pour l'immobilisation des protéines membranaires, par exemple la FhuA et de l'intégrine avß3 (humain) sur des surfaces contenant la streptavidine. Avec leurs assemblages respectifs, la constante de dissociation du complexe FhuA-pb5 a été déterminée, tandis que les interactions de l'intégrine avec vitronectine (son ligand naturel) ont été étudiées par SPR. La dernière partie de cette thèse est dédiée à l'étude d'événements de reconnaissance biomoléculaire entre une lectine (ConA) et des sucres multivalents présentés sur un châssis moléculaire, RAFT.

Mots-clés : assemblages supramoléculaires, bicouches, monocouches, thiol, amphipol